UNIVERSITY OF CALIFORNIA,
IRVINE

Interplay of Climate, Human Activities, and Urban Runoff: Implications for Streamflow Dynamics and Green Stormwater Infrastructure

DISSERTATION

submitted in partial satisfaction of the requirements
for the degree of

DOCTOR OF PHILOSOPHY

in Civil and Environmental Engineering

by

Azadeh Hemati

Dissertation Committee:
Professor Stanley B. Grant, Chair
Professor Russell Detwiler
Professor Amir AghaKouchak

2023

DEDICATION

To My Dearest Parents,
My Beloved Husband,
and My Precious Daughter

TABLE OF CONTENTS

LIST OF FIGURES

ACKNOWLEDGMENTS

I wish to express my profound gratitude to my committee chair, Professor Stanley Grant, from the University of California, Irvine, and Virginia Tech. Professor Grant embodies both the attitude and substance of a visionary scholar. He consistently and persuasively conveyed a spirit of exploration in research and scholarship, alongside an unwavering enthusiasm for teaching. This dissertation owes its existence to his steadfast guidance and unwavering support.

I extend my heartfelt thanks to my committee members, Professor Russell Detwiler and Professor Amir AghaKouchak, whose invaluable feedback and shared insights enriched my work and fueled my passion for research. I also had the privilege of collaborating closely with Dr. Megan Rippy at Virginia Tech, whose expertise in statistical analysis and thoughtful critiques significantly enhanced the quality of my research.

I gratefully acknowledge the financial support that made this journey possible, including funding from the U.S. National Science Foundation Partnerships for International Research and Education (OISE-1243543), an Australian Research Council Discovery Project (DPI30103619), and the UC Office of the President Multi-campus Research Program Initiative award (MRPI-17-455083).

To my fellow peers who shared this academic odyssey with me, I extend my sincere thanks. Your daily interactions, shared knowledge, and constructive feedback have been invaluable, shaping my growth and learning in countless ways.

To my parents and family, I am deeply indebted for their unwavering patience, empathy, and support throughout this journey. Lastly, I extend my heartfelt appreciation to my beloved husband, Mazyar, whose unyielding support and encouragement have been my steadfast companions from the inception of my Ph.D. to this very day.

Without the collective support of the individuals mentioned above, I would not have reached this significant milestone, and this dissertation would remain unrealized. My sincere thanks go out to everyone who invested their time and support throughout my Ph.D. I am profoundly grateful and will forever cherish the profound life lessons learned during these transformative years.

VITA

Azadeh Hemati

EDUCATION

Doctor of Philosophy in Civil and Environmental Engineering **2023**
University of California, Irvine *Irvine, CA*

Master of Science in Civil and Environmental Engineering **2016**
University of California, Irvine *Irvine, CA*

Master of Science in Mechanical Engineering **2011**
Purdue School of Engineering and Technology *Indianapolis, IN*

Bachelor of Science in Mechanical Engineering **2008**
Aachen University of Applied Sciences *Juelich, Germany*

WORK EXPERIENCES

Stormwater Design Engineer **2022–2023**
Q3 Consulting *Foothill Ranch, CA*

Intern at Orange County Environmental Resources **2021–2022**
Orange County Public Works *Orange, CA*

Mechanical Engineer **2012–2013**
Eli-Lilly Technology Center, LTC Utilities *Indianapolis, IN*

RESEARCH AND TEACHING EXPERIENCES

Graduate Research Assistant **2014–2021**
University of California, Irvine *Irvine, California*

Teaching Assistant–CEE11 **2017–2018**
University of California, Irvine *Irvine, CA*

Adjunct Faculty–MET220 **2013–2014**
Indiana University-Purdue University (IUPUI) *Indianapolis, IN*

Graduate Research Assistant **2009–2011**
Purdue School of Engineering and Technology *Indianapolis, IN*

JOURNAL PUBLICATIONS

Stormwater Biofilter Response to High Nitrogen Loading under Transient Flow Conditions: Ammonium and Nitrate Fates, and Nitrous Oxide Emissions. **2023**
Water Research, https://doi.org/10.1016/j.watres.2022.119501.

Deconstructing Demand: The Anthropogenic and Climatic Drivers of Urban Water Consumption **2016**
Environmental Science and Technology, https://doi.org/10.1021/acs.est.6b02938

Layer-by-Layer Nanoassembly of Copper Indium Gallium Selenium Nanoparticle Films for Solar Cell Applications. **2012**
Journal of Nanomaterials, https://doi.org/10.1155/2012/512409

Breast Tumor Detection by Flexible Wearable Antenna System. **2012**
International Journal of Computer Aided Engineering and Technology, https://doi.org/10.1504/IJCAET.2012.049574

ABSTRACT OF THE DISSERTATION

Interplay of Climate, Human Activities, and Urban Runoff: Implications for Streamflow Dynamics and Green Stormwater Infrastructure

By

Azadeh Hemati

Doctor of Philosophy in Civil and Environmental Engineering

University of California, Irvine, 2023

Professor Stanley B. Grant, Chair

As water imports dwindle, and climate changes, southern California is progressively turning to non-traditional water resources, including water reclamation, ocean water desalination, and the capture and fit-for-purpose use of dry and wet weather urban runoff. All three approaches are being employed to various degrees in the region, but capture and use of urban runoff has the potential to not only increase water supply but also provide habitat for rare and endangered flora and fauna, pollutant removal services, urban greening, and mitigation of the urban heat island effect.

This thesis explores both the water supply and water quality challenges and opportunities associated with using green stormwater infrastructure (GSI) to capture and treat urban runoff in Southern California. On the supply side, Chapter 2 presents an analysis of streamflow trends across the region, with the goal of assessing how reliable this source of water is likely to be into the future, given current trajectories in water conservation and climate change. The results suggest that, generally speaking, streamflow was increasing across the region until around 1990, and has been steadily falling since. In most of the 37 streams analyzed here, current summertime flows are less than 50% of 1990 levels. This precipitous decline reflects a combination of human and hydrological factors, including reduced water imports

to the region and outdoor water conservation measures initiated during, and following, the drought of 2011-2016.

On the water quality side, two complementary mathematical fate and transport frameworks are presented for assessing, and predicting, the removal of pollutants in a form of GSI called bioretention systems. The two frameworks take distinctly different approaches for addressing a primary challenge for modeling pollutant removal in these systems; namely, the intermittent nature of storms implies that flow through these systems is inherently unsteady.

The first mathematical framework (Chapter 3) hypothesizes that, by flow weighting time, pollutant breakthrough in these systems can be represented by a standard one-dimensional advective-dispersion model for pollutant transport through porous media. This hypothesis is validated using bromide breakthrough data collected during a pilot-scale bioretention experiment at Orange County Public Works (OCPW). This experiment, which was conducted in Spring of 2019, explicitly accounts for the highly variable (flashy) storm flows generated from impervious areas in Southern California.

The second mathematical framework (Chapter 4), hypothesizes that transient transit-time distribution theory (T-TTD) can be coupled to a biokinetic model of nitrogen cycling, to estimate the fate and transport of nitrogen species (ammonium and nitrate) in the same pilot-scale bioretention system described above. A particular advantage of T-TTD theory is that it can account for loss of water by both gravitational drainage and evapotranspiration– both of which can exert significant controls on nitrogen cycling during the long antecedent dry periods typical of Southern California's summers. The breakthrough of both ammonium and nitrate in OCPW's pilot scale facility can be reproduced, after accounting for adsorption and nitrification (ammonium) and nitrification (nitrate) in the soil media component of this system.

By shedding light on both the supply and water quality dimensions of urban stormwater

runoff, this thesis supports Southern California's long-term goal of reducing its reliance on imported sources of water. It also informs adaptive water management approaches under changing conditions and guides bioretention design enhancements for improved stormwater quality.

Chapter 1

Introduction

1.1 Introduction

Southern California, with its sun-soaked landscapes and burgeoning population, faces a pressing challenge: water scarcity. This region relies heavily on imported water sources, which makes it vulnerable to water supply disruption. The existing water supply system is also energy and carbon intensive. Approximately 12% of Califonia's energy is used for treating water, moving water from one location to another, and pumping from underground aquifers [1]. For these reasons, innovative solutions and strategies are urgently needed to both make southern California's water supply infrastructure more energy efficient and sustainable in the long-run [2, 3].

For decades, Southern California has depended on centralized water infrastructure for its drinking water, sewage, and stormwater drainage. While this system has served its purpose, it is not without drawbacks. Maintenance is costly, and this centralized approach can reduce resilience in the face of water supply disruptions. The drought of 2011-2017, which led to zero water allocation from the California State Water Project, highlighted the region's

vulnerability [4–8].

Climate change adds another layer of complexity to Southern California's water woes. Projections suggest a temperature rise of up to 2°C by 2050, contributing to the reduction of snowpack in the Sierra Nevada Mountains, a critical natural reservoir. This diminished snowpack threatens water supply, and its decline also exacerbates warming by reducing the Earth's albedo. Additionally, higher temperatures and prolonged droughts have led to more frequent and intense wildfires, releasing greenhouse gases and worsening climate conditions [9–14].

Moreover, Southern California faces an increased risk of hydrological extreme events such as heavy rainfall and runoff due to continued warming. These events can result in flash floods, mudslides, and disruptions to water supply and infrastructure, posing substantial challenges to both urban and rural communities [10, 15, 16].

To address the three-fold challenge of population growth, limited water resources, and environmental consequences, many municipalities in the region are diversifying their water supply portfolios. This includes the recycling of treated municipal wastewater for non-potable purposes and indirect potable reuse. While progress has been made in water reclamation, one underutilized water resource remains: urban runoff [5, 17–24]. Urban runoff, which includes both stormwater and dry weather flow, has the potential to provide a significant water source. However, several challenges, including the need for treatment, cost calculations, and public acceptance, have hindered its widespread utilization. Nonetheless, capturing and reusing stormwater runoff alone could provide water for a substantial portion of Southern California's population [25–27].

Additionally, according to Townsend-Small et. al (2013)[25] dry weather flow in urban rivers has been on the rise, driven by factors such as groundwater seeps, treated wastewater, and freshwater "leaks" into stormwater drainage systems. These flows represent another

opportunity for water capture and reuse, with benefits including reduced pollution in coastal waters and preservation of important ecological processes [28–30].

Historically, large-scale projects have supported the capture and recharge of stormwater runoff for groundwater replenishment. Recent initiatives, such as Los Angeles County's Measure W, have further emphasized the importance of capturing and cleaning stormwater to mitigate pollution and provide additional water supply [31, 32].

Amidst these challenges and opportunities, this doctoral thesis seeks answers to two fundamental questions:

1. How is streamflow in Southern California's urban streams evolving over time? This question focuses on assessing long-term trends in streamflow across both large and small streams throughout the region. Understanding how streamflow patterns are evolving over time is crucial for predicting future water availability and devising effective water management strategies.

2. To what extent can Green Stormwater Infrastructure be counted on to remove pollutants in urban runoff? The second critical question focuses on the removal of contaminants in stormwater or dry weather runoff in biofilters, an increasingly popular form of Green Stormwater Infrastructure (GSI) in Southern California and beyond. In particular, a modeling framework is developed for quantifying pollutant removal in soil component of GSI.

1.2 Thesis Roadmap

The thesis is organized as follows.

In **Chapter 2**, an analysis of summer and winter streamflow across multiple sites was

conducted to understand how climate and human activities influence streamflow in Southern California's urban streams. Change point detection was applied to average streamflow, maximum stream flow, and zero discharge days, and the results were correlated with Palmer Drought Severity Index (PDSI) trends. The results indicate a post-1990 decrease in all streamflow indicators.

Regarding the reliability of urban runoff as a water source, my findings suggest that declining streamflow could present long-term challenges for the capture and use of urban runoff as an alternative water resource for the region. Comprehensive water resource management strategies must address these complexities, incorporating climate resilience, sustainable land use practices, and adaptive management. Collaboration, research, and informed policies are essential for securing a sustainable water future in Southern California.

In Chapter 3, the focus shifts to the potential of bioretention systems or biofilters to remove human pathogens in urban runoff, a known source of health risks. These pathogens result from combined sewer overflows, illicit sewer connections, and failing septic systems. While research has yielded variable results in pathogen removal, the study aims to uncover the underlying mechanisms.From a technical standpoint, this chapter makes progress toward this end-goal by introduced and testing the concept of flow-weighting microbial breakthrough curves, which can then be fit to conventional solutions of the advection-dispersion equation, for example to infer rates of filtration, die-off, regrowth in the soil media component of these systems.

Chapter 4 In this chapter, an unsteady transit time distribution (TTD) theory of pollutant transport through soil media is combined with a process-based N-cycling model to predict nitrogen export from bioretention systems across various timescales. The focus is on understanding how biofilters function as either nitrogen sinks or sources, depending on the observation timescale, especially during and between storm events. For example, during dry periods between storms, nitrate may be initially generated through ammonification-

nitrification when oxygen levels are high, but later removed via denitrification as anaerobic conditions develop. Hence, nitrogen export depends on the antecedent dry period (ADP), rising and falling with increasing ADP.

The study also evaluated the impact of ADP on biofilter functionality with or without a submerged zone, designed to enhance denitrification by extending water residence time. Results from TTD theory for simulated storm sequences in the Orange County region were compared with those obtained by assigning the biofilter a single hydraulic residence time, a common engineering practice for estimating treatment credit in green stormwater infrastructure.

Chapter 2

Streamflow Trends in Southern California: Implications for the Capture and Use of Wet and Dry Weather Urban Runoff

2.1 Introduction

Many urban communities in the U.S. rely on highly centralized water infrastructure for drinking water, sewage, and storm water drainage. This civil infrastructure is expensive to build and maintain, and ironically can diminish a society's resilience to water supply disruptions [17, 18, 28, 33–39]. A case in point is Southern California, which relies on a network of reservoirs, canals, and pipelines to import approximately 60% of its drinking water from regions located hundreds of kilometers to the north and east [5]. During the drought of 2011-2017 and for the first time in its 54-year history, the California State Water

Project, which alone supplies 30% of Southern California's drinking water, announced zero water allocation to all 29 of its public water agency customers [5–7]. Water supply shortages are an ongoing challenge in the region due to continued population growth (expected to increase ∼0.8% annually by 2040) [40–42].

Adding to these challenges, California is grappling with the profound impacts of climate change. Projections indicate that by 2050, the southwestern United States, including California, could see an additional 2 °C of warming [10]. This temperature rise sets off a chain reaction of interconnected consequences.

One significant consequence is the reduction in snow depth during winter and spring, especially in the Sierra Nevada Mountains [43–45]. This decline in snowpack poses a direct threat to the state's water supply since snowpack functions as a vital natural reservoir, releasing water gradually throughout the year [10, 46]. Additionally, the reduced snowpack contributes to a decrease in albedo, as there is less reflective snow to bounce sunlight back into the atmosphere [47]. This, in turn, amplifies warming by absorbing more heat [10, 48].

Equally concerning is the uptick in the frequency and intensity of wildfires due to these higher temperatures and prolonged droughts. California's environment becomes a tinderbox, making it more susceptible to devastating wildfires [13, 49]. These fires pose immediate threats to human life and property while also releasing significant amounts of greenhouse gases, further worsening the climate conditions that fuel them[50].

Furthermore, the state faces an increased risk of hydrological extreme events such as heavy rainfall and runoff. This heightened risk is likely a result of continued warming, which intensifies the water cycle. Such events can lead to flash floods, mudslides, and disruptions to water supply and infrastructure, presenting substantial challenges for both urban and rural communities [10, 15, 16].

To cope with the twin challenge of population growth and limited water resources, many

municipalities in the region are diversifying their water supply portfolios to include local and non-traditional water resources [5, 24, 51–58]. For example, steady progress has been made statewide to recycle treated municipal wastewater for both non-potable purposes such as irrigation and to replenish drinking water supplies or indirect potable reuse [5, 17–24]. Each year approximately 670,000 acre-feet ($\sim$ 13%) of treated municipal wastewater is recycled in California, approximately 60% of which occurs in Southern California [59].

Capture and reuse of urban runoff, on the other hand, remains a relatively untapped water resource for several reasons [60–67]. Rainfall in the region typically occurs in a three-month window (January through March) which leads to a mismatch between when the rain falls (winter) and when the water is most needed (summer) [68, 69]. While stormwater capture and storage can alleviate some of this seasonal mismatch [70], as has been demonstrated in Australia [52, 71–73] and China [74–76], there are additional challenges including the need for treatment before use in many applications, difficulties in calculating the benefits and costs of infrastructure, and barriers to public acceptability [51, 73, 77]. However, if these challenges can be overcome, the potential benefits are enormous [26]. By one estimate, capturing and reusing stormwater runoff in Los Angeles alone would provide enough water for one-third of the city's nearly 4 million residents [27].

And the opportunity is not limited to storms. From 1935 to 2010, summertime (June, July, August) dry weather discharge in urban rivers in southern California increased by up to 250% [25]. The ultimate cause for this increase is the region's reliance on water importation, but proximal causes include groundwater seeps, treated wastewater, over-irrigation of ornamental landscaping, and a myriad of freshwater "leaks" that find their way to streams through stormwater drainage systems [25, 78]. Dry weather flows in the Los Angeles River alone exceed 90 GL per year [25].

As with stormwater urban runoff [79–81], distributed capture and reuse of dry weather urban runoff in Southern California has many co-benefits, including a reduction in the discharge

of polluted runoff to coastal waters [28–30, 82] and less disruption of important hydrological processes (inlet opening, salinity regimes) and associated ecological processes (e.g., reproduction of fish) in the region's tidal sloughs and estuaries, where species are not adapted to perennial inputs of freshwater [83]. Thus, capture and use of summertime flow in urban streams (e.g., for groundwater recharge and fit-for-purpose activities, such as irrigation) has many of the same advantages articulated above for stormwater capture, but without the extreme storage demands imposed by winter storms.

Southern California has a long history of capturing summer and winter flows in its major rivers (e.g., the San Gabriel, Los Angeles, and Santa Ana), primarily for groundwater recharge. The County of Los Angeles has more than 20 groundwater recharge facilities that collectively capture and recharge approximately 345 GL of stormwater runoff annually, enough water to supply roughly 2.2 million people [84]. A similar project along the banks of the Santa Ana River, in Orange County, has been operating for over 80 years (since the Prado dam was completed in 1940) and currently recharges approximately 166 GL of dry and wet weather runoff annually [85]. Historically, funding for the construction of smaller-scale systems (at the residential to city scale) has been supported by one-off State and local bonds. However, in 2018 Los Angeles County voters passed Measure W, a property tax increment of 2.5 cents per square foot of impermeable surface, to raise $285M annually allocated to capture and clean-up storm water to alleviate runoff of contaminants into streams and estuaries and procure additional supply for various end uses [31, 32].

Given the increasing interest and investment in large and small-scale facilities for the capture, treatment, and reuse of summer and winter urban runoff in Southern California, it is reasonable to ask: *How reliable is this source of water?* On the one hand, the study mentioned earlier suggests that summer baseflow in Southern California urban streams has been increasing over time [25, 86]. On the other hand, increased water conservation in the region (e.g., resulting from a nearly $500M investment by the Southern California Metropolitan

Water District in outdoor water conservation programs during the 2012-2016 drought [87]) may have reduced summer flows toward the end of the time window [88]. Indeed, recent reductions in baseflow in Southern California's urban drainages has been credited with improving coastal water quality [89, 90]. In this study we set out to answer the above question, and specifically to clarify whether summer and winter stream flow in Southern California's urban drainages is increasing or decreasing over time over a 52-year period, from 1971 to 2022.

2.2 Site Description

Southern California's Mediterranean climate is characterized by dry summers and mild wet winters [91]. Most precipitation occurs during the winter months, primarily in the form of rain, with occasional winter storms bringing significant rainfall [92]. Precipitation patterns vary considerably across the region due to its diverse topography. Coastal areas and lower elevations tend to receive moderate to low amounts of rainfall, while mountainous regions, such as San Gabriel and San Bernardino Mountains, experience higher precipitation. The region is prone to multi-year periods of below-average precipitation, leading to reduced water availability and increased stress on water supplies [93].

2.3 Methods

2.3.1 Stream Gauge Selection

Stream gauge stations in the region were evaluated for inclusion in our study based on the following criteria: (1) they should have more-or-less continuous daily streamflow measurements from 1971 to 2022, with no more than six years of contiguous missing data; (2) both

perennial and intermittent streams should be represented in the overall dataset; and (3) stream catchment information should be available, including land use, topography, climate, and geology. Based on these three criteria, 36 U.S. Geological Survey (USGS) gauging stations were selected in Los Angeles, Orange, San Diego, Riverside, San Bernardino, Santa Barbara, Ventura, and Imperial Counties. An additional (non-USGS) gauge operated by the Orange County Public Works (OCPW) was added on the downstream portion of San Diego Creek in Orange County. For all sites we retrieved metadata on watershed characteristics, local climate, and stream management controls. These data are summarized for all 37 sites in the Supplemental Information.

2.3.2 Standardized JJA and JFM Streamflow

At each gauge station, we retrieved from either the USGS or OCPW (for the San Diego Creek Station) daily average streamflow from 1971 to 2022 (nominally corresponding to 18615 streamflow measurements per site). From these data we calculated standardized annual summer and winter streamflow as follows: (1) the daily flow measurements at each gauge station were separated into summer (June, July and August, JJA) and winter (January, February, March, JFM) periods; (2) daily stream flow measurements in the JJA and JFM periods were then log (base-10) transformed (to reduce skew) and standardized (i.e., Z-scored), $Z_{i,j} = (Q_{i,j} - \bar{Q}_i)/\sigma_{Q,i}$, where $Q_{i,j}$ is the log-transformed daily average stream flow measurement at the ith station on the jth day, and $\bar{Q}_i$ and $\sigma_{Q,i}$ are the average and standard deviation, respectively, of the log-transformed daily average JJA or JFM streamflow at the ith station for the entire 51-year period; and (3) the annual average and standard deviation of the log-transformed and Z-scored stream flow values at the ith station, $\bar{Z}_i$ and $\sigma_{Z,i}$, were calculated for every JJA and JFM in the 51-year period of interest.

2.3.3 Change Point Detection (CPD)

The R package "chngpt" [94] was used to identify a change in slope of the standardized and log-transformed annual JJA and JFM streamflow data (i.e., the $\bar{Z}_i$ values described in the last section). Change points were deemed significant if the slope of $\bar{Z}_i$ with time was significantly different ($p < 0.05$) before and after the change point.

2.3.4 Palmer Drought Severity Index (PDSI)

Streamflow patterns were compared to the Palmer Drought Severity Index (PDSI), which takes into account changes in precipitation, temperature, and soil moisture within a region [95–97]. Monthly values of PDSI were retrieved from the National Centers for Environmental Information (NCEI) for the California Climate Division 6 region over the 51-year time period of interest, from 1971 to 2022. Average annual summer (JJA) and winter (JFM) PDSI timeseries were calculated from these monthly data.

2.3.5 Percent Impervious Cover (%IC)

The drainage area associated with each of the 37 gauge stations was delineated (ArcGIS Pro, Version 2.9.1) and then intersected with 30 m resolution Percent Impervious Cover (%IC) raster files for 2001, 2011, and 2019 obtained from the National Land Cover Database (NLCD) [98]. The average %IC in each drainage area was calculated for all three years (results reported for each station in Supplemental Information) along with the percent change in impervious cover from 2001 to 2019: $\Delta\%\text{IC} = 100 \times \frac{\%\text{IC}_{2019} - \%\text{IC}_{2001}}{\%\text{IC}_{2001}}$.

2.3.6 Principal Component Analysis (PCA)

To identify dominant temporal and spatial patterns across all stream sites, PCA was performed on the standardized and log-transformed annual JJA and JFM streamflow timeseries. A resampling-based stopping rule [99, 100] was used to identify PC modes that explained more variance in JJA and JFM flows than expected by chance (significant at $p < 0.05$). A non-parametric bootstrap approach [101] was used to determine the statistical uncertainty about significant PC modes and their corresponding scores and site-specific coefficients.

2.4 Results and Discussions

2.4.1 Stream Gauge Sites

The 37 sites included in our study captured a broad range of stream sizes (geometric mean discharge from 0.01 to 1127 acre-feet per year in JJA, and from 1.1 to 155,927.3 acre-feet per year in JFM), stream type (including both perennial ($N = 29$) and intermittent ($N = 8$) streams), and catchment landcover, soil, geology and topography (2.1 and Appendix A). For 26 of the 37 sites, daily average streamflow was reported every day in the 51-year period of interest. For the 11 remaining sites, the percent of days with missing streamflow data ranged from 0.02 to 12% (median 1.92%) and 0 to 12% (median 2.11 %) for JJA and JFM periods, respectively (N-values for all 37 streams are reported in the Supplemental Information).

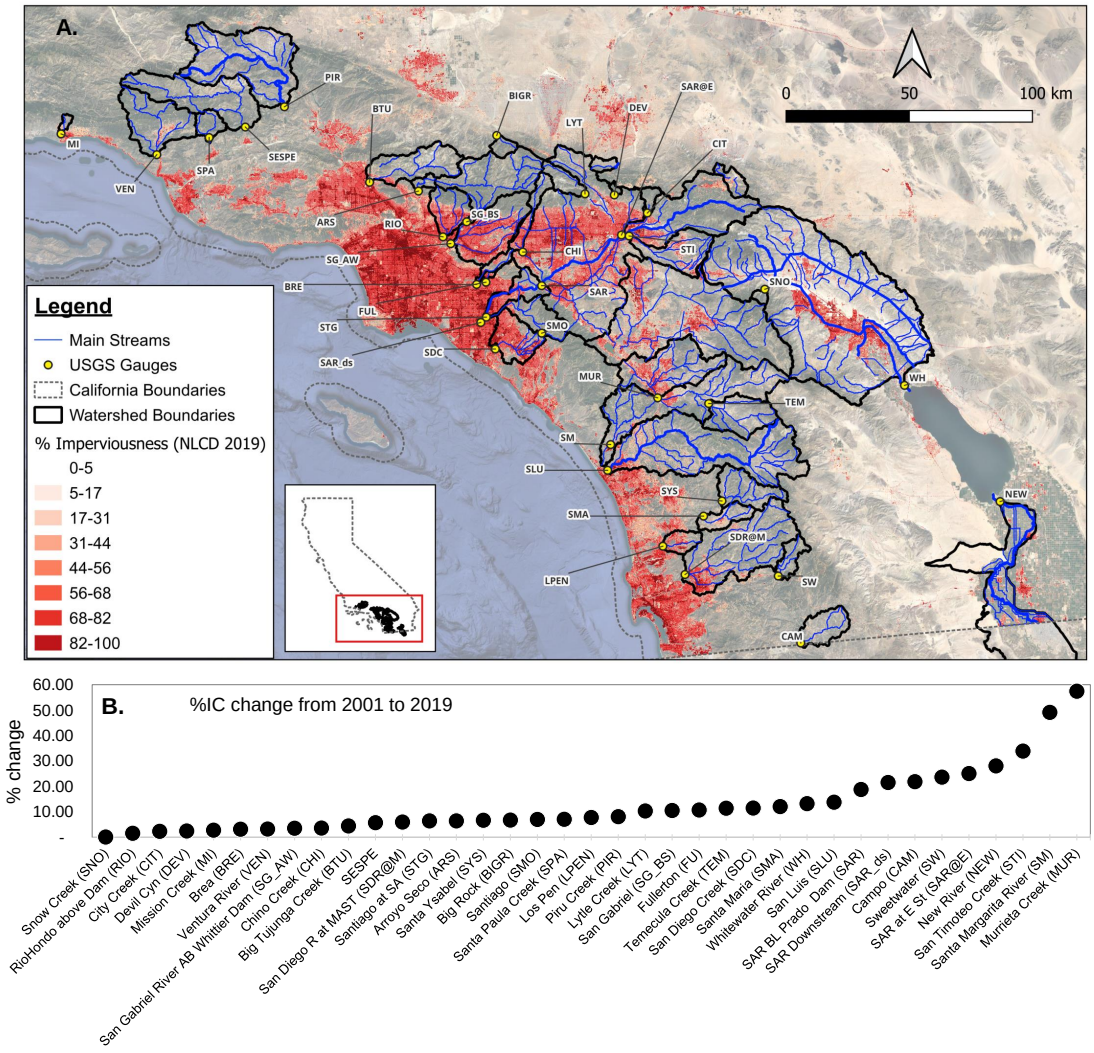

Figure 2.1: **A.** Drainage areas and 2019 percent impervious landcover for the 37 stream sites included in this study. Lower impervious landcover is an indicative of more natural catchments, while higher impervious cover reflectws urbanization. **B.** Change in impervious Cover, expressed as percent increase from 2001 to 2019, for the catchment draining to each stream.

2.4.2 Change Point Analysis: JJA Streamflow

Classification of Streamflow Patterns

The change point analysis identified a significant ($p < 0.05$) change in trend or slope of the standardized summertime (JJA) annual streamflow measured at all 37 sites. The distribution

of these inferred change points is bimodal, with a prominent mode around the year 1980 and a less prominent mode around the late 1990s (Figure 2.2A). Across all sites, the expected value of the change point distribution is the year μ =1990, signaling a regional shift in stream flow patterns occcurred in Southern California around that time. However, the change in streamflow took markedly different forms in different streams, reflecting the strong influence that climate, hydrology, and human behavior—and non-linear feedback between all three—have on local water resources, especially in densely populated areas like Southern California.

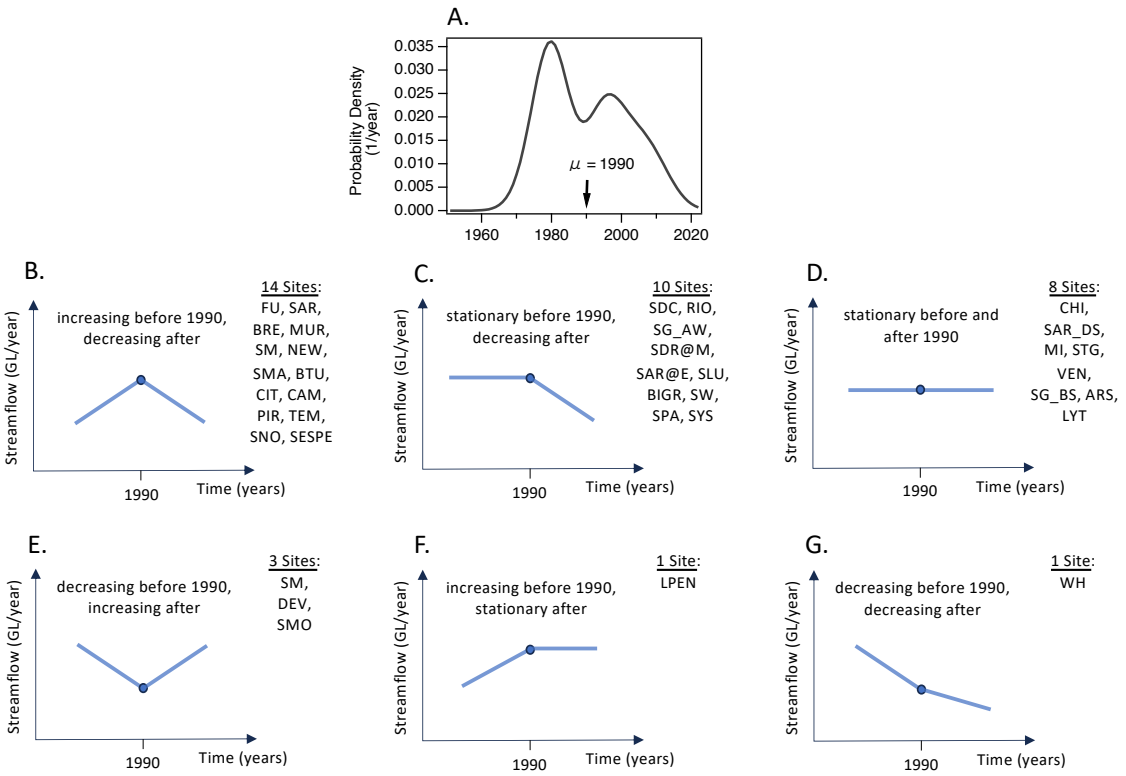

Figure 2.2: Results of the change-point analysis on (standardized and log-transformed) daily average summer (JJA) streamflow measured at 37 sites over 52-years from 1971 to 2022. **A** The probability distribution of inferred change-points. The expected value is the year μ =1990. **B** - **G** Conceptual diagrams of the pre- and post-1990 summer streamflow trends, along with the stream sites where these trends were observed (site labels are defined in Figure 1).

In particular, for the 37 stream sites analyzed here, we identified at least six distinct patterns in streamflow trends pre- and post-1990 (Figure 2.2B-G). These patterns were identified by performing a two-segment linear regression on the standardized streamflow data at each site,

adopting the expected value, μ =1990, as a common breakpoint. Streamflow was assumed to be stationary over a particular segment if the regression slope's 95% confidence interval overlapped zero. Timeseries plots of measured streamflow and the corresponding segmented linear regression are presented for each site in the Supplemental Information.

Streamflow at most of our sites (32 out of 37) fell into one of three categories (Figure 2.2B-D); namely, either streamflow was (1) increasing prior to 1990 and decreasing thereafter ($N = 14$); (2) stationary prior to 1990 and decreasing thereafter ($N = 10$); or (3) stationary both before and after 1990 ($N = 8$). For streams in the first category, increasing streamflow pre-1990 can be reasonably attributed to increasing water imports to the region, as suggested by Townsend-Small et al (2013). The fact that flow in these same streams has been declining post-1990 is also not surprising, given that the region has more recently experienced several multi-year droughts [102].

However, what happens at a particular stream appears to be both context specific and path-dependent, as is typical for complex socio-hydrological systems [103]. For example, a stream in the second category, SAR@E, experienced an abrupt decline in flow in 1996 when an upstream water reclamation plant stopped discharging to the stream (see notes in Supplemental Information). In this case a change in infrastructure, not the onset of drought conditions, caused a shift from stationary flow (pre-1990) to declining flow (post-1990).

Regardless of the underlying mechanisms, the fact that flow is declining in so many streams across Southern California (24 out of 37, or 68%) has important implications for future capture and use of urban runoff in the region. Indeed, five streams in the stationary category (Figure 2.2D, MI, SARDS, STG, SGBS, and LYT) are periodically dry in the summer. In these cases, streamflow is stationary because there is no flow to reduce. Thus, the percentage of streams in our study for which flows are either currently declining or intermittent is around 78%.

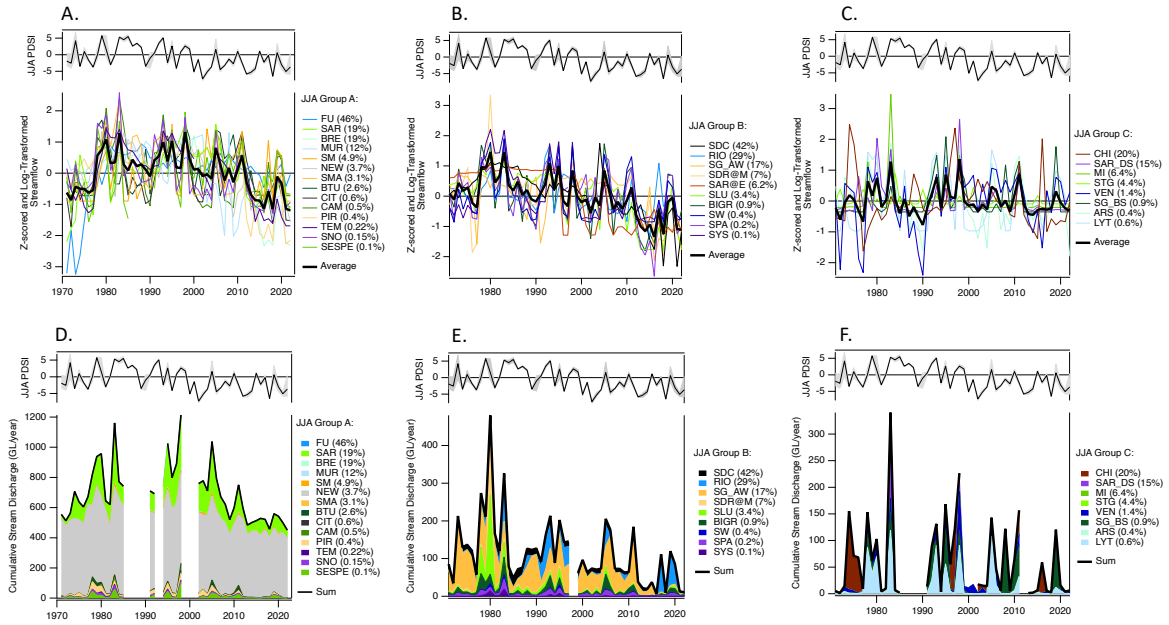

Figure 2.3: Average summer (JJA) streamflow trends for the three most common categories of change pre- and post-1990: **A,D** increasing and then decreasing flow ; **B,E** stationary then decreasing flow; and **C,F** stationary flow in both time periods. The average trend for all stations within a category is shown (dark black curve, panels **A-C**), along with the total flow from all stations within a category (dark black curves, panels **D-F**). The 2019 NLCD average catchment imperviousness is shown for each site in parentheses.

Climate Forcing

Imprinted on the broad pre- and post-1990 patterns described above are interannual climate patterns, including El Nino—La Nina rainfall cycles and the multi-year droughts mentioned earlier. For each of the main three categories described above (panels B, C, and D in Figure 2.2), the average streamflow pattern (thick black curves in panels A,B, and C in Figure 2.3) is correlated ($p < 0.05$) with PDSI ($R^2 = 0.33$, 0.43, and 0.19, respectively). The correlations with PDSI are $R^2 = 0.25$, 0.21, and 0.20, respectively, if the comparison is the cumulative flow contributed by all streams in each category (thick black curves in panels D, E, and F in Figure 2.3) indicating that PDSI explains a portion of the variation in streamflow, but other factors also play a role.

The latter analysis also allows us to quantify the magnitude of the post-1990 decline in

streamflow. For example, cumulative streamflow in the first category has declined by more than 50%, falling from just under 1200 GL/year in the mid-1990s to below 600 GL/year today (Figure 2.3D).

Annual Extremes in Streamflow

For this analysis we extracted for all sites the maximum stream flow and number of days with zero(no) flow in both summer and winter months, as described below.

Maximum Stream Flow: Maximum stream flow refers to the highest stream discharge measured in a stream over a year. By analyzing the maximum stream flow data, we gained insights into the extreme hydrological events that may occur in the streams, such as intense rainfall events or rapid snowmelt, which can lead to significant changes in water levels.

The violin plots presented in Figures 2.4B and 2.4C provide a visualization of the trends in z-scored and log-transformed maximum summer and winter discharge data pre- and post-1990 (i.e., expected breakpoint) for the studied watersheds. These plots reveal interesting patterns that are categorized based on catchment imperviousness levels.

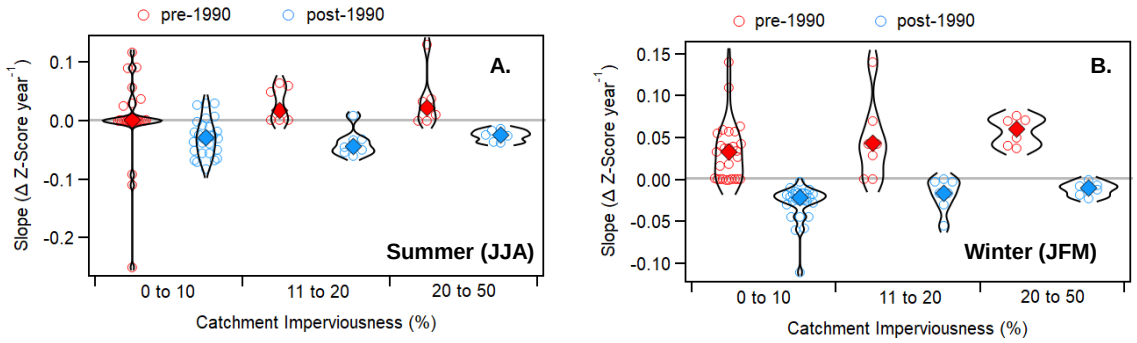

Figure 2.4: Linear trendline slopes pre- and post 1990 for the summer (B.) and winter(C.) months are presented in red and blue circles, respectively, and categorized based on the percent of catchment imperviousness. The medians of each category is shown with a diamond-shape markers.

For the maximum stream discharge trend in summer months, the pre-1990 period displayed

differing patterns. Watersheds with 0-10% imperviousness showed a median slope close to zero, indicating a relatively stable maximum discharge trend. However, watersheds falling within the 12-20% and 20-50% imperviousness ranges in summer and all impervious categories in winter months demonstrated positive median slopes, suggesting an increasing maximum discharge trend.

In both summer and winter months post-1990 period, the maximum stream discharge trend exhibited a uniform negative median slope across all three imperviousness categories. This points towards a decreasing trend in maximum discharge for all levels of watershed development.

Furthermore, Figure 2.5 provides a spatial representation of the slope trends for both winter (top panels) and summer months (bottom panels), contrasting the periods before (left panels) and after (right panels) 1990. This visual depiction offers a geographical context to complement our understanding of the observed changes in the maximum stream discharge.

The results highlight a coherent post-1990 trend: a systematic reduction in maximum stream discharge across the entire study area, irrespective of the level of catchment imperviousness or the specific spatial distribution of the streams.

Number of Days with Zero Discharge (NZD):

The number of days with zero discharge (NZD) represents the frequency of days when the stream's flow completely ceases or reaches a negligible level. This measure is indicative of drought conditions or extremely low water availability in the streams, which could be influenced by various water resource management activities undertaken by humans.

Regarding the analysis of the number of days with zero discharge (NZD), a similar approach to the maximum stream flow trend analysis was undertaken. We examined the trends both before and after 1990 and have presented them spatially in Figure 2.7.

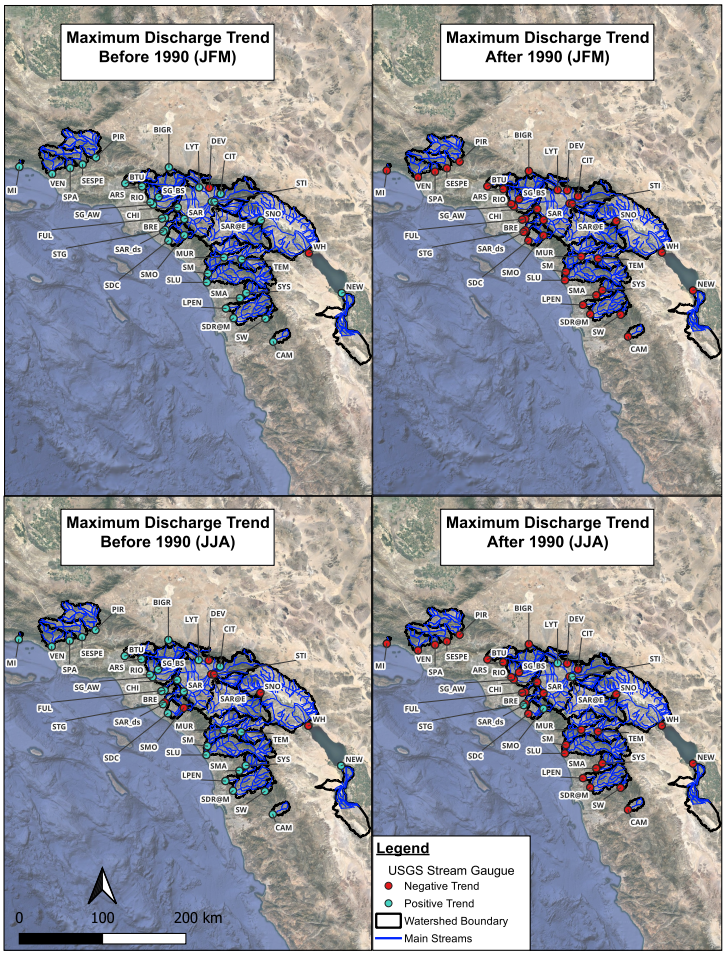

Figure 2.5: Trends in maximum stream discharges before (left panels) and after (right panels) the breakpoint (year 1990) for winter months (JFM; top panels) and summer months (JJA; bottom panels) are shown for the studied gauges. Blue(red) circles represent the gauge stations with increasing (decreasing) trend in maximum seasonal streamflows, respectively.

The slope trends for both winter (top panels) and summer months (bottom panels), during periods before (left panels) and after (right panels) 1990, are depicted in the figure. Sites that consistently reported no instances of zero discharge were represented in yellow, while streams with decreasing (red) or increasing (blue) trends in the number of zero discharge days were highlighted.

In essence, blue-colored gauges indicate that more water was allowed, resulting in fewer days with zero discharges, while red gauges signify an increase in the number of zero discharge days due to a reduction in water flow. This visual representation provides a clear indication

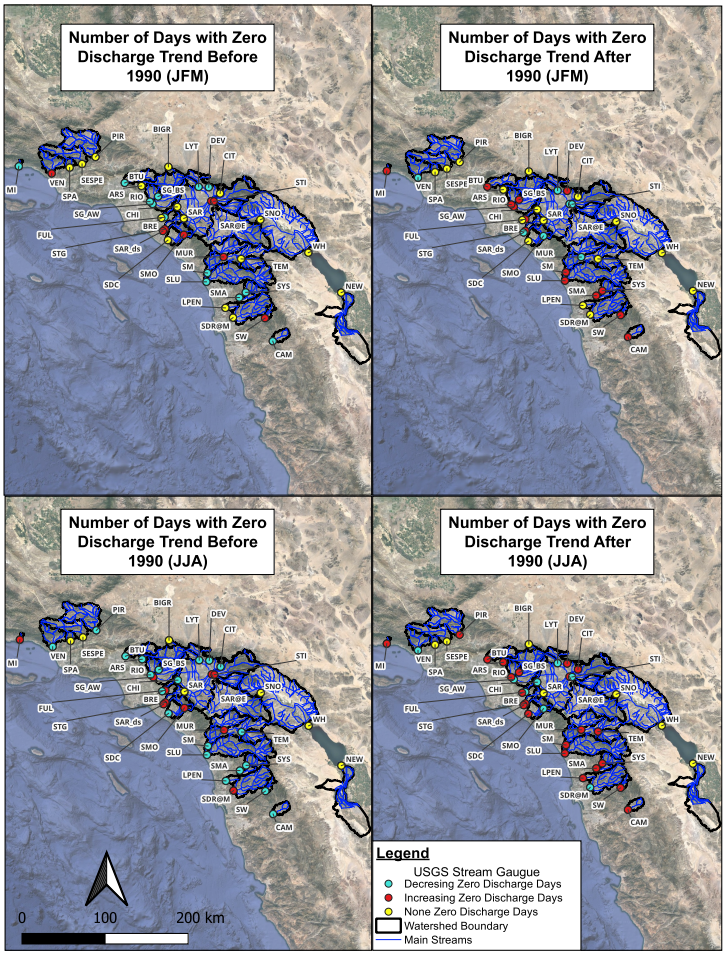

Figure 2.6: Trends in number of days with zero stream discharge before (left panels) and after (right panels) the breakpoint (year 1990) for winter months (top panels) and summer months (bottom panels) are shown for the studied gauges. Blue (red) circles represent the gauge stations with decreasing (increasing) trend in the number of days with zero discharges, respectively. There were no days detected with zero discharge for the yellow circles (gauges).

of the impact of the examined trends on the occurrence of zero discharge days in the streams.

In the broader context, the outcomes of our analysis reveal noteworthy trends post-1990, encompassing both summer and winter months. An evident pattern emerges, showing an increased frequency of streams displaying an escalating trend in the number of zero discharge days (represented by red-colored gauges). This shift signifies a reduction in water availability after 1990, potentially attributable to warmer climate conditions and the occurrence of multiple extreme drought events.

However, a distinction emerges for streams within some watersheds experiencing more than a 7% change in impervious cover since 2001. In winter months, these streams exhibit a declining trend in the number of zero discharge days (increasing number of flow days) post-1990. This trend might be attributed to the alteration in hydrological dynamics caused by urbanization-induced changes in land use.

A study by Pagan et al. (2016) [10] support our findings, suggesting that despite inconsistencies in total annual precipitation and streamflow, a discernible upswing prevails in the intensity and frequency of extreme single-day precipitation and streamflow events. These events, coupled with alterations in the temporal distribution of streamflow and an increased proportion of rainfall over snow due to warmer climate, necessitate potential adaptations in winter reservoir releases and flood channel capacities to ensure effective flood control.

In essence, our results underscore that areas experiencing heightened urbanization since 2001 are more susceptible to flooding during intense storm events. These regions often confront constraints in reservoir storage capacities, leading to the necessity of releasing stored water to accommodate runoff from new events. Consequently, the increased water discharge observed in these streams can be attributed to the complex interplay between urban development, hydrological alterations, and flood control strategies, culminating in the observed trends in streamflow dynamics.

Conversely, in the context of summer months, a distinct pattern emerges. Streams within certain watersheds that have experienced marginal development since 2001 (with less than a 7% change in impervious cover) display a diminishing trend in the number of zero discharge days. This phenomenon is accompanied by an increase in the number of flow days post-1990.

This intriguing shift in behavior can potentially be attributed to evolving hydrology. Specifically, the increasing annual forest fire area within these regions might play a significant role. Remarkably, recent research by Williams et al. (2022) [50] reveals a surge of over 1,100% in

annual forest fire area during the 1984 to 2020 period in the western United States (WUS).

This increase in forest fire area could have significant implications for streamflow. Williams et al. (2022) [50] reported a substantial increase in postfire streamflow across all four seasons. This implies that wildfire has emerged as a pivotal catalyst for altering the dynamics of runoff. The intensified postfire streamflow has far-reaching implications, significantly modifying the influence of climate on water availability and exacerbating the risks associated with runoff-related events.

The interaction between wildfire, hydrological dynamics, and subsequent changes in streamflow patterns is a testament to the evolving landscape of climate-induced impacts on water resources. This trend emphasizes the need for a comprehensive understanding of the multiple factors influencing hydrological behavior, especially in regions vulnerable to changing environmental conditions.

In order to uncover the relationship between large-scale climate patterns and the variability in maximum stream discharge, the Maximum Palmer Drought Severity Index (PDSI) for summer and winter months are compared against Principal Component Analysis (PCA) scores for Mode 1 and Mode 2 (Figure 2.7) .The choice of number of principals was based on the cumulative proportion of variance explained, which accounted for approximately 67% and 73% of the total variance for summer and winter streamflow, respectively. These two principal components were chosen as they effectively summarized the essential patterns and relationships present in each seasonal dataset.

The Maximum PDSI serves as a valuable indicator of drought severity, offering insights into the aridity levels during specific time periods. Trend analysis before and after 1990 was conducted on the maximum PDSI for the summer (Figure 2.7A) and winter months (Figure 2.7B). A decreasing trend after 1990 in maximum PDSI indicates more extreme drought, and warmer climate is occurring after 1990 which supports our previous analysis that the

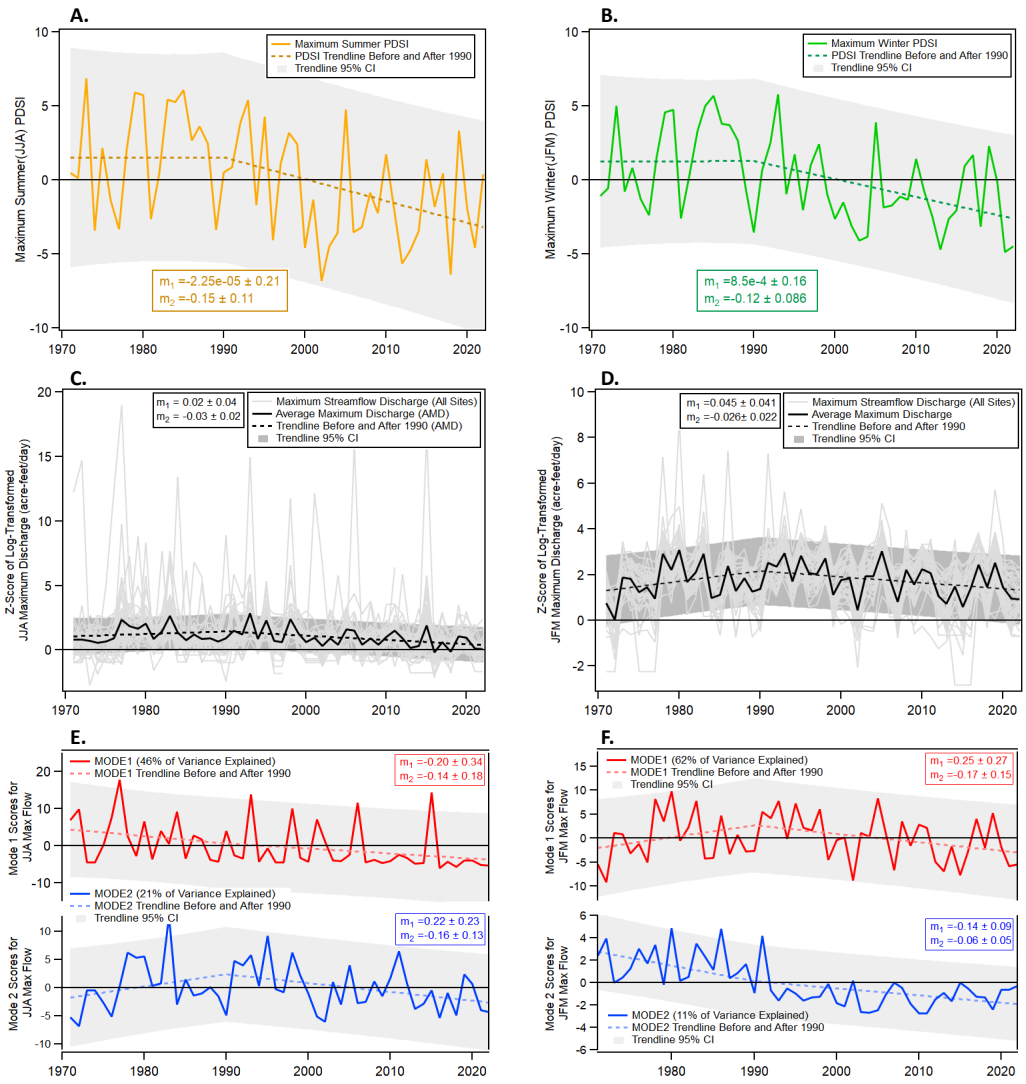

Figure 2.7: Summer/winter months analyses are showing in the left/right panels, respectively. **A. and B.** Maximum Palmer Drought Severity Index (PDSI) for summer and winter months including the trendline before and after 1990. **C. and D.** maximum annual summer (C.) and winter (D.) stream discharges (for all sites), plotted in light grey lines, and the averaged (across all sites) maximum discharge, plotted in a thick black line. **E. and F.** Scores for the top two significant detected CPA Modes (Modes 1 and 2), plotted in red and blue lines, respectively. In each panle, the linear trends before and after the breakpoint (year 1990) are plotted in dashed lines and m_1 and m_2 on each plot represents the slopes of the trendline before and after 1990. The %95 trendline confidence interval is shown by a light grey highlight band. **E.** For summer streamflows, PCA Mode 1 explained %46 of variance, and PCA Mode 2 explaind %21 of variance. **F.** For winter streamflows, PCA Mode 1 explained %62 of variance and PCA Mode 2 explained %11 of variance.

majority of the studied streams were showing negative trend in their maximum discharge and water availability post 1990. Maximum discharge for all sites are presented in light grey lines in Figures 2.7C for the summer months and 2.7D for the winter months. The average maximum discharges for both summer and winter months are calculated and shown in black line, which both are showing a negative trend after 1990.

PCA identified two marginally significant PC modes ($p < 0.05$) that together capture approximately 67% of the summer and 73% flow variability among the thirty seven sites (Figures 2.7E and 2.7F, respectively).

PC Mode 1, our primary discharge pattern, plays a pivotal role in capturing variations in flow, accounting for 46% and 61% of the variance in summer and winter flows, respectively. Notably, its correlation with the Palmer Drought Severity Index (PDSI) is stronger during winter (R^2 =0.30) than summer (R^2 =0.04). This discrepancy can be attributed to winter typically being associated with wetter conditions, rendering it more responsive to shifts in drought intensity and climate fluctuations. The prominent climatic patterns that influence winter streamflow fluctuations are effectively encapsulated by the primary mode's PCA scores, thereby fostering a robust connection between these scores and PDSI. This phenomenon implies a heightened association between identified climate patterns and drought severity, especially during the moisture-laden winter months.

In contrast, the secondary pattern, Mode 2, while being a secondary contributor to variance (explaining 21% and 11% of summer and winter flow variations,respectively), exhibits a more potent correlation with PDSI during summer (R^2 =0.29) as compared to winter (R^2 =0.1). This intriguing observation suggests that the patterns governing maximum summer discharge are not predominantly influenced by climatic conditions. Instead, external factors, such as human-induced activities, likely play a more significant role. For instance, factors like leaky infrastructure pipelines, treated wastewater runoff, escalating urban runoff, as posited by Townsend et al. (2013) [25], could precipitate augmented stream flow discharge. Addition-

ally, it's reasonable that water conservation practices imposed due to drought conditions curtail outdoor water consumption, including irrigation, leading to reduced urban usage and subsequently diminished summer streamflow. This highlights the multifaceted nature of factors impacting summer discharge patterns, extending beyond climatic influences.

2.5 Conclusions

In this study, an extensive analysis of summer and winter streamflow patterns was conducted across multiple sites to elucidate the interplay between climate influences and human activities on hydrological behavior. The investigation revolved around change point detection, examining average, maximum stream flow, and the number of days with zero discharge, and correlating these findings with climate patterns. The analysis of Maximum Palmer Drought Severity Index (PDSI) trends revealed a post-1990 decrease, suggesting an increase in extreme drought conditions associated with a warming climate. This aligns with the observed reduction in maximum stream discharge, evident in both summer and winter months.

The comprehensive analysis of the maximum stream flow patterns and the frequency of days with zero discharge shed light on the evolving dynamics of water availability in the studied streams. The post-1990 period exhibited a trend of decreasing maximum stream discharge, which can be attributed to the intricate relationship between urbanization-induced alterations in hydrology and flood control strategies. Concurrently, the number of days with zero discharge demonstrated a nuanced interplay between evolving climate conditions, urbanization, and forest fire activity.

Principal Component Analysis (PCA) elucidated two significant modes, explaining a substantial portion of variance in streamflow patterns. The primary mode exhibited a stronger connection with drought severity in winter, signifying its effectiveness in capturing climate-

related influences. Conversely, the secondary mode, more prominent during summer, was associated with external factors such as human-driven activities, including leaky infrastructure pipelines and runoff from urban areas.

In response to the central question of whether capturing urban runoff is a reliable source, the findings of this study suggest that the reliability of urban runoff as a water source for Southern California faces notable challenges. The region's streams are experiencing significant changes, characterized by declining flows, increased zero discharge days, and shifting patterns influenced by various factors. While urban runoff remains a valuable and sustainable water resource, its reliability may be influenced by evolving hydrological dynamics.

To ensure the sustainability of urban runoff as a water source, comprehensive water resource management strategies are imperative. These strategies must account for the intricate and evolving dynamics of Southern California's water systems, incorporating climate resilience, sustainable land use practices, and adaptive management approaches. Further research, collaboration, and informed policy decisions are essential to address the challenges posed by these evolving streamflow patterns and secure a sustainable water future for Southern California.

This study serves as a foundational resource, offering valuable insights for future research endeavors and policy initiatives related to water resource management in the region. It is imperative that stakeholders work together to develop and implement effective strategies to safeguard water security in Southern California while recognizing the complexities of its hydrological systems.

Chapter 3

Mechanisms of Pathogen Fate and Transport in a Pilot-Scale Stormwater Bioretention System following Exposure to Sewage-Contaminated Runoff

3.1 Introduction

Conventional stormwater drainage systems are designed to quickly move stormwater runoff away from urban areas during rain events. While these systems significantly reduce the risk of urban flooding, especially for small and medium-sized storms [92], they also cause a host of downstream ecosystem and water quality problems [34, 104, 105]. To address these problems, conventional drainage systems are increasingly being augmented with green

stormwater infrastructure (GSI), which aims to reduce the volume of stormwater runoff discharged to ambient waters by retaining the runoff as close as possible to where the rain falls [71].

Bioretention Systems (also known as raingardens, biofilters, and bioretention filters) are a popular form of GSI. These systems are engineered vadose zones, in which stormwater is directed into a ponding zone, and from there flows vertically by gravity and capillary forces through transiently saturated engineered soil media. The soil media is planted with vegetation to promote nutrient uptake and nutrient cycling, and to provide aesthetic co-benefits [106, 107]. As stormwater passes through the engineered media, a variety of pollutants (e.g., phosphorous, heavy metals, and pathogens) are removed by physicochemical filtration, adsorption, ion exchange, microbial processing and other physical and ecological processes [19, 55, 108, 109]. The treated storm water then passes through transition and drainage layers (made of sand and gravel, respectively) and exits by one of two routes, depending on the system's design. If the bioretention system is unlined, the treated water drains into the underlying soil and shallow groundwater [110]. If the bioretention system is lined, the treated water drains through an "under drain" to a conventional stormwater drainage network (e.g., a municipal separate storm sewer system (MS4)) or is captured for irrigation or other non-potable purposes [34, 54, 66, 71, 111, 112]. If the drain is elevated above the bottom of the system, a more-or-less permanently saturated zone, or "submerged zone", is created. Submerged zones have been shown to facilitate nitrogen removal by denitrification [113, 114] and the removal of fecal indicator bacteria, such as enterococci bacteria and *Escherichia coli* [55, 113], which are frequently monitored in surface waters as a potential indicator of human waste [115, 116].

The possibility that bioretention systems can be designed to remove human pathogens from urban runoff is of particular interest, given that (i) dry and wet weather runoff from urban areas is a well documented source of human pathogenic viruses [117–119],

bacteria [116, 120] and protozoa [121, 122]; and (ii) recreating in urban runoff-contaminated fresh and coastal waters is associated with an increased risk of contracting various recreational waterborne illnesses [117, 123]. Human pathogens are typically introduced to storm drain systems in association with human and animal fecal waste, for example from combined sewer overflows [124, 125], illicit sewer connections [126, 127] and failing septic systems [128, 129]. Previous studies have measured the removal of viruses, bacteria and protozoa in both laboratory and field-scale analogs of bioretention systems. Generally speaking, these studies report highly variable treatment performance, depending on system design (e.g., whether or not the bioinfiltration system has submerged zone [130, 131], the specific microbe being studied [132], soil media [133, 134], vegetation type [135], flow rates and flow variability, antecedent conditions, rainfall patterns (dry/wet cycle), and temperature [136–140].

The aforementioned variability in the removal of human pathogens and indicator microorganisms raises several questions: (1) What are the underlying mechanisms responsible for the high degree of variability in pathogen and indicator organism removal in bioretention systems? (2) Are the dominant removal mechanisms similar across all microbial contaminants, or are they microbe-specific? and (3) What are the microbe-specific rates of key non-conservative processes responsible for pathogen removal or amplification in these systems, such as filtration, die-off, and growth? Answers to these questions would not only clarify the mechanisms controlling pathogen fate and transport through GSI, but might also open the door to new bioretention system designs that enhance pathogen removal and thereby reduce the human health risk associated with stormwater pollution.

In this study we hypothesized that much of the previously noted variation in treatment performance can be explained by a few fundamental fate and transport processes, microbe-specific properties, antecedent conditions, and the extreme variability in flow routinely experienced by bioretention systems during, and in the intervals between, storm events. To test this hypothesis, the performance of 12 different formulations of a parsimonious (analytical)

pathogen fate and transport model were evaluated using previously published measurements of microbial removal in a pilot-scale bioretention system operated under realistic storm flow conditions [132]. The pilot-scale study consisted of seven simulated storm events with varying antecedent dry periods conducted over the course of one week in Southern California, USA, including two conditioning storms followed by a sewage- and bromide-spiked storm, followed by four sewage- and bromide-free "flushing" storms. During each of these storms the breakthrough concentration of six microorganisms was measured using culture-based and molecular approaches, including fecal indicator virus (coliphage), fecal indicator bacteria (enterococci bacteria, *Echerichia coli*, and Entero1a), human-associated fecal source marker (HF183), and an antibiotic resistant bacterial pathogen responsible for 300,000 hospitalizations and 10,000 deaths in the U.S. annually (methicillin-resistant *Staphylococcus aureus*, MRSA) [141, 142]. While most MRSA infections are hospital acquired (i.e., develop while patients are hospitalized for other conditions), up to one-third are acquired outside of hospital settings [143] and stormwater runoff, beach sand and recreational waters are known enviromental reservoirs of these organisms [144–146].

In this chapter we derive the fundamental equations that will be used for analyzing the previously pilot scale results described above. In particular, we show that by flow-weighting breakthrough curves, conventional analytical solutions to the advection-dispersion equation (e.g., [147]) can be used to characterize both conservative and, potentially, non-conservative processing responsible for microbial breakthrough patterns in bioinfiltration systems operated under realistic storm-flow conditions. The concept of flow-weighting breakthrough curves in unsteady hydrologic systems has been previously described in the literature [148, 149], but not to our knowledge in the context of GSI and certainly not for modeling the removal of microbial pollution in bioretention systems.

3.2 Theoretical Framework

In this section we derive formulae for the interstitial fluid concentration $C(z,t)$ and surface-attached concentration $C_s(z,t)$ of a microbial contaminant (units of microbial count per interstitial fluid volume and per dry weight of soil, respectively) at any depth z and time t in the soil media. Below we outline key assumptions and processes, governing equations, and analytical solutions.

3.2.1 Key Assumptions and Processes

The modeling framework is premised on the following six assumptions.

Assumption 1: mass transport through the soil media occurs primarily in the vertical or $z-$direction, where the variable z (units of meters) represents depth into the media;

Assumption 2: the vertical seepage velocity, $v_z(t)$ (units of meters per hour), varies with time in accordance with the time-varying inflow of stormwater from the ponding zone, but does not vary with depth in the soil media; i.e., external flow variability exerts a stronger influence on microbial transport through the soil media than does internal flow variability [150].

Assumption 3: the rate of longitudinal mixing by mechanical dispersion in the soil media can be approximated from the product of a constant dispersivity α_D (units of meters) and the time-varying vertical seepage velocity, $D(t) = \alpha_D v_z(t)$ (units of meters squared per second) [151].

Assumption 4: microorganisms in the interstitial fluids and attached to the soil media may undergo first-order decay or growth with rate constants k and μ, respectively (both units of inverse hour).

Assumption 5: microorganisms can attach to the surface of the soil media by filtration. Furthermore, soil-attached microorganisms can be transferred into the interstitial fluid by re-entrainment [152]. Here, the rates of filtration and re-entrainment are assumed to be first-order in the free and attached microorganism concentrations $C(z,t)$ and $C_s(z,t)$, respectively, and proportional to the local seepage velocity, $v_z(t)$, consistent with the role that hydrodynamics plays in colloid-collector interactions (refs). The constants of proportionality are the "filtration constant" (λ_f, units of inverse meter) and "re-entrainment constant" (λ_s, units of inverse meter).

Assumption 6: microorganisms may enter the bioinfiltration system with runoff during one or more storms, or may have originated from growth on the soil media itself, for example in association with biofilms [153, 154].

3.2.2 Governing Mass Conservation Equations

Given the above assumptions, the following two mass balance equations can be written for the accumulation of free and attached microorganisms in a differential slice of soil media located a depth z below the ponding zone:

$$\frac{\partial C}{\partial t} = -v_z(t)\frac{\partial C}{\partial z} + v_z(t)\alpha_D\frac{\partial^2 C}{\partial z^2} - \lambda_f v_z(t)C(z,t) + \frac{\rho_b\lambda_s}{\theta}v_z(t)C_s(z,t) + (\mu - k)C(z,t) \tag{3.1a}$$

$$\frac{\partial C_s}{\partial t} = \frac{\theta\lambda_f}{\rho_b}v_z(t)C(z,t) - \lambda_s v_z(t)C_s(z,t) + (\mu - k)C_s(z,t) \tag{3.1b}$$

Equation (3.1a) relates the accumulation of free microorganisms in the interstitial pore fluids (left hand side) to the divergence of the vertical advective and dispersive fluxes (first and second terms on the right hand side), the transfer of microorganisms to and from the soil media by filtration and re-entrainment (third and fourth terms), and first-order growth or

decay in the interstitial pore fluids (last term). The variables ρ_b (units of g cm^{-3}) and θ (unitless) represent the bulk density and porosity, respectively, of the soil media.

Equation (3.1b) relates the accumulation of soil-attached microorganisms (left hand side) to their addition and removal by filtration and re-entrainment (first and second terms on the right hand side), and first-order growth or decay on the surface of the soil media (last term). For simplicity, we have assumed that rate constants for first-order growth or decay are the same for free and attached microorganisms.

3.2.3 Simplifying the Governing Equations

We solved the governing equations above to yield explicit expressions for the concentration of free and attached microorganisms $C(z,t)$ and $C_s(z,t)$. This was accomplished by: (1) eliminating the growth or decay terms from equations (3.1a) and (3.1b) by application of an integrating factor; (2) eliminating the time-dependent seepage velocity, $v_z(t)$, from equations (3.1a) and (3.1b) by introducing flow-weighted time; (3) solving the simplified form of equation (3.1b) to yield an expression for the concentration of soil-attached microorganisms, $C_s(z,t)$; and finally (4) solving the simplified form of equation (3.1a) to yield an expression for the concentration of free microorganisms $C(z,t)$. These steps are described in turn.

Applying the Integrating Factor

The first-order growth or decay terms in equations (3.1a) and (3.1b) were eliminated by applying the integrating factor: $\bar{C}(z,t) = C(z,t)e^{-(\mu-k)(t-t_0)}H(t-t_0)$ and $\bar{C_S}(z,t) = C_S(z,t)e^{-(\mu-k)(t-t_0)}H(t-t_0)$, where t_0 is an initial condition dependent time delay (see below) and $H(t)$ is the unit step or Heaviside function (equal to zero for $t < 0$ and unity for $t \geq 0$).

Flow-Weighting Time

The time-varying seepage velocity variable, $v_z(t)$, appearing in equations (3.1a) and (3.1b) can be replaced with a constant velocity, $u = \alpha_V K_s$, by transferring the equations from calendar time t to flow-weighted time [148]:

$$\tau(t) = \frac{1}{K_s} \int_0^t q(x)\, dx \tag{3.2}$$

Here, K_s (units meters per hour) is the saturated hydraulic conductivity of the soil media and α_V is a constant of proportionality between seepage velocity and the Darcy flux $q(t)$ (units of meters per hour): $v_z(t) = \alpha_V q(t)$. The constant α_V is nominally equal to the inverse of the soil media's porosity, $\alpha_V \approx 1/\theta$ [155]. As the name implies, flow-weighted time progresses more quickly during storm events (when the Darcy flux $q(t)$ is large in magnitude) and more slowly in the interval between storms (when the Darcy flux is small in magnitude). While the seepage velocity can be arbitrarily small in magnitude, the transformation from calendar to flow-weighted time requires that it can never be exactly equal to zero; i.e., $v_z(t) = \alpha_V q(t) > 0$.

3.2.4 Solution for Soil-attached Microorganisms

After applying the integrating factor and flow-weighting time, the governing equation for soil-attached microorganisms (equation (3.1b)) becomes: $\frac{\partial \bar{C}_S}{\partial \tau} = \frac{\theta k_f}{\rho_b} \bar{C}(z,\tau) - k_s \bar{C}_S(z,\tau)$, where $k_f = u\lambda_f$ and $k_s = u\lambda_s$ (both units of inverse hours) are filtration and re-entrainment rate constants, respectively. For an initial condition, we assume that a population of microorganisms is attached to the soil media at depth $z = z_0$ at flow-weighted time $\tau = 0$: $\bar{C}_s(z,0) = M_s'' \delta(z - z_0)/\rho_b$, where M_s'' is the number of soil-attached microorganisms per unit cross-sectional area and $\delta(z)$ is the Dirac Delta function (units of inverse meters). Given this

initial condition, the governing equation for surface-attached microorganisms can be readily solved in flow-weighted time, where the function $f(\tau) = k_s e^{-k_s \tau}$ is referred to as a "memory function" [156] and the symbol "$*$" denotes a convolution integral: $f * g = \int_0^t f(t-x)g(x)dx$:

$$\bar{C}_s(z,\tau) = \frac{\theta k_f}{k_s \rho_b} \bar{C}(z,\tau) * f(\tau) + \frac{M_s'' \delta(z - z_0)}{\rho_b k_s} f(\tau) \tag{3.3}$$

The appearance of a convolution integral on the right hand side of equation (3.3) implies that the attached concentration of microorganisms, $\bar{C}_s(z,\tau)$, depends on the entire concentration history of free microorganisms, $\bar{C}(z,\tau)$, "filtered" through the memory function, $f(\tau)$. The memory function, in turn, is a probability density function (PDF) of wait times for attached microorganisms to become re-entrained. Typically, the exponential form of the memory function is associated with a linear (e.g., as opposed to fractal [156]) exchange between free and attached states . But in our case, the dependent variable of the memory function is flow-weighted time, not calendar time. Because flow-weighted time speeds up during storm events and slows down during antecedent dry periods, our memory function will likely be heavy-tailed in calendar time. That is, some soil-attached microorganisms will wait a very long time before becoming re-entrained, reflecting both the exponential PDF for re-entrainment in flow-weighted time and the fact that flow-weighted time progresses slowly between storms.

3.2.5 Two Solutions for Free Microorganisms

A simplified form of the governing equation for free microorganisms (equation (3.1a)) can be obtained by applying the integrating factor (Section 3.3.1), moving the equation to flow-weighted time (Section 3.3.2), and substituting equation (3.3):

$$\frac{\partial \bar{C}}{\partial \tau} = -u \frac{\partial \bar{C}}{\partial z} + u \alpha_D \frac{\partial^2 \bar{C}}{\partial z^2} - k_f \bar{C}(z,\tau) + k_f \bar{C}(z,\tau) * f(\tau) + \frac{M_s'' \delta(z - z_0)}{\theta} f(\tau) \tag{3.4}$$

In this section we derive from equation (3.4) two fundamental solutions for the concentration of free microorganisms based on two different "origin stories" for microorganisms in the soil media. For Solution I, we assume that all microorganisms were initially attached to the soil media (e.g., in association with biofilms), and then re-entrained into the interstitial fluids during one or more storm events. For Solution II, we assume that all microorganisms were initially transported into the soil media with runoff during storm events. The superposition of these two fundamental solutions yields a solution that incorporates the potential contributions of both initially attached microorganisms (Solution I) and stormwater-associated microorganisms (Solution II) to the concentration of microorganisms within, and discharged from, the soil media. Solutions I and II are distinguished by the set of initial and boundary conditions applied to equation (3.4), as outlined next.

Solution I: Microorganisms Initially Soil-Attached

Given the origin story for Solution I, the initial concentration of surface-attached microorganisms is non-zero (i.e., $M_s'' > 0$) at some depth $z = z_0$ in the soil media, the initial concentration of free microorganisms in the interstitial fluids of the soil media is zero, and all stormwater entering the soil media is microbe free. The initial condition for free microorganisms (equation (3.4)) is therefore, $\bar{C}^{\mathrm{I}}(z, 0) = 0$, where the superscript "I" denotes Solution I. Because the soil column is represented mathematically as an infinite domain (more on this later), the two boundary conditions follow from conservation of mass: $\bar{C}^{\mathrm{I}}(z \to \pm\infty, \tau) = 0$. Given these initial and boundary conditions, Solution I takes on the following form, where the variable $t(\tau)$ represents the inverse function of flow-weighted time, $t(\tau) = \tau^{-1}(t)$, and

$I_0[\cdot]$ is the Bessel Function of the first kind (derivation in Supplemental Information):

$$C^{\mathrm{I}}(z,\tau,z_0) = \frac{k_s M_s'' e^{\frac{z-z_0}{2\alpha_D} - k_s\tau - (k-\mu)t(\tau)}}{2\theta\sqrt{\pi}} \times \int_0^\tau I_0\Big[2\sqrt{k_f k_s \xi(\tau-\xi)}\Big] e^{-(k_f - k_s + \frac{u}{4\alpha_D})\xi} \Big(\frac{e^{-\frac{(z-z0)^2}{4\alpha_D u\xi}}}{\sqrt{\alpha_D u\xi}}\Big) d\xi \quad (3.5)$$

For this solution, the time delay in the integrating factor is equal to zero, $t_0 = 0$, because all microorganisms are initially present in the soil media at time $t = \tau = 0$ (see Section 3.3.1).

Before this solution can be implemented, we must first specify an initial depth profile for the soil-attached microorganisms. For a uniform initial depth profile (roughly consistent with the soil core measurements in our pilot study [132]), we begin by writing the differential mass released at depth $z = z_0 \in [0, d]$ as follows: $\Delta M_s'' = \rho_b C_{si} \Delta z_0$, where C_{si} is the initial soil-attached concentration (units of microorganism count per dry soil weight), d is the thickness of the soil media (units of meters), and Δz_0 is a differential source depth. Substituting this differential source expression into equation (3.5) and integrating over all source depths yields the following expression for Solution I:

$$C^{\mathrm{I}}(z,\tau) = \frac{k_s \rho_b C_{si} e^{-k_s\tau - (k-\mu)t(\tau)}}{2\theta} \times \int_0^\tau I_0\Big[2\sqrt{k_f k_s \xi(\tau-\xi)}\Big] e^{-(k_f - k_s)\xi} \Big(\mathrm{erf}\Big[\frac{d - z + u\xi}{2\sqrt{\alpha_D u\xi}}\Big] + \mathrm{erf}\Big[\frac{z - u\xi}{2\sqrt{\alpha_D u\xi}}\Big]\Big) d\xi \quad (3.6)$$

Solution II: Microorganisms Initially from Stormwater Inflow

For Solution II, the initial concentration of surface-attached microorganisms is zero (i.e., $M_s'' = 0$) and all microorganisms are transported into the soil media with runoff during one or more storms. If a pulse of microbial pollution enters the soil column at $\tau = 0$, the initial concentration of free microorganisms becomes: $\bar{C}^{\mathrm{II}}(z, \tau = 0) = \frac{M_R'' \delta(z)}{\theta}$, where the superscript II indicates Solution II, M_R'' is the source strength of the pollution pulse (in units

of microorganism count per unit cross-sectional area), and $\delta(z)$ is the Dirac Delta function (units of inverse meters). To allow for the superposition of Solutions I and II, we adopt the same two boundary conditions used for Solution I: $\bar{C}^{\mathrm{II}}(z \to \pm\infty, \tau) = 0$. Given these initial and boundary conditions, and after shifting the flow-weighted entrance time of the pulse by $\tau = \tau_i$, Solution II takes the following form (derivation in Supplemental Information):

$$C^{\mathrm{II}}(z,\tau,\tau_i) = e^{-(k-\mu)(t(\tau)-t(\tau_i))}\left(e^{-k_s(\tau-\tau_i)}\int_0^{\tau-\tau_i} e^{-(k_f-k_s)\xi}\sqrt{\frac{k_f k_s \xi}{\tau-\tau_i-\xi}}\right.$$
$$\left.\times\, I_1\left[2\sqrt{k_f k_s \xi(\tau-\tau_i-\xi)}\right] C^{\mathrm{II}}_{\mathrm{cons}}(z,\xi)d\xi + e^{-k_f(\tau-\tau_i)} C^{\mathrm{II}}_{\mathrm{cons}}(z,\tau-\tau_i)\right), \quad \tau > \tau_i \quad (3.7)$$

The function $\bar{C}^{\mathrm{II}}_{\mathrm{cons}}(z,\tau)$ is the corresponding solution for a conservative solute that does not undergo filtration, re-entrainment, or first-order growth or decay:

$$C^{\mathrm{II}}_{\mathrm{cons}}(z,\tau) = \frac{M''_R e^{-\frac{(z-u\tau)^2}{4\alpha_D u\tau}}}{2\theta\sqrt{\pi\alpha_D u\tau}} \quad (3.8)$$

These last two equations provide a precise relationship between the predicted breakthrough concentration of microorganisms entering the soil media with stormwater at $\tau = \tau_i$ (equation (3.7)) and the breakthrough concentration of a simultaneously applied pulse of conservative tracer, such as bromide in the experiments described later (equation (3.8)). Mathematically, the conservative solution serves as a Green's function for the more general solution [156–158].

Equations (3.7) and (3.8) are premised on the idea that a specific number of microorganisms per unit area, M''_R, enter the soil media from the ponding zone at a single point in flow-weighted time, $\tau = \tau_i$. In the experiments described later, microbial contaminants enter the soil media over the course of a single (sewage-contaminated) storm event, while subsequent (non-sewage-contaminated) storms have a much lower microbial concentration. Tailoring Solution II to this sewer overflow scenario requires first expressing the source strength of microorganisms entering the soil media with stormwater in differential form:

$\Delta M''_R = u\theta C_{SW}(\tau_i)\Delta\tau_i$, where the variables $C_{SW}(\tau_i)$ (units of microorganism count per volume of stormwater) and $\Delta\tau_i$ (units of flow-weighted time) represent the microbial concentration in stormwater entering the soil media at flow-weighted time $\tau = \tau_i$ and a differential increment of flow-weighted time, respectively. We then substitute this differential source strength into equation (3.8) and integrate over a step change in inflow concentration from $C_{SW}(\tau_i) = C_{\mathrm{SO}}$ for $0 \leq \tau \leq \tau_{\mathrm{SO}}$ to $C_{SW}(\tau_i) = C_f$ for $\tau > \tau_{\mathrm{SO}}$. For a conservative tracer, the result is as follows, where the variable τ_{SO} represents the duration of the sewage-contaminated storm in flow-weighted time, and the stormwater inflow concentrations, C_{SO} and C_f, are fixed constants:

$$C^{\mathrm{II}}_{\mathrm{cons}}(z,\tau) = \begin{cases} C_{\mathrm{SO}} A(z,\tau), \ 0 < \tau \leq \tau_{\mathrm{SO}} \\ C_{\mathrm{SO}} A(z,\tau) - (C_{\mathrm{SO}} - C_f) A(z, \tau - \tau_{\mathrm{SO}}), \ \tau > \tau_{\mathrm{SO}} \end{cases} \tag{3.9a}$$

$$A(z,\tau) = \frac{1}{2}\mathrm{erfc}\Big[\frac{z - \tau u}{2\sqrt{\alpha_D \tau u}}\Big] - \frac{e^{\frac{z}{\alpha_D}}}{2}\mathrm{erfc}\Big[\frac{z + \tau u}{2\sqrt{\alpha_D \tau u}}\Big] \tag{3.9b}$$

The corresponding non-conservative solution is represented as a superposition over N discrete pollution pulses, each of which has duration, $\Delta\tau$:

$$C^{\mathrm{II}}(z,\tau) = \frac{u\Delta\tau}{2\sqrt{\pi}} \times \begin{cases} C_{\mathrm{SO}} \sum_{i=0}^{N} B(z,\tau,\tau_i), \ 0 < \tau \leq \tau_{\mathrm{SO}} \\ C_{\mathrm{SO}} \sum_{i=0}^{N_{\mathrm{SO}}} B(z,\tau,\tau_i) + \\ \quad C_f \sum_{i=N_{\mathrm{SO}}+1}^{N} B(z,\tau,\tau_i), \ \tau > \tau_{\mathrm{SO}} \end{cases} \tag{3.10a}$$

$$\tau_i = i\Delta\tau \tag{3.10b}$$

$$N = \tau/\Delta\tau \tag{3.10c}$$

$$N_{\mathrm{SO}} = \tau_{\mathrm{SO}}/\Delta\tau \tag{3.10d}$$

The function $B(z, \tau, \tau_i)$ follows from equations (3.7) and (3.8):

$$B(z,\tau,\tau_i) = e^{-(k-\mu)(t(\tau)-t(\tau_i))}e^{-k_s(\tau-\tau_i)} \times \int_0^{\tau-\tau_i} e^{(k_s-k_f)\xi}\sqrt{\frac{k_f k_s \xi}{\tau-\tau_i-\xi}}I_1\Big[2\sqrt{k_f k_s \xi(\tau-\tau_i-\xi)}\Big]\frac{e^{-\frac{(z-u\xi)^2}{4\alpha_D u\xi}}}{\sqrt{\alpha_D u\xi}}d\xi \quad (3.11)$$

3.3 Experimental Design and Parameter Inference

3.3.1 Pilot-scale Bioretention Challenge Experiment

The pilot scale bioretention challenge experiment, which was designed to mimic a sewage-contaminated runoff event as might occur after a sewer overflow, was conducted over the course of one week in May 2019 at a low impact development (LID) demonstration facility in Orange County, California. In brief, seven individual storm events were simulated by discharging $\approx$ 1400 L of water over 70 to 80 minutes to the ponding zone of a 2.2 m^3 pilot-scale bioretention cell. The soil media was $L = 0.6$m deep, consisted of sand (65%), sandy loam (20%) and compost (15%), and was planted with the native sedge, *Carex spissa*. Each simulated storm event consisted of either stormwater alone (Storms S1, S2, and S4-S7) or a 50:50 mixture of stormwater and raw sewage spiked with potassium bromide at a final concentration of 124 mg Br^-/L (Storm S3). The stormwater consisted of minimally treated parking lot runoff collected the previous winter from the LID demonstration facility and stored in an underground cistern until use. In this case, minimal treatment entailed passing the runoff through an onsite hydrodynamic separator or a modular treatment wetland. Raw sewage was collected from the Orange County Sanitation District the day of Storm S3.

Several articles have already described various aspects of the experiment, including system hydrology and bromide breakthrough patterns [70], molecular analysis of bacterial commu-

nities entering, resident in, and discharged from the soil media [132], the response of the system to high nitrogen loading during and following Storm S3 [159], and the highly variable removal of human pathogens, antibiotic resistance genes, conventional fecal indicators and human-associated fecal source markers during and following Storm S3 [160]. The last study concluded that "further research is needed to determine the mechanisms underlying the substantial variation in treatment credit across the different microbial analytes." The current paper addresses this need by applying the models described in Section 3 to this unique dataset, as detailed next.

3.3.2 Rationale for the Inclusion/Exclusion of Microorganisms

During the pilot scale challenge experiment described above, Rugh et al (2022) [132] collected breakthrough data for 14 different microorganisms and antibiotic resistance genes. However, relatively complete breakthrough data (defined here as including breakthrough measurements during the sewage-contaminated storm (Storm S3) and at least two of the four sewage-free flushing storms (Storms S4-S7)) were only available for the six microorganisms included in our study: a fecal indicator virus (coliphage), three fecal indicator bacteria (enterococci bacteria (ENT), *Echerichia coli* (EC), and a genetic marker for enterococci species (Entero1a)), a human-associated fecal source marker (HF183), and the pathogen MRSA. While the breakthrough pattern of fecal coliform (FC) was also measured by Rugh et al, these data were not included in our study because: (1) EC is a subset of the organisms encompassed by F; (2) the breakthrough patterns of FC and EC were very similar (see Figure 1 in Rugh et al.[132]); and (3) compared to FC, EC is of greater regulatory and human health significance.

3.3.3 Calculating Flow-weighted Time

The time stamps of measured breakthrough data were transferred into flow weighted time by substituting into equation (3.2) a 1 Hz synthetic timeseries of the Darcy flux of water exiting the soil media, $q(t)$, over the course of the pilot scale study. The latter was generated by solving the one-dimensional Richards Equation for flow in variably saturated porous media (Hydrus 1D [161, 162]), driving the model with high frequency (10 Hz) experimental measurements of inflow to the ponding zone of the bioretention cell over storms S1 through S7 (see Parker et al. for details [70]). For the reference velocity ((K_s in equation (3.2)) we adopted the measured saturated hydraulic conductivity of the soil media, $K_s = 0.174$ m h^{-1}. Numerical integration of equation (3.2) yielded a 1 Hz timeseries of flow-weighted time expressed as a monotonically increasing function of calendar time, t: $\tau(t)$.

3.3.4 Model Parameter Inference

As mentioned earlier, the focus of this chapter is on deriving the fundamental transport equations, and inferring conservative transport parameters based on the bromide breakthrough curve measured during Storm S3. The application of these models to the microbial breakthrough data will be presented in a subsequent paper. Bromide breakthrough concentration measurements (collected at a frequency of approximately 1/10 min^{-1}, see Parker et al. for details [70]) were transferred to flow-weighted time (see Section 4.3) and then fit to the conservative solution (equations (3.9a) and (3.9b)) with $C_{SO} = 124$ mg L^{-1} and $C_f = 0$ mg L^{-1} by minimizing the root-mean-square error (RMSE) in nonlinear least squares regression between log-transformed bromide breakthrough concentrations and model predictions (Mathematica, Wolfram, V12.0). The result was numerical estimates and associated errors for the transport parameters α_D and α_V, along with the duration of the sewage-contaminated storm in flow-weighted time, $\tau_{\mathrm{CSO}} = \tau(t_{\mathrm{CSO}})$.

3.3.5 Twelve Model Formulations for Microbial Breakthrough

In total, 12 different model formulations were evaluated for their ability to represent measured microbial breakthrough during the pilot scale field experiment. These 12 solutions included nine different variations of Solutions I and II along with three hybrid models constructed from the superposition of Solutions I and II. The models are distinguished based on the presumed source of microorganisms (initially soil-attached (Solution I) or from stormwater inflow during one or more storms (Solution II)) and which physical processes are "turned on" or "turned off" (filtration (F), re-entrainment (R), and first-order growth or decay (G/D)). Each model is designated by the set of processes included (in parentheses) and the microbial source (as a superscript). For example, the model $(F+R)^{I}$ accounts for filtration and re-entrainment, and assumes that all microorganisms in outflow were initially soil-attached. All Solution I models were required to include re-entrainment, because without it the soil-attached microorganisms would remain in that state indefinitely. Furthermore, we only evaluated hybrid models for which the same set of physical processes were represented in both Solutions I and II. For example, the hybrid model $(F+R)^{I,II}$ would be allowed, because in this case filtration and re-entrainment occur in both Solutions I and II. On the other hand, the model $(F+R)^{I}+F^{II}$ would not be allowed, because it corresponds to the unlikely scenario where microorganisms that were initially soil-attached can be filtered and re-entrained, whereas microorganisms that originated in stormwater can only be filtered (i.e., they cannot be re-entrained).

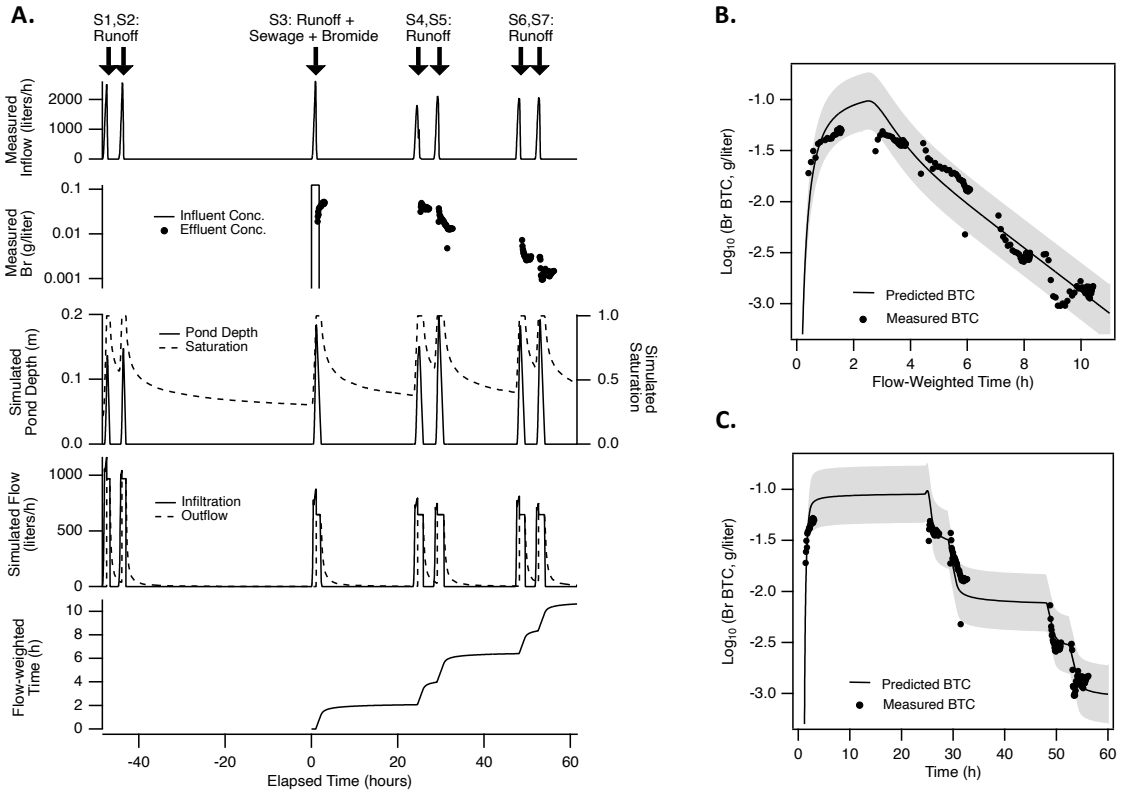

Figure 3.1: Modeling bromide breakthrough in a pilot-scale bioretention cell in flow-weighted time. **A.** Hydrological and bromide measurements plotted in real time t, where $t = 0$ is centered on Storm S3. Results plotted here include measured inflow to the ponding zone during each of the seven simulated storm events (top panel), a comparison of bromide concentration in the inflow during Storm S3 and outflow from the soil media over the course of Storms S3-S7 (second panel), Hydrus 1D simulations of ponding zone water depth and average soil media saturation during, and in the intervals between, the seven storms (third panel), comparison of simulated infiltration into, and outflow from, the soil media over the seven storms (fourth panel), and flow-weighted time calculated from the simulated outflow measurements using equation (F1a) (fifth panel). **B.** Comparison of the measured and model-predicted bromide concentration in water exiting the soil media, or bromide breakthrough curve (BTC), in flow-weighted time. The grey bands represent 95% prediction intervals for the model. **C.** The same results presented in **B** transformed back into real time.

3.4 Results and Discussion

3.4.1 System Hydrology During the Seven Simulated Storms

The simulated storms were designed to mimic the runoff generated from an 82 m^2 impervious catchment (corresponding to an area ratio of 4.5% for this pilot-scale system) during an 85th percentile storm in Orange County, California, which corresponds to 2.1 cm of stormwater depth over a 24-hour period. The resulting seven storm hydrographs (Storms S1-S7) were quite flashy, delivering $\approx$ 1400 L of water to the ponding zone over 15 to 30 minutes (top panel, Figure 3.1A). Hydrus 1D simulations of the bioretention cell's water balance, forced by measured inflow to the ponding zone, were generally consistent with field observations (third and fourth panels in Figure 3.1A). At the beginning of each storm, water accumulated in the ponding zone to a depth of 15-20 cm, before fully infiltrating to the soil media over the next 15 to 20 minutes. A mixture of new and older water previously stored in the soil media then slowly drained from the bioretention cell over the next several hours. Over the seven experimental storms, we estimated that evapotranspiration constituted $< 0.3\%$ of the bioretention cell's overall water balance [69]. Flow-weighted time, calculated from the Hydrus 1D outflow simulations (equation (3.2)), varies non-linearly with time, increasing rapidly during storm events and plateauing in the interval between storms (bottom panel, Figure 3.1A). Each storm event added approximately 2 hours of flow-weighted time, consistent with the total volume of water added during each storm ($V_S \approx 1.4$ m^3), our choice of the reference velocity ($v_0 = K_s = 0.174$ m h^{-1}), and the surface area of the pilot scale bioretention cell ($A_b = 3.7$ m^2): $\frac{V_S}{A_b v_0} \approx 2.1$ h.

3.4.2 Measured and Model-predicted Bromide BTC Patterns

The sewage-contaminated storm (Storm S3) was spiked with bromide as a conservative tracer. Some of this bromide was released in the outflow generated by Storm S3, but bromide concentrations remained elevated in the outflow from all four subsequent sewage- and bromide-free flushing storms (Storms S4-S7) (second panel, Figure 3.1A). Remarkably, these bromide breakthrough concentration (BTC) data collapse onto a single continuous curve when plotted against flow-weighted time (Figure 3.1B). The optimized analytical model (equations (3.9a)-(3.9b) with $C_0 = 0.124$ mg L^{-1} and $C_f = 0$) closely reproduces the bromide BTC (coefficient of determination, $R^2 = 0.995$) in both flow-weighted (Figure 3.1B) and calendar (Figure 3.1C) time.

Model inferred values for the duration of the sewage pulse in flow-weighted time, the dispersivity, and the constant of proportionality between the interstitial velocity and Darcy flux are as follows: $\tau_{SO} = 2.3 \pm 0.07$ h, $\alpha_D = 0.23 \pm 0.01$ m, and $\alpha_V = 2.4 \pm 0.09$. The inferred value of τ_{SO} agrees closely with our observation above that each storm adds about 2 h of flow-weighted time (Section 5.1). The inferred value of α_D is on the high-end of dispersivities values expected for transport distances of ca. 1 m (Gelhar et al., 1992). During the field experiment we observed that water and solutes in the ponding zone could bypass the soil media by traveling down the sides of the bioretention cell's walls, in effect "short-circuiting" around the primary flow path through the soil media. Short-circuit along the walls of the bioretention cell may have contributed to the higher dispersive mixing observed here. Based on the porosity of our soil media, $\theta = 0.41$, the expected constant of proportionality between the seepage velocity and Darcy velocity is precisely equal to the value inferred from the bromide breakthrough data, $\alpha_V \approx 1/\theta = 2.4$.

3.5 Discussion

From these results, it appears that the general approach adopted here–of transferring breakthrough measurements into flow-weighted time, and then modeling the resulting breakthrough curves with conventional solutions to the advection-dispersion equation–provides a reasonable representation of solute transport and dispersion in bioretention systems operated under realistic stormflow conditions. These foundational results will be the starting point, in a subsequent publication, to evaluate microbial breakthrough patterns in the pilot-scale study.

Chapter 4

Mechanisms of Nitrogen Fate and Transport in a Pilot-Scale Stormwater Bioretention System following Exposure to Sewage-Contaminated Runoff

4.1 Introduction

According to a recent analysis of The Water Reuse Foundation International Stormwater Best Management Practice (BMP) database, Clary et al. (2020) [163] found that bioinfiltration systems are effective at removing total suspended solids (TSS) and particulate forms of heavy metals, phosphorous and nitrogen, although they are often net exporters of nitrate [159, 164, 165], a bioreactive form of nitrogen commonly associated with surface water

eutrophication and harmful algal blooms [166, 167]. Similarly, in the City of Portland (Oregon), bioinfiltration systems that had been operational for between 4 and 8 years effectively removed TSS, ammonium, total copper, total zinc, and dissolved zinc, but exported, on average, 2070 percent more nitrogen than entered in storm flows [168].

There are at least two possible explanations for why bioinfiltration systems might serve as a net exporter of nitrate. First, the engineered soil media is often amended with organic material to support plant growth, and provide an electron donor for microbially mediated reactions associated with denitrification. However, as will be detailed below, aerobic and anaerobic microbial respiration of organic soil amendments (so-called autochthonous organics) can liberate ammonium by ammonification. Furthermore, if sufficient oxygen is present in the pore fluids of the biofilter, the liberated ammonium can be microbially oxidized to nitrate by nitrification. Thus, microbial processing of autochthonous organics is one possible source of nitrate in these systems. Second, stormwater mobilizes particulate organic material (e.g., leaf litter on streets) into the ponding zone of bioinfiltration systems where it can be worked into the soil media over time. Such external sources of nitrogeneous organic material (so-called allochthonous organics) may also lead to the generation of nitrate by ammonification and nitrification within the biofilter [169, 170]

In this chapter, we hypothesize that the net export of nitrate from stormwater biofilters arises not only from the biogeochemical processes described above (i.e., in-situ microbial respiration of authochtonous and allochthonous organic matter) but also from the extreme hydrological variability that defines these systems, including the stochastic nature of storm events and the transiently unsaturated nature of the vadose zone. To test this hypothesis we develop and field test a transport modeling framework that combines transient transit time distribution (T-TTD) theory, originally developed by hillslope hydrologists to describe the unsteady transport of solutes in rainfall through catchments to streams [Kim et al., 2016; Hrachowitz et al., 2016], with a process-based N-cycling model previously applied to nitrate removal in the

hyporheic zone of stream [99] and coastal [171] sediments. We specifically set out to answer the following three questions: (1) how well does our TTD/N-cycle model represent measured ammonium and nitrate export from a biofilter under realistic field operating conditions? (2) which hydrological timescales (intra-storm, inter-storm, seasonal, or annual) most influence whether biofilters are a net sink or source of nitrate? and (3) over what timescales might dead zones in the biofilter (either naturally present or deliberately engineered into the biofilter's design) mitigate the influence of hydrological variability on nitrate export? The focus of this chapter will be on developing the fundamental equations, and their initial application to measured N-transport through a pilot scale bioretention system.

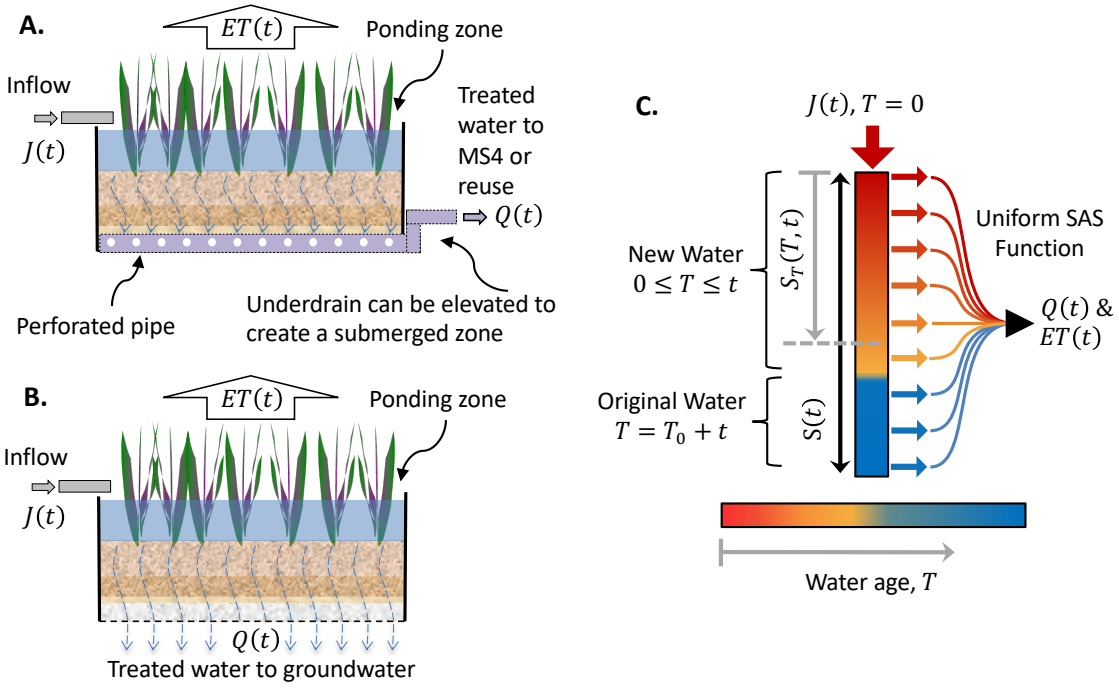

Figure 4.1: A graphical representation of a bioinfiltration system configured so that runoff travels through the soil media of the system and then is either (A) routed for use or discharge (e.g., to a MS4 system) or (B) allowed to infiltrate into underlying sediments. Panel (C) is a conceptual representation of the uniform StorAge Selection (SAS) function used to model solute transport through the bioinfiltration system (see text for details).

4.2 Field Experiments

4.2.1 Bioinfiltration System

Pilot scale challenge experiments were carried out in a bioretention cell located at the Orange County Public Works (OCPW) low impact development demonstration (LID) campus in the City of Orange, Orange County, California. The volume of the test cell was approximately 2 m^3 (dimensions 2.4 $\times$ 1.5 $\times$ 0.6 m deep). It was filled with a soil media consisting of sand (65 percent), sandy loam (20 percent), and compost (15 percent) (v/v basis) and planted with a European gray sedge, *Carex divulsa tumulicola* (opportunist ruderal weed species, such as the common dandelion, were also present at the time of the experiment). While the bioinfiltration system was open to the atmosphere, no measurable rainfall occurred during our field study. The test cell was retrofitted with an upstream 1,890 L inflow tank (Custom Roto-Molding, Inc., Caldwell, ID) which drained by gravity through a programmable control valve (Sigma Controls, Inc., Perkasie, PA) to the ponding zone. The weight of the inflow tank was monitored continuously at approximately 10 Hz (WinWedge, TAL Technologies Inc., Philadelphia, PA) with a calibrated industrial scale (PCE-SW 3000N Pallet Scale, PCE Americas Inc., Jupiter, FL). These weight measurements were low pass filtered, differentiated, and divided by the density of water to yield approximately 1 min^{-1} estimates for the volumetric discharge of water entering the test cell's ponding zone. Water exited the test cell through an underdrain, and then flowed by gravity to an underground sump that was open to the atmosphere. The depth, porosity, and maximum storage of the soil media were, respectively, d_b = 0.6m, θ_s = 0.41, and $S_{max} = d_b\theta_s$ = 0.246 m (estimated from six cores collected post-experiment with a 7.6 cm diameter carbon steel corer).

4.2.2 Simulated Storm Events

Using the field experimental set-up described above, a sequence of seven storms were simulated over a 5-day period in the summer of 2019 (June 1-5). The inlet control valve was programmed to replicate the 85th percentile storm in Santa Ana California, which at this site corresponds to 2.1 cm of storm water depth over a 24h-period, with a biofilter-to-catchment area ratio of 4.5 percent, typical for urban landscapes in Southern California [110]. With one exception, the source water for these simulated storms consisted of actual stormwater runoff that had been captured the previous winter from OCPW's LID campus and subsequently stored in an 80,000 gallon underground cistern (Storm Capture System, Oldcastle Infrastructure, Inc., Atlanta, GA). The exception was the third storm event, which consisted of a bromide-spiked 50:50 mixture of stormwater from the underground cistern and raw sewage from the local wastewater treatment plant (Orange County Sanitation District). Raw sewage was added to the third storm, to evaluate the removal of common storm water contaminants under a worst case scenario, as might occur during a sewer overflow event [171], including heavy metals, nutrients, and microbial pathogens. Previous publications have addressed breakthrough measurements of bromide [70], bacterial and viral indicators and pathogens [132, 160], antibiotic resistance genes [132, 172], and nitrogen species [173, 174]. In this study we focus on modeling the export of nitrate and ammonium from the biofilter.

4.2.3 Measurements of Nitrate and Ammonium

During the first two storms, influent samples were collected from the inflow tank, and effluent samples were collected from the biofilter underdrain with a peristaltic pump (flow rate 0.23 L per minute). During the last five storms, 13 influent samples were collected from the inflow tank and 116 samples were collected from a sump located at the end of a manifold through which the biofilter effluent drained. Effluent water from the biofilter was periodically

pumped (Model 98 Sump Pump, Zoeller Pump Company, Louisville, KY) from the sump into a continuously overflowing 5 L bucket, which was continuously sub-sampled (40 mL min $^{-1}$ by a peristaltic pump (BioLogic LP, Bio-Rad, Hercules, CA) and fractionated into 50 mL conical tubes (Falcon, Corning Life Sciences, Tewksbury, MA) every 5 minutes until biofilter outflow ceased. All samples were filtered through a 0.45-micron syringe filter (Model, manufacturer, City, State). Samples were refrigerated at 4C until analysis. All samples were analyzed for nitrate by ion chromatography (Dionex DX-120, Thermo Fisher Scientific, Waltham, MA) and ammonium by colorimetry (EPA method 350.1 [175]) using UV-visible spectroscopy (Dual Fluorometer, HORIBA scientific, Irvine, CA). The detection limit of both methods was 0.1mg/L. Method blanks and samples with known concentrations were used for quality control and to correct instrument drift.

4.3 Modeling Framework

4.3.1 Biofilter Hydrology

Transient unsaturated flow through the biofilter media was simulated with a previously calibrated bucket model developed specifically for the OCPW biofilter test cell [70] (for details, see Text S1 of the Supplemental Information). For the sequence of experimental storms described above, the model generated high frequency (1 min^{-1}) time series estimates for the hydrological variables required for the TTD theory described in the next section, including the infiltration rate of water into the biofilter from the ponding zone, $J(t)$ (units meters per hour), the volume of water present in the biofilter media (hereafter referred to as the biofilter's water storage), $S(t)$ (units of meters), and the discharge rate of water out the biofilter's underdrain, $Q(t)$ (units of meters per hour), where all volumes and flows have been divided by the area of the biofilter. The model was forced with measured inflow to the

ponding zone (see Section 2.2) and hourly estimates of potential evapotranspiration (cPET) using the Penmen-Monteith equation and local meteorological measurements. Gravitational discharge from the biofilter's underdrain was represented by a power-law relationship of storage [176] which allows for the specification of a minimum storage, S_{min}, below which gravitational drainage ceases. The latter parameter can be manipulated to represent different bottom boundary conditions: (1) if the drain is not raised then the minimum storage is set to, $S_{min} = 0$ (Figure 4.1B); (2) if the drain is raised the minimum storage is set equal to the height of the drain above the bottom of the biofilter (Figure 4.1A). Previous analysis of bromide transport through the OCPW biofilter indicated that, as a result of lateral exchange of water and solutes between the biofilter's soil media and surrounding soil, the effective size of the biofilter is approximate 1.7 times larger than its physical size [70]. Consequently, for all water balance calculations the maximum storage was set to $S_{max} = 0.42$m.

4.3.2 T-TTD Theory and Age-Ranked Storage

T-TTD theory is a control volume analysis that tracks the evolving age distribution of water stored in, and leaving, an unsteady hydrologic system. In our case the control volume is drawn around the soil media of a biofilter, and we let the variable, T (units of hours), represent the age of a water parcel in the control volume; i.e., the time a water parcel has spent in the soil media since it infiltrated from the ponding zone. The evolution of both the volume and age distribution of water stored in the control volume is described by the age-ranked storage function, $S_T(T,t)$ [m], defined as the area-normalized volume of water in storage with a particular age, T, or younger at time t. Mathematically, the age-ranked storage function is the product of the area-normalized storage $S(t)$ and the cumulative distribution function (CDF) form of the residence time distribution (RTD) of water in the control volume, $P_{RTD}(T,t)$: $S_T(T,t) = S(t)P_{RTD}(T,t)$.

Following [177], age-ranked storage can be conceptualized as a vertical ranking by age of the water stored in a control volume. The age-ranked storage function, $S_T(T,t)$, is the portion of age-ranked storage with age T or younger (see grey arrow and dashed line in Figure 4.1C). In the figure we also distinguished between "original" and "new" water, where the former refers to water that was initially present in the biofilter at time $t = 0$ and the latter refers to water that infiltrated into the biofilter from the ponding zone some time later, $t > 0$. In the analysis presented below, we mathematically tag original water by assigning it an initial age of T_0; thus, for $t \geq 0$ all original water will have a single age equal to $T = T_0 + t$. By definition, all new water flowed into the biofilter from the ponding zone at times $t \geq 0$. Consequently, new water stored in the biofilter will have a distribution of ages bounded by the inequality, $0 \leq T \leq t$. The evolution of age-ranked storage with time in the control volume is governed by the age conservation equation (ACE) [177, 178]. Before the ACE can be solved, an additional closure relationship, called the StorAgeSelection (SAS) function, must be specified to determine how the selection of water for outflow (by discharge or ET) is biased by age.

In our previous study of the OCPW biofilter [70], we found that bromide breakthrough data were well described by a uniform SAS, implying that water in outflow is selected more-or-less randomly from storage (colored discharge arrows in Figure 4.1C). Uniform SAS functions can apply to unsteady hydrologic systems, such as ours, that are far from well-mixed [179–181]. For the choice of a uniform SAS, the ACE can be solved to yield exact solutions for age-ranked storage in the biofilter's soil media and, importantly, the breakthrough concentration of the m-th solute (i.e., bromide, dissolved organic carbon, oxygen, nitrate or ammonium),

$C_{Q,m}(t)$, in water draining from the biofilter:

$$C_{Q,m}(t) = \frac{S_0 e^{-\bar{\tau}(t,0)}}{R_m S(t)} C_m^{\text{original}}(T=t) + \frac{1}{R_m S(t)} \int_0^t C_{J,m}^{\text{new}}(t_i, T=t-t_i) \, J(t_i) e^{-\bar{\tau}(t,t_i)} \, dt_i \tag{4.1a}$$

$$\bar{\tau}(t,\nu) = \int_\nu^t \frac{Q(x)+ET(x)}{S(x)} \, dx \tag{4.1b}$$

The first and second terms on the right hand side of equation (4.1a) represent the contribution of original and new water, respectively, to the breakthrough concentration of the m-th solute. New variables appearing here include the retardation coefficient for the m-th solute, R_m, the concentration of the m-th solute in original water of age $T = t$, $C_m^{\text{original}}(T = t)$, and the concentration of the m-th solute in new water of age $T = t - t_i$ that infiltrated into the biofilter from the ponding zone at time $t = t_i$, $C_{J,m}^{\text{new}}(t_i, T = t - t_i)$. We have set the initial age of original water equal to zero, $T_0 = 0$; as noted above, this parameter only serves to mathematically "tag" original water and therefore its value is arbitrary. Solute adsorption to the biofilter media is presumed to follow a linear equilibrium isotherm; the magnitude of the retardation coefficient indicates whether the m-th solute adsorbs to the biofilter media ($R_m > 1$) or not ($R_m = 1$). The variable $\bar{\tau}(t_2, t_1)$ in equation (4.1b) can be interpreted as the number of storage volumes of water that are transferred out (or "washed out") of the biofilter by gravitational discharge and ET from time $t = t_1$ to $t = t_2$. The exponential terms, $e^{-\bar{\tau}(t,0)}$ and $e^{-\bar{\tau}(t,t_i)}$, appearing on the right hand side of equation (4.1a), therefore account for the wash-out of solute mass in original and new water, respectively. To integrate equation (4.1a) we must first specify how the concentration of the m-th solute evolves as a water parcel ages. In the next section we present a N-cycle model for the age-dependence of DOC, oxygen, ammonium and nitrate concentrations in a water parcel as it transits through a biofilter.

4.3.3 N-Cycle Model

Our N-cycle model captures the following five microbially mediated redox reactions: (1) mineralization of dissolved organic carbon by aerobic and anaerobic respiration (mineralization, MIN); (2) consumption of oxygen by the aerobic respiration of dissolved organic carbon (aerobic respiration, AR); (3) liberation of ammonium by the aerobic and anaerobic respiration of organic material (ammonification, AM); (4) oxidation of ammonium to nitrate (nitrification, NI); and (5) removal of nitrate by reduction to the gases N_2 or N_2O (denitrification, DN) [99]. We further assume that each water parcel passing through the biofilter behaves like its own well-mixed batch reactor (the so-called streamline segregation hypothesis [182], see discussion in Section 2.2 of Azizian et al. 2017[99]). Mass balance over a single water parcel then yields the following set of coupled ordinary differential equations for the age-dependent concentration (units of mol m^{-3}) of allocthonous dissolved organic carbon $C_{\mathrm{DOC}}^{\mathrm{alloc}}$, molecular oxygen $C_{\mathrm{O_2}}$, nitrate $C_{\mathrm{NO_3^-}}$ and ammonium $C_{\mathrm{NH_4^+}}$ in a water parcel passing through the biofilter:

$$\frac{dC_{\mathrm{DOC}}^{\mathrm{alloc}}}{dT} = -R_{\mathrm{MIN}}^{\mathrm{alloc}}(T) \tag{4.2a}$$

$$\frac{dC_{\mathrm{O_2}}}{dT} = -R_{\mathrm{AR}}(T) - 2R_{\mathrm{NI}}(T) \tag{4.2b}$$

$$\frac{dC_{\mathrm{NH_4^+}}}{dT} = R_{\mathrm{AM}}(T) - R_{\mathrm{NI}}(T) \tag{4.2c}$$

$$\frac{dC_{\mathrm{NO_3^-}}}{dT} = R_{\mathrm{NI}}(T) - R_{\mathrm{DN}}(T) \tag{4.2d}$$

The function $R_{\mathrm{MIN}}^{\mathrm{alloc}}$ represents the mineralization rate of allocthonous organic material entering the biofilter with new water during storms, while R_{AM}, R_{NI} and R_{DN} represent, respectively, the rates of ammonification, nitrification and denitrification (all units of mol m^{-3} h^{-1}). The factor of two on the right hand side of equation (4.2b) reflects the stoichiometry of nitrification in which two molecules of oxygen are consumed for every molecule of nitrate produced [171]. To specify the reaction rates on the right hand side of the above

rate equations we assume: (1) the total mineralization rate, $R_{\mathrm{MIN}}^{\mathrm{total}}$, equals the sum of the mineralization rates of autochthonous, $R_{\mathrm{MIN}}^{\mathrm{auto}}$, and allochthonous, $R_{\mathrm{MIN}}^{\mathrm{alloc}}(T)$, organic material (equation (4.3a)); (2) the mineralization rate of autochthonous organic material, $R_{\mathrm{MIN}}^{\mathrm{auto}}$, is a fixed constant that depends on, for example, the nature and quantity of the organic material mixed into the biofilter media; (3) the mineralization rate of allocthonous organic material, $R_{\mathrm{MIN}}^{\mathrm{alloc}}(T)$, is first-order in the concentration of allocthonous DOC entering the biofilter with new water during storms, where $k_{\mathrm{MIN}}^{\mathrm{alloc}}$ is the first-order mineralization rate constant (equation (4.3b)); (4) aerobic respiration is proportional to the total mineralization rate but declines with decreasing oxygen concentration (equation (4.3c)); (5) ammonification is a fixed fraction ($\gamma_{CN} = 14$) of the total mineralization rate [183] (equation (4.3d)); (6) nitrification is second-order in oxygen and ammonium concentrations (equation (4.3e)); and (7) denitrification consumes roughly $\kappa = 0.3$ moles of carbon for every mole of nitrate reduced (equation (4.3f)) [99, 184], exhibits a Monod-type saturation dependence on nitrate concentration with a half-saturation constant of $K_{\mathrm{NO_3^-}}^{\mathrm{sat}}$, and is inhibited in the presence of oxygen (equation (4.3g)) where $K_{\mathrm{O_2}}^{\mathrm{inh}}$ is the half-saturation constant for noncompetitive oxygen inhibition (Sawyer, 2015).

$$R_{\mathrm{MIN}}^{\mathrm{total}}(T) = R_{\mathrm{MIN}}^{\mathrm{auto}} + R_{\mathrm{MIN}}^{\mathrm{alloc}}(T) \tag{4.3a}$$

$$R_{\mathrm{MIN}}^{\mathrm{alloc}}(T) = k_{\mathrm{MIN}}^{\mathrm{alloc}} C_{\mathrm{DOC}}^{\mathrm{alloc}}(T) \tag{4.3b}$$

$$R_{\mathrm{AR}}(T) = R_{\mathrm{MIN}}^{\mathrm{total}}(T)\Big(1 - \theta_{\mathrm{O_2}}^{\mathrm{inh}}(T)\Big) \tag{4.3c}$$

$$R_{\mathrm{AM}}(T) = \frac{1}{\gamma_{CN}} R_{\mathrm{MIN}}^{\mathrm{total}}(T) \tag{4.3d}$$

$$R_{\mathrm{NI}}(T) = k_{\mathrm{NI}} C_{\mathrm{O_2}}(T) C_{\mathrm{NH_4^+}}(T) \tag{4.3e}$$

$$R_{\mathrm{DN}}(T) = \kappa \theta_{\mathrm{O_2}}^{\mathrm{inh}}(T) \frac{R_{\mathrm{MIN}}^{\mathrm{total}}(T) C_{\mathrm{NO_3^-}}(T)}{C_{\mathrm{NO_3^-}}(T) + K_{\mathrm{NO_3^-}}^{\mathrm{sat}}} \tag{4.3f}$$

$$\theta_{\mathrm{O_2}}^{\mathrm{inh}}(T) = \frac{K_{\mathrm{O_2}}^{\mathrm{inh}}}{C_{\mathrm{O_2}}(T) + K_{\mathrm{O_2}}^{\mathrm{inh}}} \tag{4.3g}$$

This N-cycle model neglects anerobic ammonium oxidation (Anammox) and dissimilatory nitrate reduction to ammonium (DNRA). Although important in some (e.g., freshwater) ecosystems, these alternative pathways for nitrate reduction are thought to be of secondary importance (relative to respiratory denitrification, equation (4.3f)) in urban terrestrial systems [185]. Uptake of nitrate and ammonium by upright vegetation in the biofilter is also factored into the model (even though it does not appear in the rate equations above), by including evapotranspiration as one of two outflow processes, along with gravitational drainage, in the TTD theory (see Section (3.2)). The above rate equations describe the non-linear co-evolution of DOC, oxygen, ammonium and nitrate in a single water parcel traveling from its point of origin in the biofilter (as either original water in the soil media, or as new water entering the biofilter from the ponding zone) to its departure from the biofilter by gravitational discharge or plant uptake (ET). When the N-cycle model is convolved with TTD predictions for the evolving age distribution of water in, and leaving, the biofilter (equation (4.1a)) we can derive model-predicted breakthrough concentrations for nitrate and ammonium, accounting for both unsteady flow through the biofilter and age-dependent N-cycle reactions. In the model-data comparisons presented later, model parameters were inferred by minimizing the root-mean-square error (RMSE) in nonlinear least squares regression between the log-transformed measured and model-predicted ammonium breakthrough curves (the log-transform was necessary because breakthrough concentrations typically varied over several orders of magnitude). Model performance was assessed based on the model's RMSE, and percent linear bias calculated as follows, $\text{PBIAS} = 100 \times \sum_{i=1}^{N}(y_{\text{sim}} - y_{\text{meas}}) / \sum_{i=1}^{N}(y_{\text{meas}})$, where y_{meas} and y_{sim} represent the measured and model-simulated breakthrough concentrations, respectively, and N is the total number of measurements.

4.4 Results

4.4.1 Field Challenge Experiments and Model Calibration

Volume Balance and Bromide Breakthrough

During each simulated storm event at the OCPW biofilter test facility, approximately 1,400 L of either stormwater runoff alone (during storms S1, S2, S4, S5, S6 and S7) or a bromide-tagged 50:50 mixture of stormwater runoff and raw sewage (during storm S3) was added to the ponding zone of the biofilter (black curve, Figure 2A). Between 19 and 46 percent of the 1,400 L was recovered as outflow from the base of the biofilter, with the difference going toward increasing the volume of water stored in the transiently saturated biofilter, lateral exfiltration to the adjacent biofilter test cell (through a hole drilled in the base of the biofilter wall to accommodate irrigation lines) and, to much smaller extent, evapotranspiration (over the five days that these field experiments were conducted, ET accounted for < 0.3 percent of the overall water budget, green curve, Figure 2A). Time series of biofilter saturation and outflow generated by the bucket model (black and green curves, Figure 2B) are concordant with field observations as well as physics-based numerical simulations of transient unsaturated flow through the system (details in Parker et al., 2021 [70]).

Under the assumption that water is randomly selected by age for discharge from the biofilter (i.e., for the choice of a uniform SAS function, see Section (4.3.2) and Figure 1C), the breakthrough concentration of a conservative tracer can be estimated from TTD theory based solely on the time-history of solute inflow to the biofilter and the measured or bucket-model predicted timeseries of inflow $J(t)$, evapotranspiration $\mathrm{ET}(t)$, water storage $S(t)$, and discharge $Q(t)$ (see equations (1a) and (1b)). Indeed, TTD theory faithfully reproduces the concentration of bromide measured in outflow from the biofilter (or the "bromide breakthrough curve," BTC) during both the bromide-spiked storm S3 and subsequent bromide-

free flushing storms (storms S4 through S7) (compare points and black curve in Figure 2C). In this figure we distinguish between TTD predictions of bromide concentration in water discharged from the biofilter during periods of active outflow (solid lines in the figure) and the average bromide concentration in water stored in the biofilter during periods of little or no outflow (dashed lines); these two concentrations are equal for the choice of a uniform SAS function [177]. These TTD simulations of bromide breakthrough, which were previously published in Parker et al. (2021)[70], required the specification of a single fitting parameter: the biofilter's effective maximum water storage (S_{max}). The inferred value used here ($S_{max} = 0.42$m) is larger than the biofilter media's pore volume ($S_{max} = 0.25$m), perhaps reflecting the exchange of water and solute between the biofilter media and adjacent soil associated with lateral exfiltration. Another plausible explanation is that the larger S_{max} compensates for the oversampling of young water by the uniform SAS (discussed in Parker et al., 2021 [70]).

Ammonium Breakthrough

To identify the physical and biological processes that most influence ammonium transport and transformation in our experimental biofilter, we adopted an iterative approach in which a simplified version of the N-cycle/TTD model was first fit to the measured ammonium BTC, and then biokinetic processes were added as needed to reproduce the observed ammonium breakthrough patterns. To facilitate this process we derived two explicit formulae for the ammonium breakthrough concentration. Both solutions incorporate all of the physical transport processes captured in the TTD model for bromide (see last section), along with ammonium adsorption, respiration, ammonification and nitrification. The two solutions differ in their assumption about where DOC involved in ammonification originates, either from organic material mixed into the biofilter media (i.e., autocthonous organic material, Solution I) or organic material brought into the biofilter with new water during storms (allochthonous

organic material, Solution II). The two solutions neglect denitrification , given that the interstitial fluids of the biofilter were repeatedly aerated with incoming stormwater during the seven back-to-back storms simulated over five days.

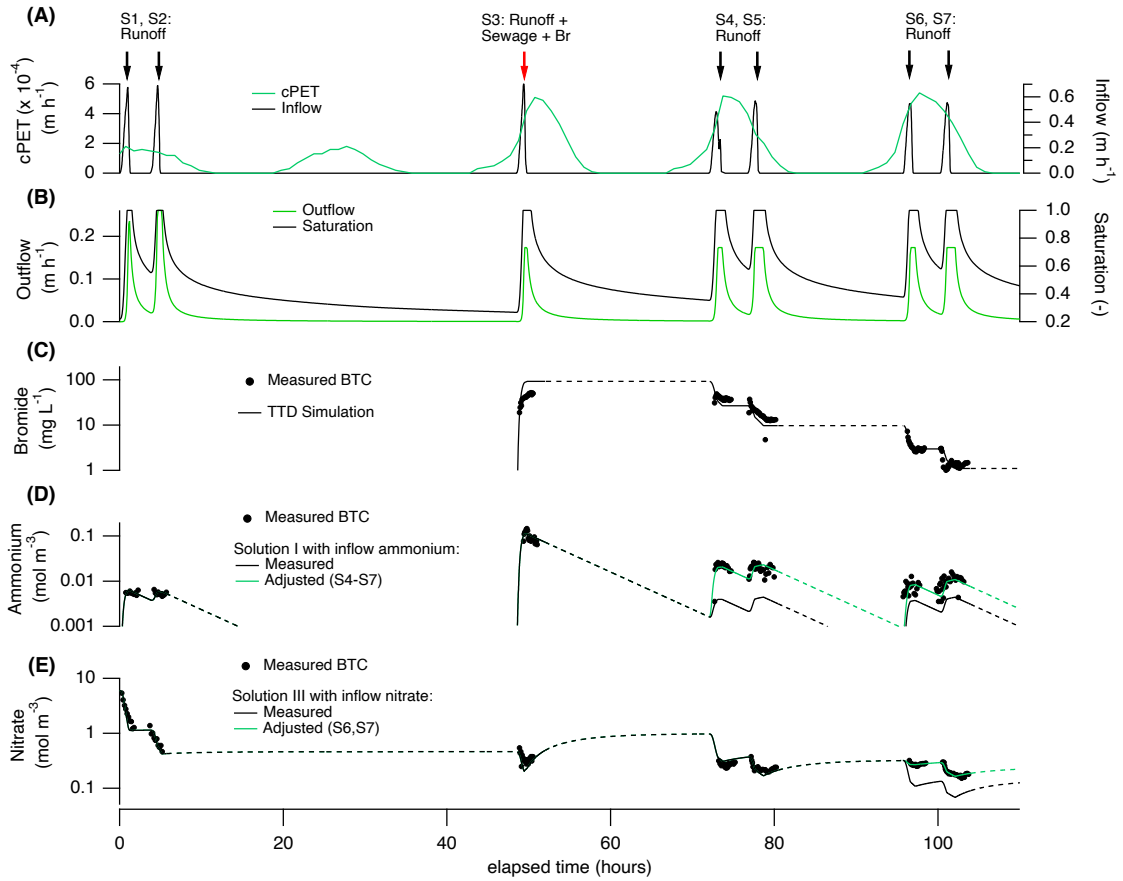

Figure 4.2: Measurements and modeling simulations for seven experimental storms at a biofilter test facility in Orange County, California. (A) Measurements of inflow to the biofilter along with estimates of the potential evapotranspiration (cPET) calculated from environmental measurements using the Penman-Montieth equation; (B) Bucket model predictions for the discharge of water from the biofilter and saturation of the biofilter media; (C) Measurements and TTD model predictions for the breakthrough curve (BTC) of bromide applied during Storm S3; (D) Measurements and TTD/N-cycle model predictions (from Solution I, see main text) for the ammonium BTC given either measured (black curve) or adjusted (green curve) ammonium inflow concentrations during Storms S4-S7; (E) Measurements and TTD/N-cycle model predictions for the nitrate BTC assuming either measured (black curve) or adjusted (green curve) nitrate inflow concentrations during Storms S6 and S7.

Within our model framework, ammonium measured in biofilter outflow could have originated either from the transport of ammonium into the biofilter during storm events, or from the

in-biofilter ammonification of autocthonous or allocthonous organic material. In the first iteration of the model we assumed that all ammonium leaving the biofilter originated in stormflow (i.e., we neglected ammonification by setting $R_{\min} = 0$ in Solution I). Because the concentration of ammonium in each storm was measured, this initial model has only two unknown parameters: the retardation coefficient for ammonium, $R_{\mathrm{NH}_4^+}$, and a pseudo-first-order nitrification rate, $k'_{\mathrm{NI}} = k_{\mathrm{NI}} C_{\mathrm{O}_2}^{\mathrm{sat}}$, where $C_{\mathrm{O}_2}^{\mathrm{sat}}$ is the concentration of oxygen in the pore fluids at oxygen saturation. Inferred values for the first-order nitrification rate constant are reasonably reproducible across all seven storms ($k'_{\mathrm{NI}} = 0.19 \pm 0.05\,\mathrm{h}^{-1}$) (Table 1). The corresponding second-order nitrification rate constant ($k_{\mathrm{NI}} = 1.9 \pm 0.5 \times 10^{-4}\,\mathrm{m}^3\,\mathrm{mol}^{-1}\,\mathrm{s}^{-1}$, assuming full oxygen saturation at 20°C, $C_{\mathrm{O}_2}^{\mathrm{sat}} = 0.28\,\mathrm{mol\,m}^{-3}$), is well within the range of nitrification rates reported in the literature. Nitrification manifests in Figure 2D as an exponential decline (or a downward sloping line in the log-linear format of the figure) in the model-predicted ammonium BTC during the recessional phase of each storm.

Inferred values for the retardation coefficient are also reproducible across Storms S1 through S3, and their average value ($R_{\mathrm{NH}_4^+} = 6.8 \pm 0.18$) is consistent with previously published estimates for the equilibrium adsorption of ammonium to sandy and loamy soils. Following Storm S3, however, the inferred retardation coefficient drops sharply ($R_{\mathrm{NH}_4^+} = 1.2 \pm 0.05$ during Storm S4) and then rebounds somewhat over the next three storms ($R_{\mathrm{NH}_4^+} = 1.3 \pm 0.07$, 3.1 ± 0.18, and 2.7 ± 0.15 for Storms S5, S6 and S7, respectively). This downshift in the retardation coefficient can be visualized by simulating the ammonium BTC with Solution I (with $R_{\mathrm{MIN}}^{\mathrm{auto}} = 0$) adopting the average nitrification rate across all seven storms ($k'_{\mathrm{NI}} = 0.19\,\mathrm{h}^{-1}$) and the average retardation coefficient for the first three storms ($R_{\mathrm{NH}_4^+} = 6.8$) (black solid and dashed curve, Figure 2D). The model closely tracks ammonium breakthrough concentrations measured during Storms S1 through S3 (RMSE = 0.08 and PBIAS=5.5%), but then significantly under-estimates the ammonium breakthrough measured during Storms S4 through S7 (RMSE = 0.59 and PBIAS = −75%).

We considered three hypotheses that might explain the increase in ammonium export after Storm S3: (H1) respiration of autochthonous organic material mixed into the biofilter media; (H2) respiration of allocthonous organic material entering the biofilter during storms; and (H3) an increase in the concentration of ammonium entering the biofilter as stormwater passes through an organic-rich mat that developed on the biofilter surface after the 50:50 mixture of storm runoff and sewage was applied during Storm S3. These are discussed in turn.

Hypothesis H1 was tested by "turning on" ammonification in Solution I (i.e., by allowing the mineralization rate, $R_{\mathrm{MIN}}^{\mathrm{auto}}$, to be non-zero) and then inferring values for both the mineralization rate and retardation coefficient (holding the nitrification rate constant at $k'_{\mathrm{NI}} = 0.19\mathrm{h}^{-1}$). The updated model performs poorly, with high error and percent bias during Storms S4 through S7 (RMSE=0.26, PBIAS= -20%), and double the error (compared to the model without mineralization, see above) for Storms S1 through S3 (RMSE=0.16, PBIAS= -1.1%) (Figure C.4, Appendix C).

To test hypothesis H2 we attempted to fit Solution II to the ammonium breakthrough data, using measured ammonium and DOC concentrations entering the biofilter with each storm as input to the model, but the inference step failed due to an equifinality issue: the model's RMSE could be equally well minimized by an infinite set of $k_{\mathrm{MIN}}^{\mathrm{alloc}}$ and $R_{\mathrm{NH}_4^+}$ values, with an increase in one balanced by an increase in the other (Figure C.5, Appendix C). For a retardation coefficient of $R_{\mathrm{NH}_4^+} = 6.8$ (the value inferred above for the first three storms), the optimal mineralization rate constant, $k_{\mathrm{MIN}}^{\mathrm{alloc}} = 6.6\mathrm{h}^{-1}$, is large compared to previously published estimates (ca., 0.06 h^{-1} [99]). Furthermore, when these two values for $R_{\mathrm{NH}_4^+}$ and $k_{\mathrm{MIN}}^{\mathrm{alloc}}$ are substituted into Solution II, the predicted ammonium concentration in water leaving the biofilter is too high (relative to measurements) during Storms S1 and S2, but too low during Storms S4 and S5 (across all seven storms, RMSE=0.27 and PBIAS= 9.8%) (Figure C.6, Appendix C).

Hypothesis H3 can be tested by noting that the linear nature of equation (1a) implies that a reduction in the retardation coefficient after Storm S3 is equivalent to a proportional increase in the inflow concentration of ammonium. Fixing the retardation coefficient at $R_{\mathrm{NH}_4^+} = 6.8$, hypothesis H3 implies that passage of stormwater through the organic-rich mat on the surface of the biofilter increased the concentration of ammonium entering the biofilter by factors of 5.7, 5.2, 2.2 and 2.5 during Storms S4, S5, S6 and S7, respectively. Multiplying these factors into the measured inflow ammonium concentration for Storms 4 through 7 brings Solution I into near perfect concordance with the ammonium breakthrough data measured during the last four storms (RMSE=0.12, PBIAS= 1.9%) (green solid and dashed curve, Figure 4.2D). Thus, of the three hypotheses evaluated here, H3 appears to be the most likely (and parsimonious) explanation for the enhanced export of ammonium during the last four storms.

Nitrate Breakthrough

In the last section we found that the ammonium BTC measured during our biofilter challenge experiment can be closely reproduced with a simple N-cycle model that accounts only for nitrification. Because nitrification transforms ammonium into nitrate, an analogous solution can be derived for the breakthrough concentration of nitrate (Solution III, Text S6, SI). If we adopt the nitrification rate constant inferred from the ammonium breakthrough data ($k'_{\mathrm{NI}} = 0.19\mathrm{h}^{-1}$, see previous section), this new model has a single fitting parameter: the initial concentration of nitrate present in original water. Fitting Solution III to the measured nitrate breakthrough curve yields an inferred value for the initial concentration of nitrate in original water of $C^{\mathrm{original}}_{0,\mathrm{NO}_3^-} = 10.2 \pm 0.39$ mol m^{-3}. The model-predicted BTC closely tracks nitrate measurements during Storms S1 through S5 (RMSE=0.09, PBIAS=-6.4%) (solid and dashed black curve, Figure 4.2E) but substantially underestimates the measured nitrate BTC during Storms S6 and S7 (RMSE=0.36, PBIAS=-57%) (solid and dashed black curve, Figure 4.2E). One possibility, concordant with hypothesis H3 above, is that the

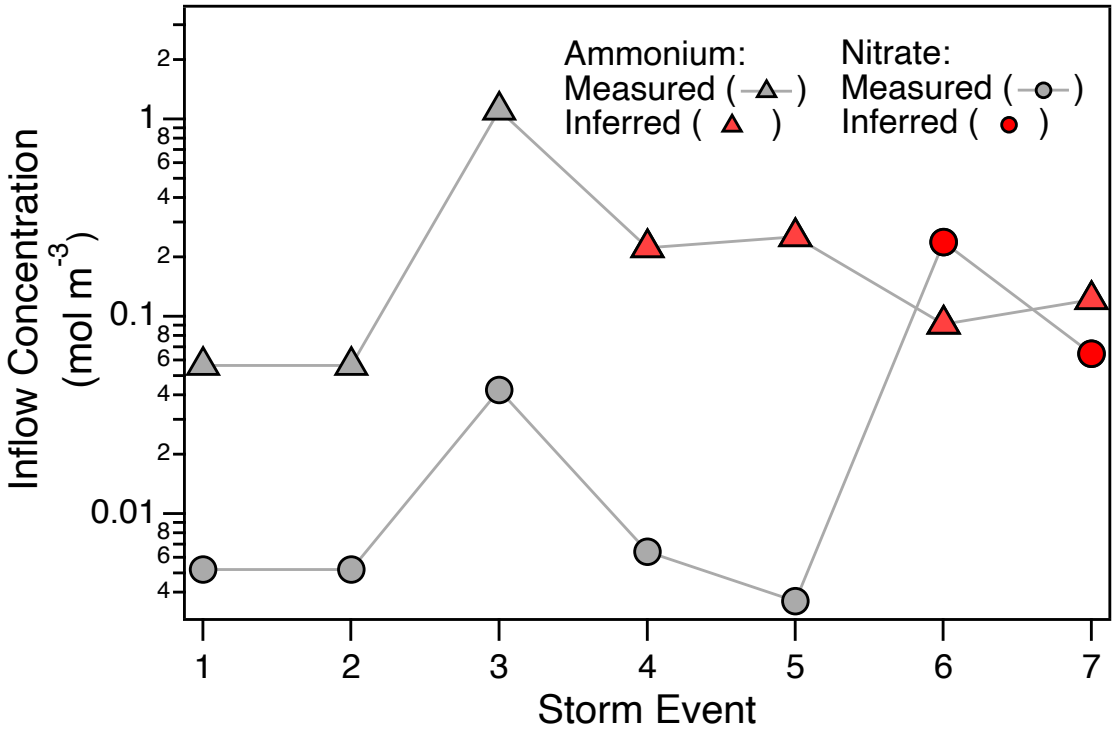

Figure 4.3: Measured and inferred concentrations of ammonium and nitrate in new water flowing into the biofilter during Storms S1 through S7. The former refers to measurements performed on samples of the runoff (Storms S1-S2 and S4-S7) or the 50:50 mixture of runoff and sewage (Storm S3) collected prior to each simulated storm. The latter refers to estimates of the inflow concentrations inferred by fitting either Solution I (ammonium) or Solution III (nitrate) to measured breakthrough concentrations, on the premise that the concentrations of these two nitrogen species increased as stormwater passed through an organic rich mat that developed on the surface of the biofilter after Storm S3. Note what appears to be a near stoichiometric conversion of ammonium to nitrate in the mat after Storm S5.

additional nitrate exported from the biofilter during Storms S6 and S7 originated from the nitrification of ammonium accumulating in the organic-rich mat present on the top of the biofilter after Storm 3. Indeed, the model fit improves substantially if the concentration of nitrate entering the biofilter during Storms S6 and S7 is increased by factors of 66 and 9.1, respectively (RMSE=0.02, PBIAS=-0.2%) (solid and dashed green curve, Figure 2E). While these multiplicative factors are large compared to what was estimated previously for ammonium (2.5 to 5.7, see last section), the implied inflow concentrations of nitrate (0.24 and 0.06 mol m^{-3} during Storms S6 and S7) are consistent with a near stoichiometric conversion of

ammonium to nitrate within the mat after Storm S5 (Figure 3). The conditions under which this particular organic-rich mat formed (through the introduction of sewage to the biofilter during Storm S3) are unlikely to be replicated frequently in practice. Nevertheless, our results point to the potential impact that organics accumulating on top of the biofilter (e.g., from leaf litter can have on ammonium and nitrate export from these systems. Specifically, our model results indicate that ammonification and nitrification within the mat increased ammonium and nitrate export from the biofilter by nearly 10-fold (compare black and green curves, Figures 4.2D and 4.2E).

4.4.2 Discussion: Toward a Stochastic Framework

The foregoing results support the contention that the TTD/N-Cycle theory developed in this study is a reasonable representation of ammonium and nitrate export under realistic field operating conditions, thus answering the first question raised in the Introduction to this paper. To answer the remaining two questions, in future evolutions of this framework we will conduct stochastic simulations of the TTD/N-cycle model designed to assess how natural hydrologic variability, particularly in Mediterranean climates like Orange County in Southern California with strongly seasonally rainfall [91], influence nitrate export over a range of temporal timescales. In particular, the modeling framework presented above can be simplified dramatically by specifying that the transfer of the four solutes of interest (DOC, oxygen, nitrate and ammonium) into the biofilter during a storm event occurs all at once and coincident in time with the storm's peak infiltration rate, t_{storm}. Importantly, this simplification applies only to the solute mass entering the biofilter, not the biofilter's water balance; i.e., the biofilter's water balance (i.e., inflows, outflows and storage) is still fully resolved over every storm event with the bucket model, at a nominal simulation frequency of 1 min^{-1}. Mathematically, this simplification is implemented by specifying the inflow concentration appearing in equation (4.1a) as follows, $C_{J,m}(t_i) = \frac{M''}{J(t_{\text{storm}})}\delta(t_i - t_{\text{storm}})$, where

M'' is the total solute mass per unit area added to the biofilter during a particular storm event, and $\delta(\cdot)$ is the Dirac Delta function. With this simplification the TTD/N-cycle model-predicted solute breakthrough concentration can be written as follows, where the vector $\overrightarrow{X} = [X_{\mathrm{DOC}}\ X_{\mathrm{O_2}}\ X_{\mathrm{NO_3^-}}\ X_{\mathrm{NH_4^+}}]$ represents the value of the quantity X for all four solutes tracked by the model:

$$\overrightarrow{C_Q}(t) = \sum_{i=1}^{N} \overrightarrow{C_J}(t, t_{\mathrm{storm},i}) e^{-\bar{\tau}(t, t_{\mathrm{storm},i})} \tag{4.4a}$$

$$\overrightarrow{C_J}(t, t_{\mathrm{storm},i}) = \begin{cases} 0,\ t < t_{\mathrm{storm},i} \\ \overrightarrow{C_{\mathrm{NC}}}(T, \overrightarrow{C_i}, \overrightarrow{R}),\ t \geq t_{\mathrm{storm},i} \end{cases} \tag{4.4b}$$

$$\overrightarrow{C_i} = \frac{\overrightarrow{M_i}''}{S(t)} \tag{4.4c}$$

New variables appearing here include the N-cycle model predictions for the concentration of all four solutes, $\overrightarrow{C_{\mathrm{NC}}}$, as a function of the age of a water parcel moving through the biofilter, $T = t - t_{\mathrm{storm},i}$, the inflow concentration associated with the i-th storm pulse, $\overrightarrow{C_i}$, and the retardation coefficients assigned to all four solutes, $\overrightarrow{R} = [R_{\mathrm{DOC}}\ R_{\mathrm{O_2}}\ R_{\mathrm{NO_3^-}}\ R_{\mathrm{NH_4^+}}]$. Under the assumption that only ammonium adsorbs to the biofilter media, the retardation coefficient vector simplifies as follows, where we have adopted the average retardation coefficient for ammonium inferred above for the first three storms, $\overrightarrow{R} = [1\ 1\ 1\ 6.8]$. The mass of the four solutes per unit area impulsively entering the biofilter during the i-th storm event is estimated from the product of the volume of stormwater that infiltrated during that storm event, V_i, and the associated stormwater solute concentrations, $\overrightarrow{C_{i,\mathrm{RS}}}$ where the subscript "RS" indicates that the concentrations have been randomly sampled from a database of stormwater measurements: $\overrightarrow{M_i}'' = V_i \overrightarrow{C_{i,\mathrm{RS}}}$. This general approach will be detailed in a future research article.

Chapter 5

References

Bibliography

(1) California, S. o. Water Energy Nexus, en, https://water.ca.gov/.

(2) Hanak, E.; Lund, J.; Mount, J.; Howitt, R.; Moyle, P.; Dinar, A.; Gray, B.; Thompson, B. Managing California's Water: From Conflict to Reconciliation, 2011.

(3) Lund, J.; Medellin-Azuara, J.; Durand, J.; Stone, K. *Journal of Water Resources Planning and Management* **2018**, *144*, Publisher: American Society of Civil Engineers, 04018067.

(4) Christensen, N. S.; Wood, A. W.; Voisin, N.; Lettenmaier, D. P.; Palmer, R. N. *Climatic Change* **2004**, *62*, 337–363.

(5) Ashoori, N.; Dzombak, D. A.; Small, M. J. *Journal of Water Resources Planning and Management* **2015**, *141*, Publisher: American Society of Civil Engineers, A4015005.

(6) Brown, E. G. Governor Brown Declares Drought State of Emergency, Office of Governor 2014, 2014.

(7) BROWN, E. G.; LAIRD, J.; COWIN, M. W. MANAGEMENT OF THE CALIFORNIA STATE WATER PROJECT, 2016.

(8) Faunt, C. C. *Groundwater Availability of the Central Valley Aquifer, California: U.S. Geological Survey*; Professional Paper 1766, Publisher: U.S. Geological Survey; USGS, 2009.

(9) Swain, D. L.; Langenbrunner, B.; Neelin, J. D.; Hall, A. *Nature Climate Change* **2018**, *8*, Number: 5 Publisher: Nature Publishing Group, 427–433.

(10) Pagán, B. R.; Ashfaq, M.; Rastogi, D.; Kendall, D. R.; Kao, S.-C.; Naz, B. S.; Mei, R.; Pal, J. S. *Environmental Research Letters* **2016**, *11*, Publisher: IOP Publishing, 094026.

(11) Diffenbaugh, N. S.; Swain, D. L.; Touma, D. *Proceedings of the National Academy of Sciences* **2015**, *112*, Publisher: Proceedings of the National Academy of Sciences, 3931–3936.

(12) Westerling, A. L.; Hidalgo, H. G.; Cayan, D. R.; Swetnam, T. W. *Science* **2006**, *313*, 940–943.

(13) Williams, A. P.; Abatzoglou, J. T.; Gershunov, A.; Guzman-Morales, J.; Bishop, D. A.; Balch, J. K.; Lettenmaier, D. P. *Earth's Future* **2019**, *7*, 892–910.

(14) Diffenbaugh, N. S.; Field, C. B. *Science (New York, N.Y.)* **2013**, *341*, 486–492.

(15) Huang, X.; Swain, D. L. *Science Advances* **2022**, *8*, Publisher: American Association for the Advancement of Science, eabq0995.

(16) Maina, F. Z.; Rhoades, A.; Siirila-Woodburn, E. R.; Dennedy-Frank, P.-J. *Hydrology and Earth System Sciences* **2022**, *26*, Publisher: Copernicus GmbH, 3589–3609.

(17) Gleick, P. H. *Proceedings of the National Academy of Sciences* **2010**, *107*, Publisher: Proceedings of the National Academy of Sciences, 21300–21305.

(18) Larsen, T. A.; Hoffmann, S.; Lüthi, C.; Truffer, B.; Maurer, M. *Science (New York, N.Y.)* **2016**, *352*, 928–933.

(19) Roy-Poirier, A.; Champagne, P.; Filion, Y. *Journal of Environmental Engineering* **2010**, *136*, Publisher: American Society of Civil Engineers, 878–889.

(20) Pataki, D. E.; Boone, C. G.; Hogue, T. S.; Jenerette, G. D.; McFadden, J. P.; Pincetl, S. *Ecohydrology* **2011**, *4*, 341–347.

(21) Ge, Y.; Priester, J. H.; Mortimer, M.; Chang, C. H.; Ji, Z.; Schimel, J. P.; Holden, P. A. *Environmental Science & Technology* **2016**, *50*, Publisher: American Chemical Society, 3965–3974.

(22) Cao, Y.; Green, P. G.; Holden, P. A. *Applied and Environmental Microbiology* **2008**, *74*, Publisher: American Society for Microbiology, 7585–7595.

(23) Alidina, M.; Li, D.; Drewes, J. E. *Water Research* **2014**, *56*, 172–180.

(24) *Water Reuse: Potential for Expanding the Nation's Water Supply Through Reuse of Municipal Wastewater*; National Academies Press: Washington, D.C., 2012.

(25) Townsend-Small, A.; Pataki, D. E.; Liu, H.; Li, Z.; Wu, Q.; Thomas, B. *Geophysical Research Letters* **2013**, *40*, ADS Bibcode: 2013GeoRL..40.4643T, 4643–4647.

(26) A Sustainable Water Future For California, https://www.nrdc.org.

(27) Gaffield, S. J.; Goo, R. L.; Richards, L. A.; Jackson, R. J. *American Journal of Public Health* **2003**, *93*, 1527–1533.

(28) Rippy, M.; Stein, R.; Sanders, B.; Davis, K.; Mclaughlin, K.; Skinner, J.; Kappeler, J.; Grant, S. *Environmental science & technology* **2014**, *48*, DOI: 10.1021/es503139h.

(29) *Meeting Water Quality Standards for San Diego's Recreational Waters: A Cost Benefit Analysis*; tech. rep.; Fermanian Business & Economic Institute, 2011.

(30) Stein, E. D.; Ackerman, D. *JAWRA Journal of the American Water Resources Association* **2007**, *43*, 398–413.

(31) Los Angeles County Flood Control District, California, Measure W, Parcel Tax (November 2018), en.

(32) LA County Passed Measure W in 2018. Let's Make It Fuel Our Recovery. en-US, https://ourwaterla.org, 2020.

(33) Sedlak, D. L., *Water 4.0: the past, present, and future of the world's most vital resource*; Yale Univ. Press: New Haven, 2014.

(34) Walsh, C. J.; Fletcher, T. D.; Burns, M. J. *PLOS ONE* **2012**, *7*, Publisher: Public Library of Science, e45814.

(35) *Urban Stormwater Management in the United States*; National Academies Press: Washington, D.C., 2009.

(36) Division, E.-W. P. Results of the Nationwide Urban Runoff Program; Volume I - Final Report, 1983.

(37) Grebel, J. E.; Mohanty, S. K.; Torkelson, A. A.; Boehm, A. B.; Higgins, C. P.; Maxwell, R. M.; Nelson, K. L.; Sedlak, D. L. *Environmental Engineering Science* **2013**, *30*, Publisher: Mary Ann Liebert Inc., 437–454.

(38) Reeves, R. L.; Grant, S. B.; Mrse, R. D.; Copil Oancea, C. M.; Sanders, B. F.; Boehm, A. B. *Environmental Science & Technology* **2004**, *38*, Publisher: American Chemical Society, 2637–2648.

(39) *Using Graywater and Stormwater to Enhance Local Water Supplies: An Assessment of Risks, Costs, and Benefits*; National Academies Press: Washington, D.C., 2016.

(40) Population Even slow growth will put pressure on infrastructure and public services, 2018.

(41) Chou, B. Mismatched: A Comparison of Future Water Supply and Demand for the Metropolitan Water District of Southern California and Its Member Agencies, en, 2017.

(42) Freeman, G. *Securing Reliable Water Supplies for Southern California*; tech. rep.; LAEDC, 2008.

(43) Ikeda, K.; Rasmussen, R.; Liu, C.; Newman, A.; Chen, F.; Barlage, M.; Gutmann, E.; Dudhia, J.; Dai, A.; Luce, C.; Musselman, K. *Climate Dynamics* **2021**, *57*, 2191–2215.

(44) Huning, L. S.; AghaKouchak, A. *Proceedings of the National Academy of Sciences* **2018**, *115*, Publisher: Proceedings of the National Academy of Sciences, 10932–10937.

(45) Pepin, N. et al. *Nature Climate Change* **2015**, *5*, Number: 5 Publisher: Nature Publishing Group, 424–430.

(46) Lepley, K.; Touchan, R.; Meko, D.; Shamir, E.; Graham, R.; Falk, D. *The Holocene* **2020**, *30*, Publisher: SAGE Publications Ltd, 1266–1278.

(47) Kumar, S.; Mocko, D.; Vuyovich, C.; Peters-Lidard, C. *Remote Sensing* **2020**, *12*, Number: 4 Publisher: Multidisciplinary Digital Publishing Institute, 645.

(48) Ouyang, Z.; Sciusco, P.; Jiao, T.; Feron, S.; Lei, C.; Li, F.; John, R.; Fan, P.; Li, X.; Williams, C. A.; Chen, G.; Wang, C.; Chen, J. *Nature Communications* **2022**, *13*, Number: 1 Publisher: Nature Publishing Group, 3800.

(49) Goss, M.; Swain, D. L.; Abatzoglou, J. T.; Sarhadi, A.; Kolden, C. A.; Williams, A. P.; Diffenbaugh, N. S. *Environmental Research Letters* **2020**, *15*, Publisher: IOP Publishing, 094016.

(50) Williams, A. P.; Livneh, B.; McKinnon, K. A.; Hansen, W. D.; Mankin, J. S.; Cook, B. I.; Smerdon, J. E.; Varuolo-Clarke, A. M.; Bjarke, N. R.; Juang, C. S.; Lettenmaier, D. P. *Proceedings of the National Academy of Sciences* **2022**, *119*, Publisher: Proceedings of the National Academy of Sciences, e2114069119.

(51) Cooley, H.; Phurisamban, R.; Gleick, P. *Environmental Research Communications* **2019**, *1*, Publisher: IOP Publishing, 042001.

(52) Grant, S. B.; Fletcher, T. D.; Feldman, D.; Saphores, J.-D.; Cook, P. L. M.; Stewardson, M.; Low, K.; Burry, K.; Hamilton, A. J. *Environmental Science & Technology* **2013**, *47*, Publisher: American Chemical Society, 10727–10734.

(53) Wong, T.; Allen, R.; Beringer, J.; Brown, R.; Chaudhri, V.; Deletic, A. *The Centre for Water Sensitive Cities, Clayton, VIC* **2011**.

(54) Grant, S. B. et al. *Science (New York, N.Y.)* **2012**, *337*, 681–686.

(55) Rippy, M. A. *WIREs Water* **2015**, *2*, 577–592.

(56) Parker, E. A.; Rippy, M. A.; Mehring, A. S.; Winfrey, B. K.; Ambrose, R. F.; Levin, L. A.; Grant, S. B. *Environmental Science & Technology* **2017**, *51*, Publisher: American Chemical Society, 5703–5712.

(57) AghaKouchak, A.; Feldman, D.; Hoerling, M.; Huxman, T.; Lund, J. *Nature* **2015**, *524*, Number: 7566 Publisher: Nature Publishing Group, 409–411.

(58) Stormwater Funding Options Report, en-US.

(59) The Untapped Potential of California's Water Supply: Effi ciency, Reuse, and Stormwater, California Drought Capstone, 2014.

(60) Walsh, C. J.; Booth, D. B.; Burns, M. J.; Fletcher, T. D.; Hale, R. L.; Hoang, L. N.; Livingston, G.; Rippy, M. A.; Roy, A. H.; Scoggins, M.; Wallace, A. *Freshwater Science* **2016**, *35*, 398–411.

(61) Tzoulas, K.; Korpela, K.; Venn, S.; Yli-Pelkonen, V.; Kaźmierczak, A.; Niemela, J.; James, P. *Landscape and Urban Planning* **2007**, *81*, 167–178.

(62) Chau, H.-F. *Green Infrastructure for Los Angeles: Addressing Urban Runoff and Water Supply through Low Impact Development*; tech. rep.; 2009.

(63) Elliott, A. H.; Trowsdale, S. A. *Environmental Modelling & Software* **2007**, *22*, 394–405.

(64) INT'L STORMWATER BMP DBASE, en-US, https://bmpdatabase.org.

(65) Watershed Management Programs — Los Angeles Regional Water Quality Control Board, https://www.waterboards.ca.gov.

(66) Jiang, S. C.; Lim, K.-Y.; Huang, X.; McCarthy, D.; Hamilton, A. J. *WIREs Water* **2015**, *2*, 683–699.

(67) Walsh, C. J.; Roy, A.; Feminella, J.; Cottingham, P.; Groffman, P.; Morgan II, R. *Am. Benthol. Soc* **2005**, *24*, 706–723.

(68) Rantz, S. E. *Runoff Characteristics of California Streams*; tech. rep.; GEOLOGICAL SURVEY WATER-SUPPLY PAPER 2009-A, 2009.

(69) Parker, E. A.; Grant, S. B.; Sahin, A.; Vrugt, J. A.; Brand, M. W. *ACS ES&T Water* **2022**, *2*, Publisher: American Chemical Society, 10–21.

(70) Parker, E. A.; Grant, S. B.; Cao, Y.; Rippy, M. A.; McGuire, K. J.; Holden, P. A.; Feraud, M.; Avasarala, S.; Liu, H.; Hung, W. C.; Rugh, M.; Jay, J.; Peng, J.; Shao, S.; Li, D. *Water Resources Research* **2021**, *57*, e2020WR028579.

(71) Askarizadeh, A.; Rippy, M. A.; Fletcher, T. D.; Feldman, D. L.; Peng, J.; Bowler, P.; Mehring, A. S.; Winfrey, B. K.; Vrugt, J. A.; AghaKouchak, A.; Jiang, S. C.; Sanders, B. F.; Levin, L. A.; Taylor, S.; Grant, S. B. *Environmental Science & Technology* **2015**, *49*, 11264–11280.

(72) Aghakouchak, A.; Feldman, D.; Stewardson, M. J.; Saphores, J.-D.; Grant, S.; Sanders, B. *Science* **2014**, *343*, 1430–1431.

(73) Low, K. G.; Grant, S. B.; Hamilton, A. J.; Gan, K.; Saphores, J.-D.; Arora, M.; Feldman, D. L. *WIREs Water* **2015**, *2*, 315–328.

(74) Cheng, H.; Hu, Y.; Zhao, J. *Environmental Science & Technology* **2009**, *43*, Publisher: American Chemical Society, 240–244.

(75) Maciejewska, E. *Acta Scientiarum Polonorum Architectura* **2020**, *19*, 11–19.

(76) Li, H.; Ding, L.; Ren, M.; Li, C.; Wang, H. *Water* **2017**, *9*, Number: 9 Publisher: Multidisciplinary Digital Publishing Institute, 594.

(77) Akram, F.; Rasul, M. G.; Khan, M. M. K.; Amir, M. S. I. I. *International Journal of Environmental and Ecological Engineering* **2014**, *8*, 188–197.

(78) Stein, E.; Federico, F.; Booth, D.; Bledsoe, B.; Bowles, C.; Rubin, Z.; Kondolf, G. M.; Sengupta, A. **2012**, Hydromodification Assessment and Management in California.

(79) Burns, M. J.; Schubert, J. E.; Fletcher, T. D.; Sanders, B. F. *WIREs Water* **2015**, *2*, _eprint: https://onlinelibrary.wiley.com/doi/pdf/10.1002/wat2.1078, 291–300.

(80) Coutts, C.; Hahn, M. *International Journal of Environmental Research and Public Health* **2015**, *12*, 9768–9798.

(81) Clar, M. L. Document Display — NEPIS — US EPA, en, 2004.

(82) Stein, E. D.; Yoon, V. K. *Water, Air, and Soil Pollution* **2008**, *190*, 183.

(83) Barbier, E. B. *Review of Environmental Economics and Policy* **2012**, *6*, Publisher: Association of Environmental and Resource Economists, 1–19.

(84) LA County Public Works, en-US, https://dpw.lacounty.gov/.

(85) Orange County Water District, en-US, https://www.ocwd.com/.

(86) Grantham, T.; Mount, J.; Stein, E. D. *Public Policy Institute of California* **2020**.

(87) Grant, S. B.; Duong, K.; Rippy, M. A.; Pierce, G.; Feldman, D.; Zanetti, E.; McNulty, A. *Environmental Research Letters* **2020**, *15*, Publisher: IOP Publishing, 054010.

(88) Hanak, E.; Lund, J.; Mount, J.; Moyle, P. What If California's Drought Continues?, Public Policy Institute of Southern California: https://www.ppic.org/, 2015.

(89) *Heal The Bay's 2021-2022 Annual Beach Report Card*; tech. rep.; Heal the Bay, 2021.

(90) Miller, O. L.; Miller, M. P.; Longley, P. C.; Alder, J. R.; Bearup, L. A.; Pruitt, T.; Jones, D. K.; Putman, A. L.; Rumsey, C. A.; McKinney, T. *Geophysical Research Letters* **2021**, *48*, e2021GL095085.

(91) California Climate Change Basics, https://water.ca.gov/Water-Basics/Climate-Change-Basics.

(92) Sanders, B. F.; Grant, S. B. *WIREs Water* **2020**, *7*, e1414.

(93) Climate of California, https://wrcc.dri.edu/Climate/narrative_ca.php.

(94) Fong, Y.; Huang, Y.; Gilbert, P. B.; Permar, S. R. *BMC Bioinformatics* **2017**, *18*, 454.

(95) Alley, W. M. *Journal of Applied Meteorology and Climatology* **1984**, *23*, Publisher: American Meteorological Society Section: Journal of Applied Meteorology and Climatology, 1100–1109.

(96) Rhee, J.; Carbone, G. J. *Journal of Climate* **2007**, *20*, Publisher: American Meteorological Society Section: Journal of Climate, 6033–6044.

(97) U.S. Gridded Palmer Drought Severity Index (PDSI) from gridMET, Drought.gov.

(98) Dewitz, J. National Land Cover Database (NLCD) 2019 Products, 2021.

(99) Azizian, M.; Boano, F.; Cook, P. L. M.; Detwiler, R. L.; Rippy, M. A.; Grant, S. B. *Water Resources Research* **2017**, *53*, 3941–3967.

(100) Rippy, M. A.; Deletic, A.; Black, J.; Aryal, R.; Lampard, J.-L.; Tang, J. Y.-M.; McCarthy, D.; Kolotelo, P.; Sidhu, J.; Gernjak, W. *Water Research* **2017**, *115*, 245–255.

(101) Babamoradi, H.; van den Berg, F.; Rinnan, Å. *Chemometrics and Intelligent Laboratory Systems* **2013**, *120*, 97–105.

(102) California, S. o. Drought, en, 2023.

(103) Di Baldassarre, G. et al. *Water Resources Research* **2019**, *55*, 6327–6355.

(104) Müller, A.; Österlund, H.; Marsalek, J.; Viklander, M. *Science of The Total Environment* **2020**, *709*, 136125.

(105) Lee, H.; Swamikannu, X.; Radulescu, D.; Kim, S.-j.; Stenstrom, M. K. *Water Research* **2007**, *41*, 4186–4196.

(106) Clar, M. B.; Barfield, B. J.; O'Connor, T. *STORMWATER BEST MANAGEMENT PRACTICES DESIGN GUIDE VOLUME 2 - VEGETATIVE BIOFILTERS*; tech. rep., EPA/600/R-04/121a; Washington, DC: U.S. Environmental Protection Agency (EPA), 2004.

(107) Payne, E. G. I.; Hatt, B. E.; Deletic, A.; Dobbie, M. F.; McCarthy, D. T.; Chandrasena, G. I. *Cooperative Research Centre for Water Sensitive Cities, Melbourne* **2015**.

(108) Srivastava, N. K.; Majumder, C. B. *Journal of hazardous materials* **2008**, *151*, Publisher: Elsevier, 1–8.

(109) Peng, J.; Cao, Y.; Rippy, M. A.; Afrooz, A. N.; Grant, S. B. *Water* **2016**, *8*, Publisher: MDPI, 600.

(110) Ambrose, R. F.; Winfrey, B. K. *WIREs Water* **2015**, *2*, 131–146.

(111) Lim, K.-Y.; Jiang, S. C. *Water research* **2013**, *47*, Publisher: Elsevier, 7273–7286.

(112) Lim, K.-Y.; Hamilton, A. J.; Jiang, S. C. *Science of the Total Environment* **2015**, *523*, Publisher: Elsevier, 95–108.

(113) Nabiul Afrooz, A. R. M.; Boehm, A. B. *Ecological Engineering* **2017**, *102*, 320–330.

(114) Zhang, Z.; Rengel, Z.; Liaghati, T.; Antoniette, T.; Meney, K. *Ecological Engineering* **2011**, *37*, 1833–1841.

(115) Tyre, K. N.; Brewton, R. A.; Kreiger, L. B.; Lapointe, B. E. *Science of The Total Environment* **2023**, *879*, 162716.

(116) Ferguson, C.; Husman, A. M. D. R.; Altavilla, N.; Deere, D.; Ashbolt, N. *Critical Reviews in Environmental Science and Technology* **2003**, *33*, 299–361.

(117) Viau, E. J.; Lee, D.; Boehm, A. B. *Environmental Science & Technology* **2011**, *45*, Publisher: American Chemical Society, 7158–7165.

(118) Sidhu, J. P. S.; Hodgers, L.; Ahmed, W.; Chong, M. N.; Toze, S. *Water Research* **2012**, *46*, 6652–6660.

(119) Jiang, S.; Chu, W. *Journal of Applied Microbiology* **2004**, *97*, 17–28.

(120) Jin, D.; Kong, X.; Cui, B.; Jin, S.; Xie, Y.; Wang, X.; Deng, Y. *Scientific Reports* **2018**, *8*, Number: 1 Publisher: Nature Publishing Group, 13368.

(121) Arnone, R. D.; Perdek Walling, J. *Journal of Water and Health* **2006**, *5*, 149–162.

(122) Zhang, L.; Seagren, E. A.; Davis, A. P.; Karns, J. S. *Journal of Environmental Engineering* **2011**, *137*, Publisher: American Society of Civil Engineers, 669–677.

(123) Boehm, A. B.; Soller, J. A. In *Environmental Toxicology: Selected Entries from the Encyclopedia of Sustainability Science and Technology*, Laws, E. A., Ed.; Springer: New York, NY, 2013, pp 441–459.

(124) Botturi, A.; Ozbayram, E. G.; Tondera, K.; Gilbert, N. I.; Rouault, P.; Caradot, N.; Gutierrez, O.; Daneshgar, S.; Frison, N.; Akyol, Ç.; Foglia, A.; Eusebi, A. L.; Fatone, F. *Critical Reviews in Environmental Science and Technology* **2021**, *51*, 1585–1618.

(125) Rizzo, A.; Tondera, K.; Pálfy, T. G.; Dittmer, U.; Meyer, D.; Schreiber, C.; Zacharias, N.; Ruppelt, J. P.; Esser, D.; Molle, P.; Troesch, S.; Masi, F. *Science of The Total Environment* **2020**, *727*, 138618.

(126) Levin, R.; Housh, M.; Portnov, B. A. *Environmental Management* **2020**, *65*, 748–757.

(127) Tran, N. H.; Reinhard, M.; Khan, E.; Chen, H.; Nguyen, V. T.; Li, Y.; Goh, S. G.; Nguyen, Q. B.; Saeidi, N.; Gin, K. Y.-H. *Science of The Total Environment* **2019**, *676*, 252–267.

(128) Geary, P.; Lucas, S. *Environmental Science and Pollution Research* **2019**, *26*, 2132–2144.

(129) Mallin, M. A.; McIver, M. R. *Marine Pollution Bulletin* **2012**, *64*, 1356–1366.

(130) Chandrasena, G. I.; Filip, S.; Zhang, K.; Osborne, C. A.; Deletic, A.; McCarthy, D. T. In *WSUD 2012: Water sensitive urban design; Building the water sensitive community; 7th international conference on water sensitive urban design*; ISSN: 9780858258952, Australia, 2012, pp 609–617.

(131) Chandrasena, G. I.; Pham, T.; Payne, E. G.; Deletic, A.; McCarthy, D. T. *Journal of Hydrology* **2014**, *519*, 814–822.

(132) Rugh, M. B. et al. *Water Research* **2022**, *219*, 118525.

(133) Valenca, R.; Borthakur, A.; Le, H.; Mohanty, S. K. In *Advances in Chemical Pollution, Environmental Management and Protection*, Sarmah, A. K., Ed.; Biochar: Fundamentals and Applications in Environmental Science and Remediation Technologies, Vol. 7; Elsevier: 2021, pp 175–201.

(134) Maurya, A.; Singh, M. K.; Kumar, S. In *Waterborne Pathogens*, Vara Prasad, M. N., Grobelak, A., Eds.; Butterworth-Heinemann: 2020, pp 123–141.

(135) Graham, K. E.; Anderson, C. E.; Boehm, A. B. *Water Research* **2021**, *207*, 117829.

(136) Fowdar, H.; Payne, E.; Schang, C.; Zhang, K.; Deletic, A.; McCarthy, D. *Journal of Hydrology* **2021**, *603*, 126887.

(137) Zinger, Y.; Prodanovic, V.; Zhang, K.; Fletcher, T. D.; Deletic, A. *Chemosphere* **2021**, *267*, 129294.

(138) Maleki Shahraki, Z.; Mao, X. *Journal of Environmental Quality* **2022**, *51*, 129–151.

(139) Chandrasena, G. I.; Shirdashtzadeh, M.; Li, Y. L.; Deletic, A.; Hathaway, J. M.; McCarthy, D. T. *Ecological Engineering* **2017**, *102*, 166–177.

(140) Zhang, L.; Seagren, E. A.; Davis, A. P.; Karns, J. S. *Water Environment Research* **2012**, *84*, 485–496.

(141) N, P.; Cascella, M. In 2019.

(142) Pantosti, A.; Venditti, M. *The European Respiratory Journal* **2009**, *34*, 1190–1196.

(143) *RESULTS of the SURVEILLANCE of METHICILLIN RESISTANT STAPHYLOCOCCUS AUREUS FROM 1995 TO 2009*; tech. rep., https://www.phac-aspc.gc.ca/nois-sinp/projects/res2009/pdf/res2009-eng.pdf; Canada: A PROJECT of the CANADIAN NOSOCOMIAL INFECTION SURVEILLANCE PROGRAM (CNISP), 2011.

(144) Goodwin, K. D.; McNay, M.; Cao, Y.; Ebentier, D.; Madison, M.; Griffith, J. F. *Water Research* **2012**, *46*, 4195–4207.

(145) Yamahara, K. M.; Sassoubre, L. M.; Goodwin, K. D.; Boehm, A. B. *Applied and Environmental Microbiology* **2012**, *78*, Publisher: American Society for Microbiology, 1733–1745.

(146) Levin-Edens, E.; Bonilla, N.; Meschke, J. S.; Roberts, M. C. *Water Research* **2011**, *45*, 5681–5686.

(147) Genuchten, M. T. V.; Leij, F. J.; Skaggs, T. H.; Toride, N.; Bradford, S. A.; Pontedeiro, E. M. *Journal of Hydrology and Hydromechanics* **2013**, *61*, 146–160.

(148) Kim, M.; Troch, P. A. *Water Resources Research* **2020**, *56*, e2020WR027186.

(149) Humphrey, C. E.; Solomon, D. K.; Genereux, D. P.; Gilmore, T. E.; Mittelstet, A. R.; Zlotnik, V. A.; Zeyrek, C.; Jensen, C. R.; MacNamara, M. R. *Water Resources Research* **2022**, *58*, e2021WR030711.

(150) Chen, J.; Yang, L.; Chen, X.; Ripp, S.; Zhuang, J. *Frontiers in Microbiology* **2022**, *13*, 730075.

(151) Yonti Madie, C.; Kamga Togue, F.; Woafo, P. *Heliyon* **2022**, *8*, e10083.

(152) Bradford, S. A.; Morales, V. L.; Zhang, W.; Harvey, R. W.; Packman, A. I.; Mohanram, A.; Welty, C. *Critical Reviews in Environmental Science and Technology* **2013**, *43*, 775–893.

(153) Kumar, B. L.; Gopal, D. V. R. S. *3 Biotech* **2015**, *5*, 867–876.

(154) Wu, Y.; Cai, P.; Jing, X.; Niu, X.; Ji, D.; Ashry, N. M.; Gao, C.; Huang, Q. *Environment International* **2019**, *132*, 105116.

(155) Woessner, W. W.; Poeter, E. P., *4.1 Darcy's Law*, Book Title: Hydrogeologic Properties of Earth Materials and Principles of Groundwater Flow Publisher: The Groundwater Project, 2020.

(156) Schumer, R.; Benson, D. A.; Meerschaert, M. M.; Baeumer, B. *Water Resources Research* **2003**, *39*, DOI: 10.1029/2003WR002141.

(157) Grant, S. B.; Gomez-Velez, J. D.; Ghisalberti, M.; Guymer, I.; Boano, F.; Roche, K.; Harvey, J. *Water Resources Research* **2020**, *56*, e2019WR026822.

(158) Grant, S. B.; Monofy, A.; Boano, F.; Gomez-Velez, J. D.; Guymer, I.; Harvey, J.; Ghisalberti, M. *Water Resources Research* **2020**, *56*, e2020WR027967.

(159) Feraud, M. et al. *Water Research* **2023**, *230*, 119501.

(160) Li, D.; Van De Werfhorst, L. C.; Rugh, M. B.; Feraud, M.; Hung, W.-C.; Jay, J.; Cao, Y.; Parker, E. A.; Grant, S. B.; Holden, P. A. *Environmental Science & Technology* **2021**, *55*, Publisher: American Chemical Society, 9199–9208.

(161) Simunek Jirka, J.; Šejna, M.; Saito, H.; Sakai, M.; Van Genuchten, M. The Hydrus-1D Software Package for Simulating the Movement of Water, Heat, and Multiple Solutes in Variably Saturated Media, Department of Environmental Sciences, University of California Riverside, Riverside, California, 2013.

(162) Šimůnek, J.; Van Genuchten, M. T. *Vadose Zone Journal* **2008**, *7*, 782–797.

(163) Clary, J.; Jones, J. *International Stormwater BMP Database 2020 Summary Statistics*; tech. rep., https://www.waterrf.org; The Water Research Foundation, 2020.

(164) Subramaniam, D.; Mather, P.; Russell, S.; Rajapakse, J. *Journal of Environmental Engineering* **2016**, *142*, Publisher: American Society of Civil Engineers, 04015090.

(165) Bratieres, K.; Fletcher, T. D.; Deletic, A.; Zinger, Y. *Water Research* **2008**, *42*, 3930–3940.

(166) Burgin, A. J.; Hamilton, S. K. *Frontiers in Ecology and the Environment* **2007**, *5*, 89–96.

(167) Romanelli, A.; Soto, D. X.; Matiatos, I.; Martínez, D. E.; Esquius, S. *Science of The Total Environment* **2020**, *715*, 136909.

(168) Kohlsmith, E.; Morse, J.; Poor, C.; Law, J. *Journal of Sustainable Water in the Built Environment* **2021**, *7*, Publisher: American Society of Civil Engineers, 05021002.

(169) Bratt, A. R.; Finlay, J. C.; Hobbie, S. E.; Janke, B. D.; Worm, A. C.; Kemmitt, K. L. *Environmental Science & Technology* **2017**, *51*, 3138–3147.

(170) Janke, B. D.; Finlay, J. C.; Hobbie, S. E. *Environmental Science & Technology* **2017**, *51*, 9569–9579.

(171) Cook, P. L. M.; Wenzhöfer, F.; Rysgaard, S.; Galaktionov, O. S.; Meysman, F. J. R.; Eyre, B. D.; Cornwell, J.; Huettel, M.; Glud, R. N. *Limnology and Oceanography: Methods* **2006**, *4*, 294–307.

(172) Zuo, X.; Chen, S.; Wang, T.; Zhang, S.; Li, T. *Water Research* **2022**, *221*, 118735.

(173) Li, J.; Tong, J.; Xia, C.; Hu, B. X.; Zhu, H.; Yang, R.; Wei, W. *Journal of Hydrology* **2017**, *549*, 754–768.

(174) Zak, D.; Kronvang, B.; Carstensen, M. V.; Hoffmann, C. C.; Kjeldgaard, A.; Larsen, S. E.; Audet, J.; Egemose, S.; Jorgensen, C. A.; Feuerbach, P.; Gertz, F.; Jensen, H. S. *Environmental Science & Technology* **2018**, *52*, Publisher: American Chemical Society, 6508–6517.

(175) US EPA, O. EPA Method 350.1: Determination of Ammonia Nitrogen by Semi-Automated Colorimetry, en, Data and Tools, 2019.

(176) Kirchner, J. W. *Water Resources Research* **2009**, *45*, DOI: 10.1029/2008WR006912.

(177) Harman, C. J.; Kim, M. *Geophysical Research Letters* **2014**, *41*, 1567–1575.

(178) Botter, G.; Bertuzzo, E.; Rinaldo, A. *Geophysical Research Letters* **2011**, *38*, DOI: 10.1029/2011GL047666.

(179) Benettin, P.; Rinaldo, A.; Botter, G. *Hydrological Processes* **2015**, *29*, _eprint: https://onlinelibrary.v 5203–5213.

(180) Benettin, P.; Rinaldo, A.; Botter, G. *Water Resources Research* **2013**, *49*, _eprint: https://onlinelibrary.wiley.com/doi/pdf/10.1002/2013WR014708, 8539–8551.

(181) Danesh-Yazdi, M.; Klaus, J.; Condon, L. E.; Maxwell, R. M. *Hydrological Processes* **2018**, *32*, _eprint: https://onlinelibrary.wiley.com/doi/pdf/10.1002/hyp.11481, 1063–1076.

(182) Rawlings, J. B.; Ekerdt, J. G., *Chemical reactor analysis and design fundamentals*, Second edition; Nob Hill Publishing: Madison, Wisconsin, 2012.

(183) Kessler, A. J.; Glud, R. N.; Cardenas, M. B.; Larsen, M.; Bourke, M. F.; Cook, P. L. M. *Limnology and Oceanography* **2012**, *57*, _eprint: https://onlinelibrary.wiley.com/doi/pdf/10 1217–1232.

(184) Kessler, A. J.; Glud, R. N.; Cardenas, M. B.; Cook, P. L. M. *Environmental Science & Technology* **2013**, *47*, 13404–13411.

(185) Reisinger, A. J.; Groffman, P. M.; Rosi-Marshall, E. J. *FEMS Microbiology Ecology* **2016**, *92*, ed. by Muyzer, G., fiw198.

Appendix A

Suplemental Information for Chapter 2

A.1 Study Area

Watershed Characteristics and Streamflow Patterns In the following pages, the detailed information for each USGS gauging station selected for this study including the gauge information, watershed characteristics, and stream management controls are summarized (in a table) followed by a map (Figure a) on the next page. The map shows the location of the gauging station, streams, drainage area, and the groundwater basin(s) presented within the drainage area. Figure b (first row) shows the N value or the number of observations that was available for the gauge station in the summer (JJA) and winter (JFM) months. Figure b (second row) shows the monthly Palmer Drought Index (PDSI) for summer and winter months followed by the mean summer and winter streamflow observations on the last row. Figure c and d show the z-scores of the log-transformed mean streamflow observations for summer and winter months, respectively. The graphs include the break-point year 1990,

where the linear trend slope of the streamflow observations changes and the trend slopes before and after the break-point (i.e., m_1 and m_2, respectively).

FULLERTON C BL FULLERTON DAM NR BREA CA

Gauge Information	USGS Station ID	11089500
	Hydrologic Unit Code	18070106
	Latitude (NAD27)	33°53'45"
	Longitude (NAD27)	117°53'07"
	Drainage Area [Mi^2]	4.94
	Elevation of The Stream Outlet Above NAVD88 [Ft]	284
	County	Orange
Watershed Characteristics	Mean Maximum January Temperature [°F]	67.04
	Mean Minimum January Temperature [°F]	42.94
	Mean Annual Precipitation [In]	15.6
	Hydrological Soil Group (HSG) [% of Covered Area]	D (100%)
	Length of Longest Flow Path [Mi]	6
	Mean Basin Elevation [Ft]	491
	Maximum Basin Elevation [Ft]	1288
	Minimum Basin Elevation [Ft]	159
	Percentage of Area Above 6000 Ft [%]	0
	Percentage of Area Covered By Forest [%]	2.8
	Percentage of Lakes And Ponds [%]	0
	Percentage of Developed (Urban) Land (NLCD 2011 Classes 21-24) [%]	85.6
	Percentage of Imperviousness (NLCD 2001 Impervious Dataset) [%]	41.54
	Percentage of Imperviousness (NLCD 2011 Impervious Dataset) [%]	43.35
	Percentage of Imperviousness (NLCD 2019 Impervious Dataset) [%]	46.00
Stream Management Controls	Developed or Natural	Developed
	Regulation	Regulated*
	Geological or Hydrological Control	None
	Dam Outlet	Yes**
	Agricultural Control	None
	(Waste)water Inputs	None
	Water Withdrawals	None
	Other Factors Affecting Runoff	-

* Flow regulated by Fullerton Flood-Control Reservoir, capacity, 760 acre-ft (resurvey of 1970). Small tributary formerly entering below station diverted into reservoir since December 1954. Ref. waterdata.usgs.gov

**Outlet of ACOE dam, thus flow is a function of dam management.

(a)

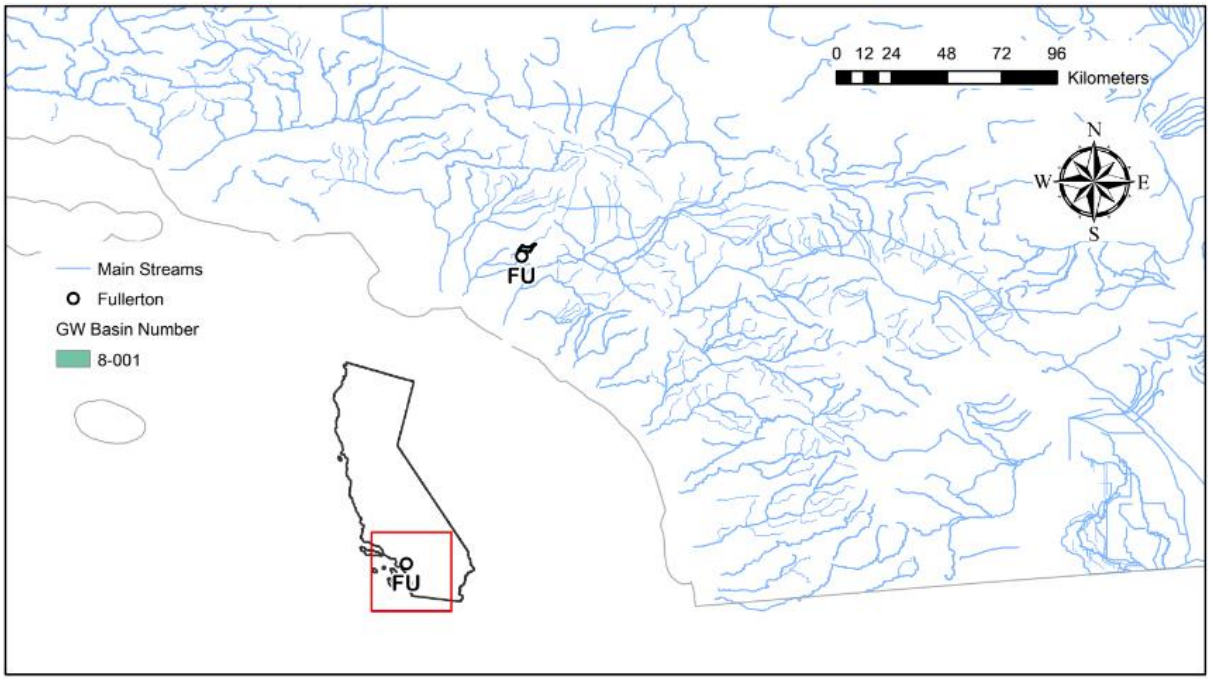
0 12 24 48 72 96
Kilometers
N
W
E
S
Main Streams
Fullerton
GW Basin Number
8-001
FU
FU

(b)

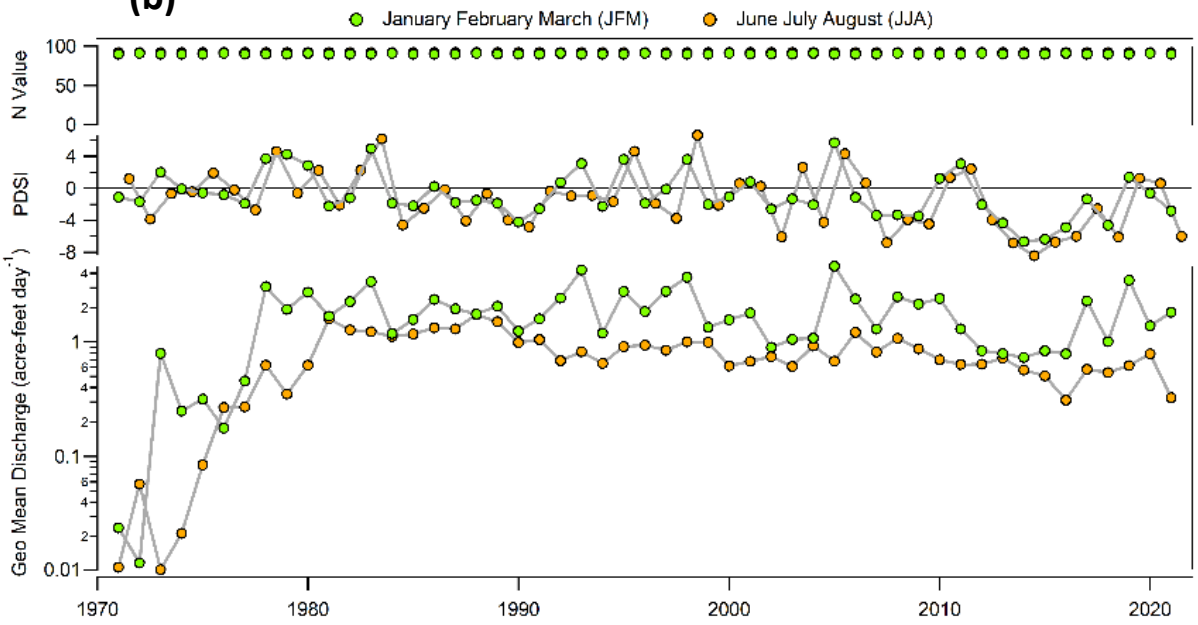
January February March (JFM)
June July August (JJA)
N Value
PDSI
Geo Mean Discharge (acre-feet day-1)
1970
1980
1990
2000
2010
2020

(c)

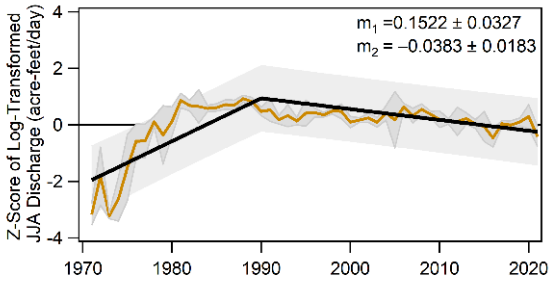
m1 =0.1522 ± 0.0327
m2 = –0.0383 ± 0.0183
Z-Score of Log-Transformed JJA Discharge (acre-feet/day)
1970
1980
1990
2000
2010
2020

(d)

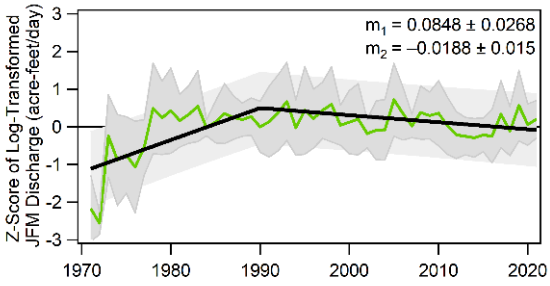
m1 = 0.0848 ± 0.0268
m2 = –0.0188 ± 0.015
Z-Score of Log-Transformed JFM Discharge (acre-feet/day)
1970
1980
1990
2000
2010
2020

SAN DIEGO C A CAMPUS DRIVE NR IRVINE CA

Gauge Information	USGS Station ID	11048555
	Hydrologic Unit Code	18070204
	Latitude (NAD27)	33°39'20"
	Longitude (NAD27)	117°50'41"
	Drainage Area [Mi^2]	111
	Elevation of The Stream Outlet Above NAVD88 [Ft]	12
	County	Orange
Watershed Characteristics	Mean Maximum January Temperature [°F]	66.51
	Mean Minimum January Temperature [°F]	43.44
	Mean Annual Precipitation [In]	14.5
	Hydrological Soil Group (HSG) [% of Covered Area]	C(28%), D(72%)
	Length of Longest Flow Path [Mi]	19
	Mean Basin Elevation [Ft]	379
	Maximum Basin Elevation [Ft]	1764
	Minimum Basin Elevation [Ft]	12
	Percentage of Area Above 6000 Ft [%]	0
	Percentage of Area Covered By Forest [%]	3.68
	Percentage of Lakes And Ponds [%]	0.24
	Percentage of Developed (Urban) Land (NLCD 2011 Classes 21-24) [%]	75.1
	Percentage of Imperviousness (NLCD 2001 Impervious Dataset) [%]	37.63
	Percentage of Imperviousness (NLCD 2011 Impervious Dataset) [%]	39.99
	Percentage of Imperviousness (NLCD 2019 Impervious Dataset) [%]	41.98
Stream Management Controls	Developed or Natural	Developed
	Regulation	Regulated
	Geological or Hydrological Control	Yes*
	Dam Outlet	No
	Agricultural Control	None
	(Waste)water Inputs	Yes**
	Water Withdrawals	Yes***
	Other Factors Affecting Runoff	-

*Lower watershed, below several dams and basins. However, these dams are mostly for sediment control in the foothills, not for water impoundment.
**There is heavy recycled water usage for irrigation, and recycled water is from both treated wastewater as well as contaminated groundwater.
***Just above the gage, there is San Joaquin Marsh that diverts 100% of flow (since 1998 when the marsh was built) to the wetland for nitrate removal. In dry years, the release from the wetlands was intermittent. The Marsh is part of the Natural Treatment System with many other smaller treatment wetlands upstream for nitrate removal as well as for infiltration.
Ref. waterdata.usgs.gov

(a)

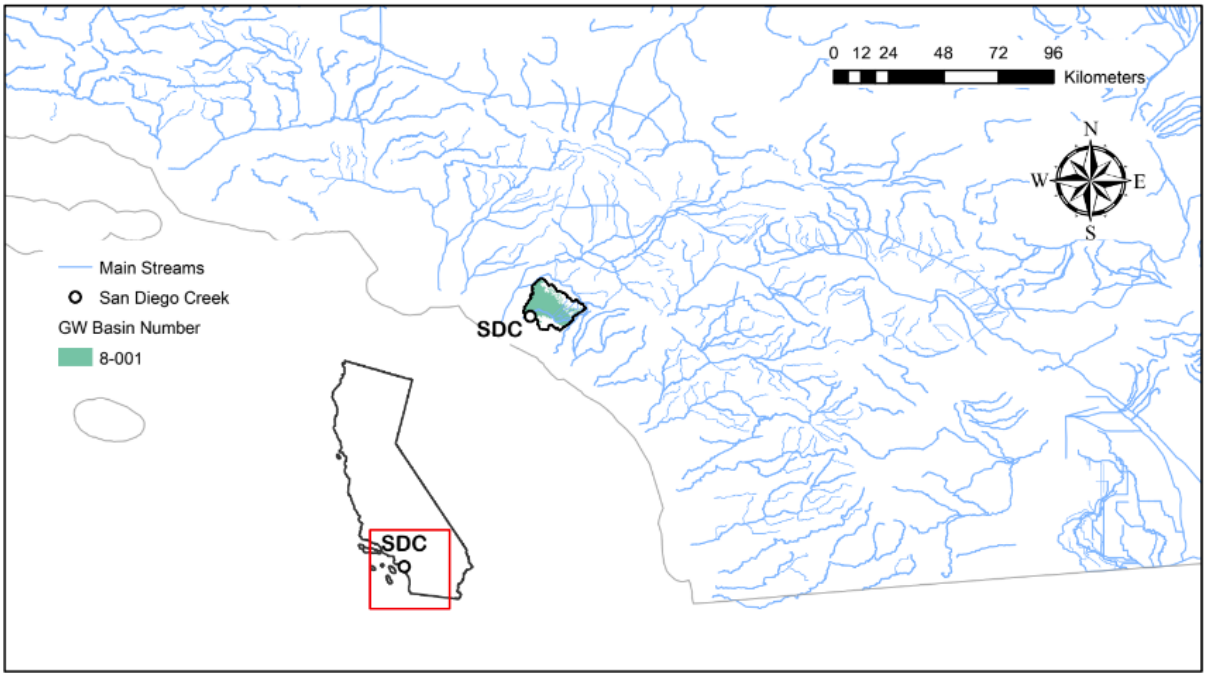
0 12 24 48 72 96
Kilometers
N
W
E
S
Main Streams
San Diego Creek
GW Basin Number
8-001
SDC
SDC

(b)

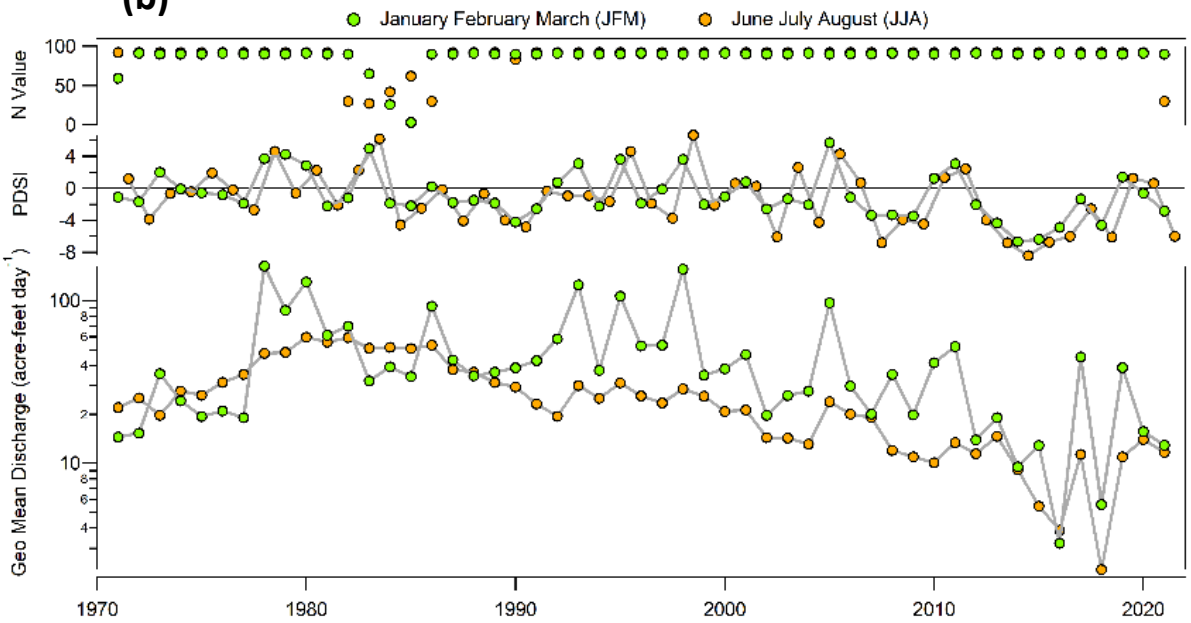
January February March (JFM)
June July August (JJA)
N Value
PDSI
Geo Mean Discharge (acre-feet day⁻¹)
1970
1980
1990
2000
2010
2020

(c)

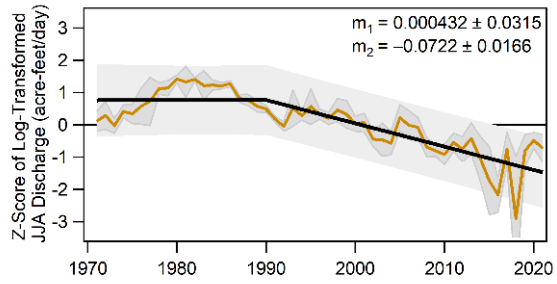
m1 = 0.000432 ± 0.0315
m2 = –0.0722 ± 0.0166
Z-Score of Log-Transformed JJA Discharge (acre-feet/day)
1970
1980
1990
2000
2010
2020

(d)

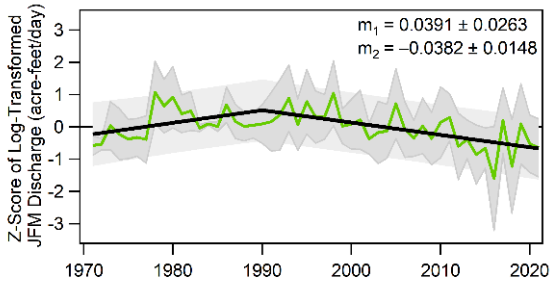
m1 = 0.0391 ± 0.0263
m2 = –0.0382 ± 0.0148
Z-Score of Log-Transformed JFM Discharge (acre-feet/day)
1970
1980
1990
2000
2010
2020

RIO HONDO AB WHITTIER NARROWS DAM CA

Gauge Information	USGS Station ID	11101250
	Hydrologic Unit Code	18070105
	Latitude (NAD27)	34°03'30"
	Longitude (NAD27)	118°04'15"
	Drainage Area [Mi^2]	91.2
	Elevation of The Stream Outlet Above NAVD88 [Ft]	209
	County	Los Angeles
Watershed Characteristics	Mean Maximum January Temperature [°F]	62.92
	Mean Minimum January Temperature [°F]	42.11
	Mean Annual Precipitation [In]	24.5
	Hydrological Soil Group (HSG) [% of Covered Area]	C(44%), D(56%)
	Length of Longest Flow Path [Mi]	18
	Mean Basin Elevation [Ft]	1542
	Maximum Basin Elevation [Ft]	6123
	Minimum Basin Elevation [Ft]	209
	Percentage of Area Above 6000 Ft [%]	0.00341
	Percentage of Area Covered By Forest [%]	13.8
	Percentage of Lakes And Ponds [%]	0.29
	Percentage of Developed (Urban) Land (NLCD 2011 Classes 21-24) [%]	60.1
	Percentage of Imperviousness (NLCD 2001 Impervious Dataset) [%]	28.9
	Percentage of Imperviousness (NLCD 2011 Impervious Dataset) [%]	29.2
	Percentage of Imperviousness (NLCD 2019 Impervious Dataset) [%]	29.4
Stream Management Controls	Developed or Natural	Developed
	Regulation	Regulated*
	Geological or Hydrological Control	Yes**
	Dam Outlet	Yes
	Agricultural Control	None
	(Waste)water Inputs	None
	Water Withdrawals	Yes***
	Other Factors Affecting Runoff	-

*Flow regulated by Big Santa Anita, Sawpit, and Eaton Flood-Control Reservoirs, and Sierra Madre, Las Flores, and Rubio debris basins, combined capacity, 2,195 acre-ft.

**Small effective drainage area; Controlled release from Peck Road reservoir

***Many diversions upstream from station for domestic use and irrigation. Los Angeles County Department of Public Works diversion from San Gabriel River below Santa Fe Dam (11085000) to Rio Hondo during water year: 2014 - no diversion; 2015 - no diversion; 2016 - 801 acre-feet; 2017 - 53,700 acre-feet; 2018 - 6,480 acre-feet; 2019 - 50,100 acre-feet; 2020 - 34,500 acre-feet; 2021 - 6,360 acre-feet.

Ref. waterdata.usgs.gov

(a)

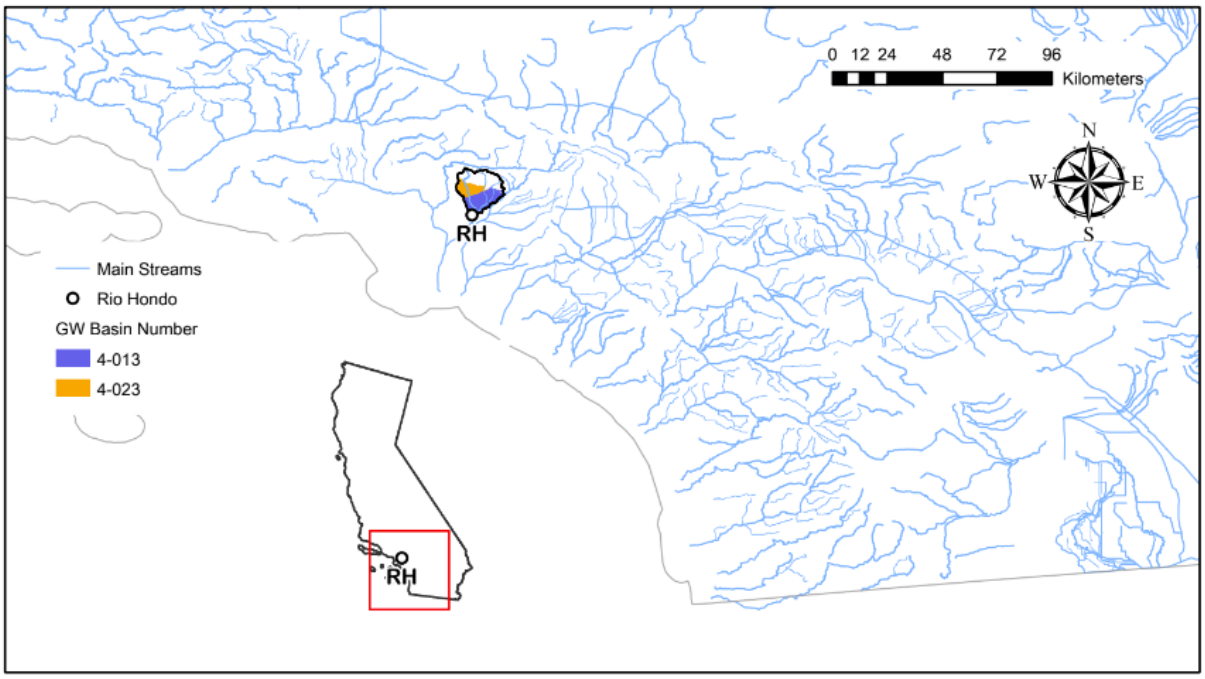
0 12 24 48 72 96
Kilometers
N
W
E
S
RH
Main Streams
Rio Hondo
GW Basin Number
4-013
4-023
RH

(b)

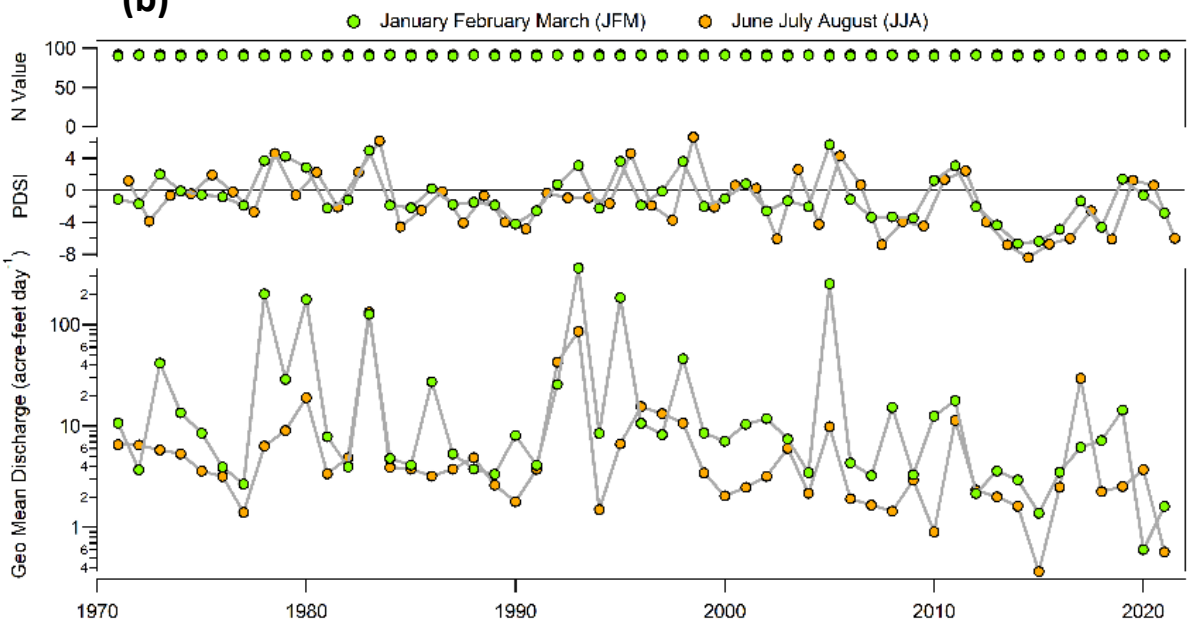
January February March (JFM)
June July August (JJA)
N Value
PDSI
Geo Mean Discharge (acre-feet day⁻¹)
1970
1980
1990
2000
2010
2020

(c)

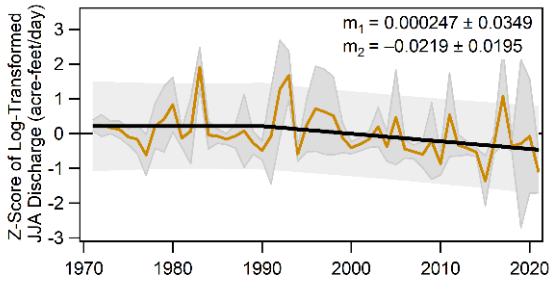
m1 = 0.000247 ± 0.0349
m2 = −0.0219 ± 0.0195
Z-Score of Log-Transformed JJA Discharge (acre-feet/day)
1970
1980
1990
2000
2010
2020

(d)

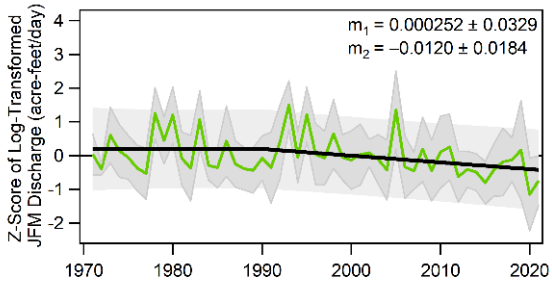
m1 = 0.000252 ± 0.0329
m2 = −0.0120 ± 0.0184
Z-Score of Log-Transformed JFM Discharge (acre-feet/day)
1970
1980
1990
2000
2010
2020

LOS PENASQUITOS C NR POWAY CA

Gauge Information	USGS Station ID	11023340
	Hydrologic Unit Code	18070304
	Latitude (NAD27)	32°56'35"
	Longitude (NAD27)	117°07'15"
	Drainage Area [Mi^2]	42.1
	Elevation of The Stream Outlet Above NAVD88 [Ft]	265
	County	San Diego
Watershed Characteristics	Mean Maximum January Temperature [°F]	66.58
	Mean Minimum January Temperature [°F]	40.76
	Mean Annual Precipitation [In]	15.4
	Hydrological Soil Group (HSG) [% of Covered Area]	C(93%), D(7%)
	Length of Longest Flow Path [Mi]	13
	Mean Basin Elevation [Ft]	861
	Maximum Basin Elevation [Ft]	2669
	Minimum Basin Elevation [Ft]	264
	Percentage of Area Above 6000 Ft [%]	0
	Percentage of Area Covered By Forest [%]	4.18
	Percentage of Lakes And Ponds [%]	0
	Percentage of Developed (Urban) Land (NLCD 2011 Classes 21-24) [%]	53.8
	Percentage of Imperviousness (NLCD 2001 Impervious Dataset) [%]	22.61
	Percentage of Imperviousness (NLCD 2011 Impervious Dataset) [%]	24.03
	Percentage of Imperviousness (NLCD 2019 Impervious Dataset) [%]	24.38
Stream Management Controls	Developed or Natural	Developed*
	Regulation	Regulated**
	Geological or Hydrological Control	None
	Dam Outlet	No
	Agricultural Control	None
	(Waste)water Inputs	Yes***
	Water Withdrawals	Yes***
	Other Factors Affecting Runoff	-

*Transition from natural to urban
** Flow partly regulated by several conservation reservoirs upstream from station.
***Pumping from wells along stream for irrigation. Flow augmented by reclaimed water from Poway area. Ref. waterdata.usgs.gov

(a)

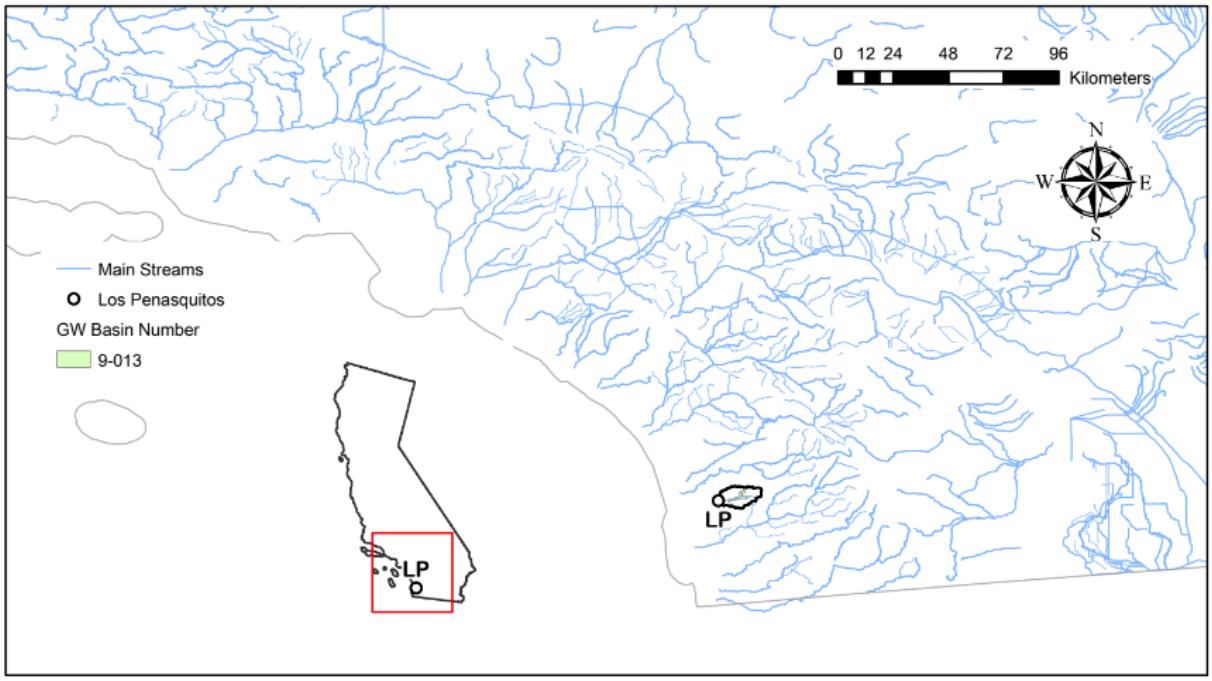
0 12 24 48 72 96
Kilometers
N
W
E
S
Main Streams
Los Penasquitos
GW Basin Number
9-013
LP
LP

(b)

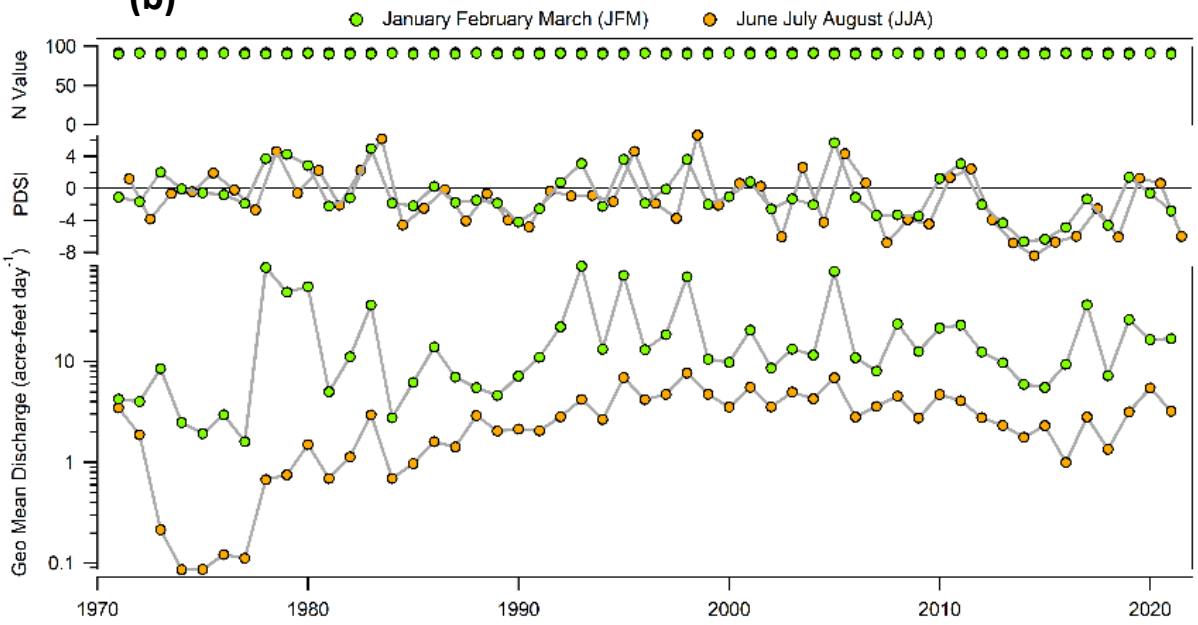
January February March (JFM)
June July August (JJA)
N Value
PDSI
Geo Mean Discharge (acre-feet day-1)
1970
1980
1990
2000
2010
2020

(c)

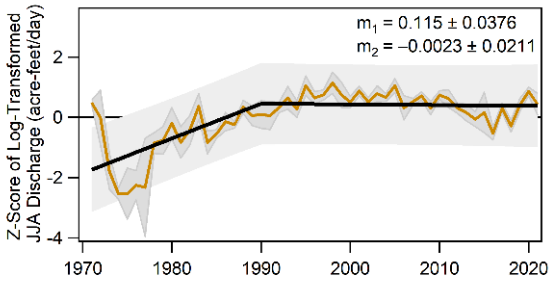
m1 = 0.115 ± 0.0376
m2 = –0.0023 ± 0.0211
Z-Score of Log-Transformed JJA Discharge (acre-feet/day)
1970
1980
1990
2000
2010
2020

(d)

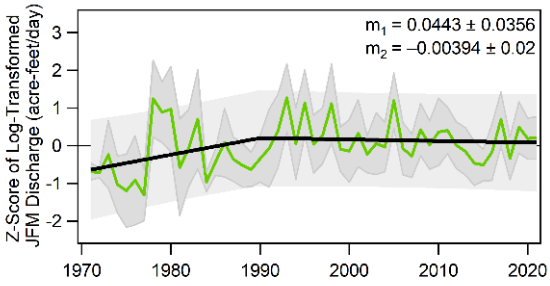
m1 = 0.0443 ± 0.0356
m2 = –0.00394 ± 0.02
Z-Score of Log-Transformed JFM Discharge (acre-feet/day)
1970
1980
1990
2000
2010
2020

ARROYO TRABUCO A SAN JUAN CAPISTRANO CA

Gauge Information	USGS Station ID	11047300
	Hydrologic Unit Code	18070301
	Latitude (NAD27)	33°29'54"
	Longitude (NAD27)	117°39'54"
	Drainage Area [Mi^2]	54.1
	Elevation of The Stream Outlet Above NAVD88 [Ft]	596
	County	Orange
Watershed Characteristics	Mean Maximum January Temperature [°F]	64.46
	Mean Minimum January Temperature [°F]	43.96
	Mean Annual Precipitation [In]	18.4
	Hydrological Soil Group (HSG) [% of Covered Area]	C(41%), D(59%)
	Length of Longest Flow Path [Mi]	24
	Mean Basin Elevation [Ft]	1386
	Maximum Basin Elevation [Ft]	5687
	Minimum Basin Elevation [Ft]	80
	Percentage of Area Above 6000 Ft [%]	0
	Percentage of Area Covered By Forest [%]	14
	Percentage of Lakes And Ponds [%]	0.4
	Percentage of Developed (Urban) Land (NLCD 2011 Classes 21-24) [%]	52.7
	Percentage of Imperviousness (NLCD 2001 Impervious Dataset) [%]	22.59
	Percentage of Imperviousness (NLCD 2011 Impervious Dataset) [%]	22.91
	Percentage of Imperviousness (NLCD 2019 Impervious Dataset) [%]	23.05
Stream Management Controls	Developed or Natural	Developed
	Regulation	Unregulated*
	Geological or Hydrological Control	None
	Dam Outlet	No
	Agricultural Control	None
	(Waste)water Inputs	None
	Water Withdrawals	None*
	Other Factors Affecting Runoff	Channelized**

*No regulation or diversion upstream from station. Ref. waterdata.usgs.gov
**Urban influence on runoff in lower watershed.

(a)

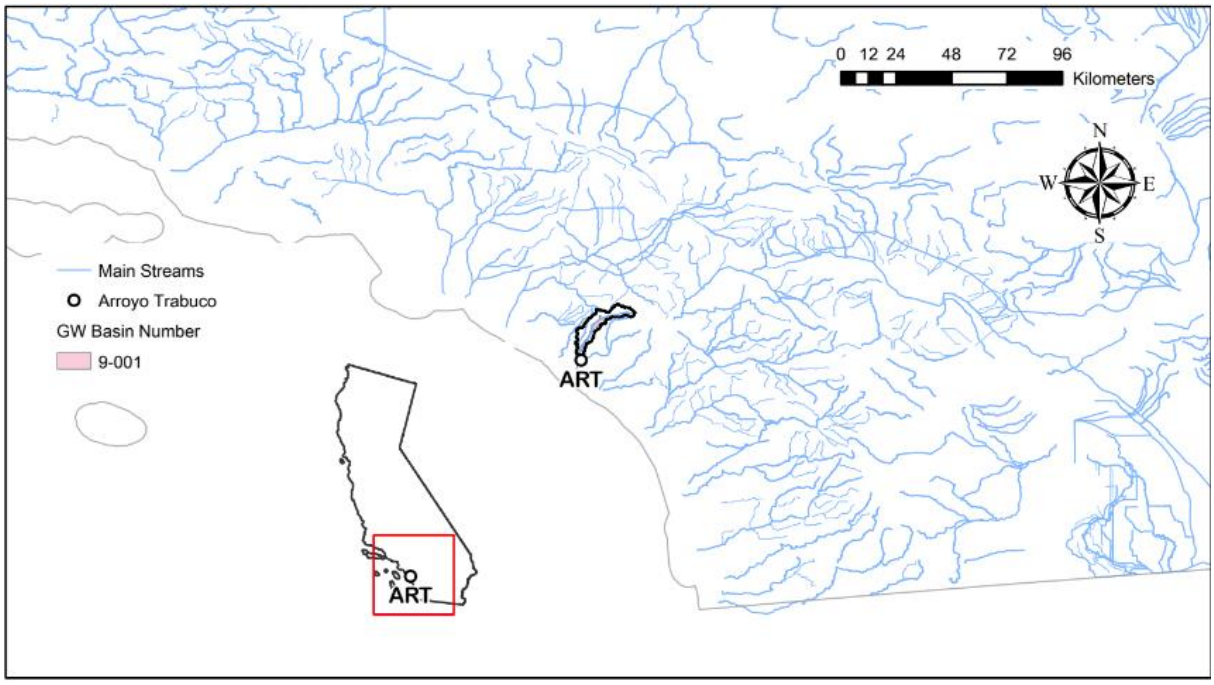
0 12 24 48 72 96
Kilometers
N
W
E
S
Main Streams
Arroyo Trabuco
GW Basin Number
9-001
ART
ART

(b)

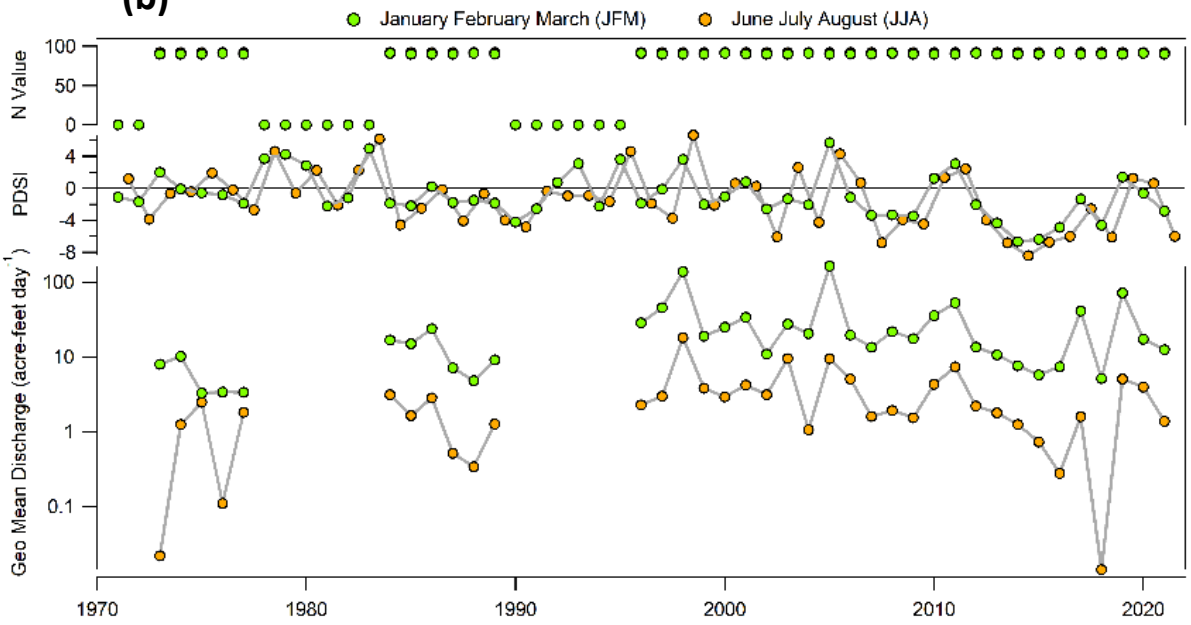
January February March (JFM)
June July August (JJA)
N Value
PDSI
Geo Mean Discharge (acre-feet day⁻¹)
1970
1980
1990
2000
2010
2020

(c)

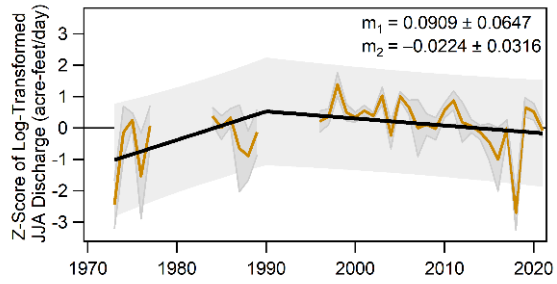
m1 = 0.0909 ± 0.0647
m2 = −0.0224 ± 0.0316
Z-Score of Log-Transformed JJA Discharge (acre-feet/day)
1970
1980
1990
2000
2010
2020

(d)

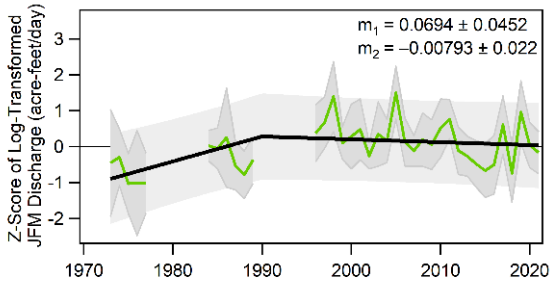
m1 = 0.0694 ± 0.0452
m2 = −0.00793 ± 0.022
Z-Score of Log-Transformed JFM Discharge (acre-feet/day)
1970
1980
1990
2000
2010
2020

CHINO C A SCHAEFER AVENUE NR CHINO CA

Gauge Information	USGS Station ID	11073360
	Hydrologic Unit Code	18070203
	Latitude (NAD27)	34°00'14"
	Longitude (NAD27)	117°43'34"
	Drainage Area [Mi^2]	48.9
	Elevation of The Stream Outlet Above NAVD88 [Ft]	679
	County	San Bernardino
Watershed Characteristics	Mean Maximum January Temperature [°F]	57.81
	Mean Minimum January Temperature [°F]	36.72
	Mean Annual Precipitation [In]	29.4
	Hydrological Soil Group (HSG) [% of Covered Area]	C(47%), D(53%)
	Length of Longest Flow Path [Mi]	24
	Mean Basin Elevation [Ft]	3441
	Maximum Basin Elevation [Ft]	10056
	Minimum Basin Elevation [Ft]	679
	Percentage of Area Above 6000 Ft [%]	22.6
	Percentage of Area Covered By Forest [%]	10.4
	Percentage of Lakes And Ponds [%]	0
	Percentage of Developed (Urban) Land (NLCD 2011 Classes 21-24) [%]	44.8
	Percentage of Imperviousness (NLCD 2001 Impervious Dataset) [%]	19.56
	Percentage of Imperviousness (NLCD 2011 Impervious Dataset) [%]	20.01
	Percentage of Imperviousness (NLCD 2019 Impervious Dataset) [%]	20.28
Stream Management Controls	Developed or Natural	Highly Developed
	Regulation	Regulated*
	Geological or Hydrological Control	None*
	Dam Outlet	No
	Agricultural Control	None
	(Waste)water Inputs	Yes**
	Water Withdrawals	Yes**
	Other Factors Affecting Runoff	Groundwater ***

*Upstream of Prado Dam; Flow mostly regulated by San Antonio Flood-Control Reservoir, capacity, 7,700 acre-ft. Since 1997, due to construction in area of gage, Schaefer Avenue no longer extends to the Chino Creek crossing. The Schaefer Avenue Bridge, however, remains.

**Natural streamflow affected by extensive groundwater withdrawals, diversions for power, domestic use, irrigation, and return flow from irrigated areas. Releases of imported water are made to the basin by the California Water Project at times in some years, via San Antonio Creek from Rialto Pipeline below San Antonio Dam, at a site approximately 11 mi upstream. During the current water year, the California Water Project reported no releases were made into the basin.

***Some influence of groundwater management.

Ref. waterdata.usgs.gov

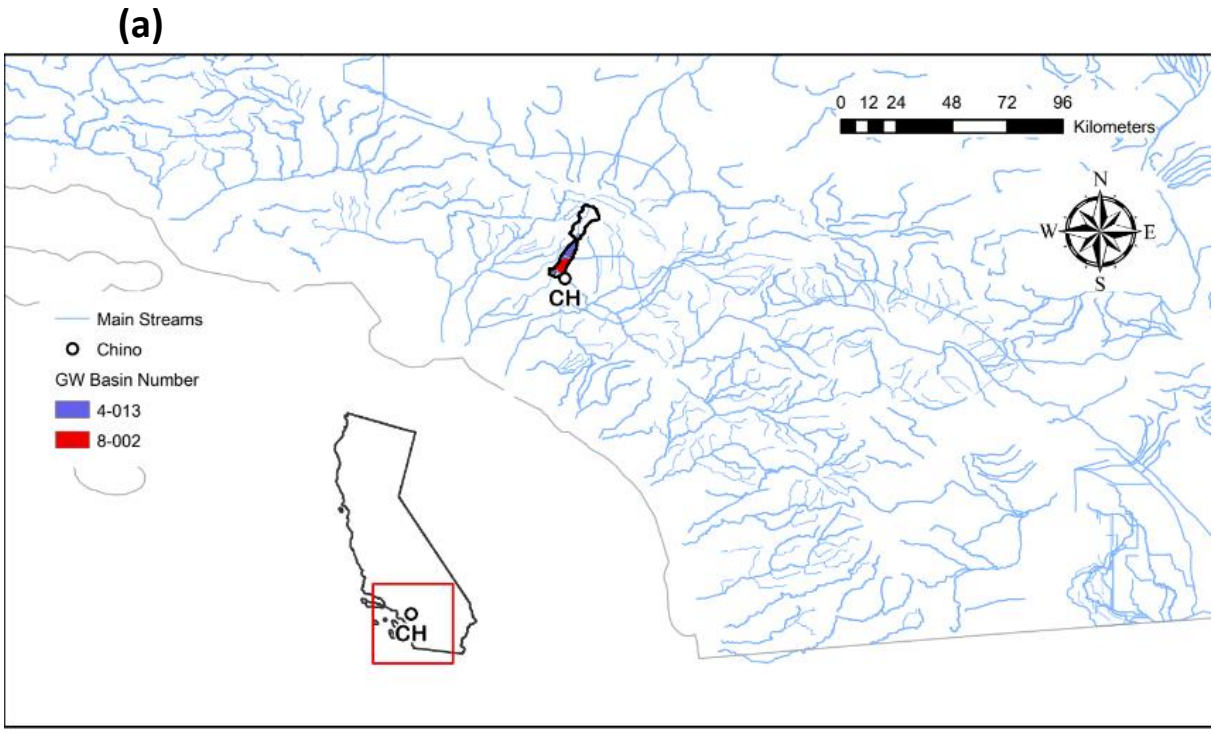
(a)
0 12 24 48 72 96
Kilometers
N
W
E
S
CH
Main Streams
Chino
GW Basin Number
4-013
8-002
CH

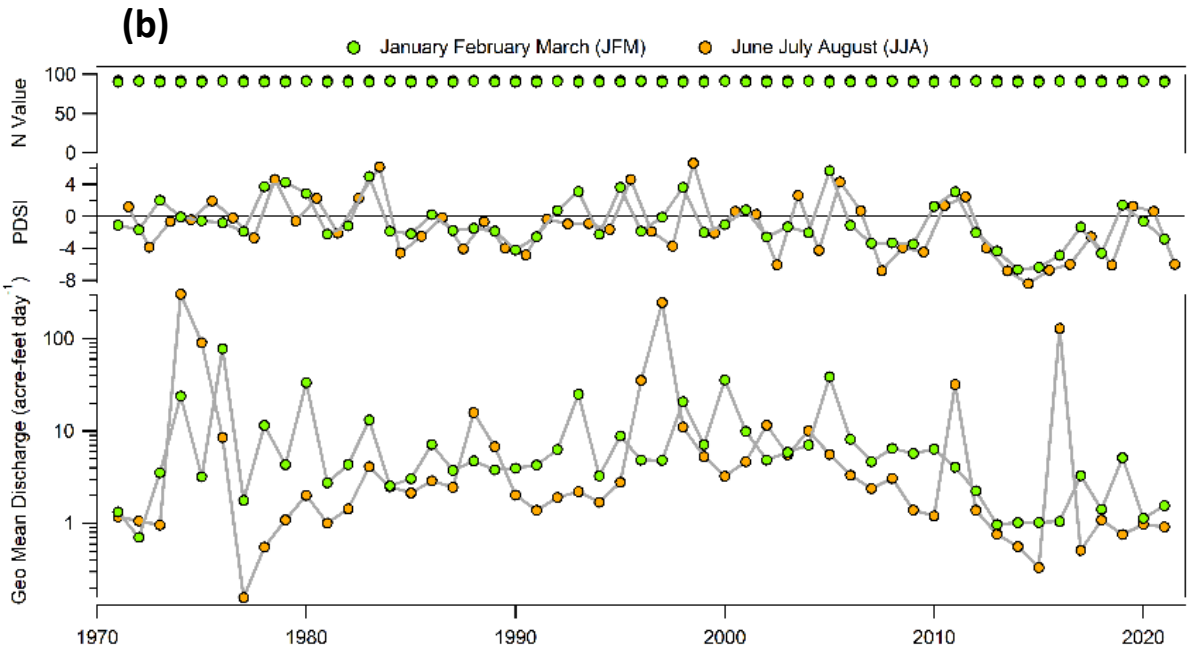
(b)
January February March (JFM)
June July August (JJA)
N Value
PDSI
Geo Mean Discharge (acre-feet day⁻¹)
1970
1980
1990
2000
2010
2020

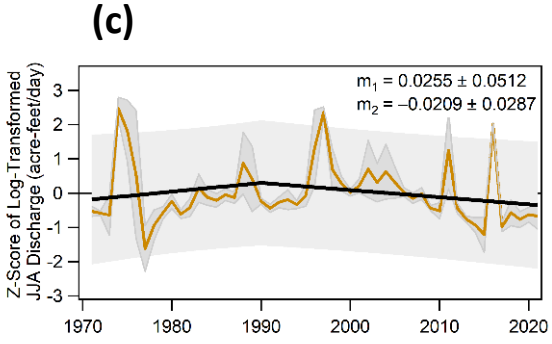
(c)
m1 = 0.0255 ± 0.0512
m2 = −0.0209 ± 0.0287
Z-Score of Log-Transformed JJA Discharge (acre-feet/day)
1970
1980
1990
2000
2010
2020

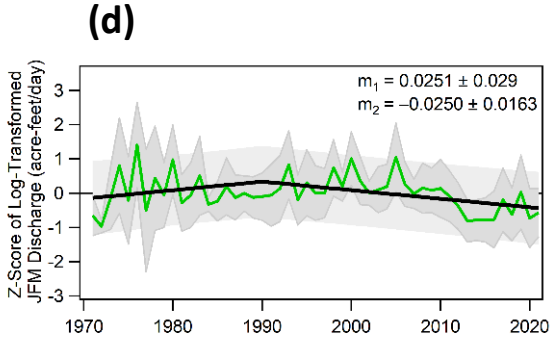
(d)
m1 = 0.0251 ± 0.029
m2 = −0.0250 ± 0.0163
Z-Score of Log-Transformed JFM Discharge (acre-feet/day)
1970
1980
1990
2000
2010
2020

BREA C BL BREA DAM NR FULLERTON CA

Gauge Information	USGS Station ID	11088500
	Hydrologic Unit Code	18070106
	Latitude (NAD27)	33°53'16"
	Longitude (NAD27)	117°55'32"
	Drainage Area [Mi^2]	21.6
	Elevation of The Stream Outlet Above NAVD88 [Ft]	210
	County	Los Angeles
Watershed Characteristics	Mean Maximum January Temperature [°F]	66.04
	Mean Minimum January Temperature [°F]	42.31
	Mean Annual Precipitation [In]	18.3
	Hydrological Soil Group (HSG) [% of Covered Area]	C(6%), D(94%)
	Length of Longest Flow Path [Mi]	16
	Mean Basin Elevation [Ft]	844
	Maximum Basin Elevation [Ft]	1463
	Minimum Basin Elevation [Ft]	210
	Percentage of Area Above 6000 Ft [%]	23.1
	Percentage of Area Covered By Forest [%]	14.4
	Percentage of Lakes And Ponds [%]	0.0646
	Percentage of Developed (Urban) Land (NLCD 2011 Classes 21-24) [%]	44.6
	Percentage of Imperviousness (NLCD 2001 Impervious Dataset) [%]	18.21
	Percentage of Imperviousness (NLCD 2011 Impervious Dataset) [%]	18.63
	Percentage of Imperviousness (NLCD 2019 Impervious Dataset) [%]	18.80
Stream Management Controls	Developed or Natural	Developed
	Regulation	Regulated*
	Geological or Hydrological Control	Yes
	Dam Outlet	Yes
	Agricultural Control	None
	(Waste)water Inputs	Yes**
	Water Withdrawals	None**
	Other Factors Affecting Runoff	Outlet of Brea Dam**

*Flow regulated and largely controlled by Brea Flood-Control Reservoir, capacity, 4,000 acre-ft.
**No diversion upstream from station. Since August 1966, low flow mostly the result of irrigation wastewater from golf course 0.8 mi upstream. Ref. waterdata.usgs.gov

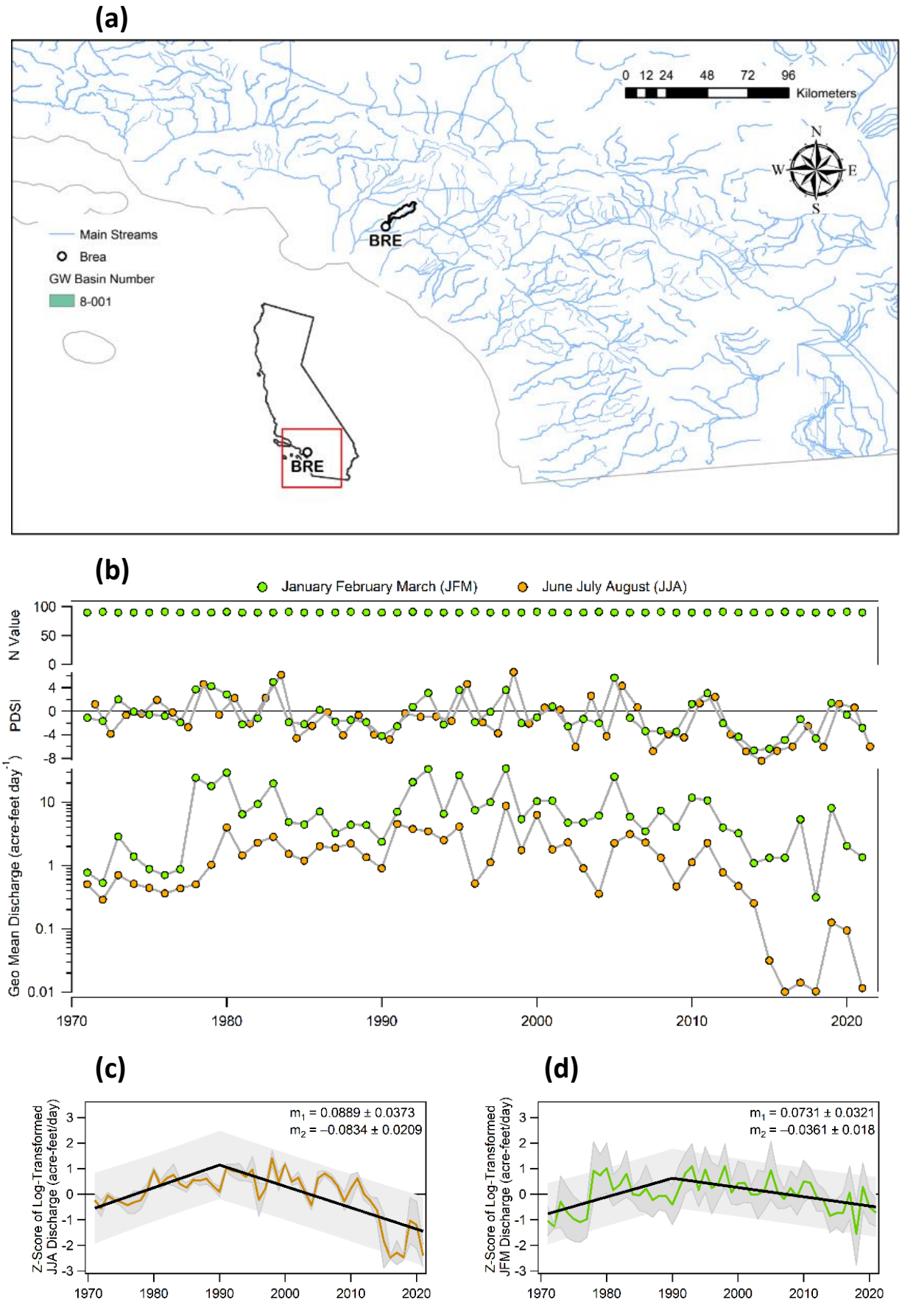
(a)
0 12 24 48 72 96
Kilometers
N
W
E
S
Main Streams
Brea
GW Basin Number
8-001
BRE
BRE
(b)
January February March (JFM)
June July August (JJA)
N Value
PDSI
Geo Mean Discharge (acre-feet day-1)
100
50
0
4
0
-4
-8
10
1
0.1
0.01
1970
1980
1990
2000
2010
2020
(c)
m1 = 0.0889 ± 0.0373
m2 = –0.0834 ± 0.0209
Z-Score of Log-Transformed JJA Discharge (acre-feet/day)
3
2
1
0
-1
-2
-3
1970
1980
1990
2000
2010
2020
(d)
m1 = 0.0731 ± 0.0321
m2 = –0.0361 ± 0.018
Z-Score of Log-Transformed JFM Discharge (acre-feet/day)
3
2
1
0
-1
-2
-3
1970
1980
1990
2000
2010
2020

SANTA ANA R BL PRADO DAM CA

Gauge Information	USGS Station ID	11074000
	Hydrologic Unit Code	18070203
	Latitude (NAD27)	33°53'00"
	Longitude (NAD27)	117°38'40"
	Drainage Area [Mi^2]	2258 (Contributing DA, 1490 Mi^2)
	Elevation of The Stream Outlet Above NAVD88 [Ft]	451
	County	Riverside
Watershed Characteristics	Mean Maximum January Temperature [°F]	60.41
	Mean Minimum January Temperature [°F]	36.09
	Mean Annual Precipitation [In]	19.8
	Hydrological Soil Group (HSG) [% of Covered Area]	C(67%), D(33%)
	Length of Longest Flow Path [Mi]	109
	Mean Basin Elevation [Ft]	2833
	Maximum Basin Elevation [Ft]	11420
	Minimum Basin Elevation [Ft]	451
	Percentage of Area Above 6000 Ft [%]	11.5
	Percentage of Area Covered By Forest [%]	9.67
	Percentage of Lakes And Ponds [%]	0.79
	Percentage of Developed (Urban) Land (NLCD 2011 Classes 21-24) [%]	35.7
	Percentage of Imperviousness (NLCD 2001 Impervious Dataset) [%]	15.74
	Percentage of Imperviousness (NLCD 2011 Impervious Dataset) [%]	17.75
	Percentage of Imperviousness (NLCD 2019 Impervious Dataset) [%]	18.71
Stream Management Controls	Developed or Natural	Developed
	Regulation	Regulated*
	Geological or Hydrological Control	Yes**
	Dam Outlet	Yes
	Agricultural Control	None
	(Waste)water Inputs	Yes**
	Water Withdrawals	Yes**
	Other Factors Affecting Runoff	Golf Course Runoff*

*Lower watershed is highly developed. Flow regulated since 1940 by Prado Flood-Control Reservoir (Prado Dam), capacity, 196,200 acre-ft, which released flood water only twice during the last 10 years. Dry weather release from the Dam is mostly for groundwater infiltration, which dries up around Angel Stadium and does not propagate further downstream.
**Natural streamflow affected by extensive groundwater withdrawals, diversion for irrigation, discharges of treated effluent, and return flow from irrigated areas (Most flows into the stream are urban runoff downstream of the golf course). Releases of imported water are also made to the basin by the California Water Project at times in some years, via San Antonio Creek from Rialto Pipeline below San Antonio Dam. The latest release according to the USGS water data was 12,780 acre-ft.
Ref. waterdata.usgs.gov

(a)

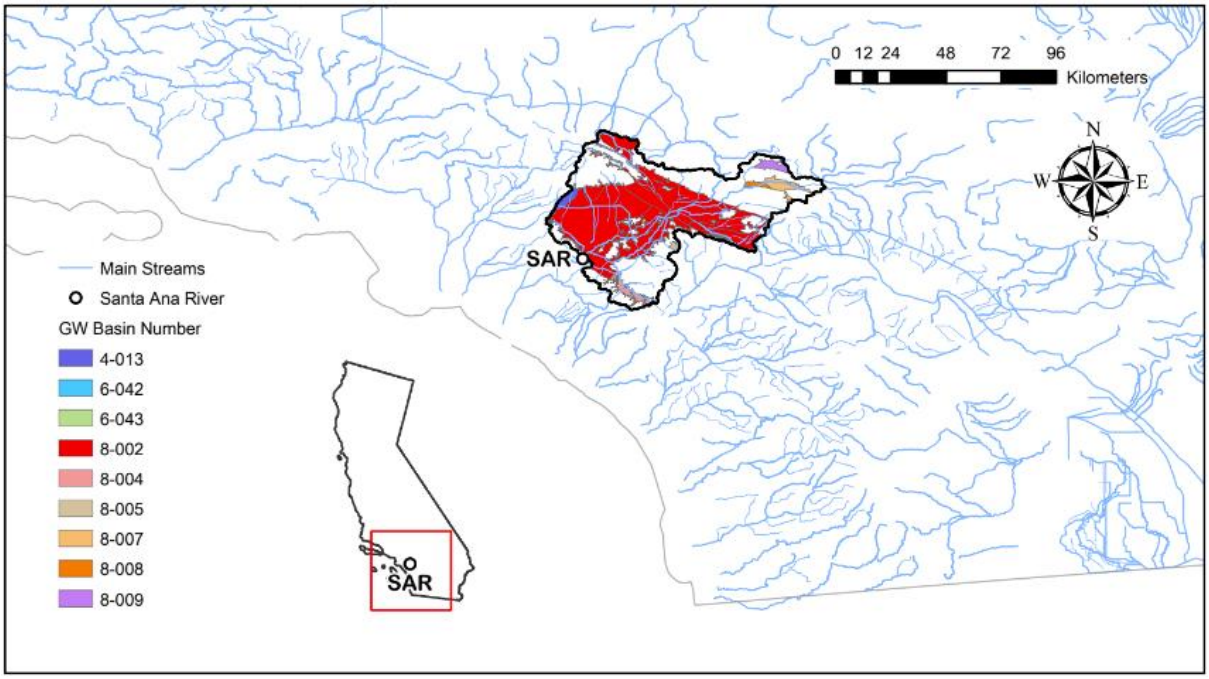
0 12 24 48 72 96
Kilometers
N
W
E
S
SAR
Main Streams
Santa Ana River
GW Basin Number
4-013
6-042
6-043
8-002
8-004
8-005
8-007
8-008
8-009
SAR

(b)

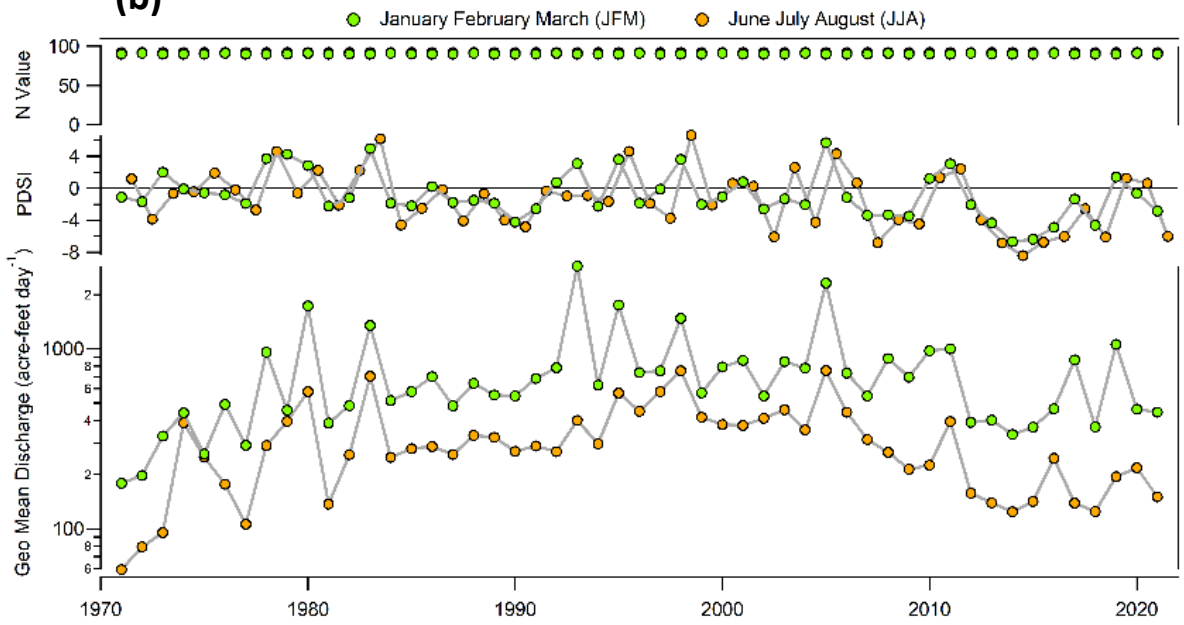
January February March (JFM)
June July August (JJA)
N Value
PDSI
Geo Mean Discharge (acre-feet day-1)
1970
1980
1990
2000
2010
2020

(c)

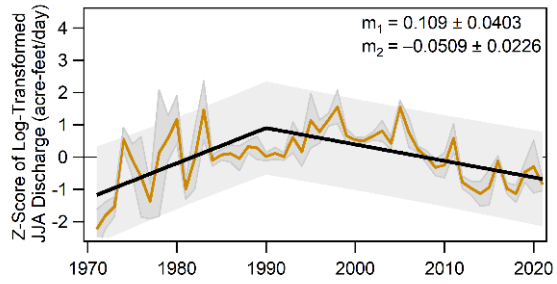
m1 = 0.109 ± 0.0403
m2 = −0.0509 ± 0.0226
Z-Score of Log-Transformed JJA Discharge (acre-feet/day)
1970
1980
1990
2000
2010
2020

(d)

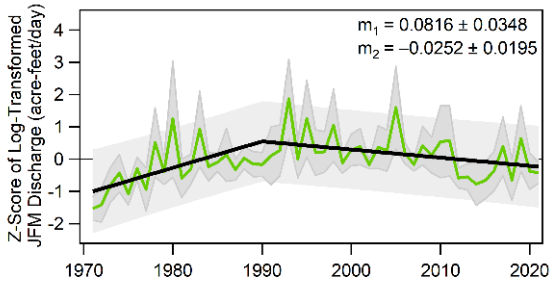
m1 = 0.0816 ± 0.0348
m2 = −0.0252 ± 0.0195
Z-Score of Log-Transformed JFM Discharge (acre-feet/day)
1970
1980
1990
2000
2010
2020

SAN GABRIEL R AB WHITTIER NARROWS DAM CA

Gauge Information	USGS Station ID	11087020
	Hydrologic Unit Code	18070106
	Latitude (NAD27)	34°02'03"
	Longitude (NAD27)	118°02'14"
	Drainage Area [Mi^2]	442
	Elevation of The Stream Outlet Above NAVD88 [Ft]	219
	County	Los Angeles
Watershed Characteristics	Mean Maximum January Temperature [°F]	59.26
	Mean Minimum January Temperature [°F]	38.99
	Mean Annual Precipitation [In]	28.2
	Hydrological Soil Group (HSG) [% of Covered Area]	C(26%), D(74%)
	Length of Longest Flow Path [Mi]	47
	Mean Basin Elevation [Ft]	2791
	Maximum Basin Elevation [Ft]	10059
	Minimum Basin Elevation [Ft]	219
	Percentage of Area Above 6000 Ft [%]	10.5
	Percentage of Area Covered By Forest [%]	17.4
	Percentage of Lakes And Ponds [%]	0.33
	Percentage of Developed (Urban) Land (NLCD 2011 Classes 21-24) [%]	35.1
	Percentage of Imperviousness (NLCD 2001 Impervious Dataset) [%]	16.77
	Percentage of Imperviousness (NLCD 2011 Impervious Dataset) [%]	17.20
	Percentage of Imperviousness (NLCD 2019 Impervious Dataset) [%]	17.34
Stream Management Controls	Developed or Natural	Developed
	Regulation	Regulated*
	Geological or Hydrological Control	Yes
	Dam Outlet	No
	Agricultural Control	None
	(Waste)water Inputs	Yes**
	Water Withdrawals	Yes**
	Other Factors Affecting Runoff	Wastewater Discharge

*Flow regulated by several reservoirs, combined capacity, 123,000 acre-ft.

**Many diversions upstream from station for irrigation, power development, and groundwater replenishment. Colorado River water released to the San Gabriel River at site 14.9 mi upstream from gage, at Metropolitan Water District aqueduct crossing on San Dimas Creek for groundwater replenishment. Los Angeles County Department of Public Works diversion from San Gabriel River below Santa Fe Dam (11085000) to Rio Hondo during water year:

2014 - no diversion
2015 - no diversion
2016 - 801 acre-feet
2017 - 53,700 acre-feet
2018 - 6,480 acre-feet
2019 - 50,100 acre-feet
2020 - 34,500 acre-feet
2021 - 6,360 acre-feet

Ref. waterdata.usgs.gov

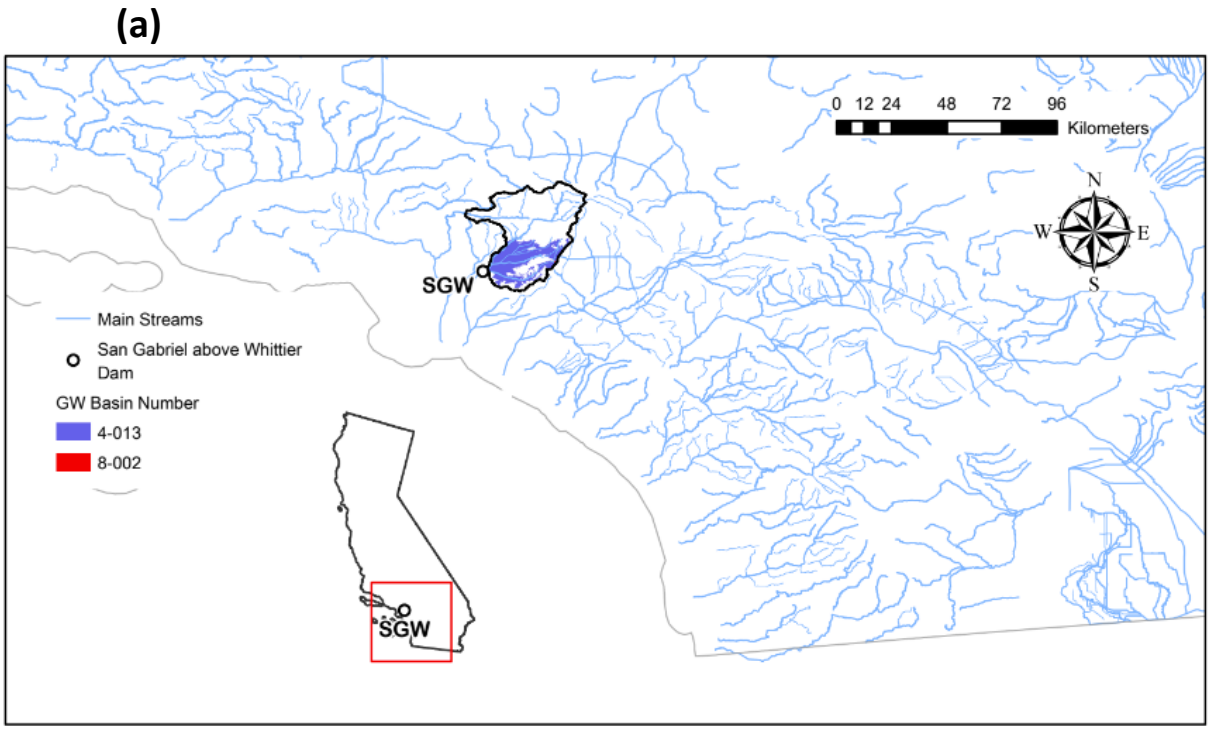
(a)
0 12 24 48 72 96
Kilometers
N
W
E
S
SGW
Main Streams
San Gabriel above Whittier Dam
GW Basin Number
4-013
8-002
SGW

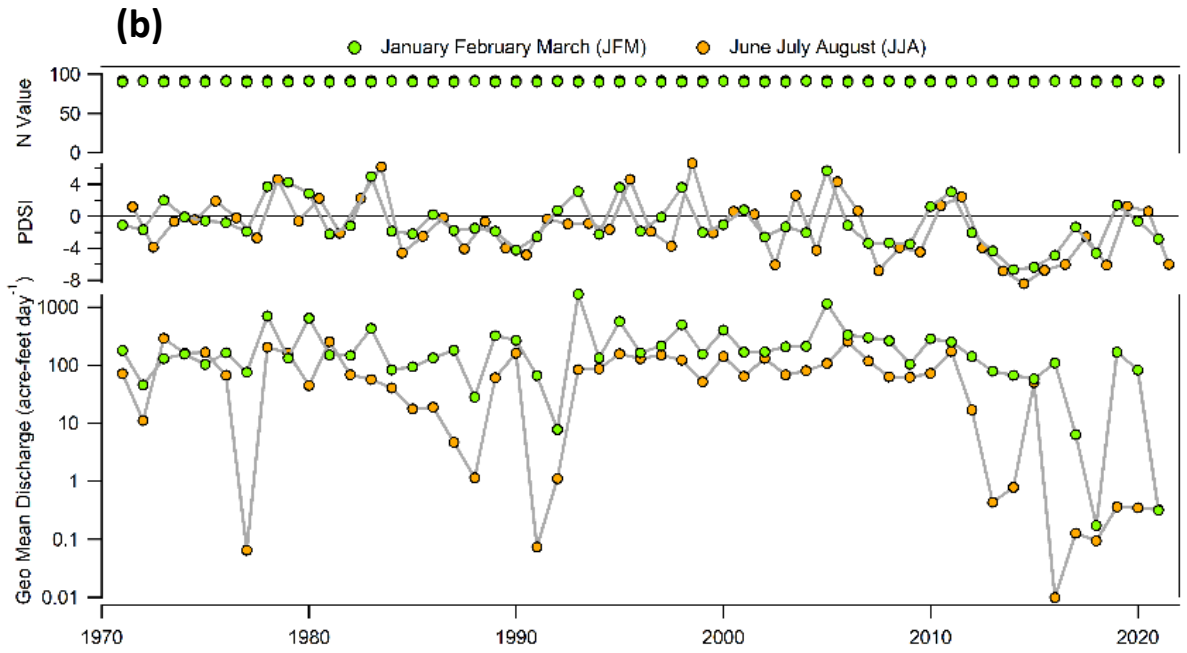
(b)
January February March (JFM)
June July August (JJA)
N Value
PDSI
Geo Mean Discharge (acre-feet day-1)
1970
1980
1990
2000
2010
2020

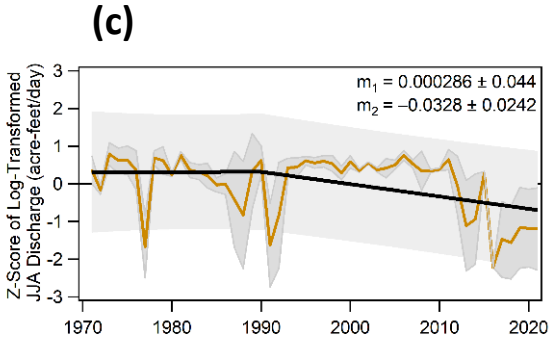
(c)
m1 = 0.000286 ± 0.044
m2 = −0.0328 ± 0.0242
Z-Score of Log-Transformed JJA Discharge (acre-feet/day)
1970
1980
1990
2000
2010
2020

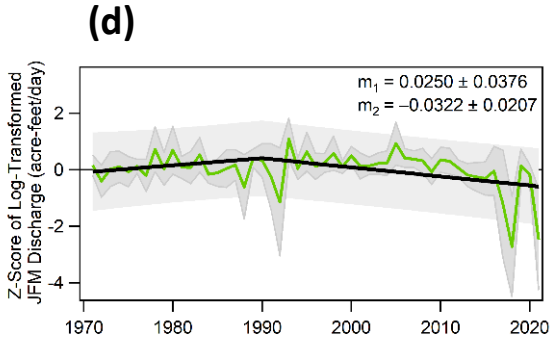
(d)
m1 = 0.0250 ± 0.0376
m2 = −0.0322 ± 0.0207
Z-Score of Log-Transformed JFM Discharge (acre-feet/day)
1970
1980
1990
2000
2010
2020

SANTA ANA R A SANTA ANA CA (SAR d/s)

Gauge Information	USGS Station ID	11078000
	Hydrologic Unit Code	18070203
	Latitude (NAD27)	33°45'04"
	Longitude (NAD27)	117°54'27"
	Drainage Area [Mi^2]	1700
	Elevation of The Stream Outlet Above NAVD88 [Ft]	79
	County	Orange
Watershed Characteristics	Mean Maximum January Temperature [°F]	60.67
	Mean Minimum January Temperature [°F]	36.62
	Mean Annual Precipitation [In]	19.8
	Hydrological Soil Group (HSG) [% of Covered Area]	C(67%), D(33%)
	Length of Longest Flow Path [Mi]	132
	Mean Basin Elevation [Ft]	2730
	Maximum Basin Elevation [Ft]	11420
	Minimum Basin Elevation [Ft]	78
	Percentage of Area Above 6000 Ft [%]	10.7
	Percentage of Area Covered By Forest [%]	9.93
	Percentage of Lakes And Ponds [%]	0.78
	Percentage of Developed (Urban) Land (NLCD 2011 Classes 21-24) [%]	35.6
	Percentage of Imperviousness (NLCD 2001 Impervious Dataset) [%]	12.19
	Percentage of Imperviousness (NLCD 2011 Impervious Dataset) [%]	13.95
	Percentage of Imperviousness (NLCD 2019 Impervious Dataset) [%]	14.81
Stream Management Controls	Developed or Natural	Developed
	Regulation	Regulated*
	Geological or Hydrological Control	Yes*
	Dam Outlet	No
	Agricultural Control	None
	(Waste)water Inputs	Yes**
	Water Withdrawals	Yes**
	Other Factors Affecting Runoff	Channelized Floodway***; Irrigation

*Since 1940, flow partially regulated by Prado Flood-Control Reservoir, capacity, 217,000 acre-ft. Natural flow affected by three small flood-control reservoirs, combined capacity, 31,900 acre-ft; Big Bear Lake (station 11049000), capacity, 73,000 acre-ft; Seven Oaks Flood-Control Reservoir, capacity, 145,600 acre-ft; and Santiago Reservoir, capacity, 25,000 acre-ft. Discharge up to 100 ft^3/s can be diverted from Carbon Creek to Coyote Creek 1.5 mi upstream from mouth of Carbon Creek.

**Natural flow affected by groundwater withdrawals, diversions, importation by Metropolitan Water District, municipal use, and return flow from irrigation. Gauge is located downstream of Santa Ana River at East street (station 11059300), thus influenced by effluent from sewage reclamation plant.

***Gage out of operation from Apr. 5, to Nov. 14, 1994, due to channel work (lining).

Ref. waterdata.usgs.gov

(a)

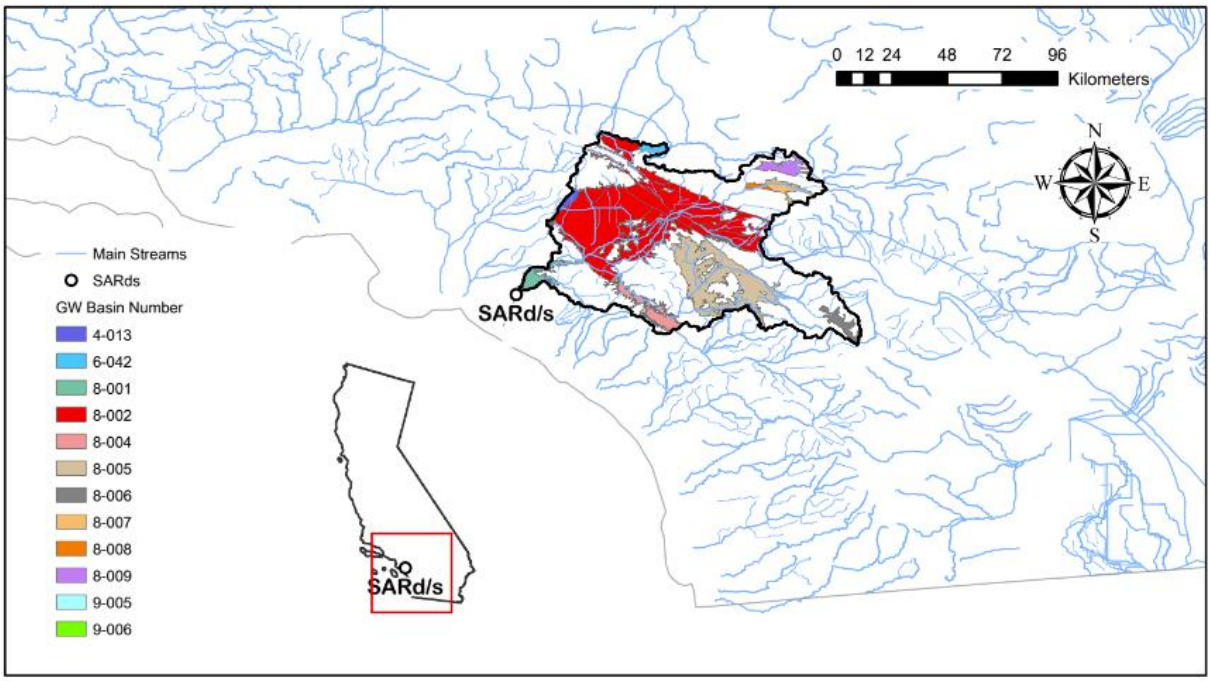
0 12 24 48 72 96
Kilometers
N
W
E
S
Main Streams
SARds
GW Basin Number
4-013
6-042
8-001
8-002
8-004
8-005
8-006
8-007
8-008
8-009
9-005
9-006
SARd/s
SARd/s

(b)

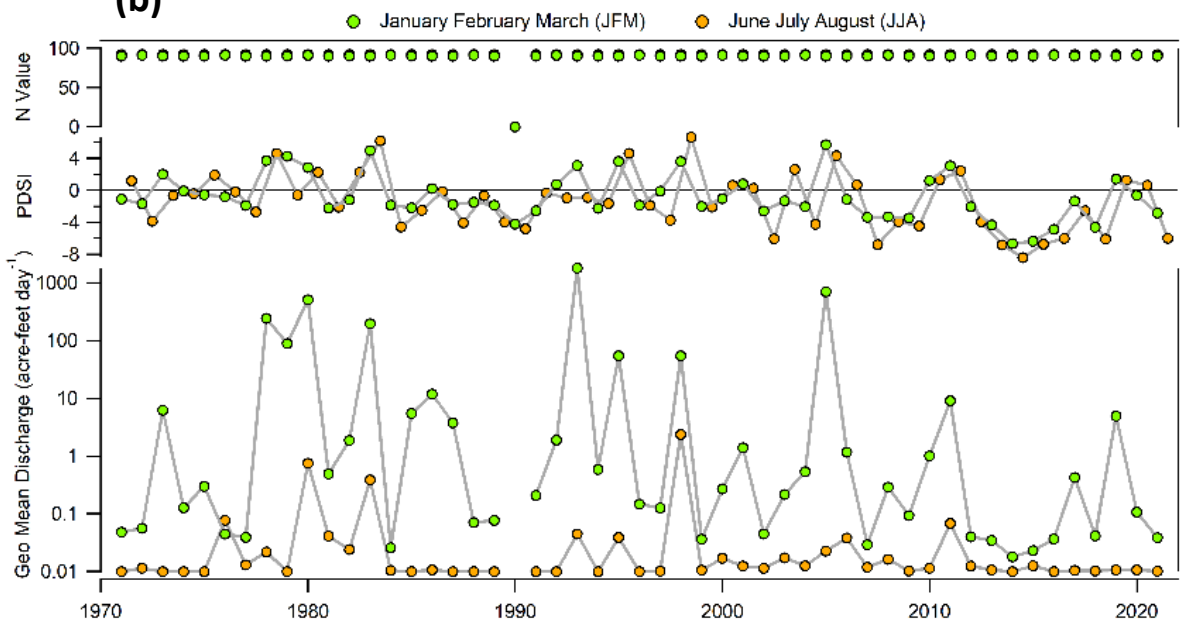
January February March (JFM)
June July August (JJA)
N Value
PDSI
Geo Mean Discharge (acre-feet day-1)
1970
1980
1990
2000
2010
2020

(c)

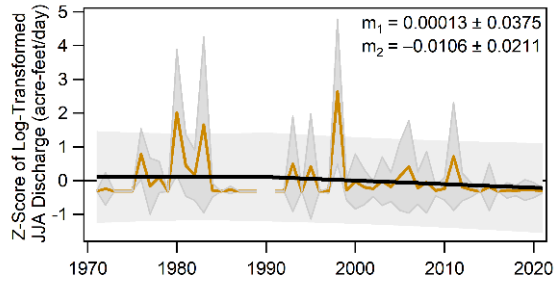
m1 = 0.00013 ± 0.0375
m2 = –0.0106 ± 0.0211
Z-Score of Log-Transformed JJA Discharge (acre-feet/day)
1970
1980
1990
2000
2010
2020

(d)

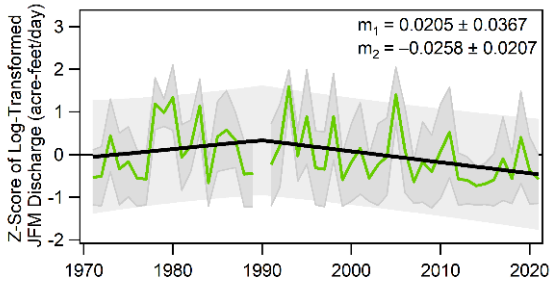
m1 = 0.0205 ± 0.0367
m2 = –0.0258 ± 0.0207
Z-Score of Log-Transformed JFM Discharge (acre-feet/day)
1970
1980
1990
2000
2010
2020

LOS COCHES C NR LAKESIDE CA

Gauge Information	USGS Station ID	11022200
	Hydrologic Unit Code	18070304
	Latitude (NAD27)	32°50'10"
	Longitude (NAD27)	116°53'58"
	Drainage Area [Mi^2]	12.2
	Elevation of The Stream Outlet Above NAVD88 [Ft]	596
	County	San Diego
Watershed Characteristics	Mean Maximum January Temperature [°F]	66.06
	Mean Minimum January Temperature [°F]	40.05
	Mean Annual Precipitation [In]	17.4
	Hydrological Soil Group (HSG) [% of Covered Area]	C(100%)
	Length of Longest Flow Path [Mi]	7
	Mean Basin Elevation [Ft]	1204
	Maximum Basin Elevation [Ft]	2237
	Minimum Basin Elevation [Ft]	544
	Percentage of Area Above 6000 Ft [%]	0
	Percentage of Area Covered By Forest [%]	6.6
	Percentage of Lakes And Ponds [%]	0
	Percentage of Developed (Urban) Land (NLCD 2011 Classes 21-24) [%]	41.1
	Percentage of Imperviousness (NLCD 2001 Impervious Dataset) [%]	10.51
	Percentage of Imperviousness (NLCD 2011 Impervious Dataset) [%]	11.41
	Percentage of Imperviousness (NLCD 2019 Impervious Dataset) [%]	11.69
Stream Management Controls	Developed or Natural	Developed
	Regulation	Unregulated*
	Geological or Hydrological Control	None
	Dam Outlet	No
	Agricultural Control	None
	(Waste)water Inputs	None
	Water Withdrawals	None*
	Other Factors Affecting Runoff	-

*No regulation or diversion upstream from station. Minimum daily discharge is 0.01 ft^3/s many days from 2014-2016. Ref. waterdata.usgs.gov

(a)

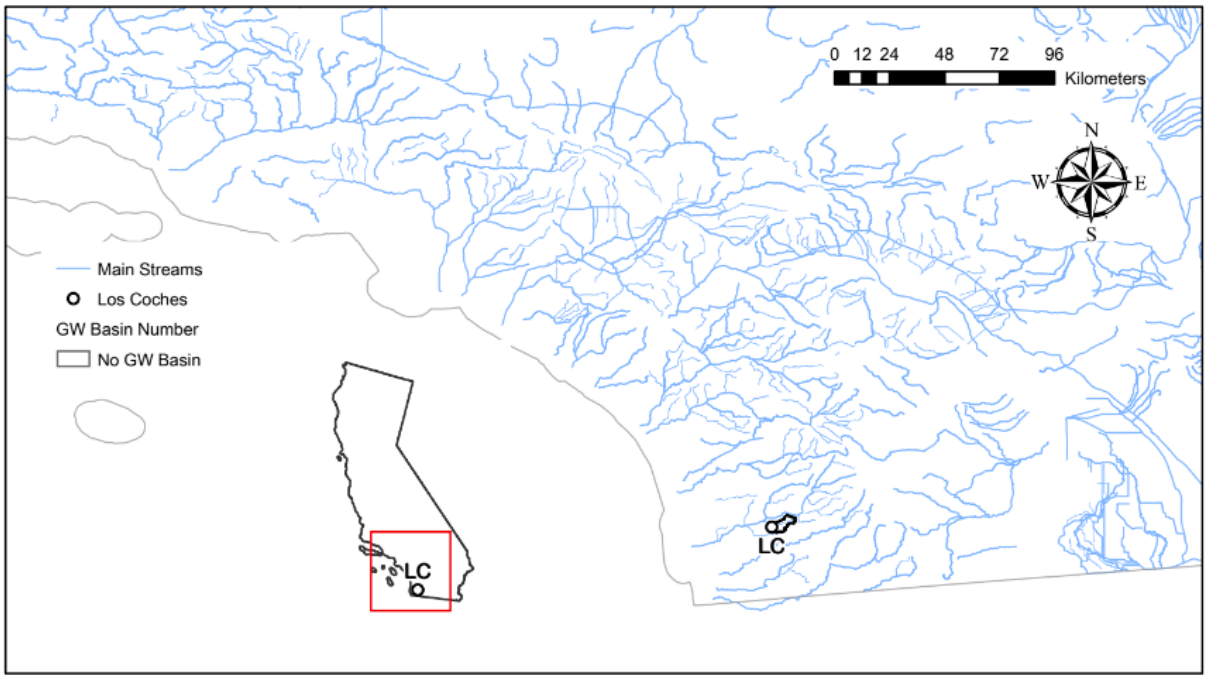
0 12 24 48 72 96
Kilometers
N
W
E
S
Main Streams
Los Coches
GW Basin Number
No GW Basin
LC
LC

(b)

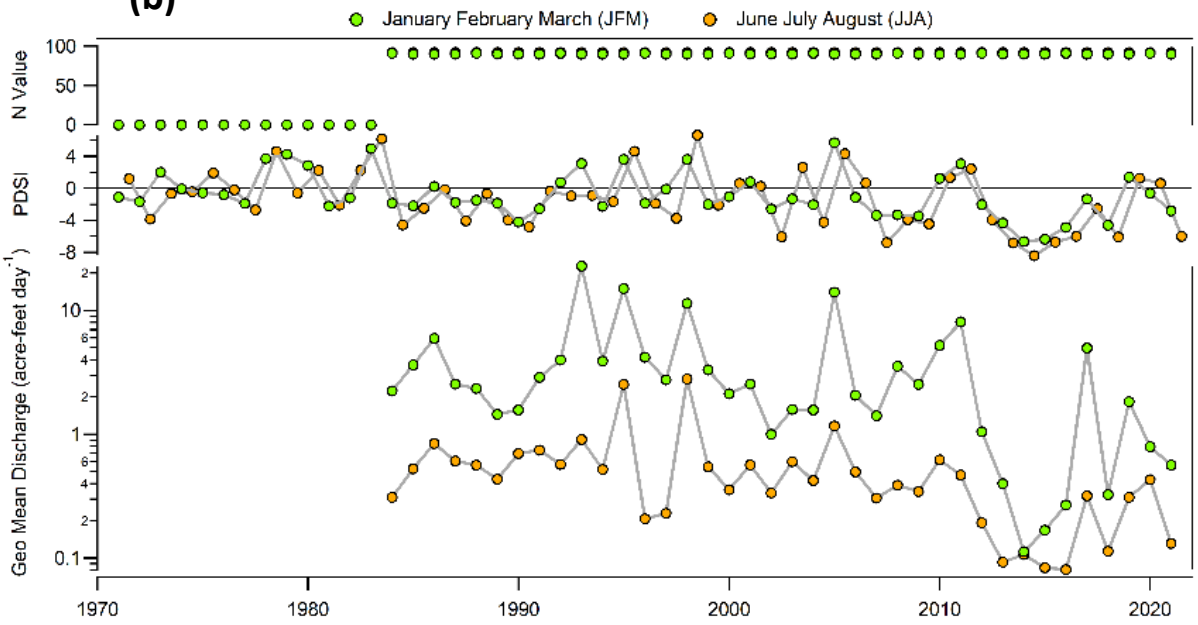
January February March (JFM)
June July August (JJA)
N Value
PDSI
Geo Mean Discharge (acre-feet day-1)
1970
1980
1990
2000
2010
2020

(c)

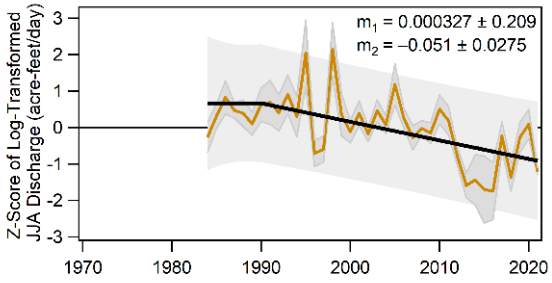
m1 = 0.000327 ± 0.209
m2 = –0.051 ± 0.0275
Z-Score of Log-Transformed JJA Discharge (acre-feet/day)
1970
1980
1990
2000
2010
2020

(d)

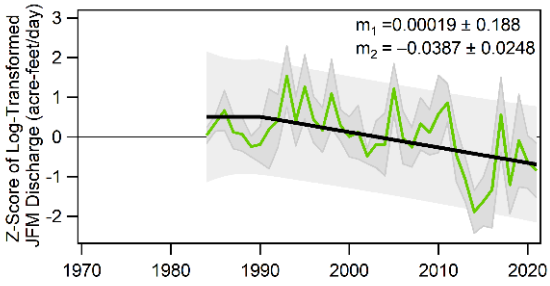
m1 =0.00019 ± 0.188
m2 = –0.0387 ± 0.0248
Z-Score of Log-Transformed JFM Discharge (acre-feet/day)
1970
1980
1990
2000
2010
2020

MURRIETA C A TEMECULA CA

Gauge Information	USGS Station ID	11043000
	Hydrologic Unit Code	18070302
	Latitude (NAD27)	33°28'47"
	Longitude (NAD27)	117°08'35"
	Drainage Area [Mi^2]	222
	Elevation of The Stream Outlet Above NAVD88 [Ft]	973
	County	Riverside
Watershed Characteristics	Mean Maximum January Temperature [°F]	65.05
	Mean Minimum January Temperature [°F]	38.61
	Mean Annual Precipitation [In]	14.7
	Hydrological Soil Group (HSG) [% of Covered Area]	C(84%), D(16%)
	Length of Longest Flow Path [Mi]	31
	Mean Basin Elevation [Ft]	1710
	Maximum Basin Elevation [Ft]	4566
	Minimum Basin Elevation [Ft]	973
	Percentage of Area Above 6000 Ft [%]	0
	Percentage of Area Covered By Forest [%]	2.74
	Percentage of Lakes And Ponds [%]	3.52
	Percentage of Developed (Urban) Land (NLCD 2011 Classes 21-24) [%]	34.3
	Percentage of Imperviousness (NLCD 2001 Impervious Dataset) [%]	7.31
	Percentage of Imperviousness (NLCD 2011 Impervious Dataset) [%]	10.61
	Percentage of Imperviousness (NLCD 2019 Impervious Dataset) [%]	11.52
Stream Management Controls	Developed or Natural	Developed
	Regulation	Regulated
	Geological or Hydrological Control	Yes*
	Dam Outlet	No
	Agricultural Control	None
	(Waste)water Inputs	None
	Water Withdrawals	None
	Other Factors Affecting Runoff	-

*Tributaries are hydrologically controlled; This reach is bedrock controlled.
**No flow during many days in several years.
Ref. waterdata.usgs.gov

(a)

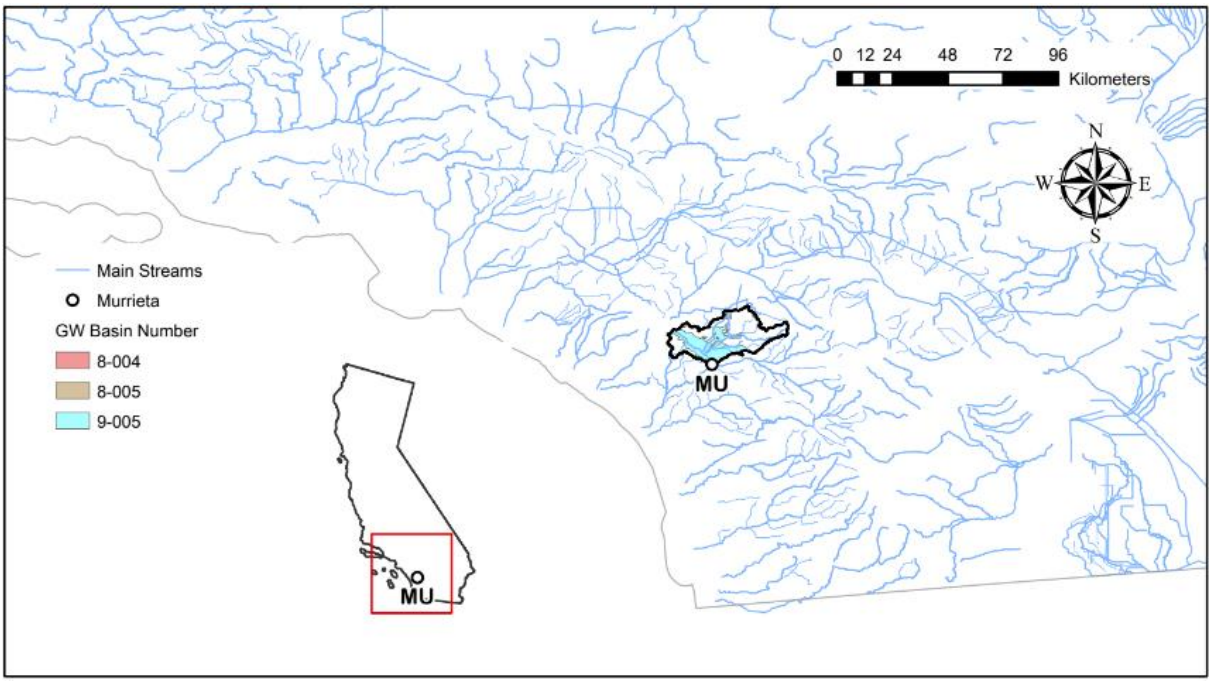
0 12 24 48 72 96
Kilometers
N
W
E
S
Main Streams
Murrieta
GW Basin Number
8-004
8-005
9-005
MU
MU

(b)

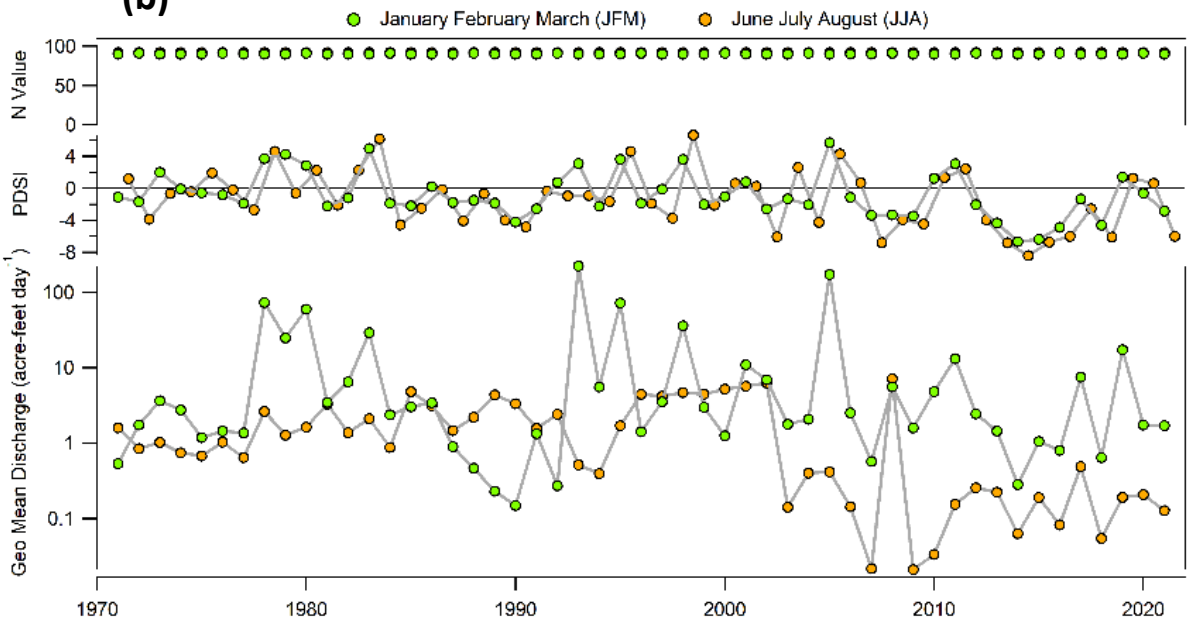
January February March (JFM)
June July August (JJA)
N Value
PDSI
Geo Mean Discharge (acre-feet day⁻¹)
1970
1980
1990
2000
2010
2020

(c)

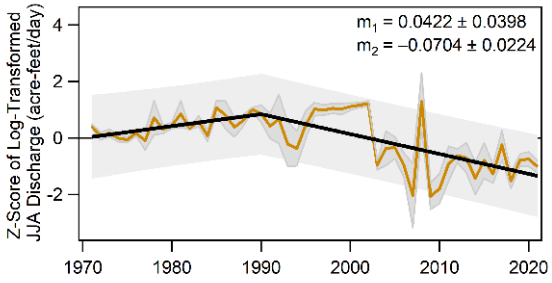
m1 = 0.0422 ± 0.0398
m2 = −0.0704 ± 0.0224
Z-Score of Log-Transformed JJA Discharge (acre-feet/day)
1970
1980
1990
2000
2010
2020

(d)

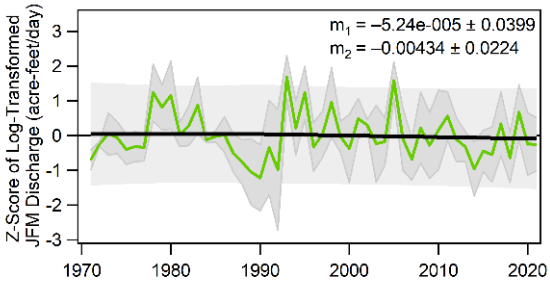
m1 = −5.24e-005 ± 0.0399
m2 = −0.00434 ± 0.0224
Z-Score of Log-Transformed JFM Discharge (acre-feet/day)
1970
1980
1990
2000
2010
2020

SAN DIEGO R A FASHION VALLEY AT SAN DIEGO CA

Gauge Information	USGS Station ID	11023000
	Hydrologic Unit Code	18070304
	Latitude (NAD27)	32°45'54"
	Longitude (NAD27)	117°10'04"
	Drainage Area [Mi^2]	429
	Elevation of The Stream Outlet Above NAVD88 [Ft]	22
	County	San Diego
Watershed Characteristics	Mean Maximum January Temperature [°F]	62.82
	Mean Minimum January Temperature [°F]	38.74
	Mean Annual Precipitation [In]	19.5
	Hydrological Soil Group (HSG) [% of Covered Area]	C(55%), D(45%)
	Length of Longest Flow Path [Mi]	53
	Mean Basin Elevation [Ft]	1867
	Maximum Basin Elevation [Ft]	6492
	Minimum Basin Elevation [Ft]	22
	Percentage of Area Above 6000 Ft [%]	0.0574
	Percentage of Area Covered By Forest [%]	11
	Percentage of Lakes And Ponds [%]	0.79
	Percentage of Developed (Urban) Land (NLCD 2011 Classes 21-24) [%]	25.9
	Percentage of Imperviousness (NLCD 2001 Impervious Dataset) [%]	10.87
	Percentage of Imperviousness (NLCD 2011 Impervious Dataset) [%]	11.13
	Percentage of Imperviousness (NLCD 2019 Impervious Dataset) [%]	11.29
Stream Management Controls	Developed or Natural	Developed*
	Regulation	Regulated**
	Geological or Hydrological Control	Yes
	Dam Outlet	No
	Agricultural Control	None
	(Waste)water Inputs	None
	Water Withdrawals	Yes***
	Other Factors Affecting Runoff	-

*Natural stream flowing through developed watershed.
**Flow regulated by upstream dams (i.e., Cuyamaca Reservoir, capacity, 11,740 acre-ft; El Capitan Reservoir (station 11020600), and San Vicente Reservoir (station 11022100)).
***Diversions by city of San Diego for municipal supply and by Helix Irrigation District.
Ref. waterdata.usgs.gov

(a)

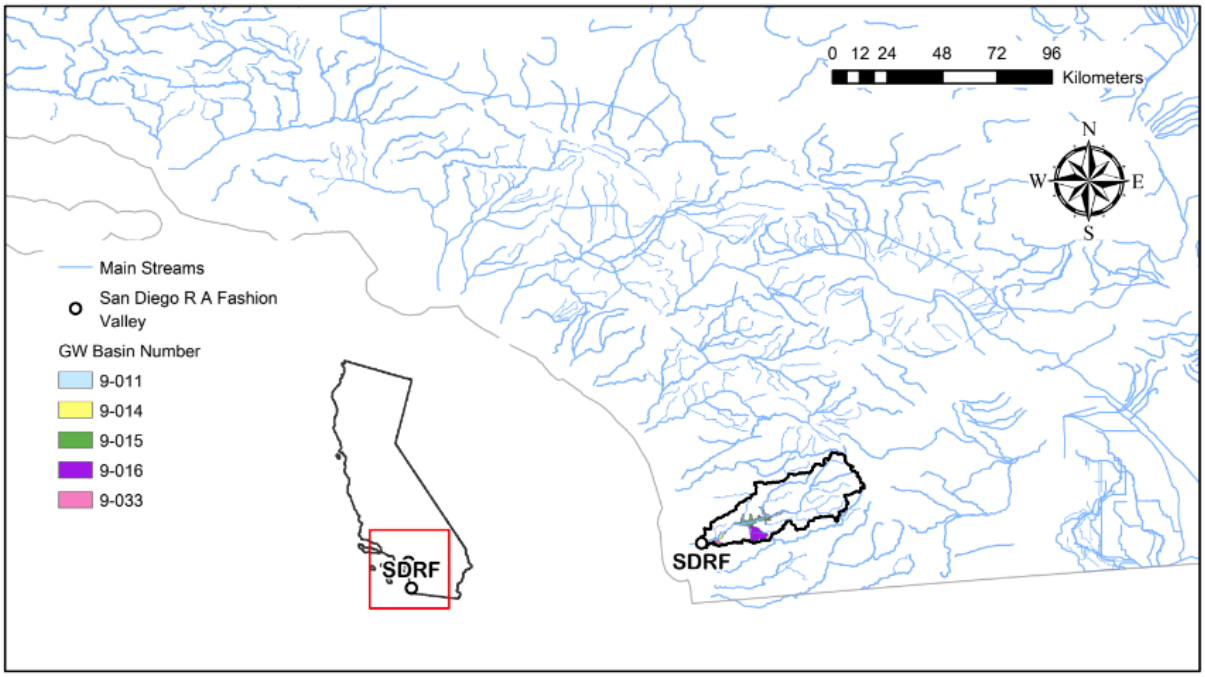
0 12 24 48 72 96
Kilometers
N
W
E
S
Main Streams
San Diego R A Fashion Valley
GW Basin Number
9-011
9-014
9-015
9-016
9-033
SDRF
SDRF

(b)

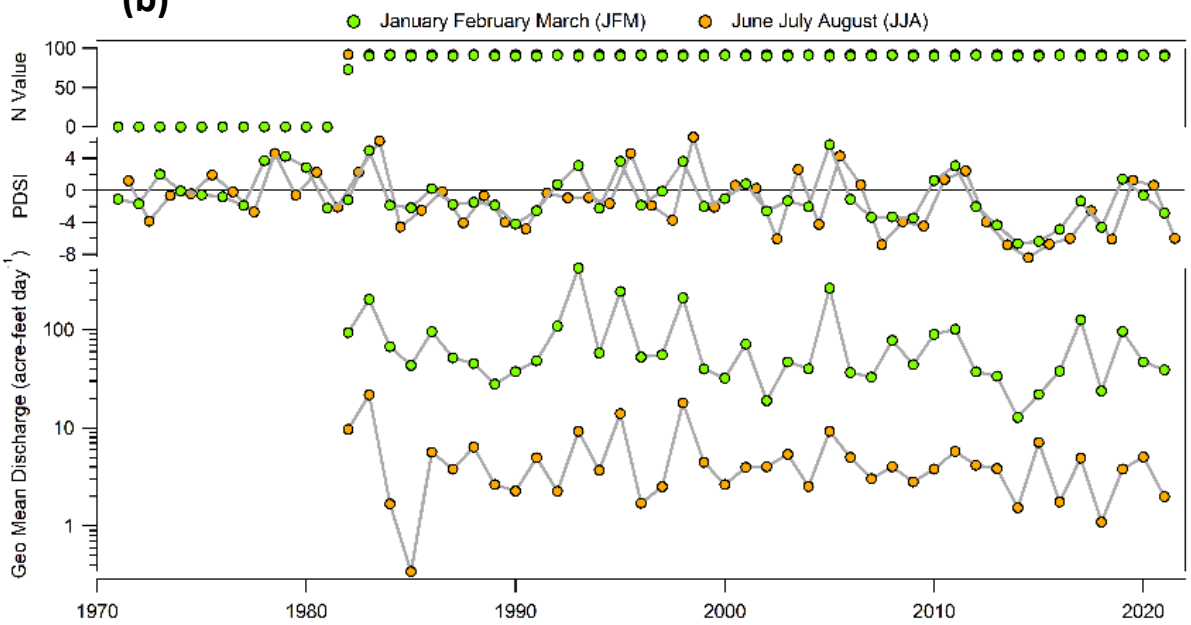
January February March (JFM)
June July August (JJA)
N Value
PDSI
Geo Mean Discharge (acre-feet day⁻¹)
1970
1980
1990
2000
2010
2020

(c)

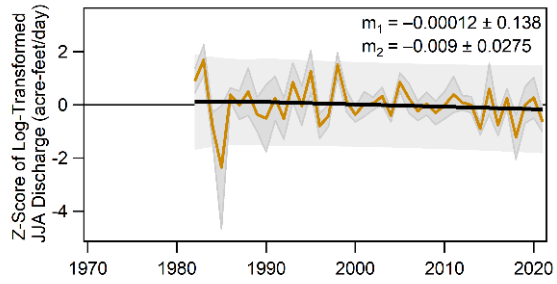
m1 = −0.00012 ± 0.138
m2 = −0.009 ± 0.0275
Z-Score of Log-Transformed JJA Discharge (acre-feet/day)
1970
1980
1990
2000
2010
2020

(d)

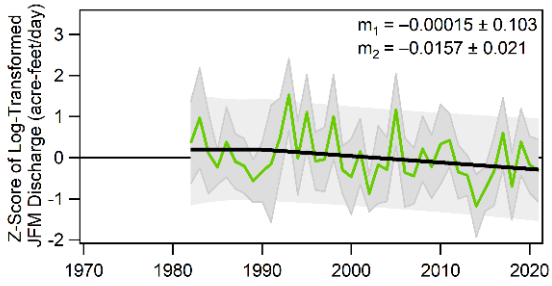
m1 = −0.00015 ± 0.103
m2 = −0.0157 ± 0.021
Z-Score of Log-Transformed JFM Discharge (acre-feet/day)
1970
1980
1990
2000
2010
2020

SAN TIMOTEO C NR LOMA LINDA CA

Gauge Information	USGS Station ID	11057500
	Hydrologic Unit Code	18070203
	Latitude (NAD27)	34°03'41"
	Longitude (NAD27)	117°16'00"
	Drainage Area [Mi^2]	125
	Elevation of The Stream Outlet Above NAVD88 [Ft]	1043
	County	San Bernardino
Watershed Characteristics	Mean Maximum January Temperature [°F]	59.82
	Mean Minimum January Temperature [°F]	36.99
	Mean Annual Precipitation [In]	20
	Hydrological Soil Group (HSG) [% of Covered Area]	C(48%), D(52%)
	Length of Longest Flow Path [Mi]	31
	Mean Basin Elevation [Ft]	2892
	Maximum Basin Elevation [Ft]	8824
	Minimum Basin Elevation [Ft]	1043
	Percentage of Area Above 6000 Ft [%]	2.8
	Percentage of Area Covered By Forest [%]	6.91
	Percentage of Lakes And Ponds [%]	0.0405
	Percentage of Developed (Urban) Land (NLCD 2011 Classes 21-24) [%]	25.6
	Percentage of Imperviousness (NLCD 2001 Impervious Dataset) [%]	5.99
	Percentage of Imperviousness (NLCD 2011 Impervious Dataset) [%]	7.48
	Percentage of Imperviousness (NLCD 2019 Impervious Dataset) [%]	8.02
Stream Management Controls	Developed or Natural	Developed*
	Regulation	Unregulated*
	Geological or Hydrological Control	None
	Dam Outlet	No
	Agricultural Control	None
	(Waste)water Inputs	None
	Water Withdrawals	Yes**
	Other Factors Affecting Runoff	Channelized Floodway; Irrigation**

*Highly developed watershed. No regulation upstream from station.
**Natural flow affected by pumping and return flow from irrigated areas. Since Dec. 7, 1997, channel is a trapezoidal concrete floodway. Ref. waterdata.usgs.gov

(a)

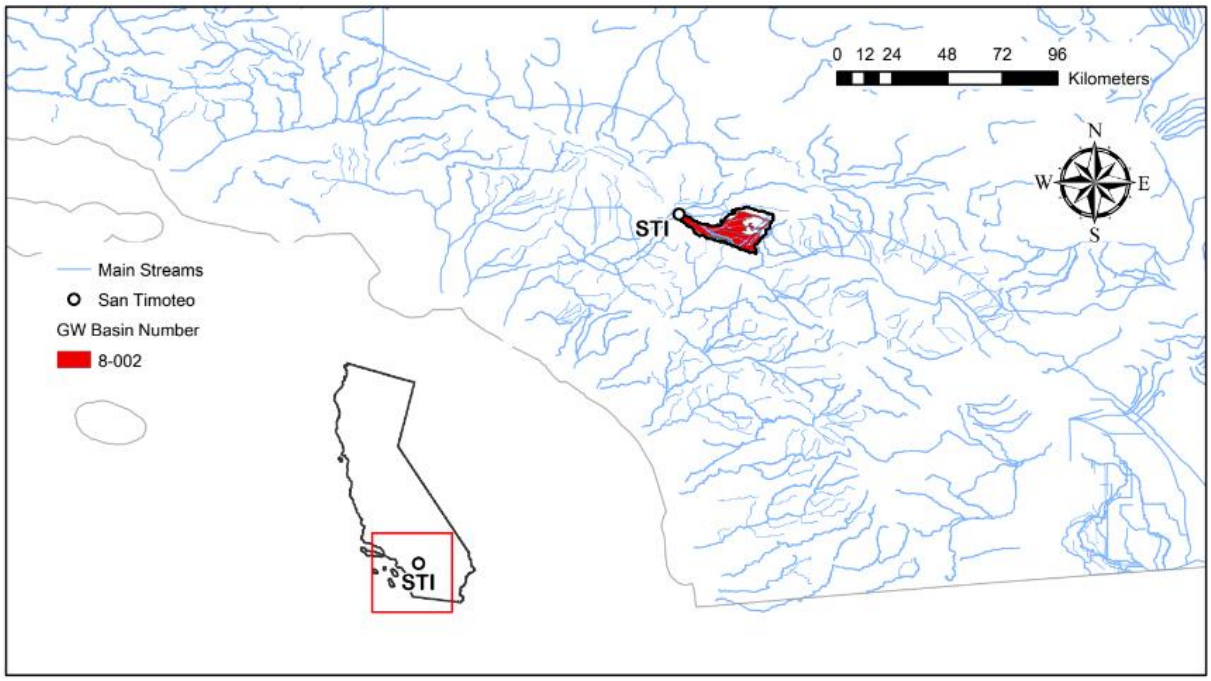
0 12 24 48 72 96
Kilometers
N
W
E
S
STI
Main Streams
San Timoteo
GW Basin Number
8-002
STI

(b)

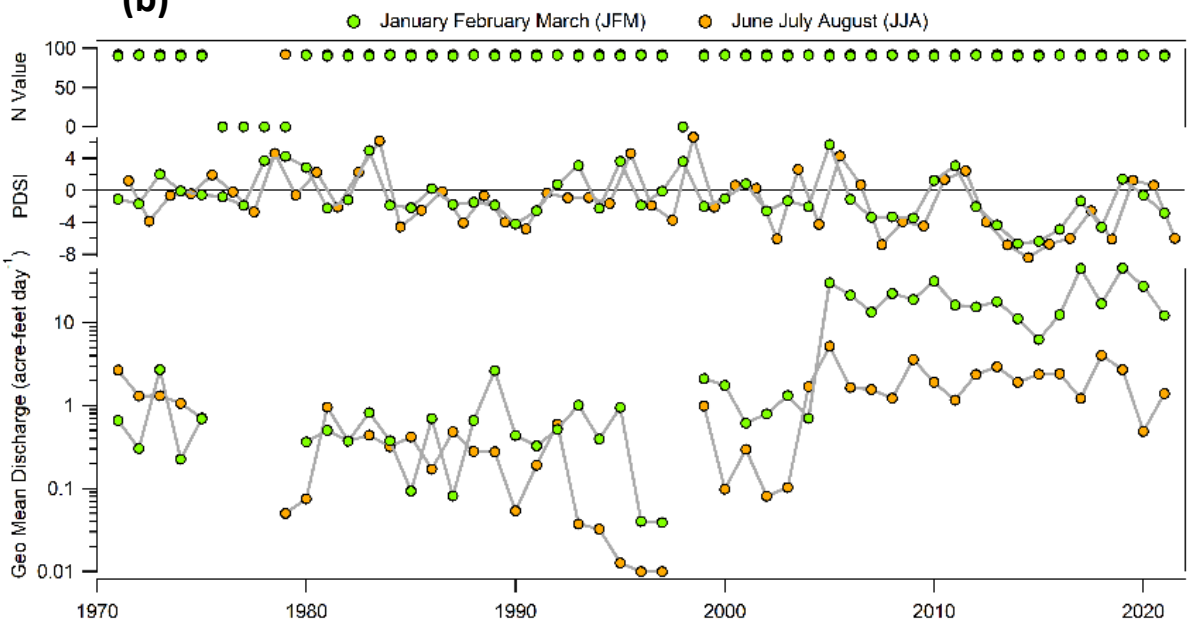
January February March (JFM)
June July August (JJA)
N Value
PDSI
Geo Mean Discharge (acre-feet day⁻¹)
1970
1980
1990
2000
2010
2020

(c)

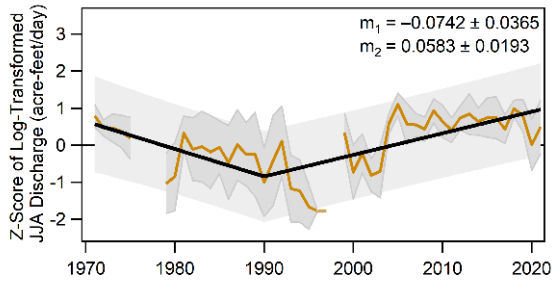
m1 = −0.0742 ± 0.0365
m2 = 0.0583 ± 0.0193
Z-Score of Log-Transformed JJA Discharge (acre-feet/day)
1970
1980
1990
2000
2010
2020

(d)

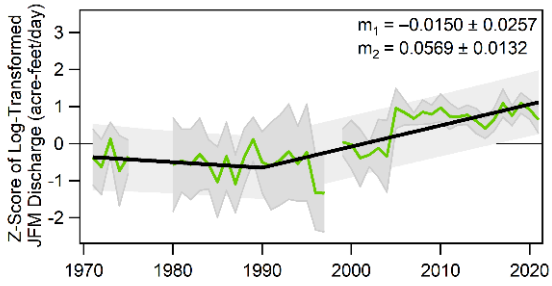
m1 = −0.0150 ± 0.0257
m2 = 0.0569 ± 0.0132
Z-Score of Log-Transformed JFM Discharge (acre-feet/day)
1970
1980
1990
2000
2010
2020

SAN DIEGO R A MAST RD NR SANTEE CA

Gauge Information	USGS Station ID	11022480
	Hydrologic Unit Code	18070304
	Latitude (NAD27)	32°50'25"
	Longitude (NAD27)	117°01'30"
	Drainage Area [Mi^2]	368
	Elevation of The Stream Outlet Above NAVD88 [Ft]	291
	County	San Diego
Watershed Characteristics	Mean Maximum January Temperature [°F]	62.27
	Mean Minimum January Temperature [°F]	38.09
	Mean Annual Precipitation [In]	20.6
	Hydrological Soil Group (HSG) [% of Covered Area]	C(55%), D(45%)
	Length of Longest Flow Path [Mi]	41
	Mean Basin Elevation [Ft]	2098
	Maximum Basin Elevation [Ft]	6492
	Minimum Basin Elevation [Ft]	291
	Percentage of Area Above 6000 Ft [%]	0.0669
	Percentage of Area Covered By Forest [%]	12.1
	Percentage of Lakes And Ponds [%]	0.85
	Percentage of Developed (Urban) Land (NLCD 2011 Classes 21-24) [%]	19.3
	Percentage of Imperviousness (NLCD 2001 Impervious Dataset) [%]	6.57
	Percentage of Imperviousness (NLCD 2011 Impervious Dataset) [%]	6.82
	Percentage of Imperviousness (NLCD 2019 Impervious Dataset) [%]	6.97
Stream Management Controls	Developed or Natural	Developed
	Regulation	Regulated*
	Geological or Hydrological Control	Yes***
	Dam Outlet	No
	Agricultural Control	None
	(Waste)water Inputs	None
	Water Withdrawals	Yes**
	Other Factors Affecting Runoff	Transition Reach***

*Flow regulated by Cuyamaca Reservoir, capacity, 11,740 acre-ft, El Capitan Reservoir (station 11020600), and San Vicente Reservoir (station 11022100).
**Diversions by city of San Diego for municipal supply and by Helix Irrigation District.
***Natural reach between two more heavily urbanized areas; Upstream is hydrologically controlled by dam.
Ref. waterdata.usgs.gov

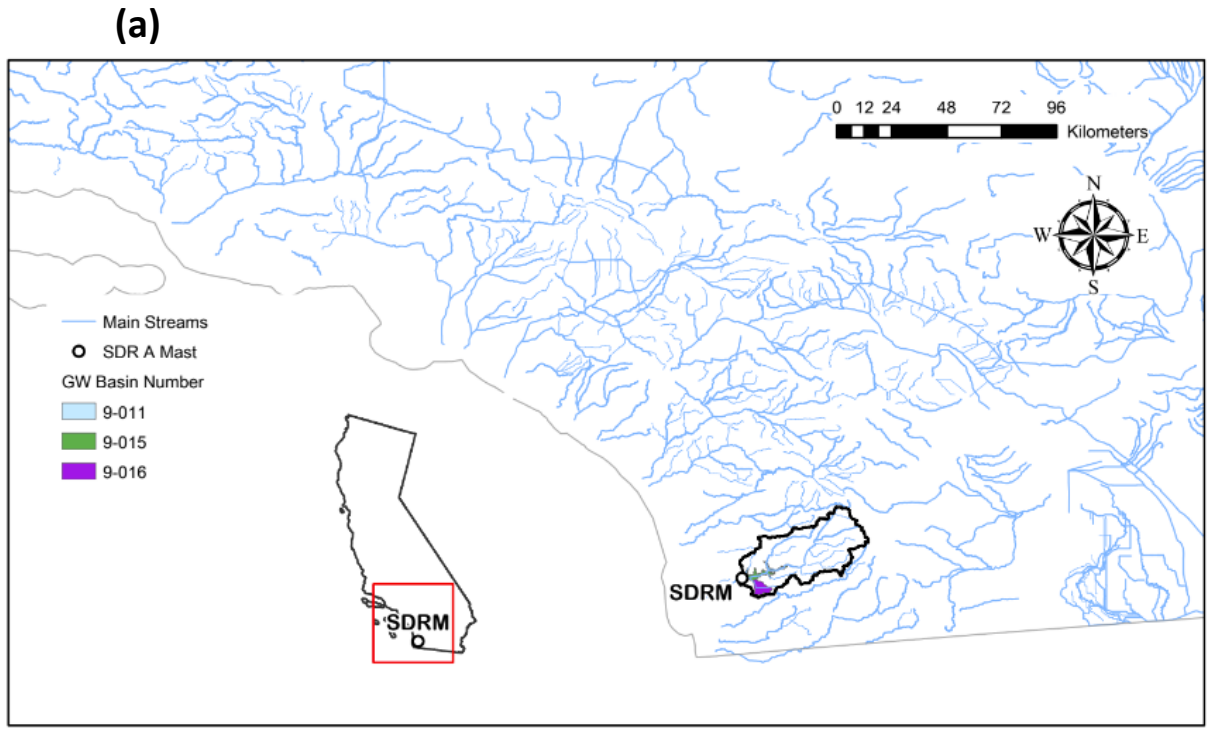
(a)
0 12 24 48 72 96
Kilometers
N
W
E
S
Main Streams
SDR A Mast
GW Basin Number
9-011
9-015
9-016
SDRM
SDRM

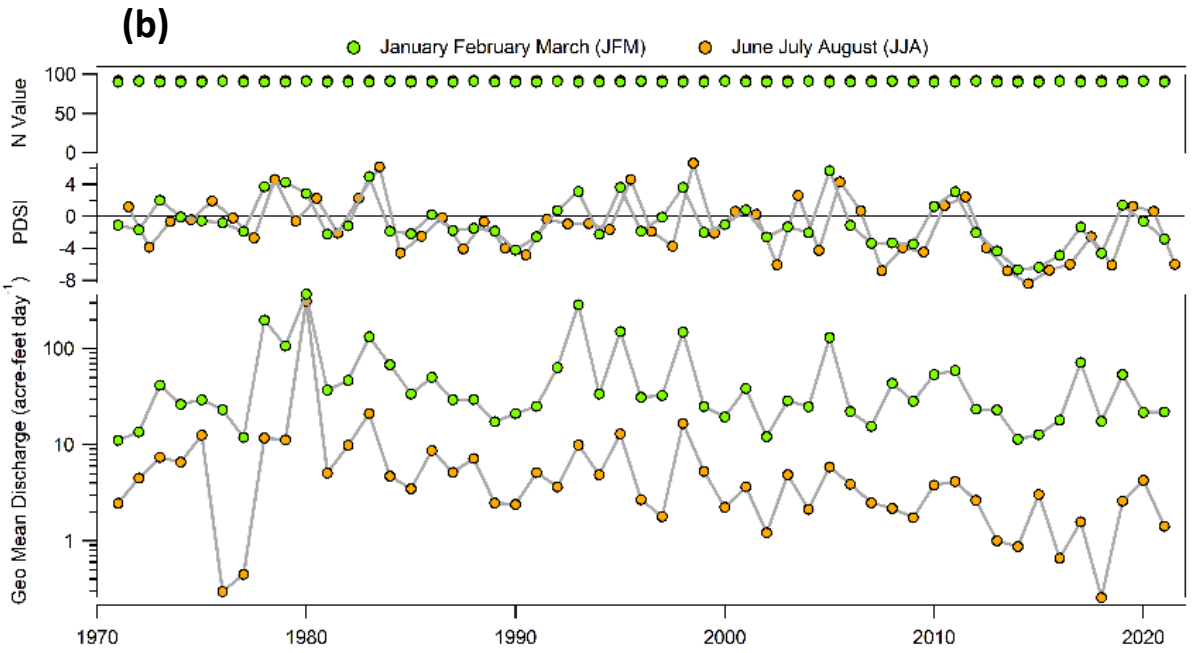
(b)
January February March (JFM)
June July August (JJA)
N Value
PDSI
Geo Mean Discharge (acre-feet day⁻¹)
1970
1980
1990
2000
2010
2020

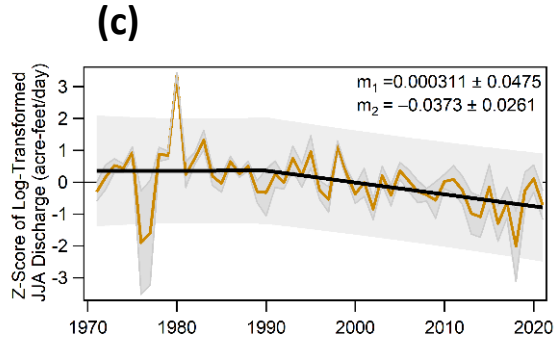
(c)
m1 =0.000311 ± 0.0475
m2 = –0.0373 ± 0.0261
Z-Score of Log-Transformed JJA Discharge (acre-feet/day)
1970
1980
1990
2000
2010
2020

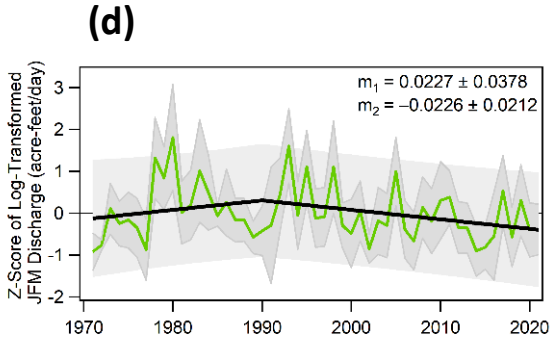
(d)
m1 = 0.0227 ± 0.0378
m2 = –0.0226 ± 0.0212
Z-Score of Log-Transformed JFM Discharge (acre-feet/day)
1970
1980
1990
2000
2010
2020

MISSION C NR MISSION ST NR SANTA BARBARA CA

Gauge Information	USGS Station ID	11119750
	Hydrologic Unit Code	18060013
	Latitude (NAD83)	34°25'39"
	Longitude (NAD83)	119°43'31"
	Drainage Area [Mi^2]	8.38
	Elevation of The Stream Outlet Above NAVD88 [Ft]	142
	County	Santa Barbara
Watershed Characteristics	Mean Maximum January Temperature [°F]	61.04
	Mean Minimum January Temperature [°F]	42.14
	Mean Annual Precipitation [In]	25.4
	Hydrological Soil Group (HSG) [% of Covered Area]	C(62%), D(38%)
	Length of Longest Flow Path [Mi]	7
	Mean Basin Elevation [Ft]	1644
	Maximum Basin Elevation [Ft]	3966
	Minimum Basin Elevation [Ft]	140
	Percentage of Area Above 6000 Ft [%]	0
	Percentage of Area Covered By Forest [%]	31.9
	Percentage of Lakes And Ponds [%]	0.24
	Percentage of Developed (Urban) Land (NLCD 2011 Classes 21-24) [%]	25.3
	Percentage of Imperviousness (NLCD 2001 Impervious Dataset) [%]	6.20
	Percentage of Imperviousness (NLCD 2011 Impervious Dataset) [%]	6.29
	Percentage of Imperviousness (NLCD 2019 Impervious Dataset) [%]	6.37
Stream Management Controls	Developed or Natural	Developed*
	Regulation	Regulated
	Geological or Hydrological Control	None
	Dam Outlet	No
	Agricultural Control	None
	(Waste)water Inputs	Yes**
	Water Withdrawals	None
	Other Factors Affecting Runoff	-

*Lower watershed is highly developed.
**At times water is released to the creek for groundwater recharge from Gibraltar Reservoir through Mission Tunnel several miles upstream; No flow most of each year. Ref. waterdata.usgs.gov

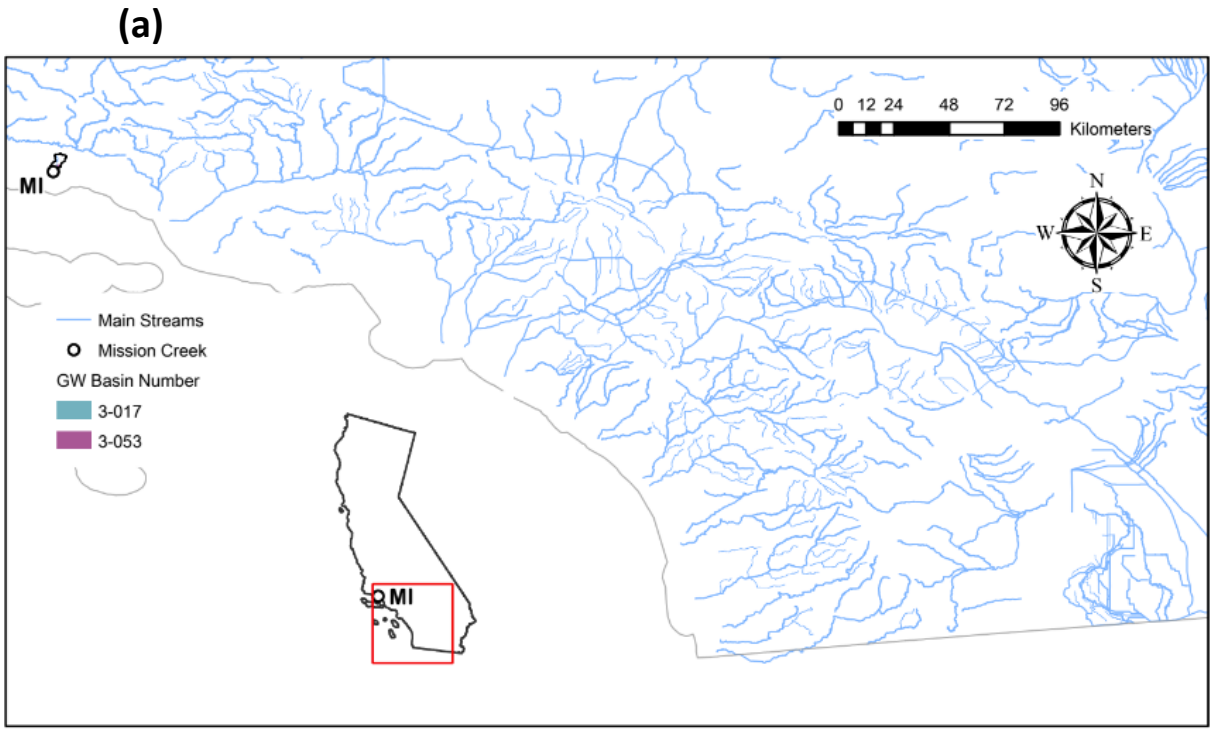
(a)
0 12 24 48 72 96
Kilometers
N
W
E
S
MI
Main Streams
Mission Creek
GW Basin Number
3-017
3-053
MI

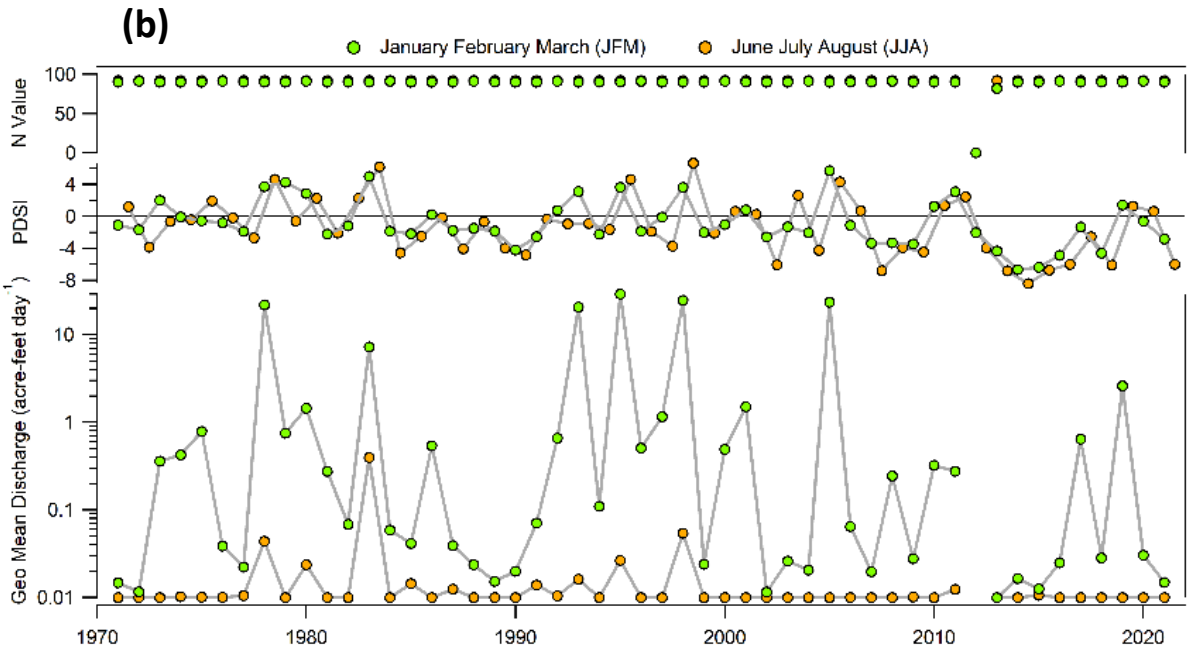
(b)
January February March (JFM)
June July August (JJA)
N Value
PDSI
Geo Mean Discharge (acre-feet day⁻¹)
1970
1980
1990
2000
2010
2020

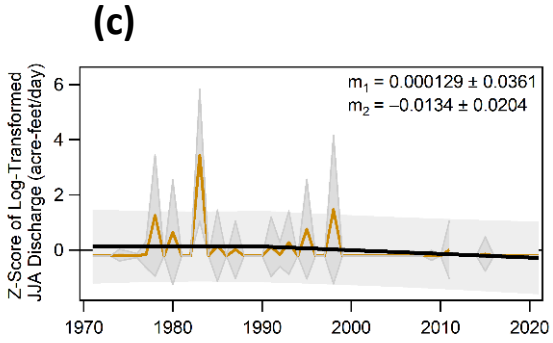
(c)
m1 = 0.000129 ± 0.0361
m2 = −0.0134 ± 0.0204
Z-Score of Log-Transformed
JJA Discharge (acre-feet/day)
1970
1980
1990
2000
2010
2020

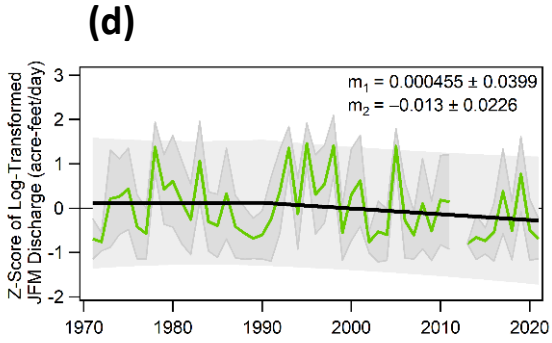
(d)
m1 = 0.000455 ± 0.0399
m2 = −0.013 ± 0.0226
Z-Score of Log-Transformed
JFM Discharge (acre-feet/day)
1970
1980
1990
2000
2010
2020

SANTA ANA R A E ST NR SAN BERNARDINO CA

Gauge Information	USGS Station ID	11059300
	Hydrologic Unit Code	18070203
	Latitude (NAD27)	34°03'54"
	Longitude (NAD27)	117°17'58"
	Drainage Area [Mi^2]	541
	Elevation of The Stream Outlet Above NAVD88 [Ft]	962
	County	San Bernardino
Watershed Characteristics	Mean Maximum January Temperature [°F]	51.56
	Mean Minimum January Temperature [°F]	27.61
	Mean Annual Precipitation [In]	26.8
	Hydrological Soil Group (HSG) [% of Covered Area]	C(63%),D(37%)
	Length of Longest Flow Path [Mi]	49
	Mean Basin Elevation [Ft]	5447
	Maximum Basin Elevation [Ft]	11420
	Minimum Basin Elevation [Ft]	959
	Percentage of Area Above 6000 Ft [%]	51.4
	Percentage of Area Covered By Forest [%]	24.5
	Percentage of Lakes And Ponds [%]	1.02
	Percentage of Developed (Urban) Land (NLCD 2011 Classes 21-24) [%]	19.8
	Percentage of Imperviousness (NLCD 2001 Impervious Dataset) [%]	4.95
	Percentage of Imperviousness (NLCD 2011 Impervious Dataset) [%]	5.69
	Percentage of Imperviousness (NLCD 2019 Impervious Dataset) [%]	6.19
Stream Management Controls	Developed or Natural	Developed
	Regulation	Regulated*
	Geological or Hydrological Control	Yes*
	Dam Outlet	No
	Agricultural Control	None
	(Waste)water Inputs	Yes**
	Water Withdrawals	Yes***
	Other Factors Affecting Runoff	Channelized reach d/s of Seven Oaks Dam

*San Bernardino County Flood Control District (SBCFCD) declared growth in channel 'semi-permanent' citing environmental regulation in 2016. Flow partly regulated by Big Bear Lake (station 11049000) and, since November 1999, by Seven Oaks Flood-Control Reservoir, capacity, 145,600 acre-ft.
**Effluent from sewage reclamation plant 1.0 mi upstream caused sustained flow past gage from 1967 to Mar. 21, 1996.
***Natural flow of stream affected by ground-water withdrawals and diversion for domestic use and irrigation upstream from station.
Ref. waterdata.usgs.gov

(a)

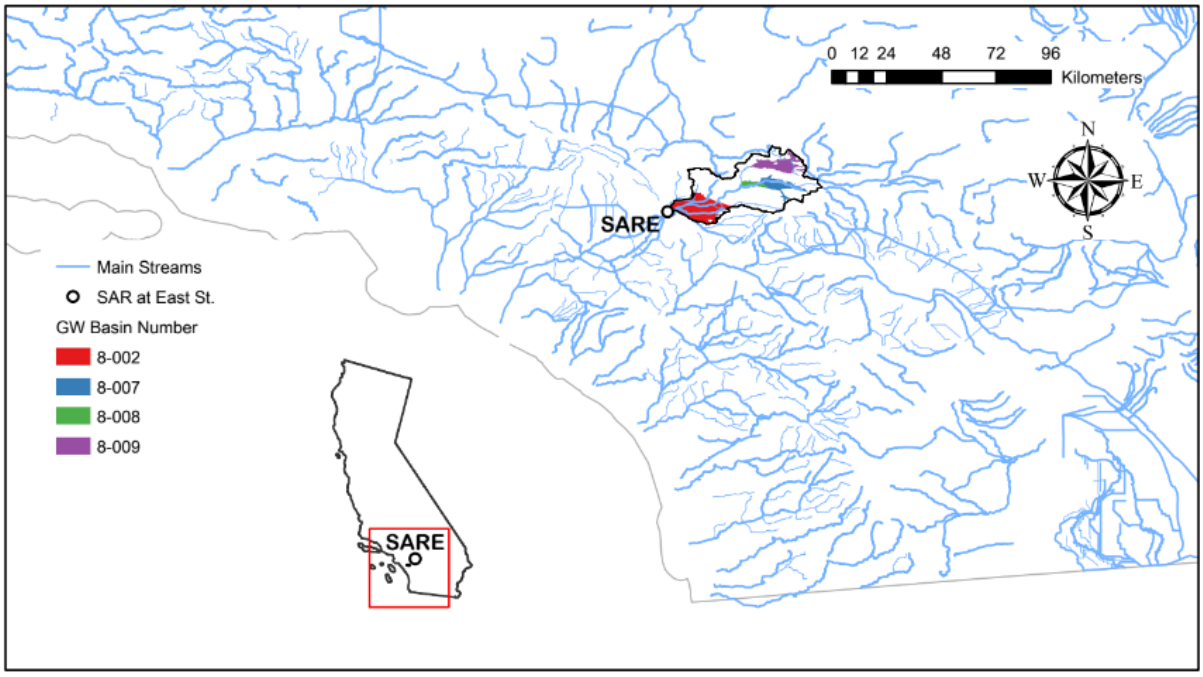
0 12 24 48 72 96
Kilometers
N
W
E
S
SARE
Main Streams
SAR at East St.
GW Basin Number
8-002
8-007
8-008
8-009
SARE

(b)

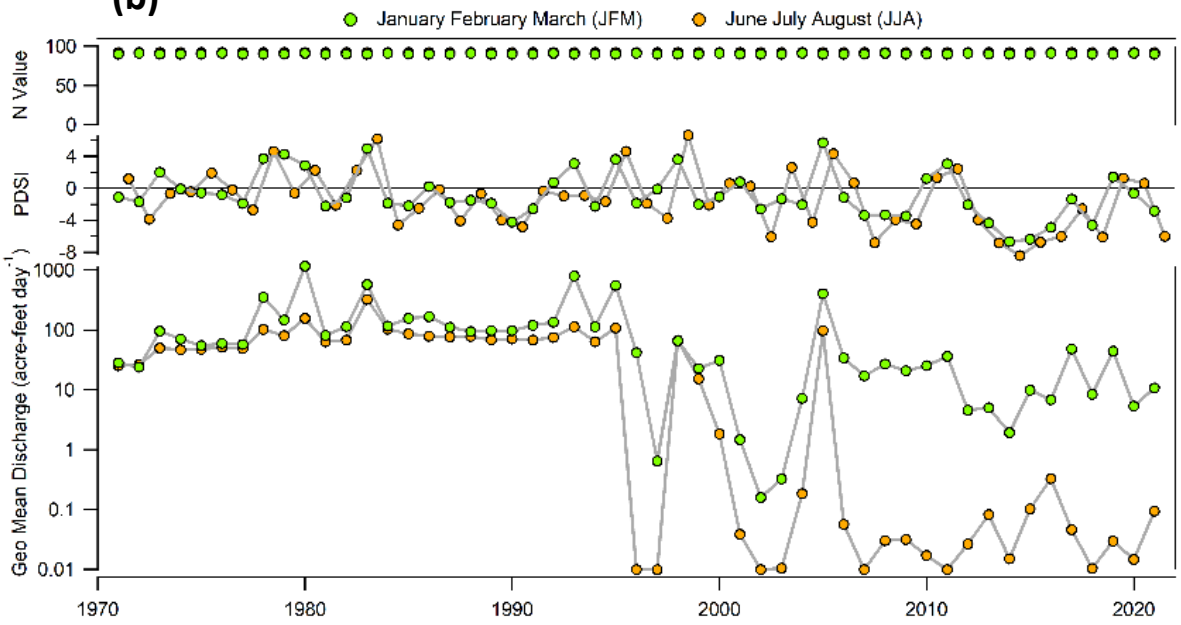
January February March (JFM)
June July August (JJA)
N Value
PDSI
Geo Mean Discharge (acre-feet day-1)
1970
1980
1990
2000
2010
2020

(c)

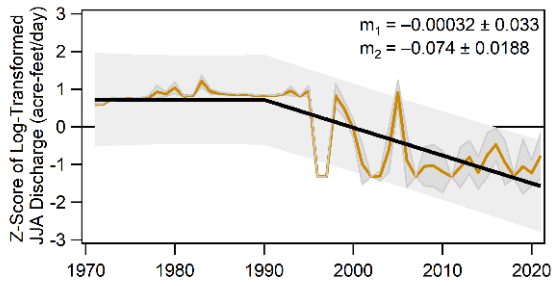
m1 = −0.00032 ± 0.033
m2 = −0.074 ± 0.0188
Z-Score of Log-Transformed JJA Discharge (acre-feet/day)
1970
1980
1990
2000
2010
2020

(d)

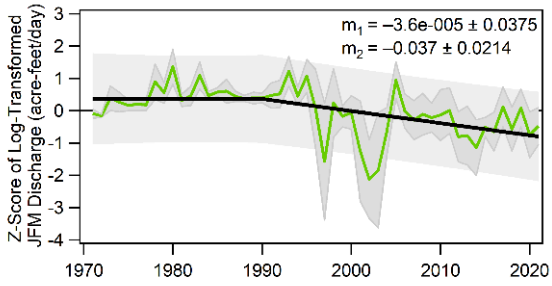
m1 = −3.6e-005 ± 0.0375
m2 = −0.037 ± 0.0214
Z-Score of Log-Transformed JFM Discharge (acre-feet/day)
1970
1980
1990
2000
2010
2020

SANTA MARGARITA R A YSIDORA CA

Gauge Information	USGS Station ID	11046000
	Hydrologic Unit Code	18070302
	Latitude (NAD27)	33°18'40"
	Longitude (NAD27)	117°20'47"
	Drainage Area [Mi^2]	723
	Elevation of The Stream Outlet Above NAVD88 [Ft]	78
	County	San Diego
Watershed Characteristics	Mean Maximum January Temperature [°F]	62.43
	Mean Minimum January Temperature [°F]	38.11
	Mean Annual Precipitation [In]	16.3
	Hydrological Soil Group (HSG) [% of Covered Area]	C(41%), D(59%)
	Length of Longest Flow Path [Mi]	64
	Mean Basin Elevation [Ft]	2360
	Maximum Basin Elevation [Ft]	6818
	Minimum Basin Elevation [Ft]	77
	Percentage of Area Above 6000 Ft [%]	0.0753
	Percentage of Area Covered By Forest [%]	8.05
	Percentage of Lakes And Ponds [%]	1.24
	Percentage of Developed (Urban) Land (NLCD 2011 Classes 21-24) [%]	16.7
	Percentage of Imperviousness (NLCD 2001 Impervious Dataset) [%]	3.27
	Percentage of Imperviousness (NLCD 2011 Impervious Dataset) [%]	4.53
	Percentage of Imperviousness (NLCD 2019 Impervious Dataset) [%]	4.87
Stream Management Controls	Developed or Natural	Developed
	Regulation	Regulated*
	Geological or Hydrological Control	Yes
	Dam Outlet	No
	Agricultural Control	None
	(Waste)water Inputs	None
	Water Withdrawals	Yes**
	Other Factors Affecting Runoff	-

*Flow partly regulated by Vail Lake (station 11042510) since November 1948 and by Skinner Reservoir since 1974. Flow in Warm Springs Creek, a tributary to Murrieta Creek, slightly regulated beginning in water year 1999 by Diamond Valley Lake, capacity, 800,000 acre-ft (see station 11042800).
**Diversions to O'Neill Lake and to groundwater recharge basins are made at point 2.3 mi upstream by Camp Pendleton personnel. Regulated return flows from O'Neill Lake can occur at times, as can unregulated spills.
Note: On Camp Pendleton, good representation of lower watershed. Stipulated judgement always requires 3 cfs flow at Santa Margarita gorge.
Ref. waterdata.usgs.gov

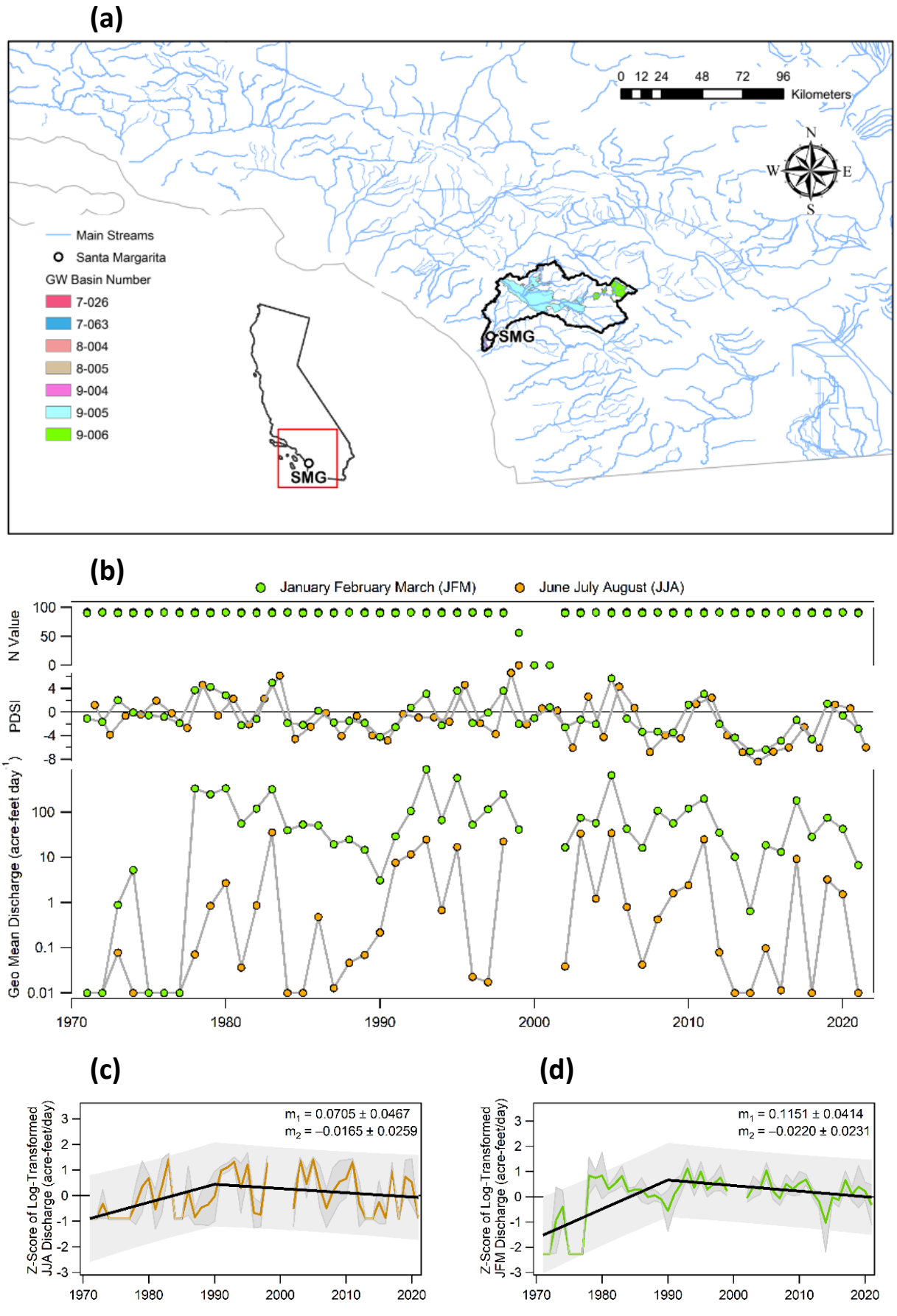
(a)
0 12 24 48 72 96
Kilometers
N
W
E
S
Main Streams
Santa Margarita
GW Basin Number
7-026
7-063
8-004
8-005
9-004
9-005
9-006
SMG
SMG
(b)
January February March (JFM)
June July August (JJA)
N Value
PDSI
Geo Mean Discharge (acre-feet day-1)
1970
1980
1990
2000
2010
2020
(c)
m1 = 0.0705 ± 0.0467
m2 = −0.0165 ± 0.0259
Z-Score of Log-Transformed JJA Discharge (acre-feet/day)
(d)
m1 = 0.1151 ± 0.0414
m2 = −0.0220 ± 0.0231
Z-Score of Log-Transformed JFM Discharge (acre-feet/day)

WHITEWATER R NR MECCA

Gauge Information	USGS Station ID	10259540
	Hydrologic Unit Code	18100201
	Latitude (NAD27)	33°31'29"
	Longitude (NAD27)	116°04'36"
	Drainage Area [Mi^2]	1495
	Elevation of The Stream Outlet Above NAVD88 [Ft]	-227
	County	Riverside
Watershed Characteristics	Mean Maximum January Temperature [°F]	68.05
	Mean Minimum January Temperature [°F]	38.95
	Mean Annual Precipitation [In]	3.81
	Hydrological Soil Group (HSG) [% of Covered Area]	C(12%), D(88%)
	Length of Longest Flow Path [Mi]	27
	Mean Basin Elevation [Ft]	158
	Maximum Basin Elevation [Ft]	2257
	Minimum Basin Elevation [Ft]	-227
	Percentage of Area Above 6000 Ft [%]	0
	Percentage of Area Covered By Forest [%]	4.26
	Percentage of Lakes And Ponds [%]	0.34
	Percentage of Developed (Urban) Land (NLCD 2011 Classes 21-24) [%]	18.3
	Percentage of Imperviousness (NLCD 2001 Impervious Dataset) [%]	3.94
	Percentage of Imperviousness (NLCD 2011 Impervious Dataset) [%]	4.28
	Percentage of Imperviousness (NLCD 2019 Impervious Dataset) [%]	4.47
Stream Management Controls	Developed or Natural	Developed
	Regulation	Regulated
	Geological or Hydrological Control	None
	Dam Outlet	No
	Agricultural Control	Yes*
	(Waste)water Inputs	None
	Water Withdrawals	None
	Other Factors Affecting Runoff	-

*Located upstream of Salton Sea. Most flow represents seepage and return flow from irrigated areas (agricultural return flows). No discharge records computed above 200 ft^3/s since October 1992. Ref. waterdata.usgs.gov

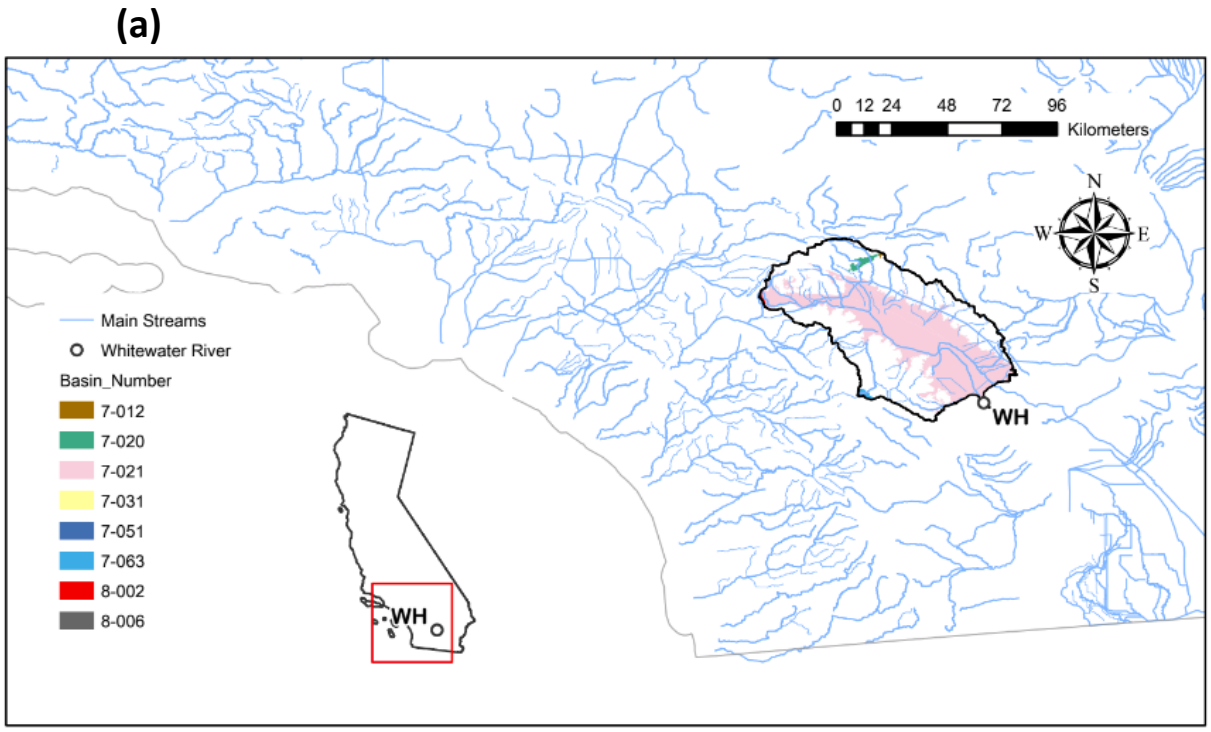
(a)
0 12 24 48 72 96
Kilometers
N
W
E
S
Main Streams
Whitewater River
Basin_Number
7-012
7-020
7-021
7-031
7-051
7-063
8-002
8-006
WH
WH

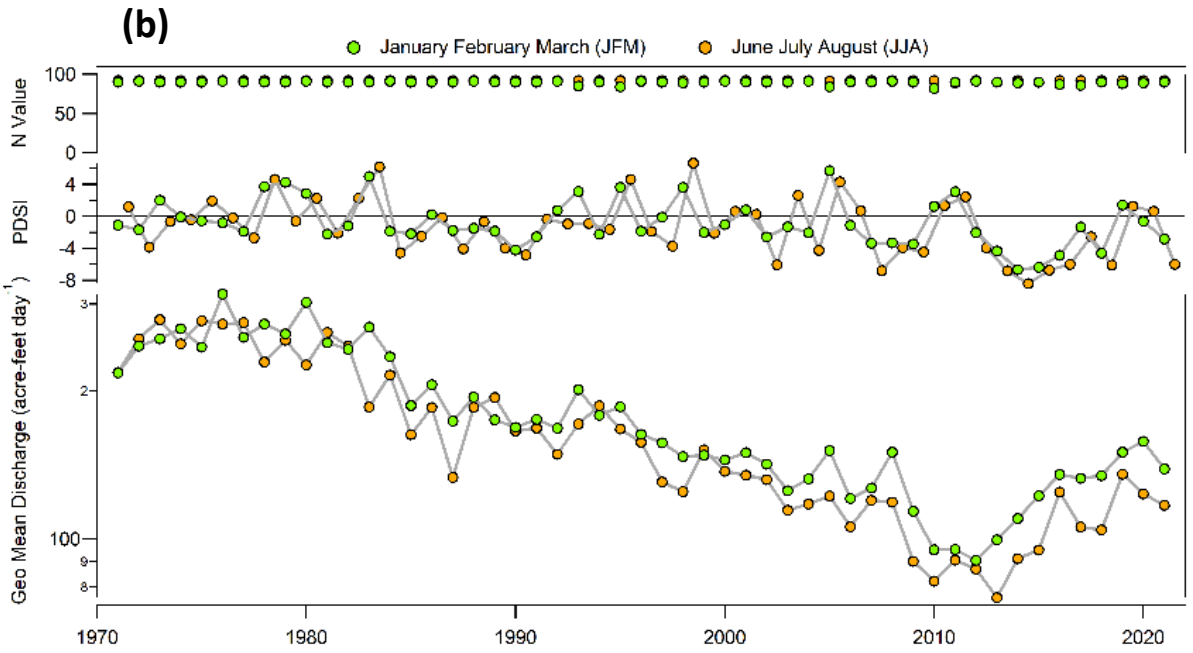
(b)
January February March (JFM)
June July August (JJA)
N Value
PDSI
Geo Mean Discharge (acre-feet day⁻¹)
1970
1980
1990
2000
2010
2020

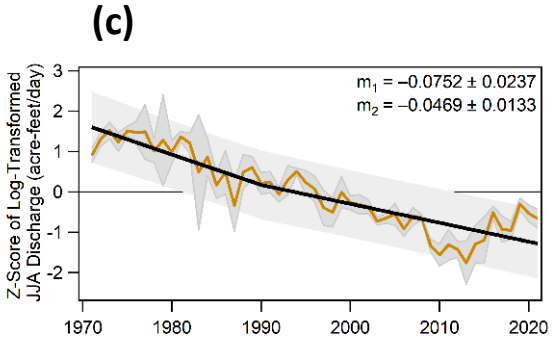
(c)
m1 = −0.0752 ± 0.0237
m2 = −0.0469 ± 0.0133
Z-Score of Log-Transformed JJA Discharge (acre-feet/day)
1970
1980
1990
2000
2010
2020

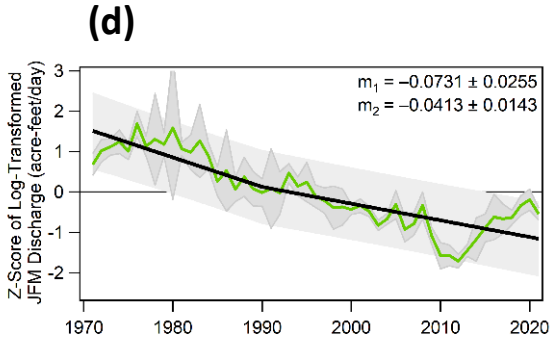
(d)
m1 = −0.0731 ± 0.0255
m2 = −0.0413 ± 0.0143
Z-Score of Log-Transformed JFM Discharge (acre-feet/day)
1970
1980
1990
2000
2010
2020

SANTIAGO C A SANTA ANA CA

Gauge Information	USGS Station ID	11077500
	Hydrologic Unit Code	18070203
	Latitude (NAD27)	33°46'13"
	Longitude (NAD27)	117°53'01"
	Drainage Area [Mi^2]	98.6
	Elevation of The Stream Outlet Above NAVD88 [Ft]	113
	County	Orange
Watershed Characteristics	Mean Maximum January Temperature [°F]	62.86
	Mean Minimum January Temperature [°F]	44.43
	Mean Annual Precipitation [In]	20.3
	Hydrological Soil Group (HSG) [% of Covered Area]	C(30%), D(70%)
	Length of Longest Flow Path [Mi]	35
	Mean Basin Elevation [Ft]	1820
	Maximum Basin Elevation [Ft]	5684
	Minimum Basin Elevation [Ft]	112
	Percentage of Area Above 6000 Ft [%]	0
	Percentage of Area Covered By Forest [%]	17.2
	Percentage of Lakes And Ponds [%]	0.77
	Percentage of Developed (Urban) Land (NLCD 2011 Classes 21-24) [%]	14.2
	Percentage of Imperviousness (NLCD 2001 Impervious Dataset) [%]	4.1
	Percentage of Imperviousness (NLCD 2011 Impervious Dataset) [%]	4.3
	Percentage of Imperviousness (NLCD 2019 Impervious Dataset) [%]	4.4
Stream Management Controls	Developed or Natural	Developed
	Regulation	Regulated*
	Geological or Hydrological Control	None
	Dam Outlet	No
	Agricultural Control	None
	(Waste)water Inputs	None
	Water Withdrawals	Yes**
	Other Factors Affecting Runoff	Lower Watershed***

*Flow regulated since December 1931 by Santiago Reservoir, capacity, 25,000 acre-ft; since January 1963 by Villa Park Flood-Control Reservoir, capacity, 15,500 acre-ft, and affected by intervening gravel pits. Gage out of operation from Aug. 8 to Dec. 18, 2002, for bridge construction.
**Diversions upstream from station by Irvine Company and Serrano and Carpenter Irrigation Districts.
***Receives runoff from developed landscape upstream.
Ref. waterdata.usgs.gov

(a)

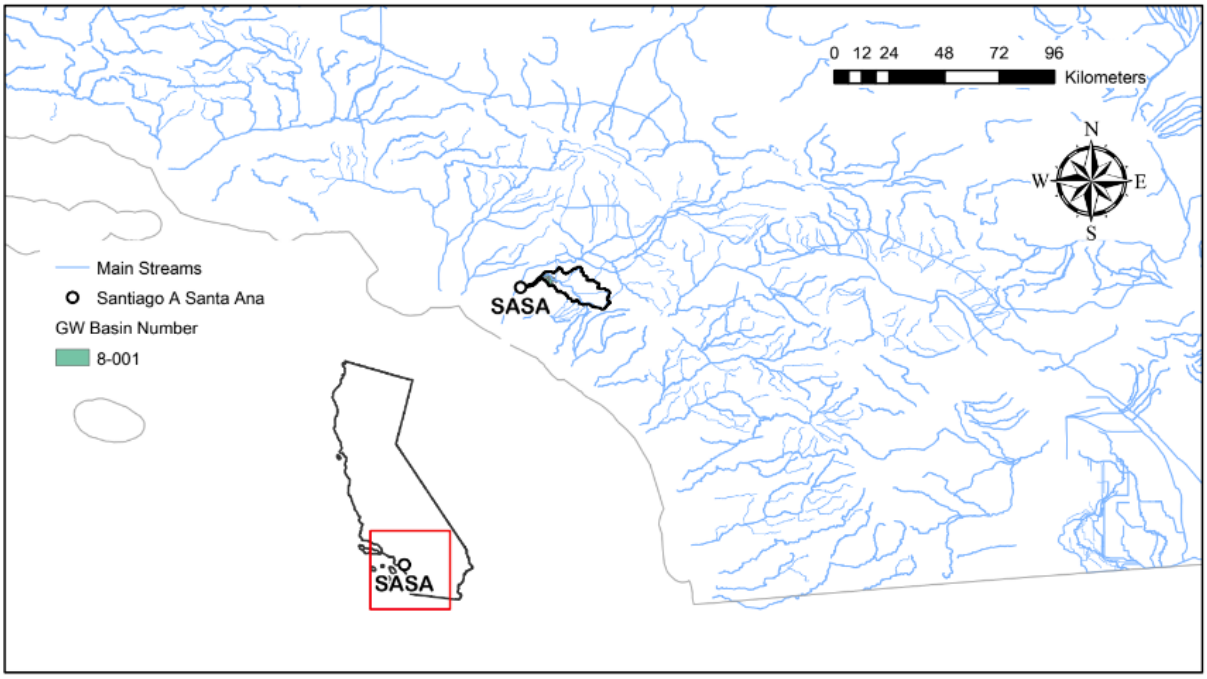
0 12 24 48 72 96
Kilometers
N
W
E
S
Main Streams
Santiago A Santa Ana
GW Basin Number
8-001
SASA
SASA

(b)

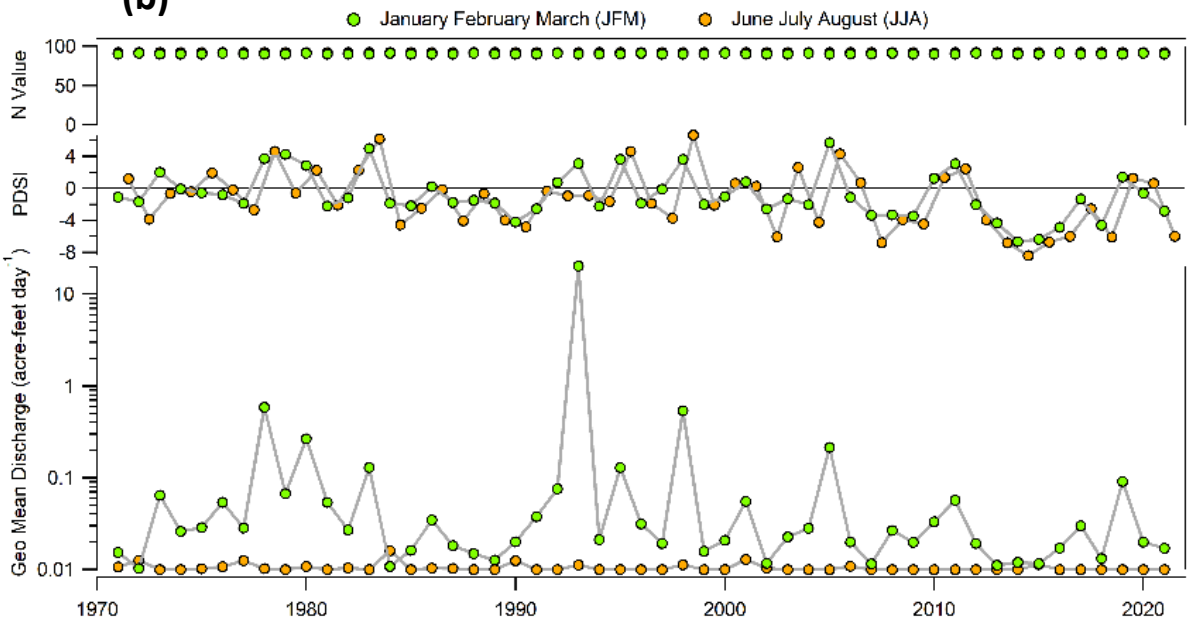
January February March (JFM)
June July August (JJA)
N Value
PDSI
Geo Mean Discharge (acre-feet day⁻¹)
1970
1980
1990
2000
2010
2020

(c)

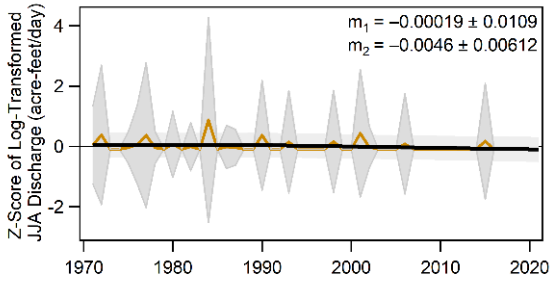
m1 = −0.00019 ± 0.0109
m2 = −0.0046 ± 0.00612
Z-Score of Log-Transformed JJA Discharge (acre-feet/day)
1970
1980
1990
2000
2010
2020

(d)

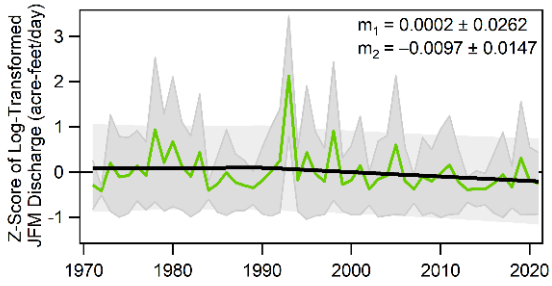
m1 = 0.0002 ± 0.0262
m2 = −0.0097 ± 0.0147
Z-Score of Log-Transformed JFM Discharge (acre-feet/day)
1970
1980
1990
2000
2010
2020

NEW R NR WESTMORLAND CA

Gauge Information	USGS Station ID	10255550
	Hydrologic Unit Code	18100204
	Latitude (NAD27)	33°06'17"
	Longitude (NAD27)	115°39'49"
	Drainage Area [Mi^2]	602
	Elevation of The Stream Outlet Above NAVD88 [Ft]	-226
	County	
Watershed Characteristics	Mean Maximum January Temperature [°F]	65.48
	Mean Minimum January Temperature [°F]	38.77
	Mean Annual Precipitation [In]	3.48
	Hydrological Soil Group (HSG) [% of Covered Area]	D(100%)
	Length of Longest Flow Path [Mi]	93
	Mean Basin Elevation [Ft]	285
	Maximum Basin Elevation [Ft]	4516
	Minimum Basin Elevation [Ft]	-227
	Percentage of Area Above 6000 Ft [%]	0
	Percentage of Area Covered By Forest [%]	0.59
	Percentage of Lakes And Ponds [%]	0.14
	Percentage of Developed (Urban) Land (NLCD 2011 Classes 21-24) [%]	38.2
	Percentage of Imperviousness (NLCD 2001 Impervious Dataset) [%]	2.84
	Percentage of Imperviousness (NLCD 2011 Impervious Dataset) [%]	3.10
	Percentage of Imperviousness (NLCD 2019 Impervious Dataset) [%]	3.65
Stream Management Controls	Developed or Natural	Developed
	Regulation	Regulated
	Geological or Hydrological Control	None
	Dam Outlet	No
	Agricultural Control	Yes*
	(Waste)water Inputs	None
	Water Withdrawals	None
	Other Factors Affecting Runoff	-

*Entirely agricultural runoff - intense agricultural production around Salton Sea and controlled by agricultural return flows.

(a)

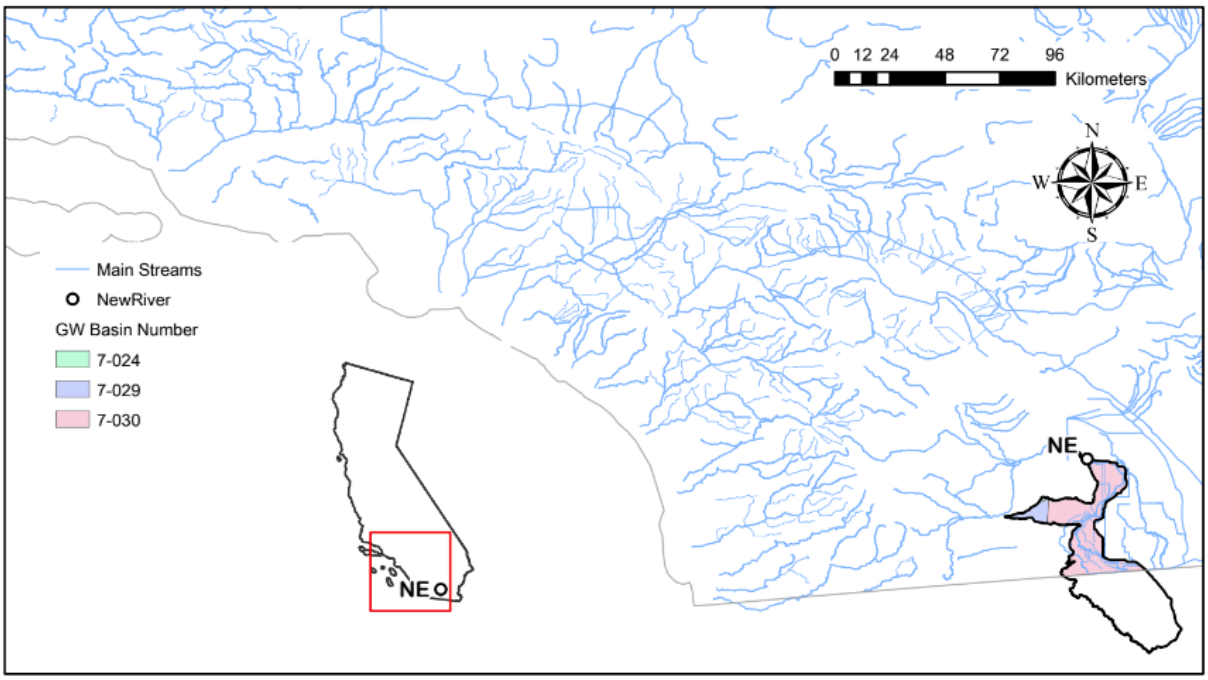
0 12 24 48 72 96
Kilometers
N
W
E
S
Main Streams
NewRiver
GW Basin Number
7-024
7-029
7-030
NE
NE

(b)

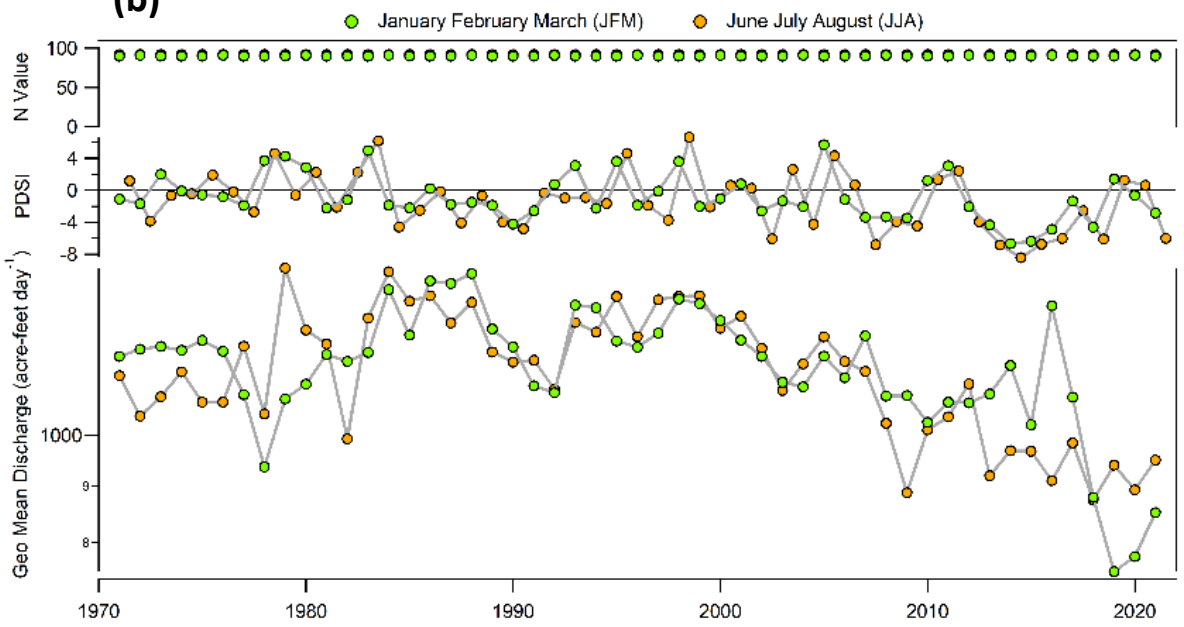
January February March (JFM)
June July August (JJA)
N Value
PDSI
Geo Mean Discharge (acre-feet day-1)
1970
1980
1990
2000
2010
2020

(c)

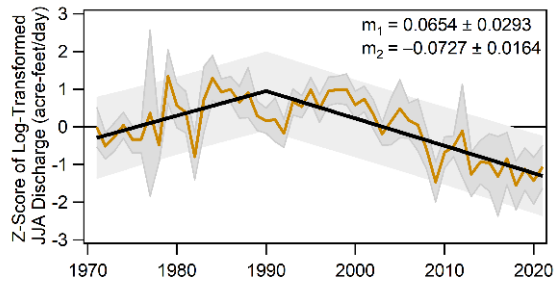
m1 = 0.0654 ± 0.0293
m2 = −0.0727 ± 0.0164
Z-Score of Log-Transformed JJA Discharge (acre-feet/day)
1970
1980
1990
2000
2010
2020

(d)

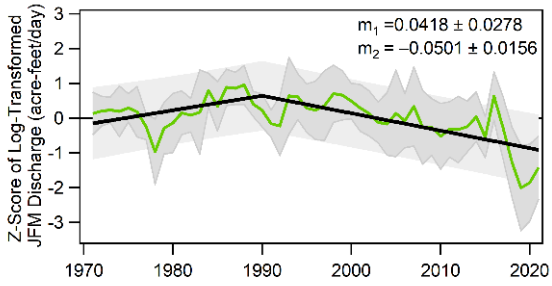
m1 =0.0418 ± 0.0278
m2 = −0.0501 ± 0.0156
Z-Score of Log-Transformed JFM Discharge (acre-feet/day)
1970
1980
1990
2000
2010
2020

SAN LUIS REY R A OCEANSIDE CA

Gauge Information	USGS Station ID	11042000
	Hydrologic Unit Code	18070303
	Latitude (NAD27)	33°13'05"
	Longitude (NAD27)	117°21'34"
	Drainage Area [Mi^2]	557
	Elevation of The Stream Outlet Above NAVD88 [Ft]	22
	County	San Diego
Watershed Characteristics	Mean Maximum January Temperature [°F]	61.54
	Mean Minimum January Temperature [°F]	37.68
	Mean Annual Precipitation [In]	19.9
	Hydrological Soil Group (HSG) [% of Covered Area]	C(22%), D(78%)
	Length of Longest Flow Path [Mi]	72
	Mean Basin Elevation [Ft]	2354
	Maximum Basin Elevation [Ft]	6525
	Minimum Basin Elevation [Ft]	22
	Percentage of Area Above 6000 Ft [%]	0.32
	Percentage of Area Covered By Forest [%]	15.4
	Percentage of Lakes And Ponds [%]	0.35
	Percentage of Developed (Urban) Land (NLCD 2011 Classes 21-24) [%]	14.1
	Percentage of Imperviousness (NLCD 2001 Impervious Dataset) [%]	3.02
	Percentage of Imperviousness (NLCD 2011 Impervious Dataset) [%]	3.30
	Percentage of Imperviousness (NLCD 2019 Impervious Dataset) [%]	3.44
Stream Management Controls	Developed or Natural	Developed
	Regulation	Regulated*
	Geological or Hydrological Control	Yes**
	Dam Outlet	No
	Agricultural Control	None
	(Waste)water Inputs	None
	Water Withdrawals	Yes**
	Other Factors Affecting Runoff	Groundwater***

*Flow regulated by Lake Henshaw, capacity, 194,300 acre-ft, since 1923. Gage was out of operation for channel work from Nov. 10, 1997, to Apr. 28, 1998.
**Several diversions for irrigation and domestic use upstream from station.
***Good flow lower watershed gage, influenced by heavy groundwater recharge upstream of the gage.
Ref. waterdata.usgs.gov

(a)

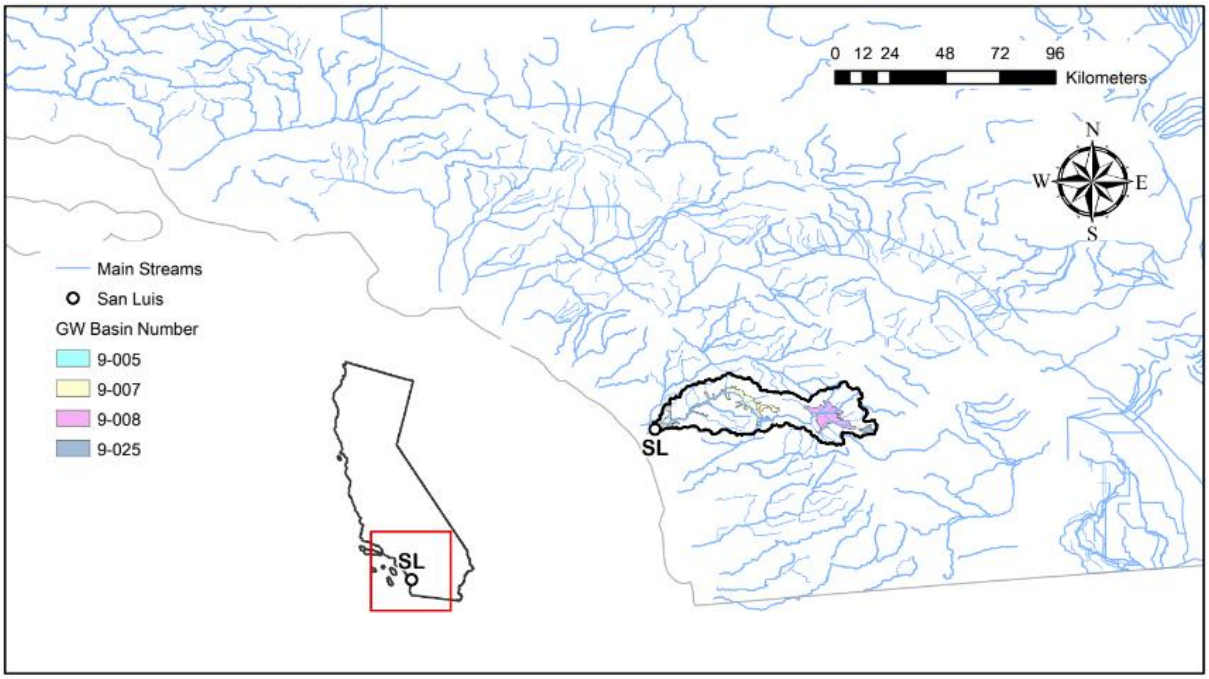
0 12 24 48 72 96
Kilometers
N
W
E
S
Main Streams
San Luis
GW Basin Number
9-005
9-007
9-008
9-025
SL
SL

(b)

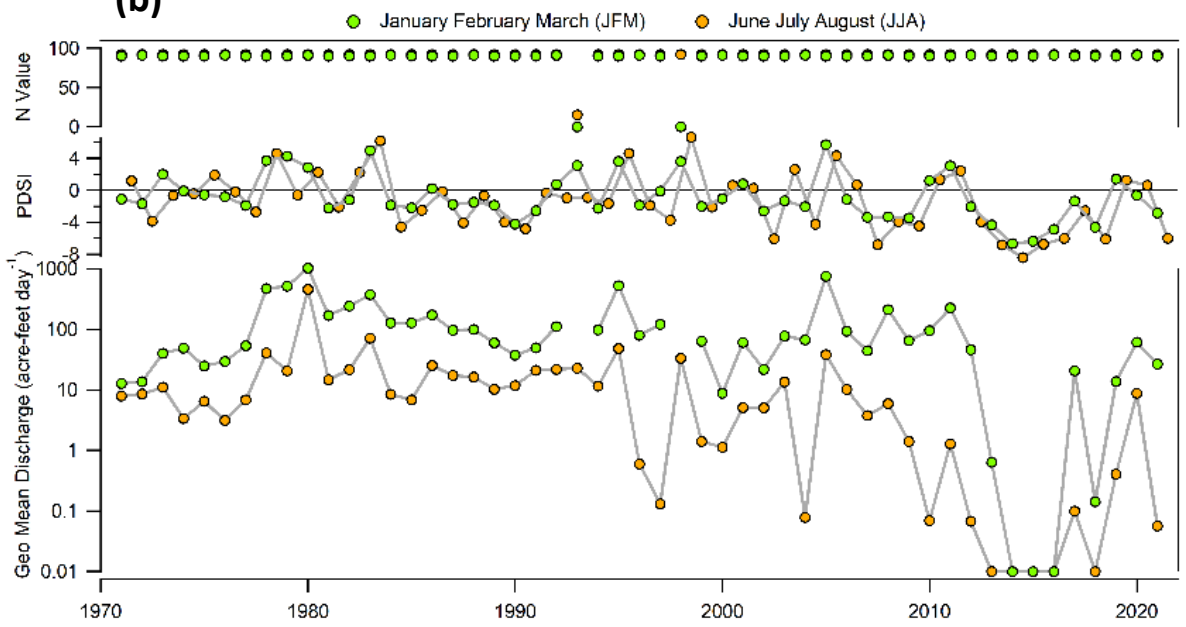
January February March (JFM)
June July August (JJA)
N Value
PDSI
Geo Mean Discharge (acre-feet day-1)
1970
1980
1990
2000
2010
2020

(c)

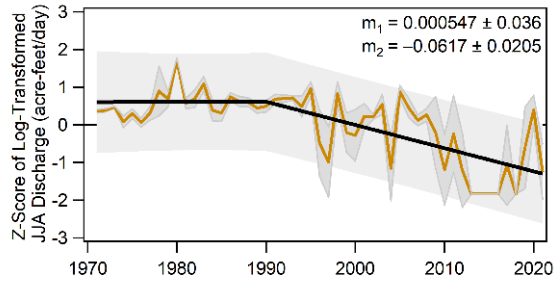
m1 = 0.000547 ± 0.036
m2 = −0.0617 ± 0.0205
Z-Score of Log-Transformed JJA Discharge (acre-feet/day)
1970
1980
1990
2000
2010
2020

(d)

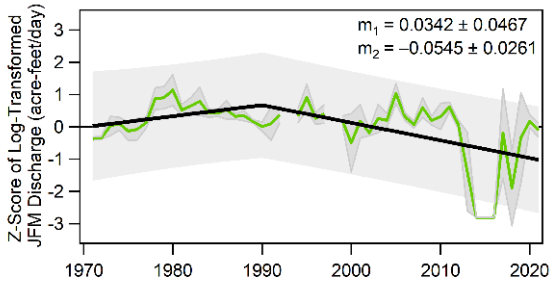
m1 = 0.0342 ± 0.0467
m2 = −0.0545 ± 0.0261
Z-Score of Log-Transformed JFM Discharge (acre-feet/day)
1970
1980
1990
2000
2010
2020

SANTA MARIA C NR RAMONA CA

Gauge Information	USGS Station ID	11028500
	Hydrologic Unit Code	18070304
	Latitude (NAD27)	33°03'08"
	Longitude (NAD27)	116°56'41"
	Drainage Area [Mi^2]	57.6
	Elevation of The Stream Outlet Above NAVD88 [Ft]	1308
	County	San Diego
Watershed Characteristics	Mean Maximum January Temperature [°F]	64.35
	Mean Minimum January Temperature [°F]	38.08
	Mean Annual Precipitation [In]	18.7
	Hydrological Soil Group (HSG) [% of Covered Area]	C(32%), D(68%)
	Length of Longest Flow Path [Mi]	18
	Mean Basin Elevation [Ft]	1845
	Maximum Basin Elevation [Ft]	3271
	Minimum Basin Elevation [Ft]	1307
	Percentage of Area Above 6000 Ft [%]	0
	Percentage of Area Covered By Forest [%]	4.65
	Percentage of Lakes And Ponds [%]	0.008
	Percentage of Developed (Urban) Land (NLCD 2011 Classes 21-24) [%]	17.3
	Percentage of Imperviousness (NLCD 2001 Impervious Dataset) [%]	2.72
	Percentage of Imperviousness (NLCD 2011 Impervious Dataset) [%]	2.93
	Percentage of Imperviousness (NLCD 2019 Impervious Dataset) [%]	3.05
Stream Management Controls	Developed or Natural	Developed*
	Regulation	Unregulated*
	Geological or Hydrological Control	None
	Dam Outlet	No
	Agricultural Control	Yes**
	(Waste)water Inputs	Yes***
	Water Withdrawals	None
	Other Factors Affecting Runoff	-

*Some development within the watershed and no regulation upstream from station. .
**Historical agriculture and vernal pool landscape;
***Land application of treated sewage effluent upstream from the gage beginning December 1972 contributes to low flows.
Ref. waterdata.usgs.gov

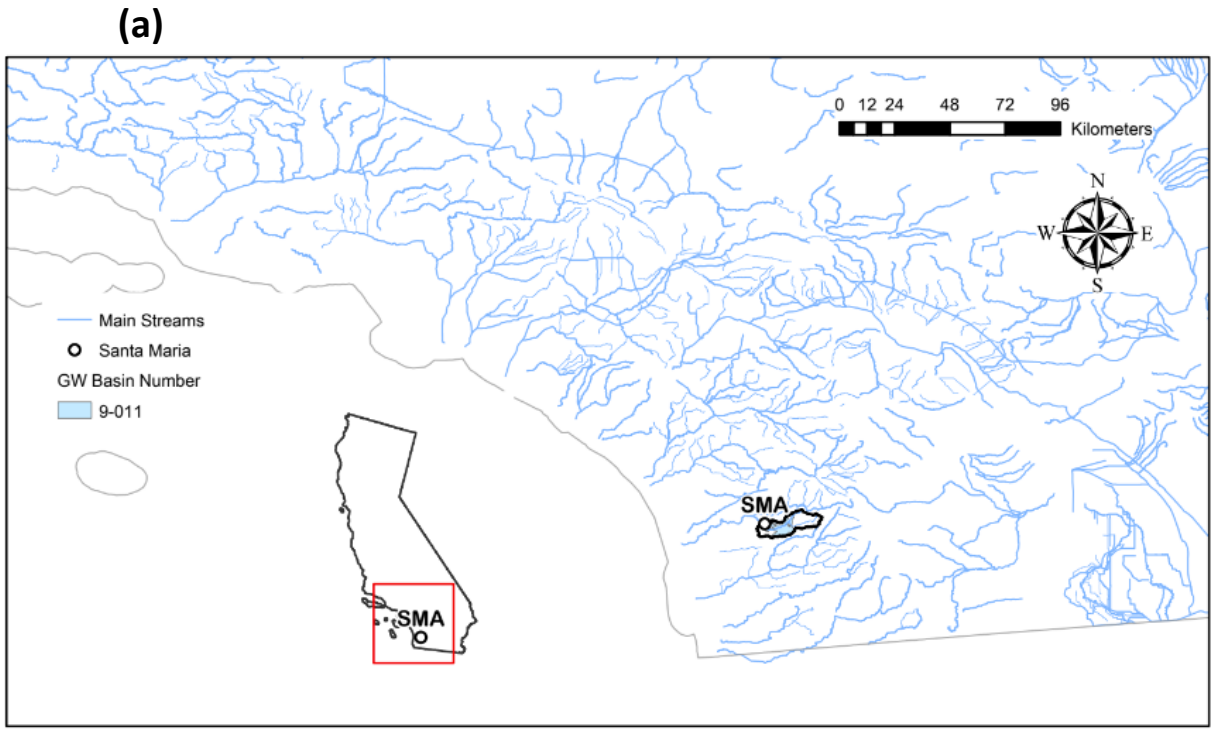
(a)
0 12 24 48 72 96
Kilometers
N
W
E
S
Main Streams
Santa Maria
GW Basin Number
9-011
SMA
SMA

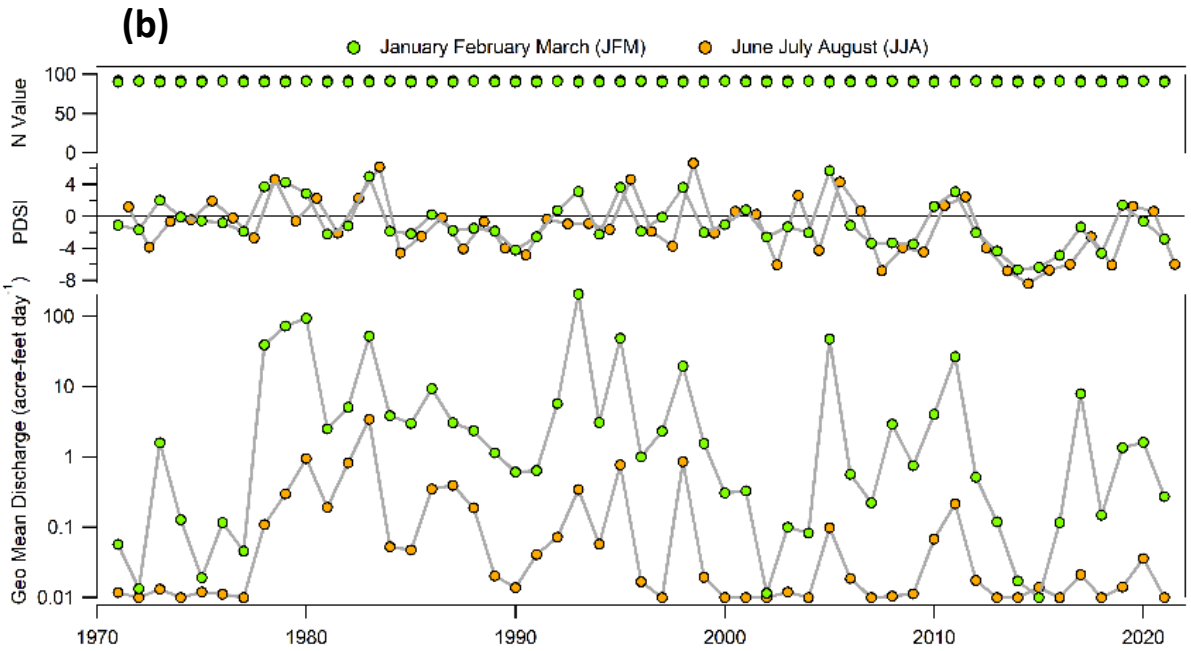
(b)
January February March (JFM)
June July August (JJA)
N Value
PDSI
Geo Mean Discharge (acre-feet day-1)
1970
1980
1990
2000
2010
2020

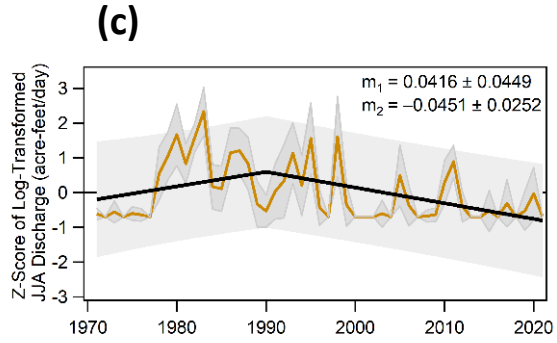
(c)
m1 = 0.0416 ± 0.0449
m2 = −0.0451 ± 0.0252
Z-Score of Log-Transformed JJA Discharge (acre-feet/day)
1970
1980
1990
2000
2010
2020

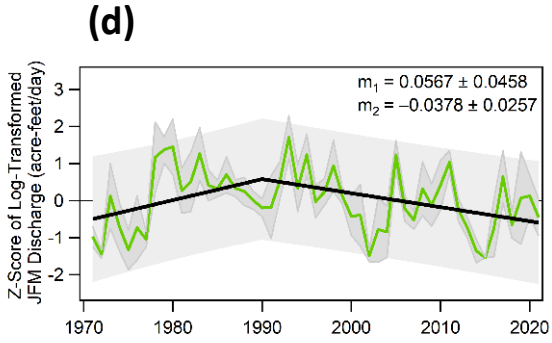
(d)
m1 = 0.0567 ± 0.0458
m2 = −0.0378 ± 0.0257
Z-Score of Log-Transformed JFM Discharge (acre-feet/day)
1970
1980
1990
2000
2010
2020

BIG TUJUNGA C BL HANSEN DAM CA

Gauge Information	USGS Station ID	11097000
	Hydrologic Unit Code	18070105
	Latitude (NAD27)	34°15'13"
	Longitude (NAD27)	118°23'17"
	Drainage Area [Mi^2]	153
	Elevation of The Stream Outlet Above NAVD88 [Ft]	945
	County	Los Angeles
Watershed Characteristics	Mean Maximum January Temperature [°F]	55.49
	Mean Minimum January Temperature [°F]	38.59
	Mean Annual Precipitation [In]	27.5
	Hydrological Soil Group (HSG) [% of Covered Area]	D(100%)
	Length of Longest Flow Path [Mi]	34
	Mean Basin Elevation [Ft]	3612
	Maximum Basin Elevation [Ft]	7107
	Minimum Basin Elevation [Ft]	945
	Percentage of Area Above 6000 Ft [%]	1.84
	Percentage of Area Covered By Forest [%]	20
	Percentage of Lakes And Ponds [%]	0.0975
	Percentage of Developed (Urban) Land (NLCD 2011 Classes 21-24) [%]	9.7
	Percentage of Imperviousness (NLCD 2001 Impervious Dataset) [%]	2.52
	Percentage of Imperviousness (NLCD 2011 Impervious Dataset) [%]	2.58
	Percentage of Imperviousness (NLCD 2019 Impervious Dataset) [%]	2.63
Stream Management Controls	Developed or Natural	Developed
	Regulation	Regulated*
	Geological or Hydrological Control	None
	Dam Outlet	Yes
	Agricultural Control	None
	(Waste)water Inputs	None
	Water Withdrawals	Yes**
	Other Factors Affecting Runoff	-

*Flow regulated since July 1931 by Big Tujunga Flood Control Reservoir, capacity, 5,690 acre-ft, and since September 1940 by Hansen Flood-Control Reservoir, capacity, 25,450 acre-ft.

**Several small diversions for domestic use and irrigation. Since about 1948, Los Angeles County Department of Public Works has diverted water 0.3 mi upstream from gage to spreading grounds. Ref. waterdata.usgs.gov

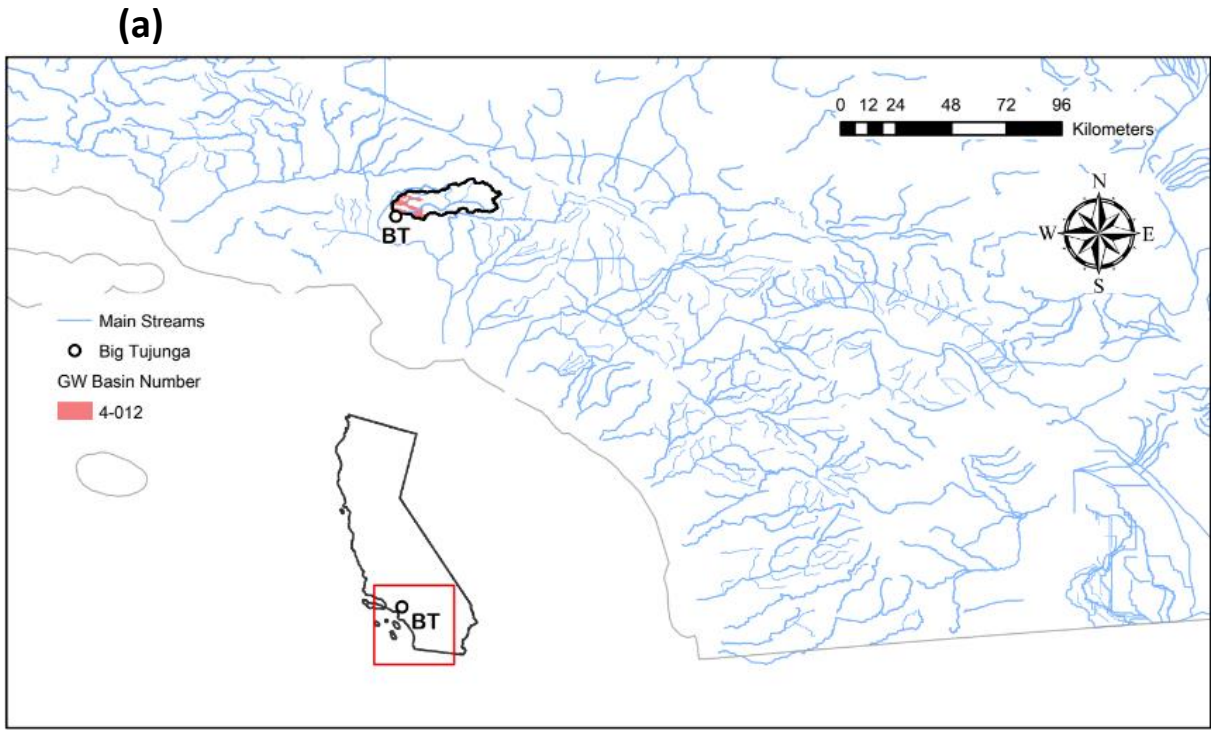
(a)
0 12 24 48 72 96
Kilometers
N
W
E
S
BT
Main Streams
Big Tujunga
GW Basin Number
4-012
BT

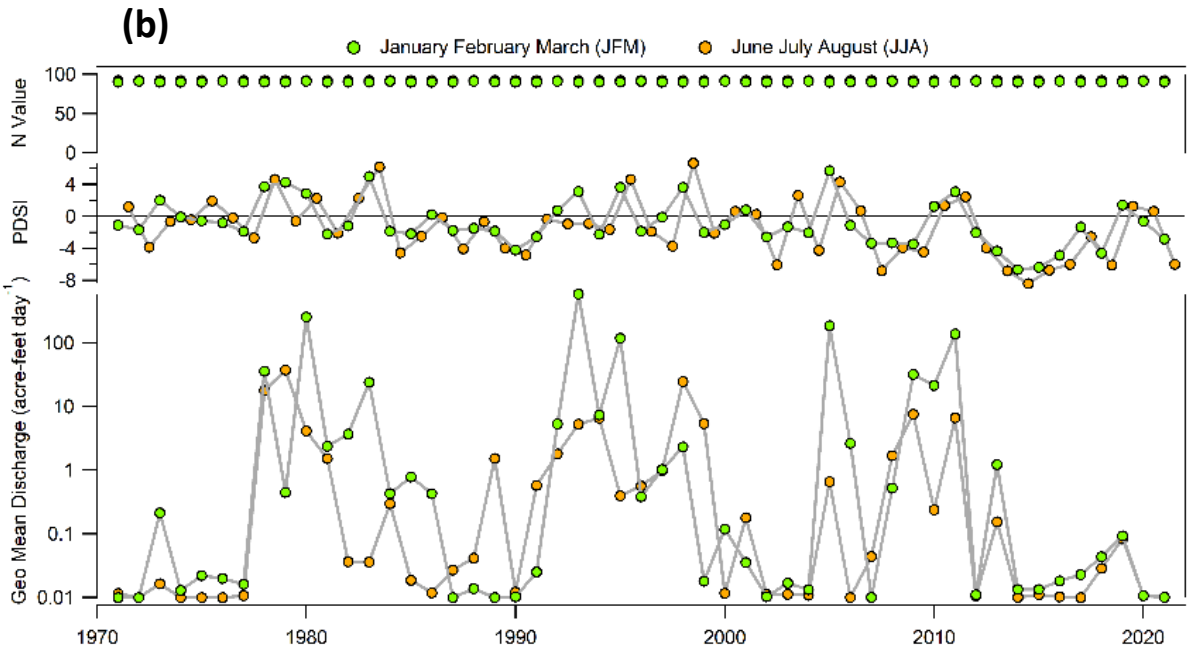
(b)
January February March (JFM)
June July August (JJA)
N Value
PDSI
Geo Mean Discharge (acre-feet day-1)
1970
1980
1990
2000
2010
2020

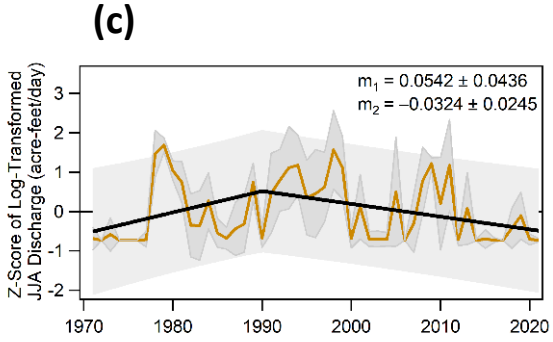
(c)
m1 = 0.0542 ± 0.0436
m2 = −0.0324 ± 0.0245
Z-Score of Log-Transformed JJA Discharge (acre-feet/day)

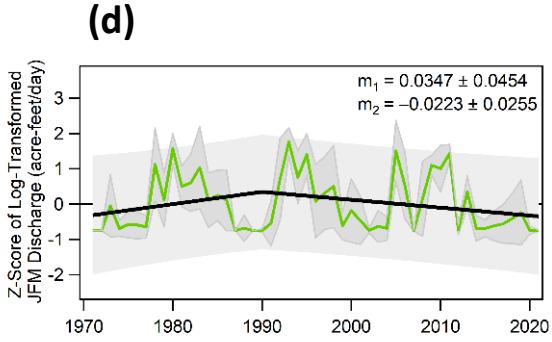
(d)
m1 = 0.0347 ± 0.0454
m2 = −0.0223 ± 0.0255
Z-Score of Log-Transformed JFM Discharge (acre-feet/day)

VENTURA R NR VENTURA

Gauge Information	USGS Station ID	11118500
	Hydrologic Unit Code	18070101
	Latitude (NAD27)	34°21'08"
	Longitude (NAD27)	119°18'27"
	Drainage Area [Mi^2]	188
	Elevation of The Stream Outlet Above NAVD88 [Ft]	220
	County	Ventura
Watershed Characteristics	Mean Maximum January Temperature [°F]	60.67
	Mean Minimum January Temperature [°F]	37.37
	Mean Annual Precipitation [In]	27.3
	Hydrological Soil Group (HSG) [% of Covered Area]	C(18%), D(82%)
	Length of Longest Flow Path [Mi]	28
	Mean Basin Elevation [Ft]	2305
	Maximum Basin Elevation [Ft]	6029
	Minimum Basin Elevation [Ft]	218
	Percentage of Area Above 6000 Ft [%]	0.001
	Percentage of Area Covered By Forest [%]	29.5
	Percentage of Lakes And Ponds [%]	1.89
	Percentage of Developed (Urban) Land (NLCD 2011 Classes 21-24) [%]	10.6
	Percentage of Imperviousness (NLCD 2001 Impervious Dataset) [%]	1.33
	Percentage of Imperviousness (NLCD 2011 Impervious Dataset) [%]	1.36
	Percentage of Imperviousness (NLCD 2019 Impervious Dataset) [%]	1.37
Stream Management Controls	Developed or Natural	Developed
	Regulation	Regulated*
	Geological or Hydrological Control	None
	Dam Outlet	No
	Agricultural Control	None
	(Waste)water Inputs	None
	Water Withdrawals	Yes**
	Other Factors Affecting Runoff	Affected by Discharge from Lake Casitas

*Flow partly regulated since March 1948 by Matilija Reservoir (station 11115000), usable capacity, 1,480 acre-ft, and since October 1959 by Lake Casitas (station 11108133), capacity, 323,700 acre-ft.

**Water diverted to Lake Casitas on Coyote Creek since January 1959. Diversion by City of Ventura for municipal supply began prior to 1911. For records of combined discharge of river and Ventura City Diversion (station 11118400), see station 11118501 (discontinued in 2007).

(a)

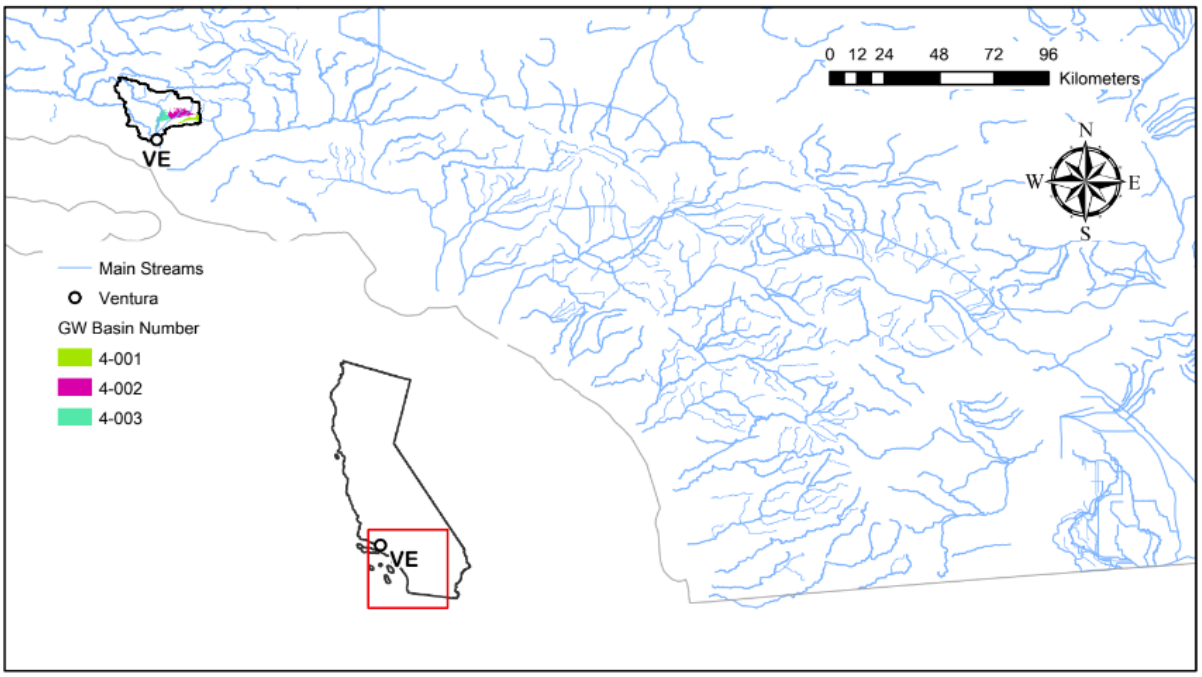
0 12 24 48 72 96
Kilometers
N
W
E
S
VE
Main Streams
Ventura
GW Basin Number
4-001
4-002
4-003
VE

(b)

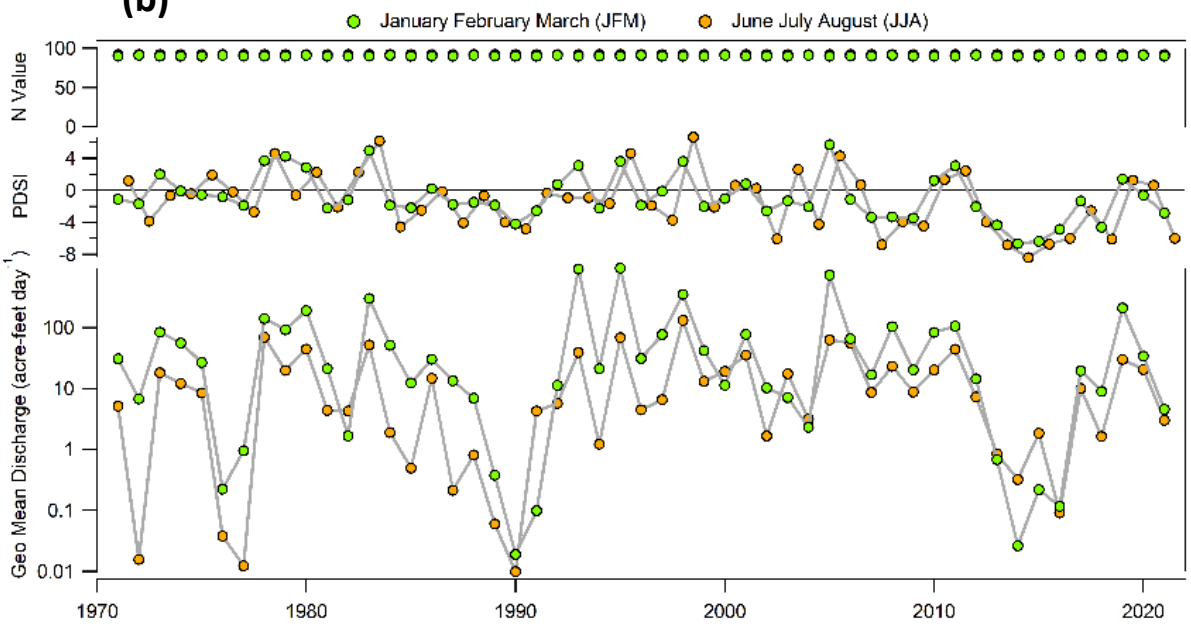
January February March (JFM)
June July August (JJA)
N Value
PDSI
Geo Mean Discharge (acre-feet day⁻¹)
1970
1980
1990
2000
2010
2020

(c)

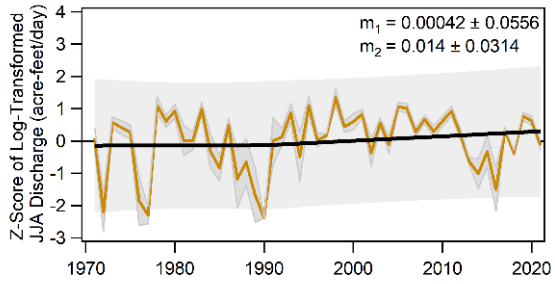
m1 = 0.00042 ± 0.0556
m2 = 0.014 ± 0.0314
Z-Score of Log-Transformed JJA Discharge (acre-feet/day)
1970
1980
1990
2000
2010
2020

(d)

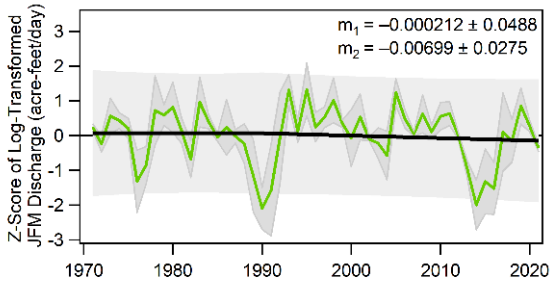
m1 = –0.000212 ± 0.0488
m2 = –0.00699 ± 0.0275
Z-Score of Log-Transformed JFM Discharge (acre-feet/day)
1970
1980
1990
2000
2010
2020

BIG ROCK C NR VALYERMO CA

Gauge Information	USGS Station ID	10263500
	Hydrologic Unit Code	18090206
	Latitude (NAD27)	34°25'15"
	Longitude (NAD27)	117°50'19"
	Drainage Area [Mi^2]	22.9
	Elevation of The Stream Outlet Above NAVD88 [Ft]	4094
	County	Los Angeles
Watershed Characteristics	Mean Maximum January Temperature [°F]	47.54
	Mean Minimum January Temperature [°F]	29.21
	Mean Annual Precipitation [In]	27.5
	Hydrological Soil Group (HSG) [% of Covered Area]	D(100%)
	Length of Longest Flow Path [Mi]	8
	Mean Basin Elevation [Ft]	6349
	Maximum Basin Elevation [Ft]	9387
	Minimum Basin Elevation [Ft]	4064
	Percentage of Area Above 6000 Ft [%]	61.1
	Percentage of Area Covered By Forest [%]	20.1
	Percentage of Lakes And Ponds [%]	0
	Percentage of Developed (Urban) Land (NLCD 2011 Classes 21-24) [%]	3
	Percentage of Imperviousness (NLCD 2001 Impervious Dataset) [%]	0.83
	Percentage of Imperviousness (NLCD 2011 Impervious Dataset) [%]	0.86
	Percentage of Imperviousness (NLCD 2019 Impervious Dataset) [%]	0.89
Stream Management Controls	Developed or Natural	Natural
	Regulation	Unregulated*
	Geological or Hydrological Control	Yes
	Dam Outlet	No
	Agricultural Control	None
	(Waste)water Inputs	None
	Water Withdrawals	None*
	Other Factors Affecting Runoff	Alluvial Fan**

*No regulation or diversion upstream from station. Ref. waterdata.usgs.gov

**Near Devils Punchbowl, below large alluvial fan that modulates runoff.

(a)

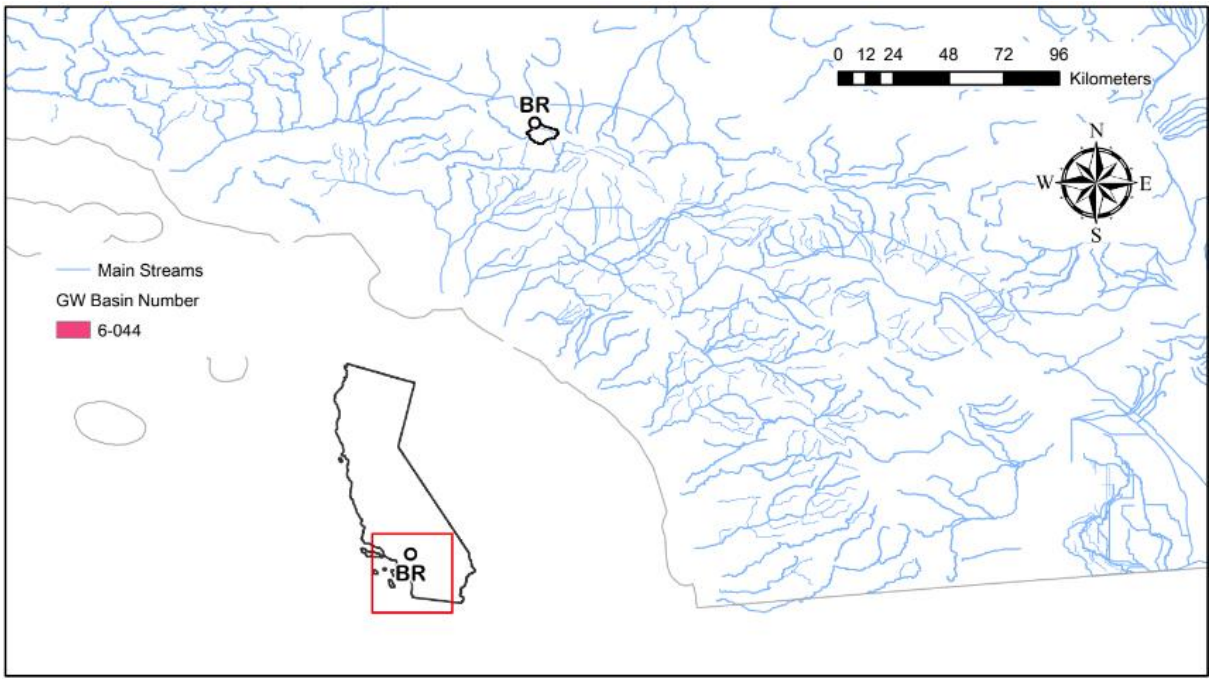
0 12 24 48 72 96
Kilometers
N
W
E
S
BR
Main Streams
GW Basin Number
6-044
BR

(b)

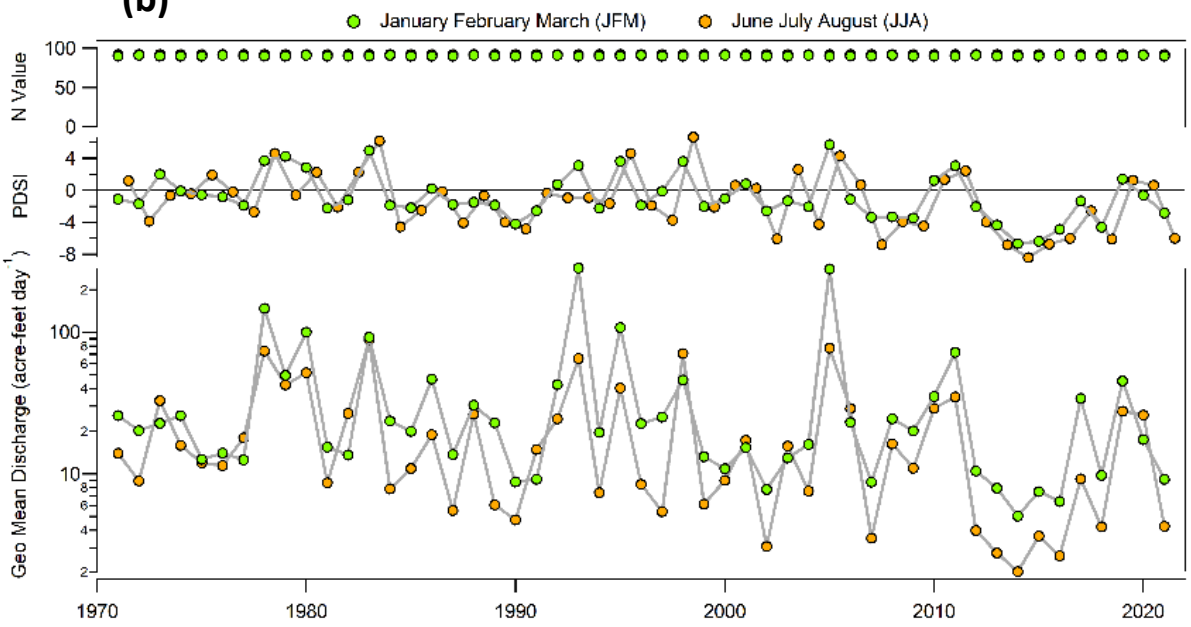
January February March (JFM)
June July August (JJA)
N Value
PDSI
Geo Mean Discharge (acre-feet day⁻¹)
1970
1980
1990
2000
2010
2020

(c)

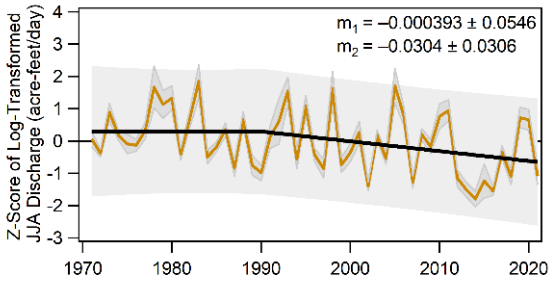
m1 = –0.000393 ± 0.0546
m2 = –0.0304 ± 0.0306
Z-Score of Log-Transformed JJA Discharge (acre-feet/day)
1970
1980
1990
2000
2010
2020

(d)

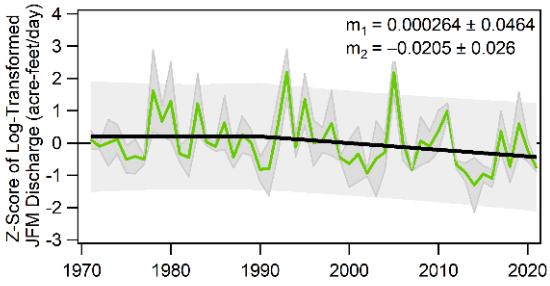
m1 = 0.000264 ± 0.0464
m2 = –0.0205 ± 0.026
Z-Score of Log-Transformed JFM Discharge (acre-feet/day)
1970
1980
1990
2000
2010
2020

SAN GABRIEL R BL SANTA FE DAM NR BALDWIN PK CA

Gauge Information	USGS Station ID	11085000
	Hydrologic Unit Code	18070106
	Latitude (NAD27)	34°06'44"
	Longitude (NAD27)	117°58'07"
	Drainage Area [Mi^2]	236
	Elevation of The Stream Outlet Above NAVD88 [Ft]	432
	County	Los Angeles
Watershed Characteristics	Mean Maximum January Temperature [°F]	54.13
	Mean Minimum January Temperature [°F]	36.3
	Mean Annual Precipitation [In]	34.9
	Hydrological Soil Group (HSG) [% of Covered Area]	C(1%), D(99%)
	Length of Longest Flow Path [Mi]	39
	Mean Basin Elevation [Ft]	4236
	Maximum Basin Elevation [Ft]	10059
	Minimum Basin Elevation [Ft]	232
	Percentage of Area Above 6000 Ft [%]	19.5
	Percentage of Area Covered By Forest [%]	25
	Percentage of Lakes And Ponds [%]	0.29
	Percentage of Developed (Urban) Land (NLCD 2011 Classes 21-24) [%]	4.7
	Percentage of Imperviousness (NLCD 2001 Impervious Dataset) [%]	0.78
	Percentage of Imperviousness (NLCD 2011 Impervious Dataset) [%]	0.86
	Percentage of Imperviousness (NLCD 2019 Impervious Dataset) [%]	0.86
Stream Management Controls	Developed or Natural	Developed
	Regulation	Regulated*
	Geological or Hydrological Control	Yes**
	Dam Outlet	Yes**
	Agricultural Control	None
	(Waste)water Inputs	None
	Water Withdrawals	Yes***
	Other Factors Affecting Runoff	-

*Flow regulated by Cogswell and San Gabriel Flood-Control Reservoirs, combined capacity, 43,170 acre-ft; Morris Reservoir, capacity, 28,800 acre-ft; and Santa Fe Flood Control Reservoir, capacity, 32,100 acre-ft.
**Outlet of Santa Fe Dam, runoff controlled by dam releases
**Diversions upstream from station for irrigation, power development, and ground-water replenishment. At times water is diverted from side of stilling basin to headwaters of Rio Hondo. Los Angeles County Department of Public Works diversion from San Gabriel River below Santa Fe Dam (11085000) to Rio Hondo during water year:2014 - no diversion; 2015-no diversion; 2016-801 acre-feet; 2017-53,700 acre-feet; 2018- 6,480 acre-feet; 2019- 50,100 acre-feet; 2020-34,500 acre-feet; 2021- 6,360 acre-feet.
Ref. waterdata.usgs.gov

(a)

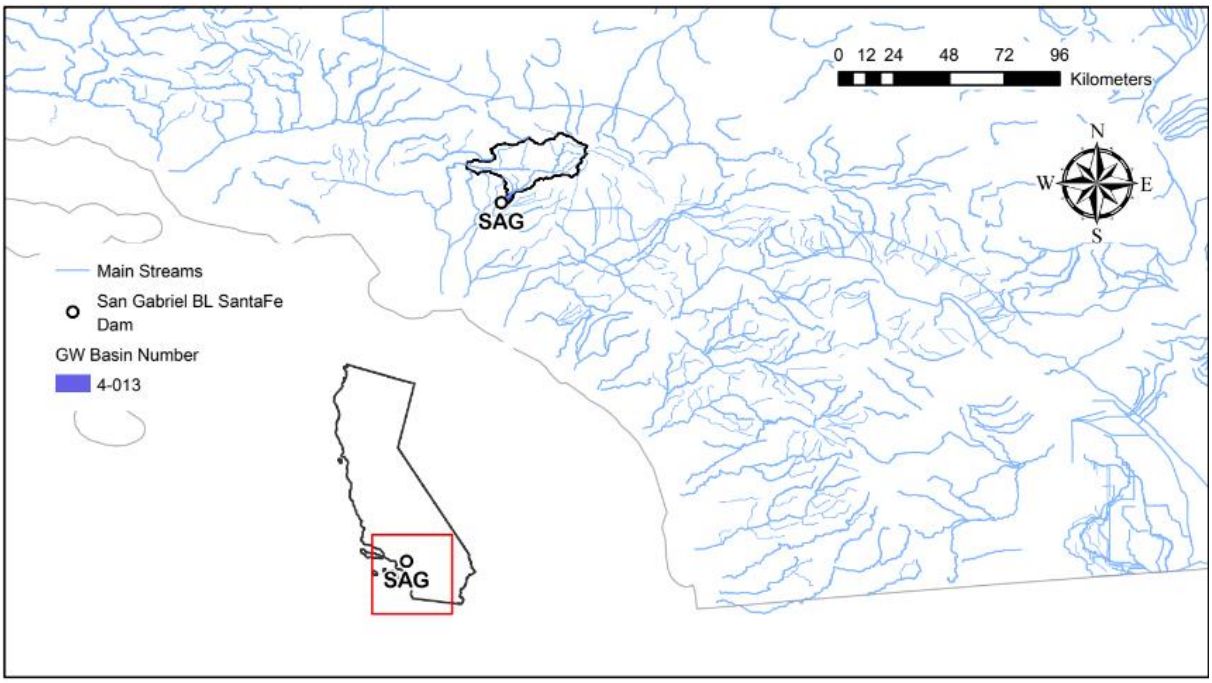
0 12 24 48 72 96
Kilometers
N
W
E
S
SAG
Main Streams
San Gabriel BL SantaFe Dam
GW Basin Number
4-013
SAG

(b)

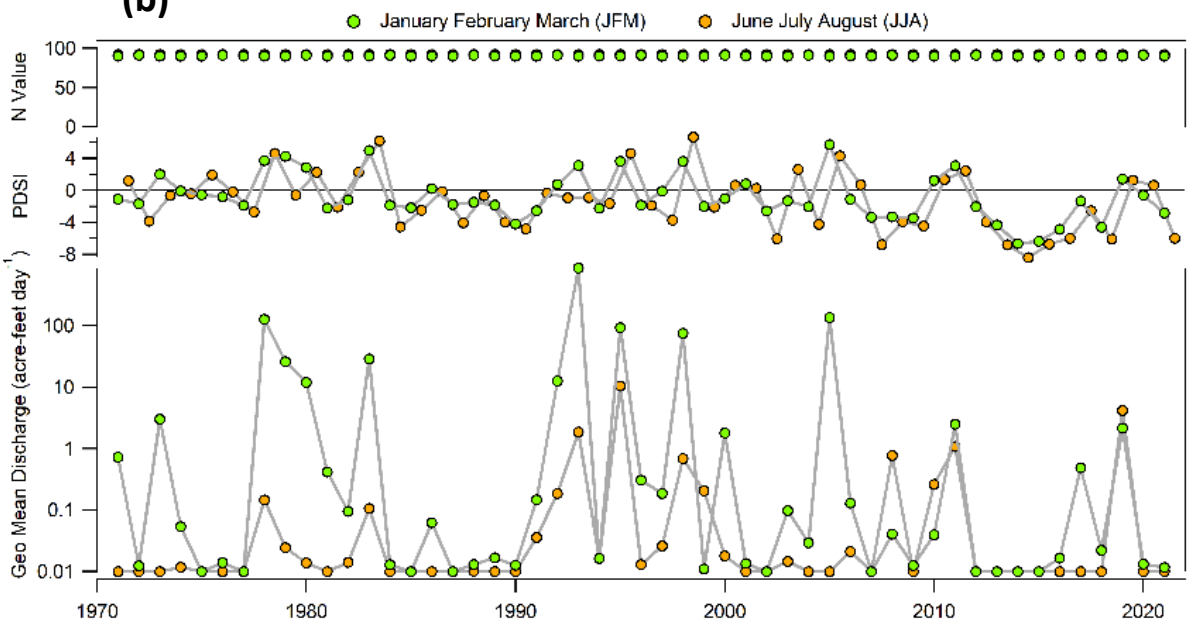
January February March (JFM)
June July August (JJA)
N Value
PDSI
Geo Mean Discharge (acre-feet day⁻¹)
1970
1980
1990
2000
2010
2020

(c)

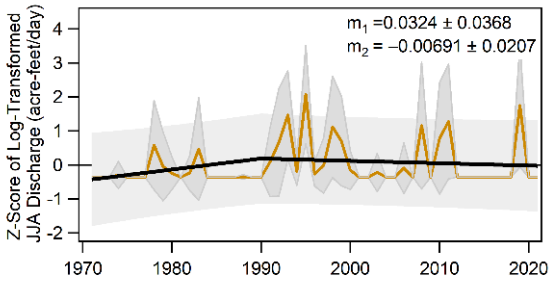
m1 =0.0324 ± 0.0368
m2 = –0.00691 ± 0.0207
Z-Score of Log-Transformed JJA Discharge (acre-feet/day)
1970
1980
1990
2000
2010
2020

(d)

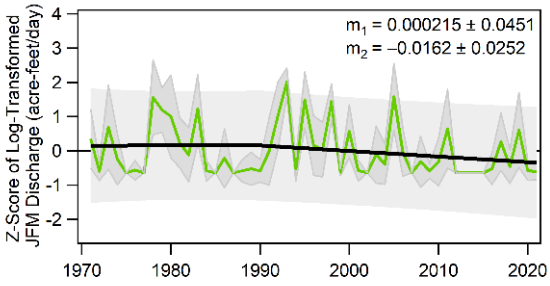
m1 = 0.000215 ± 0.0451
m2 = –0.0162 ± 0.0252
Z-Score of Log-Transformed JFM Discharge (acre-feet/day)
1970
1980
1990
2000
2010
2020

DEVIL CYN C NR SAN BERNARDINO CA

Gauge Information	USGS Station ID	11063680
	Hydrologic Unit Code	18070203
	Latitude (NAD27)	34°12'30"
	Longitude (NAD27)	117°19'50"
	Drainage Area [Mi^2]	5.49
	Elevation of The Stream Outlet Above NAVD88 [Ft]	2125
	County	San Bernadino
Watershed Characteristics	Mean Maximum January Temperature [°F]	54.13
	Mean Minimum January Temperature [°F]	34.09
	Mean Annual Precipitation [In]	36.7
	Hydrological Soil Group (HSG) [% of Covered Area]	D(100%)
	Length of Longest Flow Path [Mi]	4
	Mean Basin Elevation [Ft]	3815
	Maximum Basin Elevation [Ft]	5379
	Minimum Basin Elevation [Ft]	2125
	Percentage of Area Above 6000 Ft [%]	0
	Percentage of Area Covered By Forest [%]	32.9
	Percentage of Lakes And Ponds [%]	0
	Percentage of Developed (Urban) Land (NLCD 2011 Classes 21-24) [%]	6.4
	Percentage of Imperviousness (NLCD 2001 Impervious Dataset) [%]	0.72
	Percentage of Imperviousness (NLCD 2011 Impervious Dataset) [%]	0.74
	Percentage of Imperviousness (NLCD 2019 Impervious Dataset) [%]	0.74
Stream Management Controls	Developed or Natural	Natural*
	Regulation	Unregulated*
	Geological or Hydrological Control	None
	Dam Outlet	No
	Agricultural Control	None
	(Waste)water Inputs	None
	Water Withdrawals	Yes**
	Other Factors Affecting Runoff	-

* Adjacent to DWR reservoir and mostly natural flows; No regulation upstream from station.
**City of San Bernardino diverts upstream from station at times, with diverted flows routed to recharge basins downstream from station. Natural flow affected by pumping along creek.
Ref. waterdata.usgs.gov

(a)

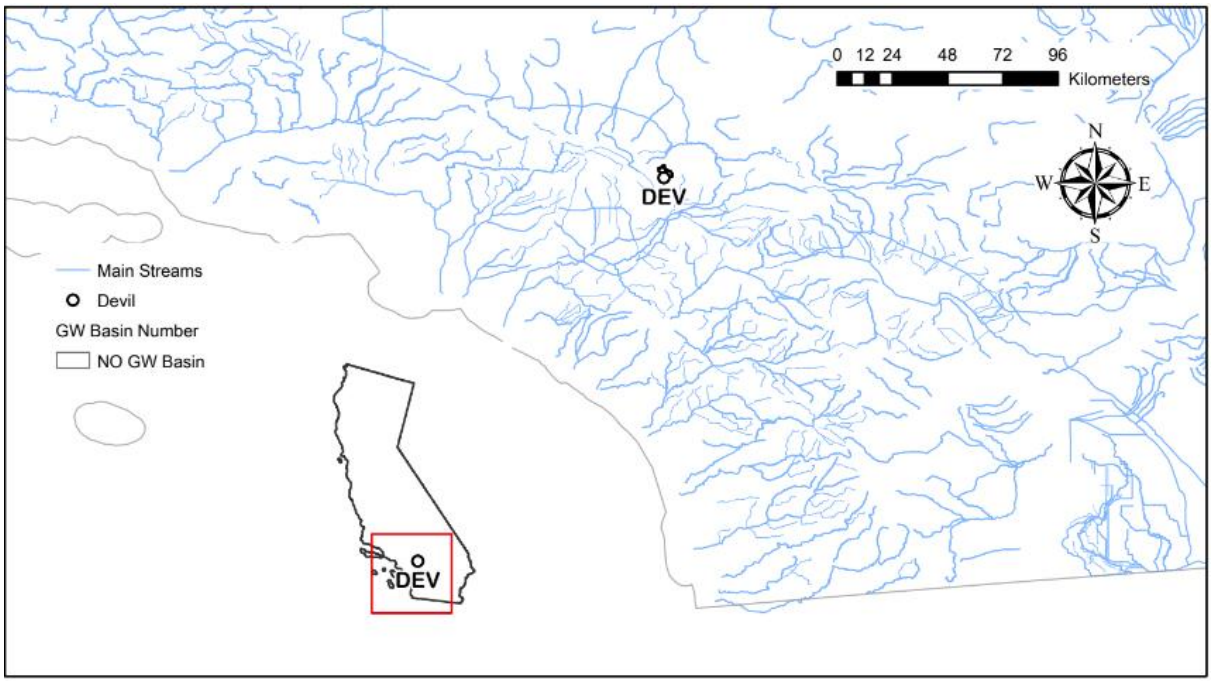
0 12 24 48 72 96
Kilometers
N
W
E
S
DEV
Main Streams
Devil
GW Basin Number
NO GW Basin
DEV

(b)

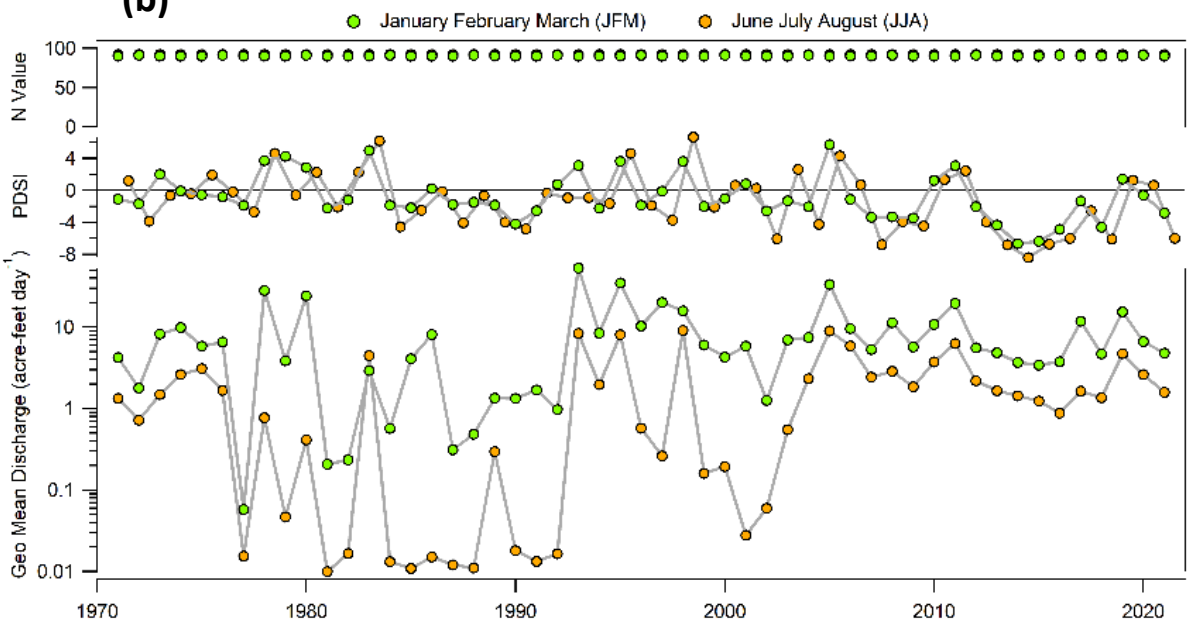
January February March (JFM)
June July August (JJA)
N Value
PDSI
Geo Mean Discharge (acre-feet day⁻¹)
1970
1980
1990
2000
2010
2020

(c)

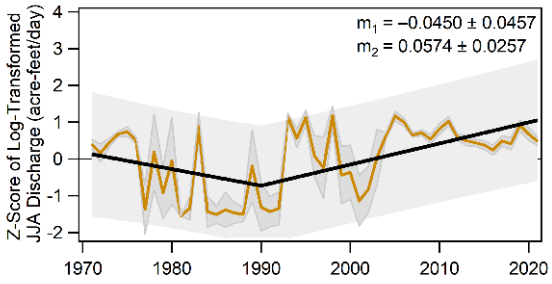
m1 = −0.0450 ± 0.0457
m2 = 0.0574 ± 0.0257
Z-Score of Log-Transformed JJA Discharge (acre-feet/day)
1970
1980
1990
2000
2010
2020

(d)

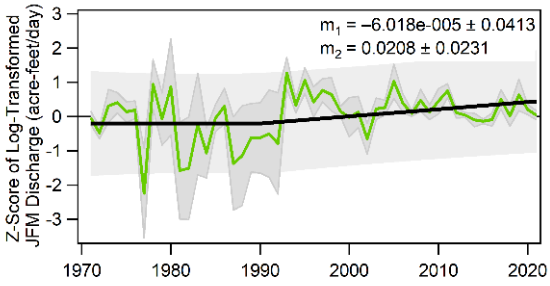
m1 = −6.018e-005 ± 0.0413
m2 = 0.0208 ± 0.0231
Z-Score of Log-Transformed JFM Discharge (acre-feet/day)
1970
1980
1990
2000
2010
2020

JAMUL C NR JAMUL CA

Gauge Information	USGS Station ID	11014000
	Hydrologic Unit Code	18070304
	Latitude (NAD27)	32°38'15"
	Longitude (NAD27)	116°53'00"
	Drainage Area [Mi^2]	70.1
	Elevation of The Stream Outlet Above NAVD88 [Ft]	524
	County	San Diego
Watershed Characteristics	Mean Maximum January Temperature [°F]	64.35
	Mean Minimum January Temperature [°F]	39.02
	Mean Annual Precipitation [In]	17.5
	Hydrological Soil Group (HSG) [% of Covered Area]	C(100%)
	Length of Longest Flow Path [Mi]	13
	Mean Basin Elevation [Ft]	1604
	Maximum Basin Elevation [Ft]	3733
	Minimum Basin Elevation [Ft]	518
	Percentage of Area Above 6000 Ft [%]	0
	Percentage of Area Covered By Forest [%]	8.15
	Percentage of Lakes And Ponds [%]	0
	Percentage of Developed (Urban) Land (NLCD 2011 Classes 21-24) [%]	7
	Percentage of Imperviousness (NLCD 2001 Impervious Dataset) [%]	0.59
	Percentage of Imperviousness (NLCD 2011 Impervious Dataset) [%]	0.62
	Percentage of Imperviousness (NLCD 2019 Impervious Dataset) [%]	0.65
Stream Management Controls	Developed or Natural	Natural
	Regulation	Unregulated*
	Geological or Hydrological Control	None
	Dam Outlet	No
	Agricultural Control	None
	(Waste)water Inputs	Yes**
	Water Withdrawals	None
	Other Factors Affecting Runoff	Pasture Grazing

* No regulation upstream from station.
**Water is diverted from Cottonwood Creek at Barrett Lake (station 11011000) via San Diego and Dulzura Conduit into Dulzura Creek, a tributary to Jamul Creek, and is included in discharge for this station. Ref. waterdata.usgs.gov
***Upstream of Otay lakes, landscape heavily grazed until about 20 years ago.
Ref. waterdata.usgs.gov

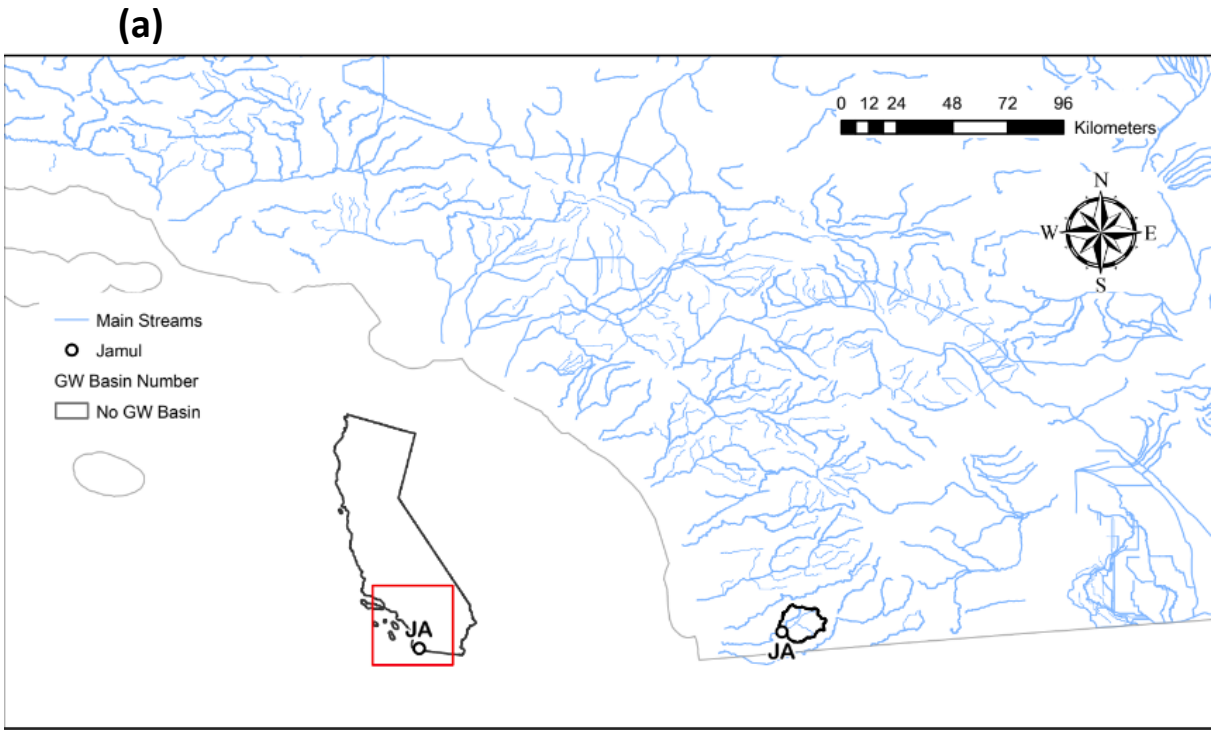
(a)
0 12 24 48 72 96
Kilometers
N
W
E
S
Main Streams
Jamul
GW Basin Number
No GW Basin
JA
JA

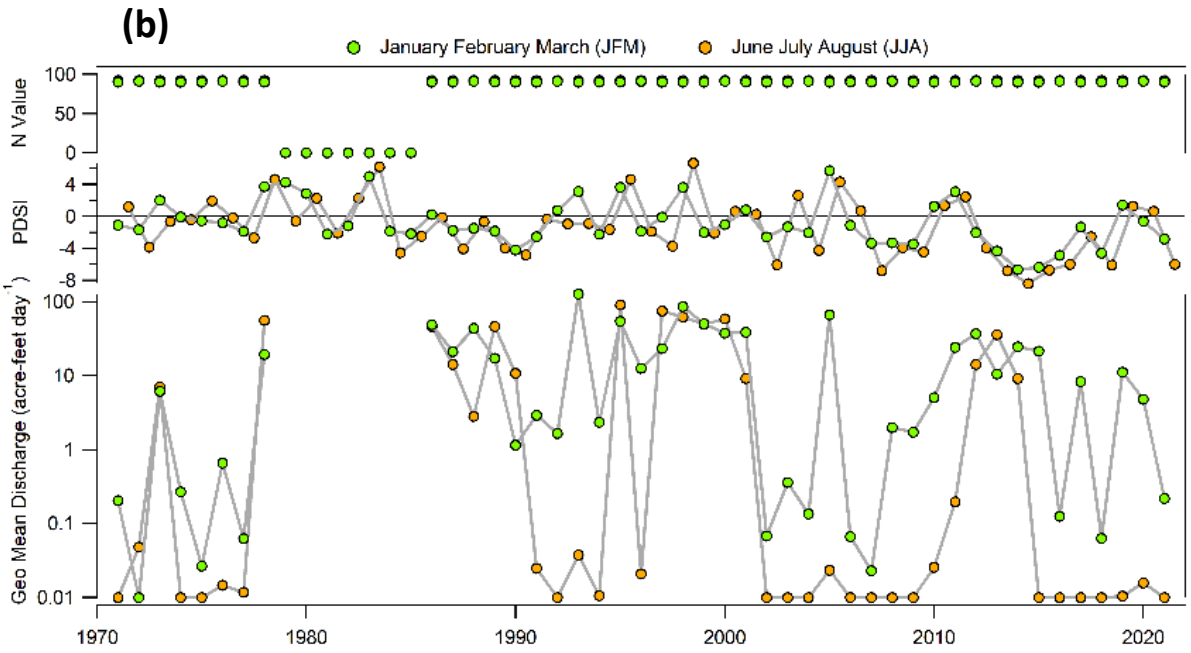
(b)
January February March (JFM)
June July August (JJA)
N Value
PDSI
Geo Mean Discharge (acre-feet day⁻¹)
1970
1980
1990
2000
2010
2020

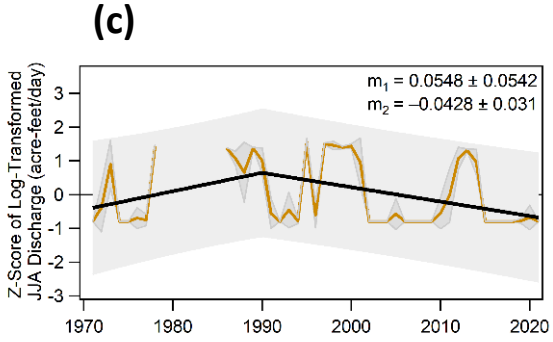
(c)
m1 = 0.0548 ± 0.0542
m2 = −0.0428 ± 0.031
Z-Score of Log-Transformed JJA Discharge (acre-feet/day)
1970
1980
1990
2000
2010
2020

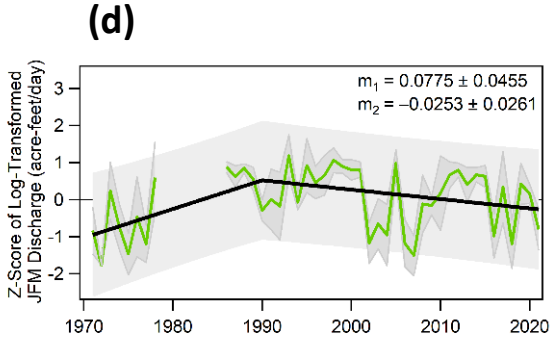
(d)
m1 = 0.0775 ± 0.0455
m2 = −0.0253 ± 0.0261
Z-Score of Log-Transformed JFM Discharge (acre-feet/day)
1970
1980
1990
2000
2010
2020

CITY C NR HIGHLAND CA

Gauge Information	USGS Station ID	11055800
	Hydrologic Unit Code	18070203
	Latitude (NAD27)	34°08'38"
	Longitude (NAD27)	117°11'16"
	Drainage Area [Mi^2]	19.6
	Elevation of The Stream Outlet Above NAVD88 [Ft]	1670
	County	San Bernadino
Watershed Characteristics	Mean Maximum January Temperature [°F]	53.02
	Mean Minimum January Temperature [°F]	33.12
	Mean Annual Precipitation [In]	30.5
	Hydrological Soil Group (HSG) [% of Covered Area]	C(28%), D(72%)
	Length of Longest Flow Path [Mi]	9
	Mean Basin Elevation [Ft]	3918
	Maximum Basin Elevation [Ft]	6442
	Minimum Basin Elevation [Ft]	1600
	Percentage of Area Above 6000 Ft [%]	2.27
	Percentage of Area Covered By Forest [%]	32.1
	Percentage of Lakes And Ponds [%]	0
	Percentage of Developed (Urban) Land (NLCD 2011 Classes 21-24) [%]	5.4
	Percentage of Imperviousness (NLCD 2001 Impervious Dataset) [%]	0.59
	Percentage of Imperviousness (NLCD 2011 Impervious Dataset) [%]	0.59
	Percentage of Imperviousness (NLCD 2019 Impervious Dataset) [%]	0.60
Stream Management Controls	Developed or Natural	Natural
	Regulation	Unregulated*
	Geological or Hydrological Control	Yes**
	Dam Outlet	No
	Agricultural Control	None
	(Waste)water Inputs	None
	Water Withdrawals	Yes**
	Other Factors Affecting Runoff	-

* No regulation upstream from station.
**Transition between upper and lower watershed; Some geologic contact that may augment surface discharge.
***City Creek Water Co.'s canal (station 11055700) diverted from a site 0.5 mi upstream from station for irrigation throughout period of record until Sep. 30, 1986; and resumed diversion on Mar. 31, 1989. Diversion canal damaged by storms of January 1993, with no flow in canal from Jan. 14, 1993, to Apr. 5, 1995.
Ref. waterdata.usgs.gov

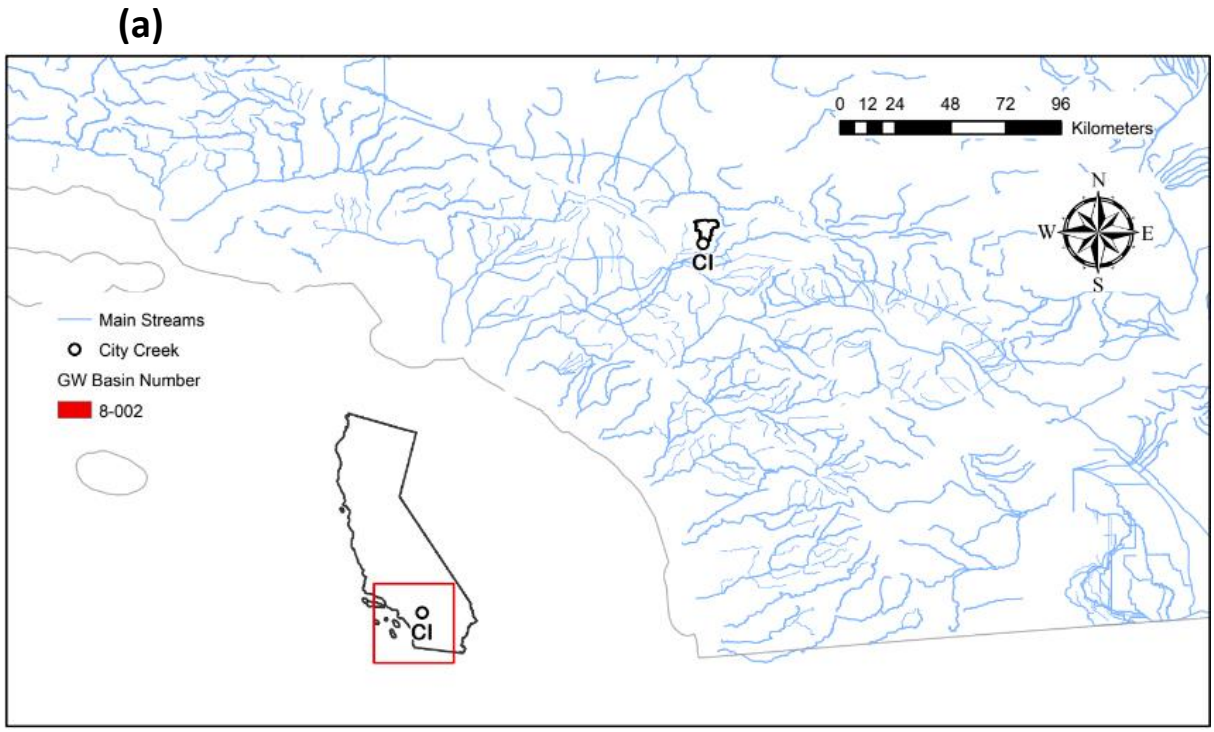
(a)
0 12 24 48 72 96
Kilometers
N
W
E
S
CI
Main Streams
City Creek
GW Basin Number
8-002
CI

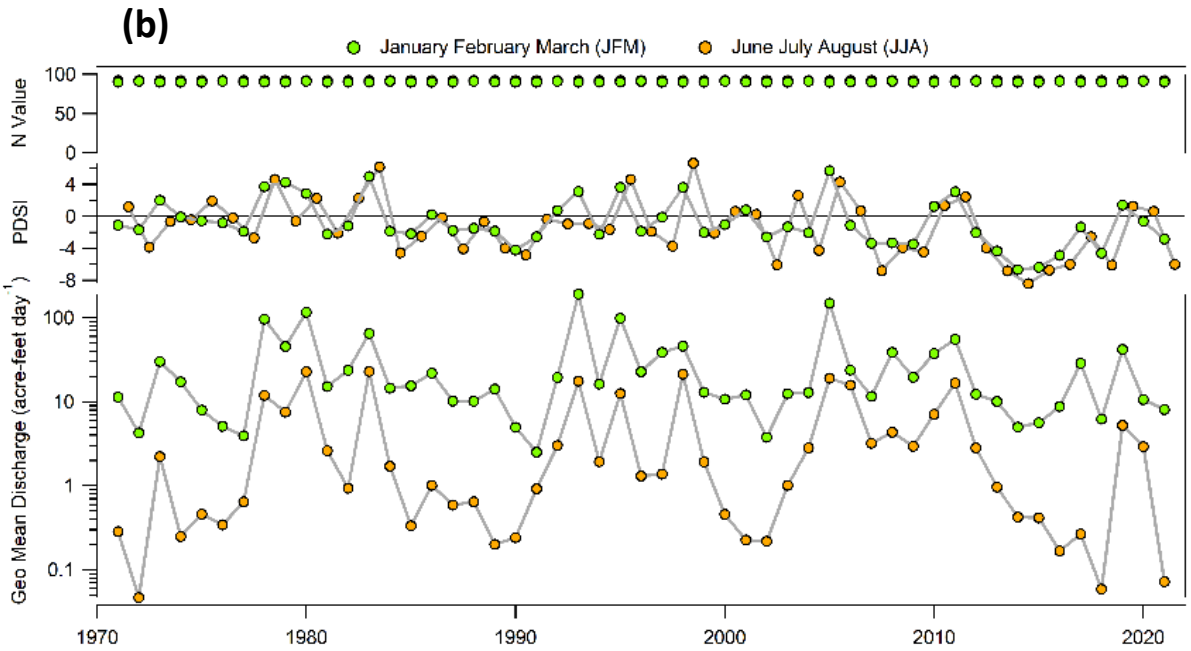
(b)
January February March (JFM)
June July August (JJA)
N Value
PDSI
Geo Mean Discharge (acre-feet day-1)
1970
1980
1990
2000
2010
2020

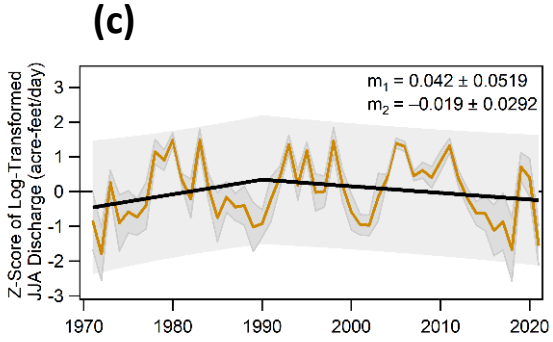
(c)
m1 = 0.042 ± 0.0519
m2 = –0.019 ± 0.0292
Z-Score of Log-Transformed JJA Discharge (acre-feet/day)
1970
1980
1990
2000
2010
2020

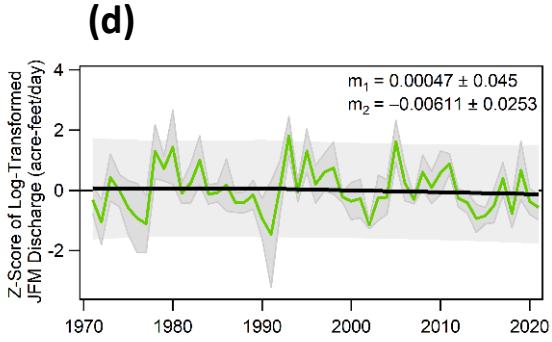
(d)
m1 = 0.00047 ± 0.045
m2 = –0.00611 ± 0.0253
Z-Score of Log-Transformed JFM Discharge (acre-feet/day)
1970
1980
1990
2000
2010
2020

LYTLE C NR FONTANA CA

Gauge Information	USGS Station ID	11062000
	Hydrologic Unit Code	18070203
	Latitude (NAD27)	34°12'44"
	Longitude (NAD27)	117°27'26"
	Drainage Area [Mi^2]	46.6
	Elevation of The Stream Outlet Above NAVD88 [Ft]	2393
	County	San Bernardino
Watershed Characteristics	Mean Maximum January Temperature [°F]	50.04
	Mean Minimum January Temperature [°F]	30.91
	Mean Annual Precipitation [In]	43
	Hydrological Soil Group (HSG) [% of Covered Area]	D(100%)
	Length of Longest Flow Path [Mi]	16
	Mean Basin Elevation [Ft]	5563
	Maximum Basin Elevation [Ft]	10061
	Minimum Basin Elevation [Ft]	2387
	Percentage of Area Above 6000 Ft [%]	39.7
	Percentage of Area Covered By Forest [%]	22.5
	Percentage of Lakes And Ponds [%]	0.0188
	Percentage of Developed (Urban) Land (NLCD 2011 Classes 21-24) [%]	2.1
	Percentage of Imperviousness (NLCD 2001 Impervious Dataset) [%]	0.52
	Percentage of Imperviousness (NLCD 2011 Impervious Dataset) [%]	0.53
	Percentage of Imperviousness (NLCD 2019 Impervious Dataset) [%]	0.58
Stream Management Controls	Developed or Natural	Natural*
	Regulation	Unregulated*
	Geological or Hydrological Control	Yes
	Dam Outlet	No
	Agricultural Control	None
	(Waste)water Inputs	None
	Water Withdrawals	Yes**
	Other Factors Affecting Runoff	Groundwater discharge***

*No regulation upstream from station and mostly natural.
**Southern California Edison Co.'s Lytle Creek Conduit (station 11060900) diverts 2.3 mi upstream for power development and Fontana Water Co. collects water from an infiltration line (station 11061000) upstream for irrigation and domestic use. Abrupt changes in the combined discharge of Lytle Creek and diversions occurs at times, due to changes in diversion, the distances between diversion and gage locations, time of travel, and changes in surface and subsurface storage. Spill can occur from Southern California Edison Co.'s Lytle Creek forebay during unusually high flows. Water can be pumped from channel by two pumps at Miller Narrows at a point approximately 2 mi upstream. No water has been pumped out of channel since 1971. Ref. waterdata.usgs.gov
*** Known groundwater discharge sources in this area.

(a)

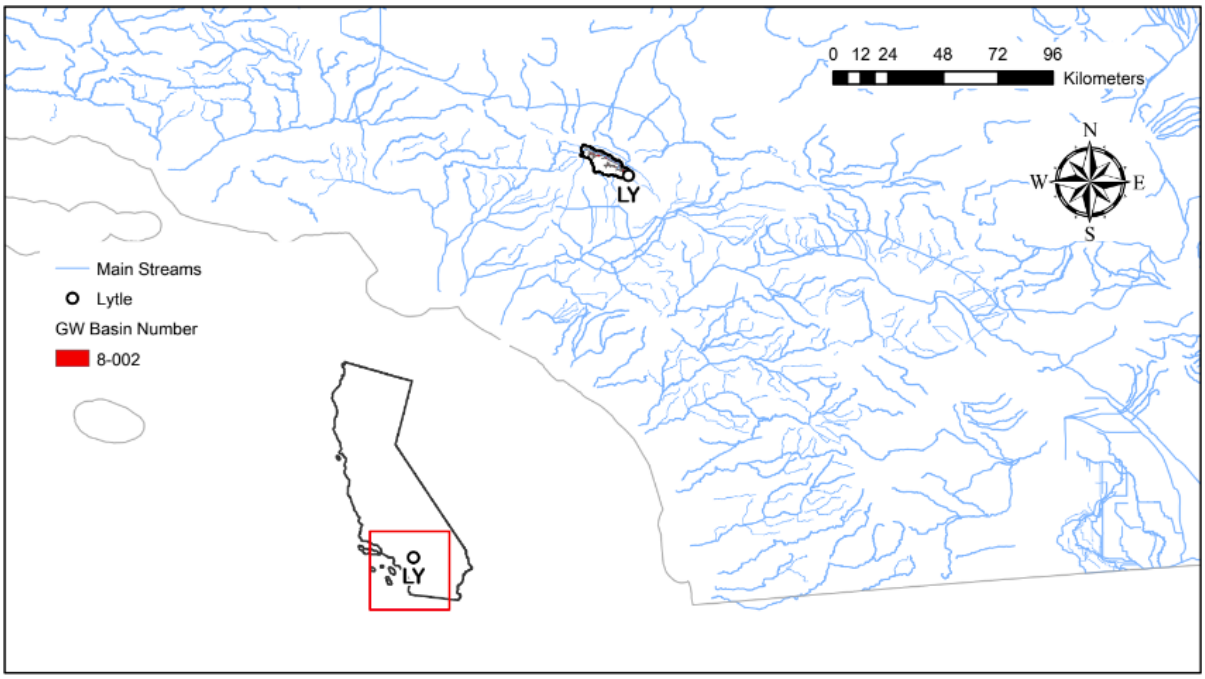
0 12 24 48 72 96
Kilometers
N
W
E
S
LY
Main Streams
Lytle
GW Basin Number
8-002
LY

(b)

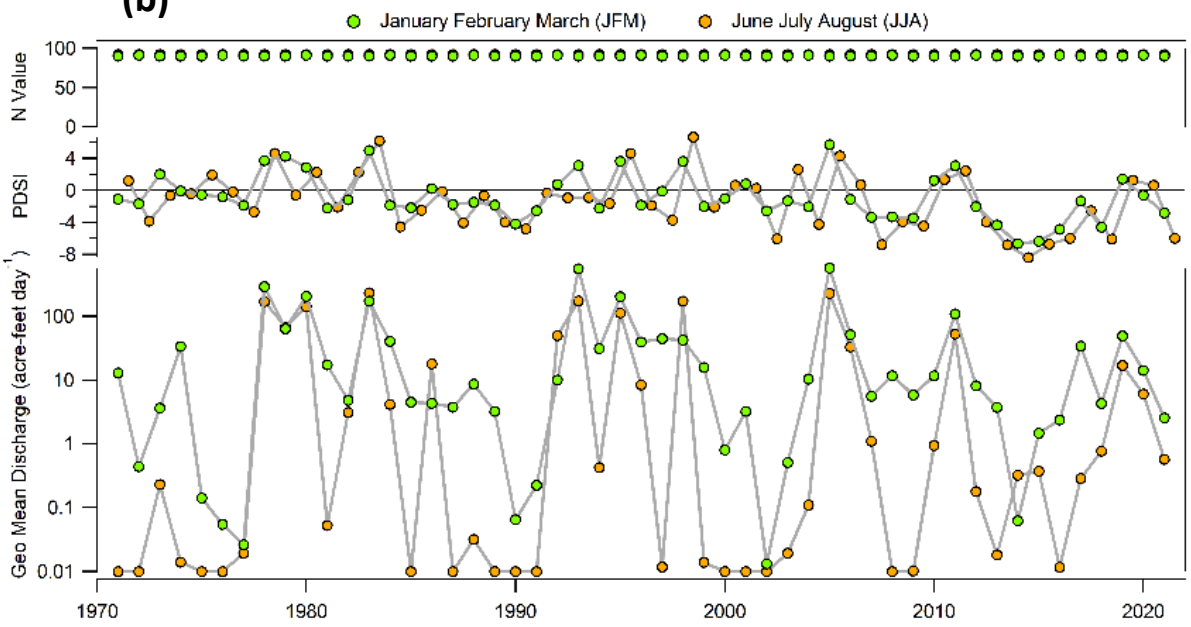
January February March (JFM)
June July August (JJA)
N Value
PDSI
Geo Mean Discharge (acre-feet day⁻¹)
1970
1980
1990
2000
2010
2020

(c)

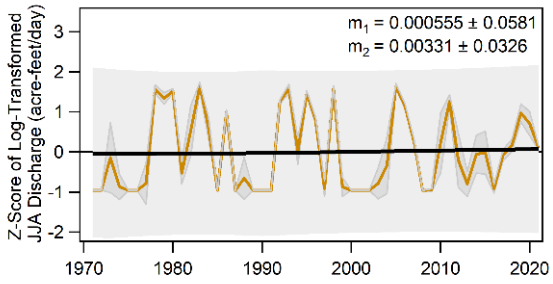
m1 = 0.000555 ± 0.0581
m2 = 0.00331 ± 0.0326
Z-Score of Log-Transformed JJA Discharge (acre-feet/day)
1970
1980
1990
2000
2010
2020

(d)

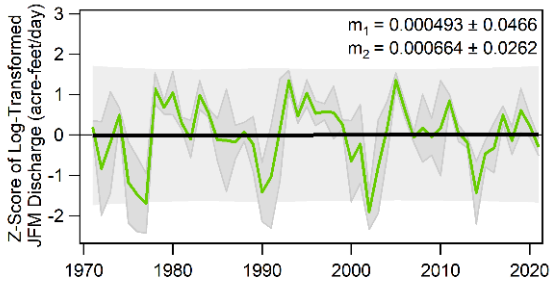
m1 = 0.000493 ± 0.0466
m2 = 0.000664 ± 0.0262
Z-Score of Log-Transformed JFM Discharge (acre-feet/day)
1970
1980
1990
2000
2010
2020

CAMPO C NR CAMPO CA

Gauge Information	USGS Station ID	11012500
	Hydrologic Unit Code	18070305
	Latitude (NAD27)	32°35'28"
	Longitude (NAD27)	116°31'29"
	Drainage Area [Mi^2]	85
	Elevation of The Stream Outlet Above NAVD88 [Ft]	2204
	County	San Diego
Watershed Characteristics	Mean Maximum January Temperature [°F]	60.01
	Mean Minimum January Temperature [°F]	32.96
	Mean Annual Precipitation [In]	18.1
	Hydrological Soil Group (HSG) [% of Covered Area]	C(8%), D(92%)
	Length of Longest Flow Path [Mi]	20
	Mean Basin Elevation [Ft]	3272
	Maximum Basin Elevation [Ft]	4604
	Minimum Basin Elevation [Ft]	2201
	Percentage of Area Above 6000 Ft [%]	0
	Percentage of Area Covered By Forest [%]	1.5
	Percentage of Lakes And Ponds [%]	0
	Percentage of Developed (Urban) Land (NLCD 2011 Classes 21-24) [%]	10.3
	Percentage of Imperviousness (NLCD 2001 Impervious Dataset) [%]	0.39
	Percentage of Imperviousness (NLCD 2011 Impervious Dataset) [%]	0.44
	Percentage of Imperviousness (NLCD 2019 Impervious Dataset) [%]	0.48
Stream Management Controls	Developed or Natural	Developed
	Regulation	Unregulated*
	Geological or Hydrological Control	Yes**
	Dam Outlet	No
	Agricultural Control	None
	(Waste)water Inputs	None
	Water Withdrawals	None*
	Other Factors Affecting Runoff	Granitic Drainage (Naturally Impervious)

*Near Mexico border; No regulation or diversion upstream from station.
**Peaks are attenuated by small conservation reservoir 1 mi upstream since August 1956.
Ref. waterdata.usgs.gov

(a)

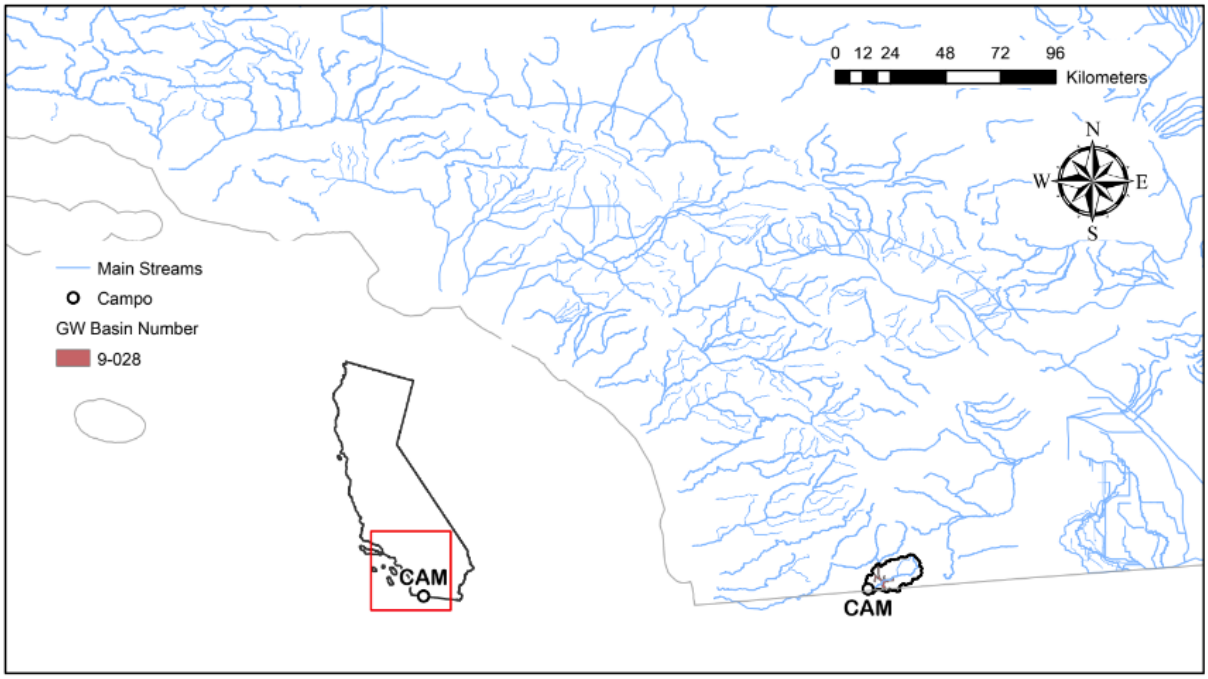
0 12 24 48 72 96
Kilometers
N
W
E
S
Main Streams
Campo
GW Basin Number
9-028
CAM
CAM

(b)

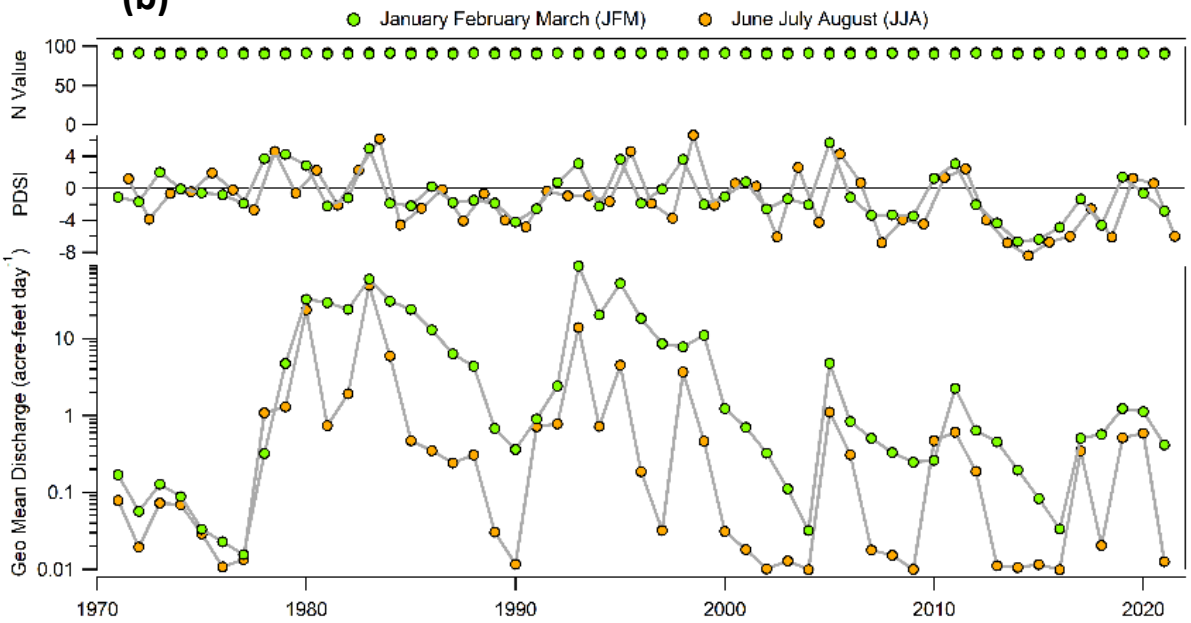
January February March (JFM)
June July August (JJA)
N Value
PDSI
Geo Mean Discharge (acre-feet day⁻¹)
1970
1980
1990
2000
2010
2020

(c)

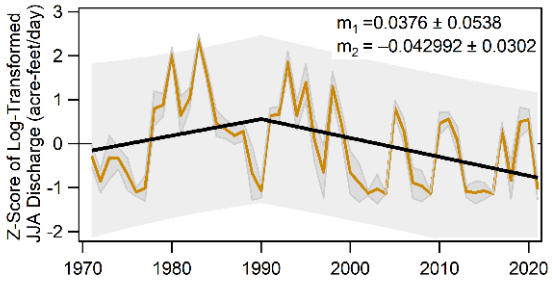
m1 =0.0376 ± 0.0538
m2 = –0.042992 ± 0.0302
Z-Score of Log-Transformed JJA Discharge (acre-feet/day)
1970
1980
1990
2000
2010
2020

(d)

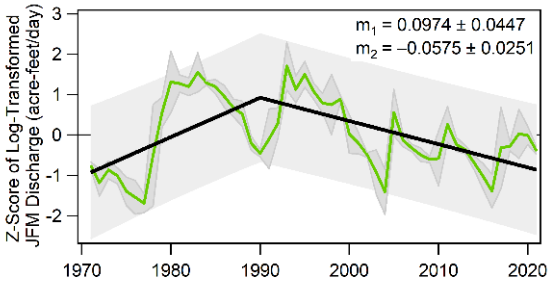
m1 = 0.0974 ± 0.0447
m2 = –0.0575 ± 0.0251
Z-Score of Log-Transformed JFM Discharge (acre-feet/day)
1970
1980
1990
2000
2010
2020

SANTIAGO C A MODJESKA CA

Gauge Information	USGS Station ID	11075800
	Hydrologic Unit Code	18070203
	Latitude (NAD27)	33°42'32"
	Longitude (NAD27)	117°38'05"
	Drainage Area [Mi^2]	12.5
	Elevation of The Stream Outlet Above NAVD88 [Ft]	1273
	County	Orange
Watershed Characteristics	Mean Maximum January Temperature [°F]	59.1
	Mean Minimum January Temperature [°F]	42.88
	Mean Annual Precipitation [In]	25.6
	Hydrological Soil Group (HSG) [% of Covered Area]	C(77%), D(23%)
	Length of Longest Flow Path [Mi]	9
	Mean Basin Elevation [Ft]	3018
	Maximum Basin Elevation [Ft]	5684
	Minimum Basin Elevation [Ft]	1272
	Percentage of Area Above 6000 Ft [%]	0
	Percentage of Area Covered By Forest [%]	28.7
	Percentage of Lakes And Ponds [%]	0
	Percentage of Developed (Urban) Land (NLCD 2011 Classes 21-24) [%]	1.6
	Percentage of Imperviousness (NLCD 2001 Impervious Dataset) [%]	0.44
	Percentage of Imperviousness (NLCD 2011 Impervious Dataset) [%]	0.45
	Percentage of Imperviousness (NLCD 2019 Impervious Dataset) [%]	0.47
Stream Management Controls	Developed or Natural	Natural
	Regulation	Unregulated*
	Geological or Hydrological Control	None
	Dam Outlet	No
	Agricultural Control	None
	(Waste)water Inputs	None
	Water Withdrawals	Yes**
	Other Factors Affecting Runoff	Fire Effects***

*Slight regulation by Modjeska Reservoir on Harding Creek.
**Santiago County Water District diverts water at Modjeska Reservoir on Harding Creek.
***Upper watershed, multiple fires, some minor development.
Ref. waterdata.usgs.gov

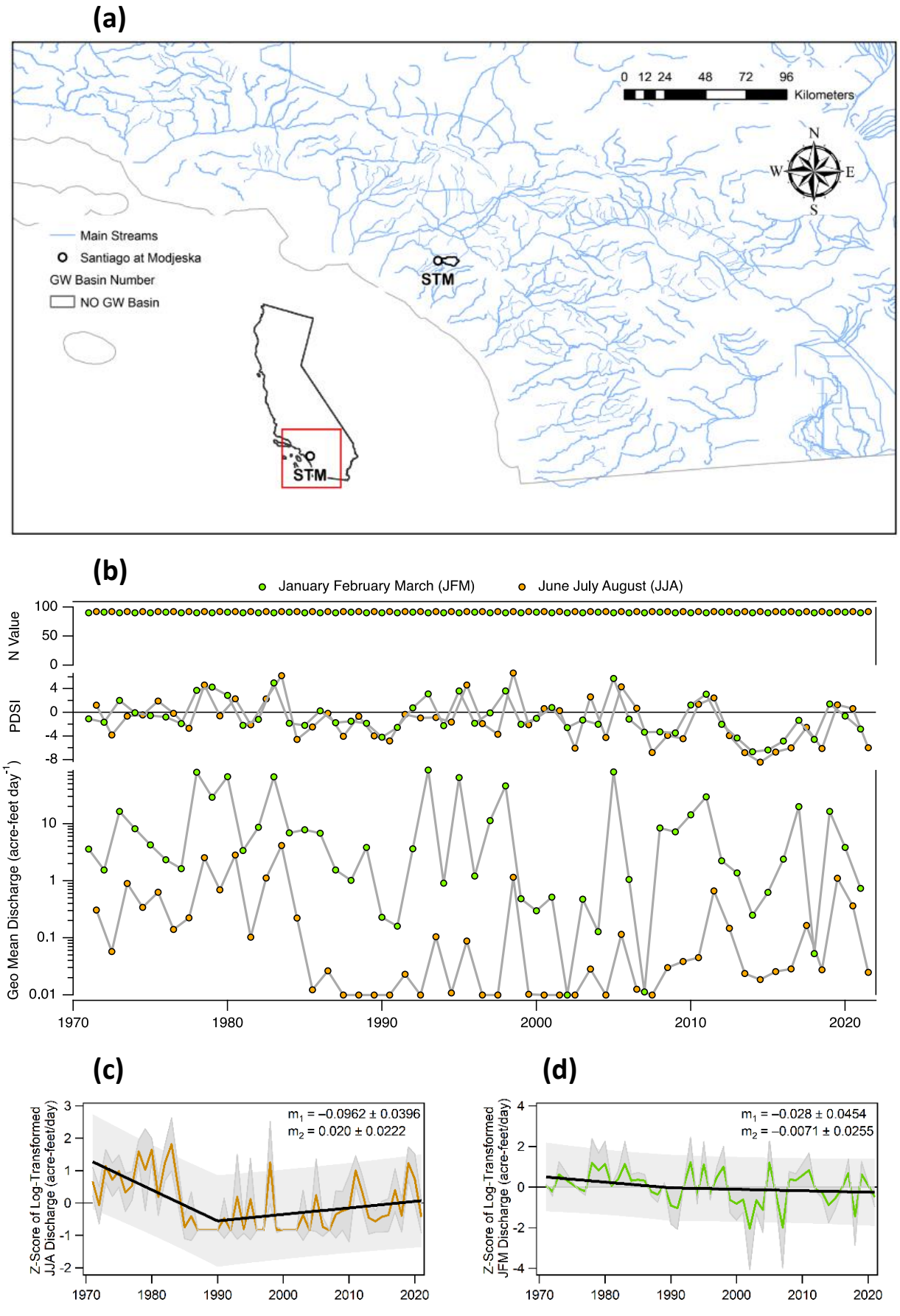
(a)
0 12 24 48 72 96
Kilometers
N
W
E
S
Main Streams
Santiago at Modjeska
GW Basin Number
NO GW Basin
STM
STM
(b)
January February March (JFM)
June July August (JJA)
N Value
PDSI
Geo Mean Discharge (acre-feet day-1)
1970
1980
1990
2000
2010
2020
(c)
m1 = −0.0962 ± 0.0396
m2 = 0.020 ± 0.0222
Z-Score of Log-Transformed JJA Discharge (acre-feet/day)
(d)
m1 = −0.028 ± 0.0454
m2 = −0.0071 ± 0.0255
Z-Score of Log-Transformed JFM Discharge (acre-feet/day)

ARROYO SECO NR PASADENA CA

Gauge Information	USGS Station ID	11098000
	Hydrologic Unit Code	18070105
	Latitude (NAD27)	34°13'20"
	Longitude (NAD27)	118°10'36"
	Drainage Area [Mi^2]	16
	Elevation of The Stream Outlet Above NAVD88 [Ft]	1410
	County	Los Angeles
Watershed Characteristics	Mean Maximum January Temperature [°F]	54.1
	Mean Minimum January Temperature [°F]	38.9
	Mean Annual Precipitation [In]	31.5
	Hydrological Soil Group (HSG) [% of Covered Area]	D (100%)
	Length of Longest Flow Path [Mi]	12
	Mean Basin Elevation [Ft]	3598
	Maximum Basin Elevation [Ft]	6158
	Minimum Basin Elevation [Ft]	1410
	Percentage of Area Above 6000 Ft [%]	0.0842
	Percentage of Area Covered By Forest [%]	31.2
	Percentage of Lakes And Ponds [%]	0
	Percentage of Developed (Urban) Land (NLCD 2011 Classes 21-24) [%]	5.3
	Percentage of Imperviousness (NLCD 2001 Impervious Dataset) [%]	0.37
	Percentage of Imperviousness (NLCD 2011 Impervious Dataset) [%]	0.37
	Percentage of Imperviousness (NLCD 2019 Impervious Dataset) [%]	0.40
Stream Management Controls	Developed or Natural	Natural
	Regulation	Unregulated*
	Geological or Hydrological Control	Yes**
	Dam Outlet	No
	Agricultural Control	None
	(Waste)water Inputs	None
	Water Withdrawals	None*
	Other Factors Affecting Runoff	-

*No regulation or diversion upstream from station. Ref. waterdata.usgs.gov
**Upper LA River; Flow controlled by Brown Canyon Dam.

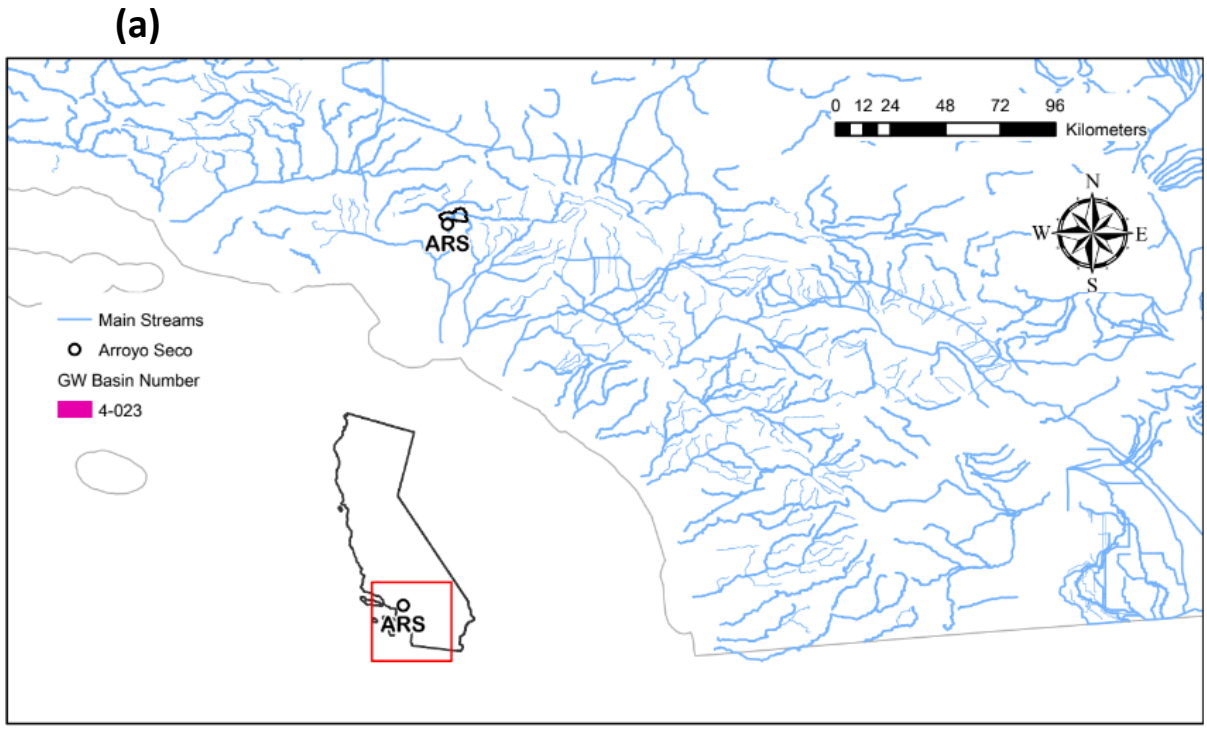
(a)
0 12 24 48 72 96
Kilometers
N
W
E
S
ARS
Main Streams
Arroyo Seco
GW Basin Number
4-023
ARS

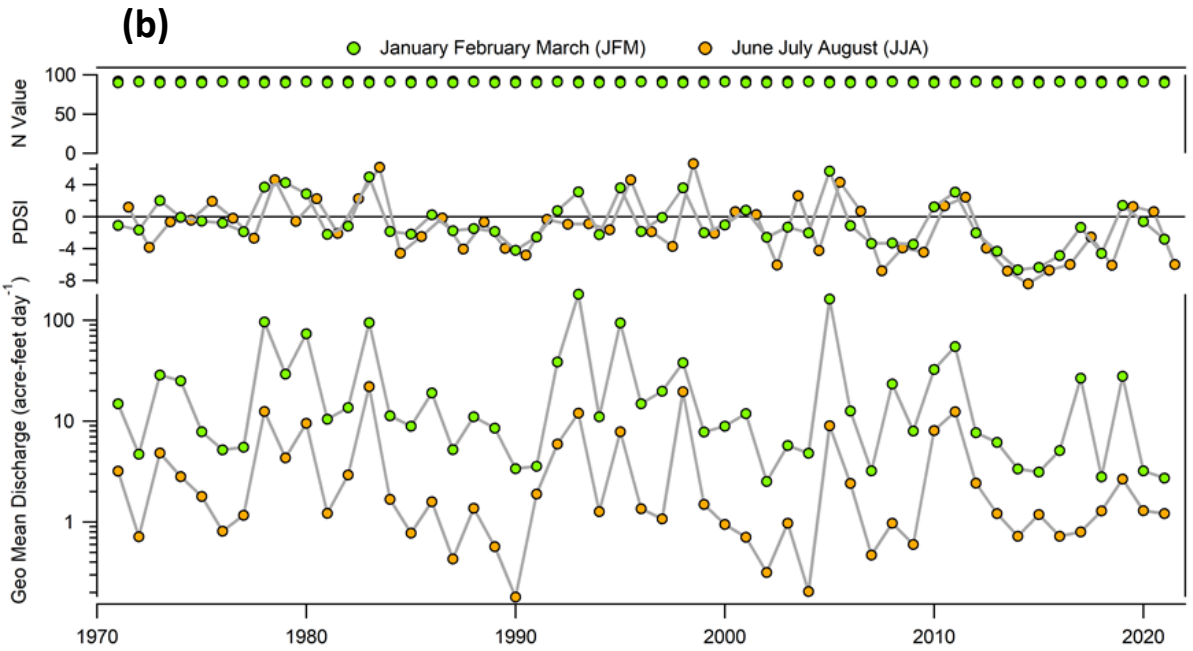
(b)
January February March (JFM)
June July August (JJA)
N Value
PDSI
Geo Mean Discharge (acre-feet day-1)
1970
1980
1990
2000
2010
2020

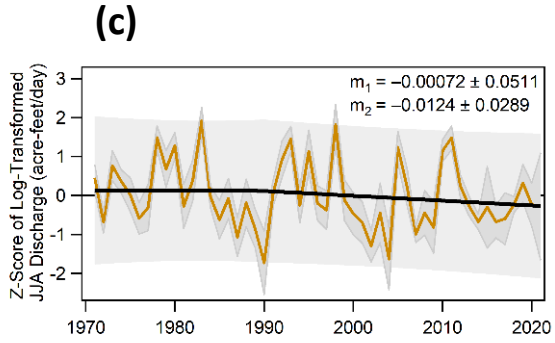
(c)
m1 = −0.00072 ± 0.0511
m2 = −0.0124 ± 0.0289
Z-Score of Log-Transformed JJA Discharge (acre-feet/day)

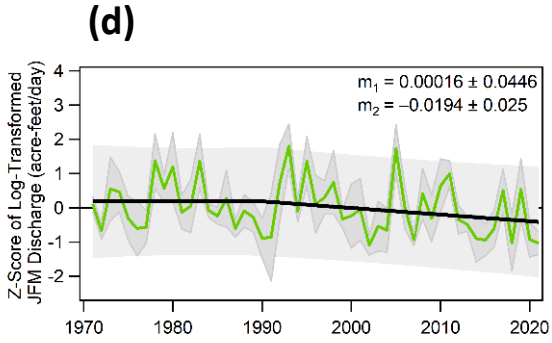
(d)
m1 = 0.00016 ± 0.0446
m2 = −0.0194 ± 0.025
Z-Score of Log-Transformed JFM Discharge (acre-feet/day)

SWEETWATER R NR DESCANSO CA

Gauge Information	USGS Station ID	11015000
	Hydrologic Unit Code	18070304
	Latitude (NAD27)	32°50'05"
	Longitude (NAD27)	116°37'20"
	Drainage Area [Mi^2]	45.4
	Elevation of The Stream Outlet Above NAVD88 [Ft]	3283
	County	San Diego
Watershed Characteristics	Mean Maximum January Temperature [°F]	54.66
	Mean Minimum January Temperature [°F]	33
	Mean Annual Precipitation [In]	29.9
	Hydrological Soil Group (HSG) [% of Covered Area]	D(100%)
	Length of Longest Flow Path [Mi]	17
	Mean Basin Elevation [Ft]	4361
	Maximum Basin Elevation [Ft]	6465
	Minimum Basin Elevation [Ft]	3281
	Percentage of Area Above 6000 Ft [%]	0.27
	Percentage of Area Covered By Forest [%]	25.2
	Percentage of Lakes And Ponds [%]	0.011
	Percentage of Developed (Urban) Land (NLCD 2011 Classes 21-24) [%]	4.9
	Percentage of Imperviousness (NLCD 2001 Impervious Dataset) [%]	0.31
	Percentage of Imperviousness (NLCD 2011 Impervious Dataset) [%]	0.34
	Percentage of Imperviousness (NLCD 2019 Impervious Dataset) [%]	0.39
Stream Management Controls	Developed or Natural	Natural
	Regulation	Unregulated*
	Geological or Hydrological Control	None**
	Dam Outlet	No
	Agricultural Control	None
	(Waste)water Inputs	None
	Water Withdrawals	None*
	Other Factors Affecting Runoff	-

*No regulation or diversion upstream from station.
**Upper watershed, some minor upstream control (Sweetwater Reservoir).
Ref. waterdata.usgs.gov

(a)

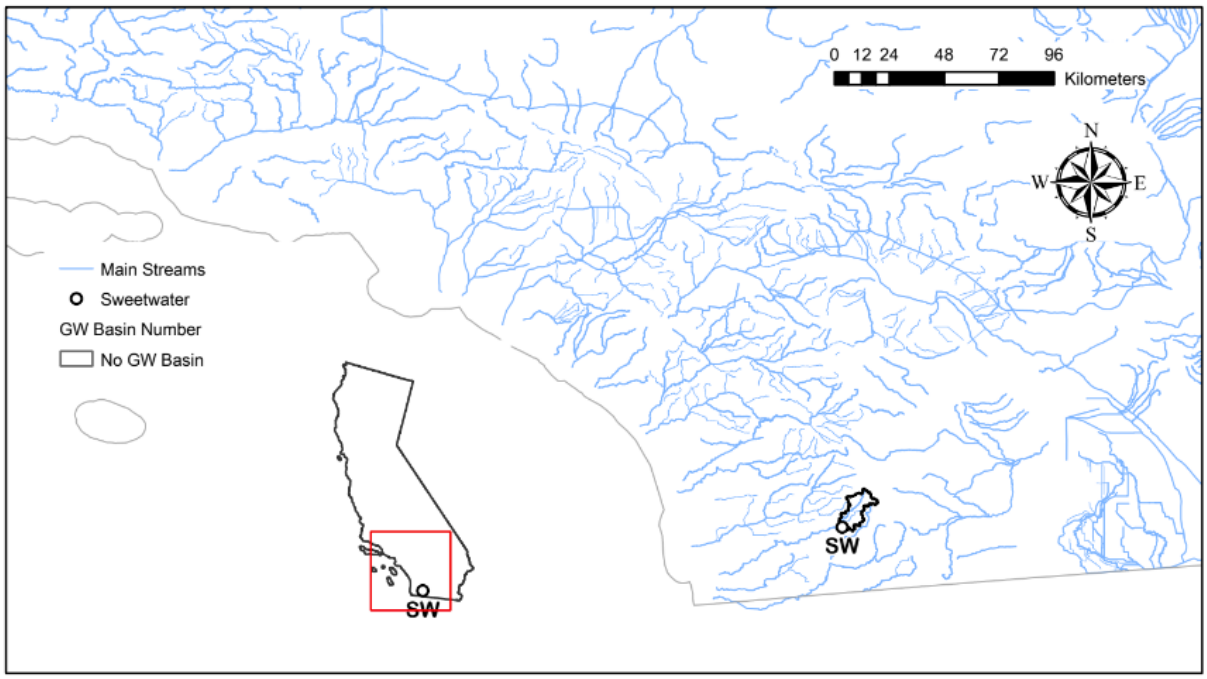
0 12 24 48 72 96
Kilometers
N
W
E
S
Main Streams
Sweetwater
GW Basin Number
No GW Basin
SW
SW

(b)

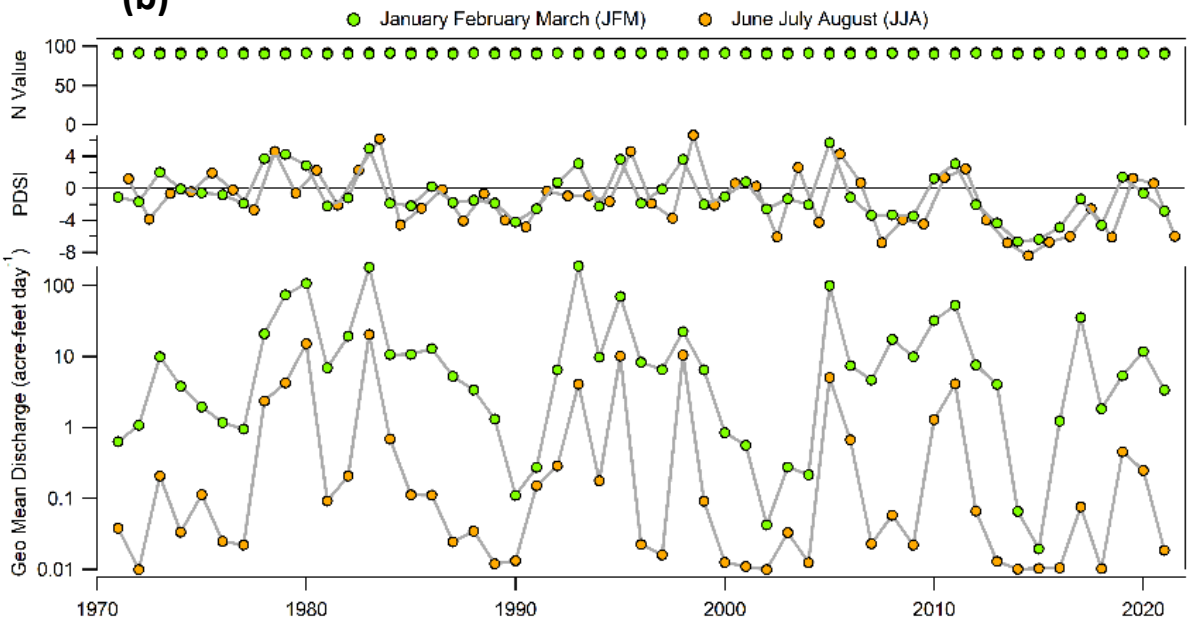
January February March (JFM)
June July August (JJA)
N Value
PDSI
Geo Mean Discharge (acre-feet day⁻¹)
1970
1980
1990
2000
2010
2020

(c)

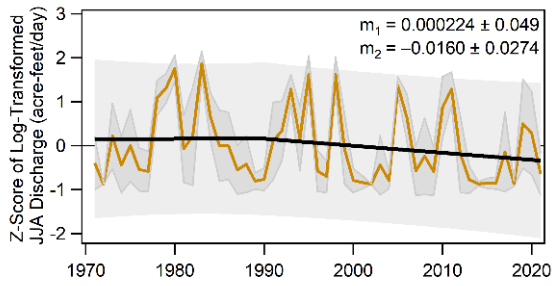
m1 = 0.000224 ± 0.049
m2 = −0.0160 ± 0.0274
Z-Score of Log-Transformed JJA Discharge (acre-feet/day)
1970
1980
1990
2000
2010
2020

(d)

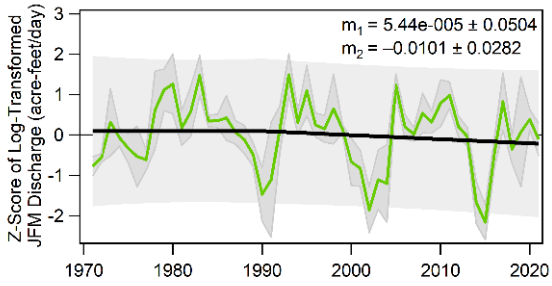
m1 = 5.44e-005 ± 0.0504
m2 = −0.0101 ± 0.0282
Z-Score of Log-Transformed JFM Discharge (acre-feet/day)
1970
1980
1990
2000
2010
2020

PIRU CREEK ABOVE LAKE PIRU CA

Gauge Information	USGS Station ID	11109600
	Hydrologic Unit Code	18070102
	Latitude (NAD27)	34°31'23"
	Longitude (NAD27)	118°45'22"
	Drainage Area [Mi^2]	372
	Elevation of The Stream Outlet Above NAVD88 [Ft]	1069
	County	Ventura
Watershed Characteristics	Mean Maximum January Temperature [°F]	51.93
	Mean Minimum January Temperature [°F]	30.99
	Mean Annual Precipitation [In]	21.8
	Hydrological Soil Group (HSG) [% of Covered Area]	C(20%), D(80%)
	Length of Longest Flow Path [Mi]	60
	Mean Basin Elevation [Ft]	4547
	Maximum Basin Elevation [Ft]	8832
	Minimum Basin Elevation [Ft]	1067
	Percentage of Area Above 6000 Ft [%]	12.8
	Percentage of Area Covered By Forest [%]	23.3
	Percentage of Lakes And Ponds [%]	0.62
	Percentage of Developed (Urban) Land (NLCD 2011 Classes 21-24) [%]	2.7
	Percentage of Imperviousness (NLCD 2001 Impervious Dataset) [%]	0.36
	Percentage of Imperviousness (NLCD 2011 Impervious Dataset) [%]	0.37
	Percentage of Imperviousness (NLCD 2019 Impervious Dataset) [%]	0.39
Stream Management Controls	Developed or Natural	Natural
	Regulation	Regulated*
	Geological or Hydrological Control	None
	Dam Outlet	No
	Agricultural Control	None
	(Waste)water Inputs	None
	Water Withdrawals	None
	Other Factors Affecting Runoff	-

*Records collected in connection with Federal Energy Regulatory Commission (FERC) project no. 2153. Flow regulated beginning December 1971 by Pyramid Lake (station 11109520).
**Imported water from the California Water Project stored and released at Pyramid Dam.
*Upstream of Lake Piru; No flow at times in some years.
Ref. waterdata.usgs.gov

(a)

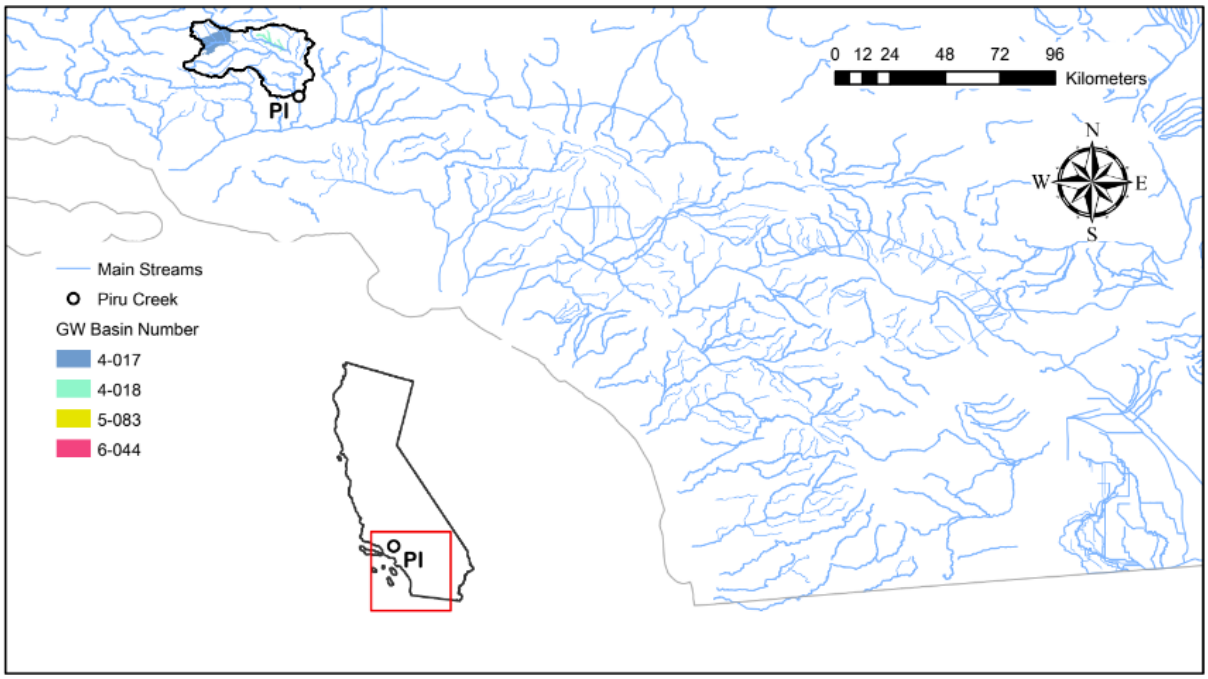
PI
0 12 24 48 72 96
Kilometers
N
W
E
S
Main Streams
Piru Creek
GW Basin Number
4-017
4-018
5-083
6-044
PI

(b)

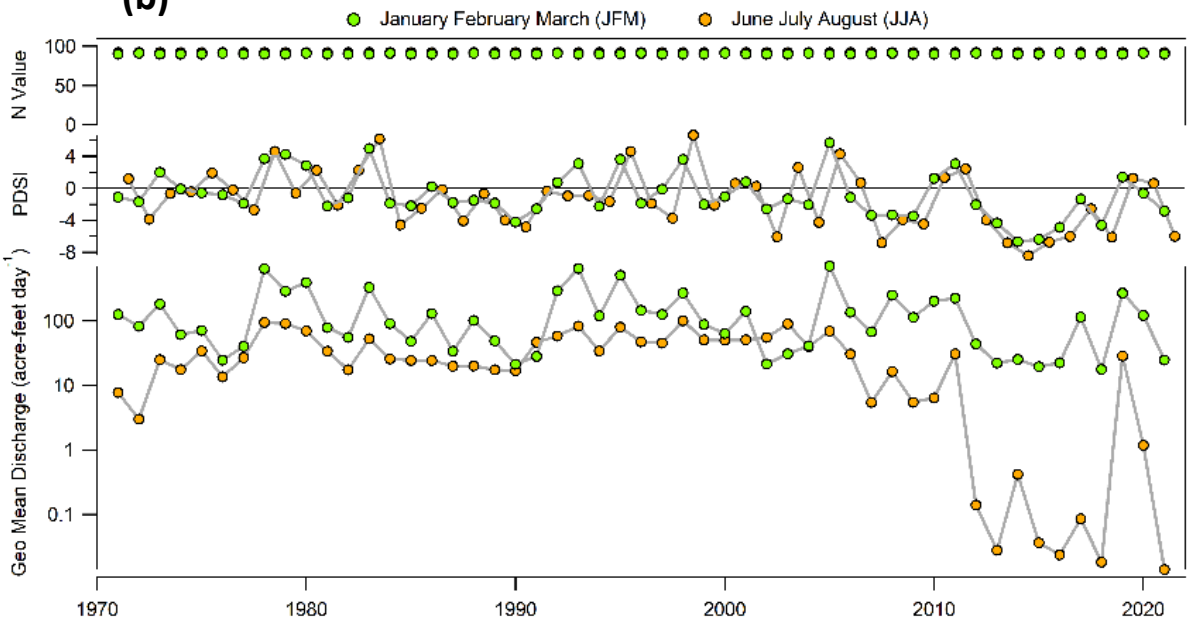
January February March (JFM)
June July August (JJA)
N Value
PDSI
Geo Mean Discharge (acre-feet day-1)
1970
1980
1990
2000
2010
2020

(c)

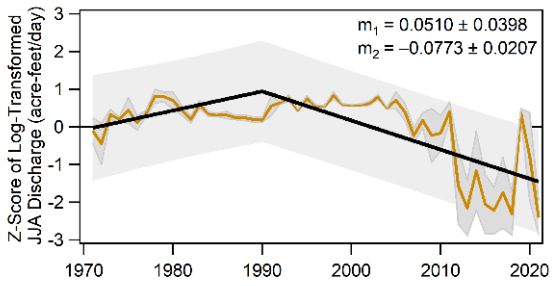
m1 = 0.0510 ± 0.0398
m2 = −0.0773 ± 0.0207
Z-Score of Log-Transformed JJA Discharge (acre-feet/day)
1970
1980
1990
2000
2010
2020

(d)

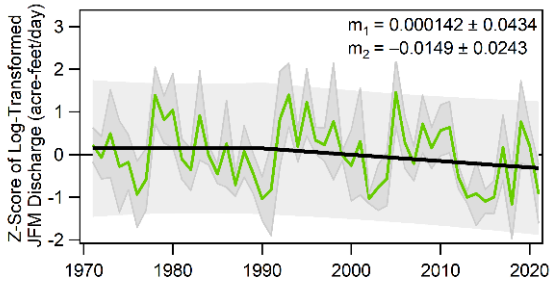
m1 = 0.000142 ± 0.0434
m2 = −0.0149 ± 0.0243
Z-Score of Log-Transformed JFM Discharge (acre-feet/day)
1970
1980
1990
2000
2010
2020

TEMECULA C NR AGUANGA CA

Gauge Information	USGS Station ID	11042400
	Hydrologic Unit Code	18070302
	Latitude (NAD27)	33°27'33"
	Longitude (NAD27)	116°55'22"
	Drainage Area [Mi^2]	131
	Elevation of The Stream Outlet Above NAVD88 [Ft]	1599
	County	Riverside
Watershed Characteristics	Mean Maximum January Temperature [°F]	57.63
	Mean Minimum January Temperature [°F]	34.73
	Mean Annual Precipitation [In]	18.3
	Hydrological Soil Group (HSG) [% of Covered Area]	D(100%)
	Length of Longest Flow Path [Mi]	24
	Mean Basin Elevation [Ft]	3680
	Maximum Basin Elevation [Ft]	6141
	Minimum Basin Elevation [Ft]	1590
	Percentage of Area Above 6000 Ft [%]	0.021
	Percentage of Area Covered By Forest [%]	12.5
	Percentage of Lakes And Ponds [%]	0.001
	Percentage of Developed (Urban) Land (NLCD 2011 Classes 21-24) [%]	3.6
	Percentage of Imperviousness (NLCD 2001 Impervious Dataset) [%]	0.20
	Percentage of Imperviousness (NLCD 2011 Impervious Dataset) [%]	0.21
	Percentage of Imperviousness (NLCD 2019 Impervious Dataset) [%]	0.22
Stream Management Controls	Developed or Natural	Natural*
	Regulation	Unregulated*
	Geological or Hydrological Control	None
	Dam Outlet	No
	Agricultural Control	None
	(Waste)water Inputs	None
	Water Withdrawals	Yes*
	Other Factors Affecting Runoff	Gravel Mining

*No regulation upstream from station. Upstream of Vail Lake, mostly natural (some gravel mining and groundwater extraction), flashy ephemeral system.
**Pumping upstream from station for irrigation of less than 1,000 acres.
Ref. waterdata.usgs.gov

(a)

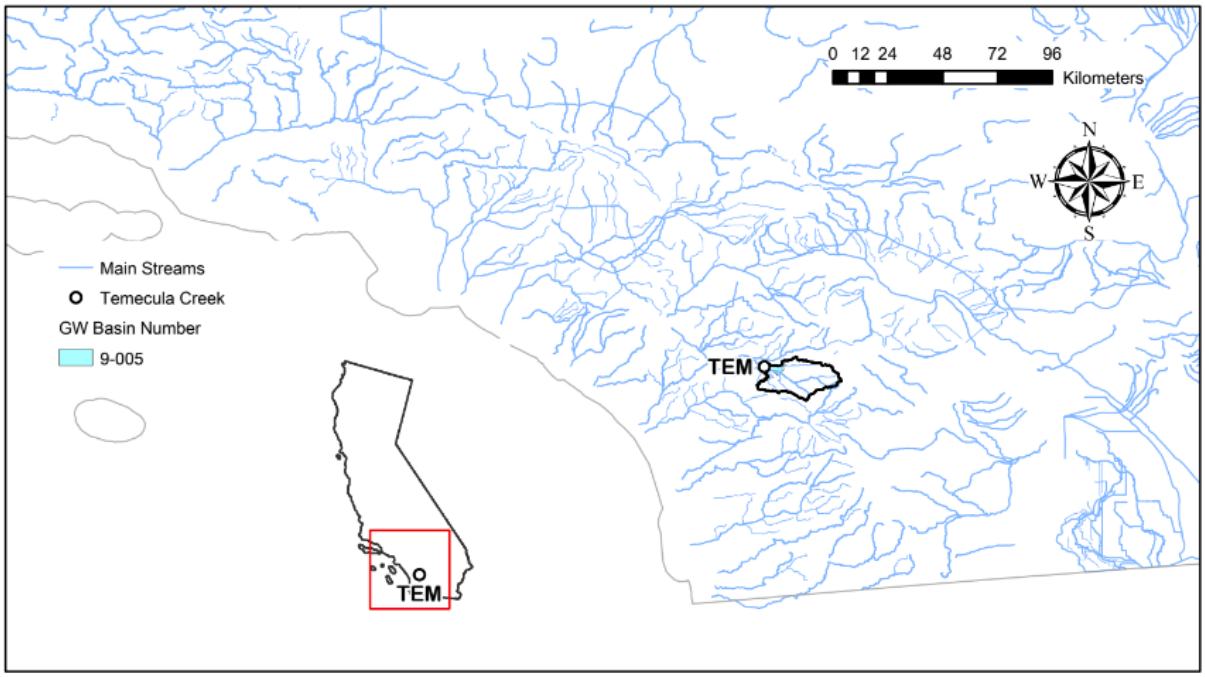
0 12 24 48 72 96
Kilometers
N
W
E
S
Main Streams
Temecula Creek
GW Basin Number
9-005
TEM
TEM

(b)

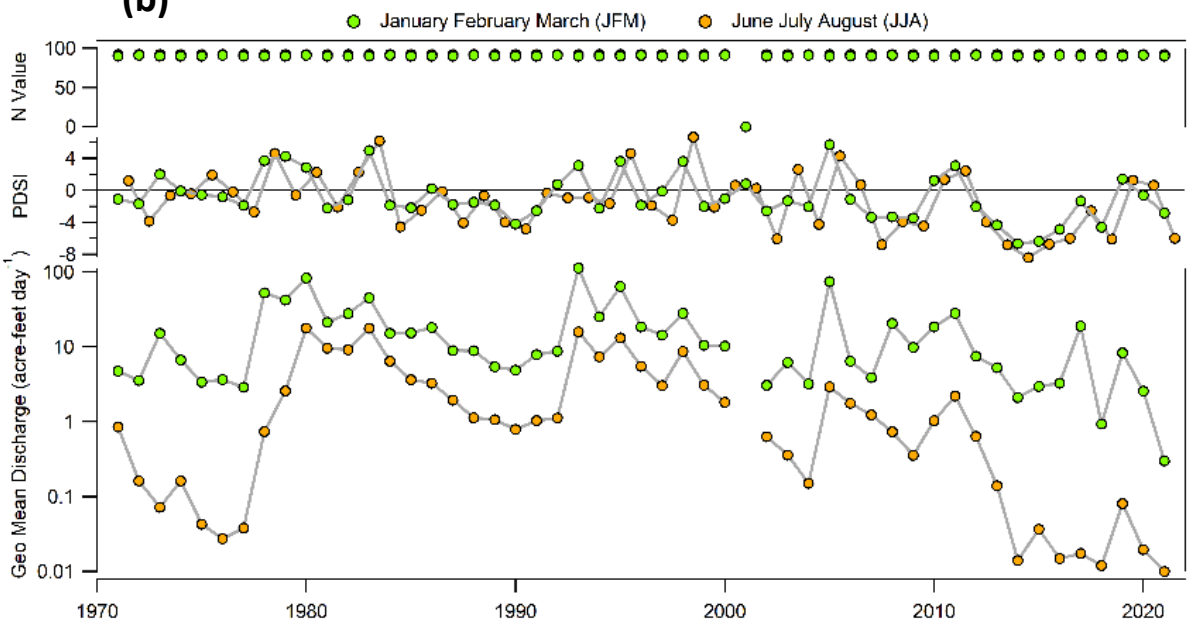
January February March (JFM)
June July August (JJA)
N Value
PDSI
Geo Mean Discharge (acre-feet day⁻¹)
1970
1980
1990
2000
2010
2020

(c)

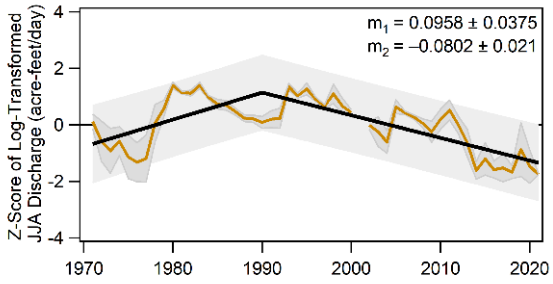
m1 = 0.0958 ± 0.0375
m2 = −0.0802 ± 0.021
Z-Score of Log-Transformed JJA Discharge (acre-feet/day)
1970
1980
1990
2000
2010
2020

(d)

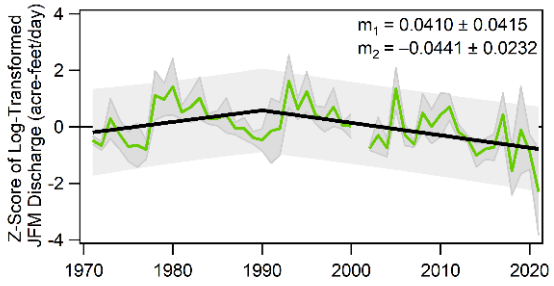
m1 = 0.0410 ± 0.0415
m2 = −0.0441 ± 0.0232
Z-Score of Log-Transformed JFM Discharge (acre-feet/day)
1970
1980
1990
2000
2010
2020

SANTA PAULA C NR SANTA PAULA

Gauge Information	USGS Station ID	11113500
	Hydrologic Unit Code	18070102
	Latitude (NAD27)	34°24'48"
	Longitude (NAD27)	119°04'53"
	Drainage Area [Mi^2]	38.4
	Elevation of The Stream Outlet Above NAVD88 [Ft]	777
	County	Ventura
Watershed Characteristics	Mean Maximum January Temperature [°F]	56.48
	Mean Minimum January Temperature [°F]	36.82
	Mean Annual Precipitation [In]	26.7
	Hydrological Soil Group (HSG) [% of Covered Area]	C(1%), D(99%)
	Length of Longest Flow Path [Mi]	12
	Mean Basin Elevation [Ft]	3356
	Maximum Basin Elevation [Ft]	6691
	Minimum Basin Elevation [Ft]	777
	Percentage of Area Above 6000 Ft [%]	2.25
	Percentage of Area Covered By Forest [%]	29.2
	Percentage of Lakes And Ponds [%]	0.019
	Percentage of Developed (Urban) Land (NLCD 2011 Classes 21-24) [%]	2.4
	Percentage of Imperviousness (NLCD 2001 Impervious Dataset) [%]	0.180
	Percentage of Imperviousness (NLCD 2011 Impervious Dataset) [%]	0.190
	Percentage of Imperviousness (NLCD 2019 Impervious Dataset) [%]	0.193
Stream Management Controls	Developed or Natural	Developed
	Regulation	Unregulated
	Geological or Hydrological Control	None
	Dam Outlet	No
	Agricultural Control	Yes*
	(Waste)water Inputs	None
	Water Withdrawals	Yes*
	Other Factors Affecting Runoff	Adjacent* Agricultural Runoff

*Natural flow affected by pumping and return flow from irrigated areas. Ref. waterdata.usgs.gov

(a)

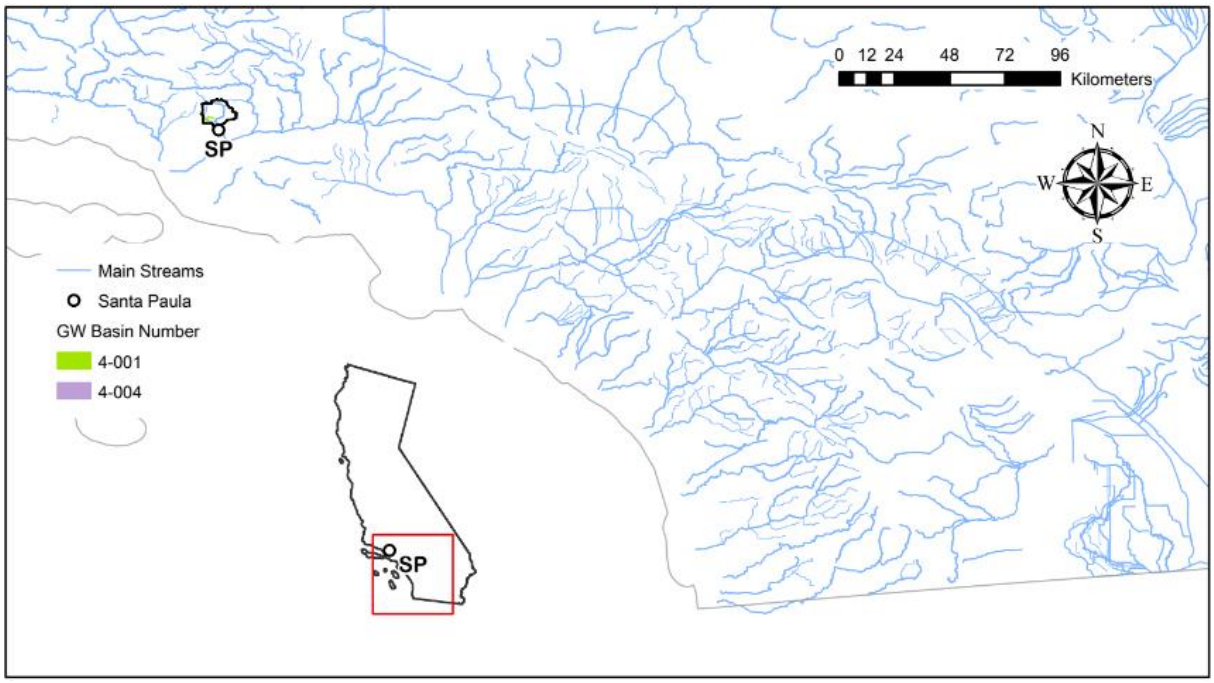
0 12 24 48 72 96
Kilometers
N
W
E
S
SP
Main Streams
Santa Paula
GW Basin Number
4-001
4-004
SP

(b)

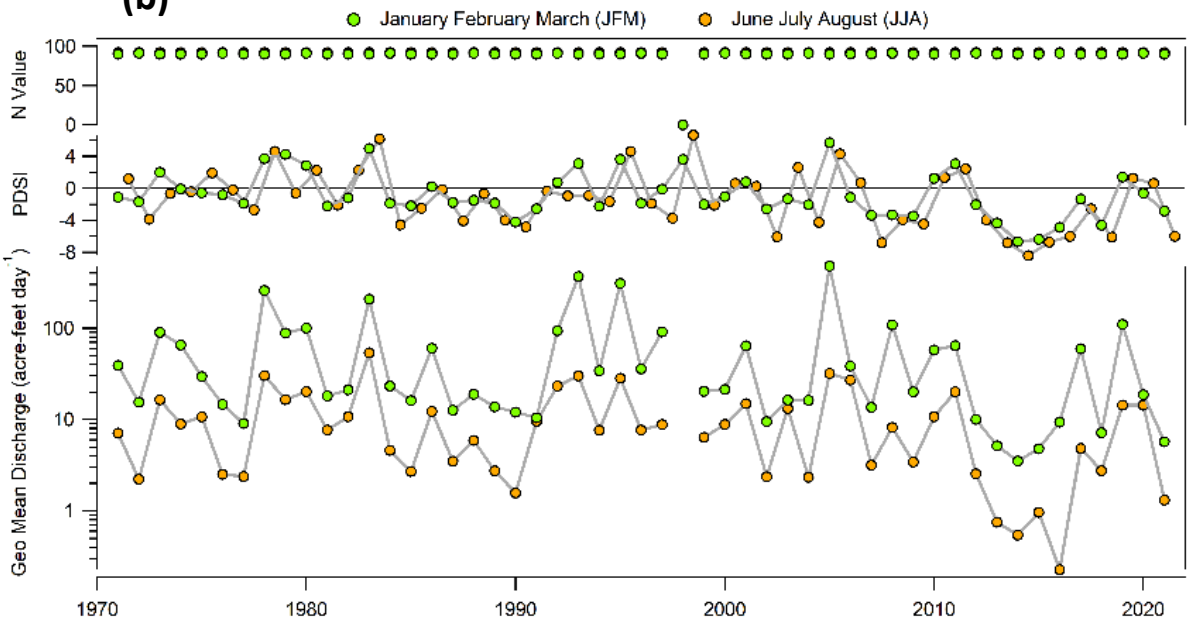
January February March (JFM)
June July August (JJA)
N Value
PDSI
Geo Mean Discharge (acre-feet day⁻¹)
1970
1980
1990
2000
2010
2020

(c)

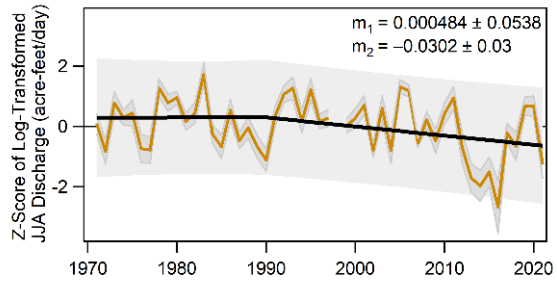
m1 = 0.000484 ± 0.0538
m2 = −0.0302 ± 0.03
Z-Score of Log-Transformed JJA Discharge (acre-feet/day)
1970
1980
1990
2000
2010
2020

(d)

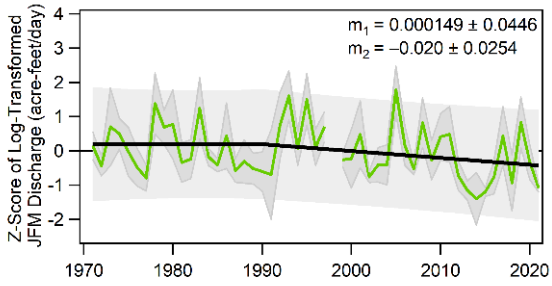
m1 = 0.000149 ± 0.0446
m2 = −0.020 ± 0.0254
Z-Score of Log-Transformed JFM Discharge (acre-feet/day)
1970
1980
1990
2000
2010
2020

SNOW C AND DIV COMBINED CA

Gauge Information	USGS Station ID	10256501
	Hydrologic Unit Code	18100201
	Latitude (NAD27)	33°52'14"
	Longitude (NAD27)	116°40'49"
	Drainage Area [Mi^2]	10.9
	Elevation of The Stream Outlet Above NAVD88 [Ft]	2008
	County	Riverside
Watershed Characteristics	Mean Maximum January Temperature [°F]	50.68
	Mean Minimum January Temperature [°F]	27.37
	Mean Annual Precipitation [In]	25.1
	Hydrological Soil Group (HSG) [% of Covered Area]	C(99%), D(1%)
	Length of Longest Flow Path [Mi]	5
	Mean Basin Elevation [Ft]	6120
	Maximum Basin Elevation [Ft]	10813
	Minimum Basin Elevation [Ft]	2008
	Percentage of Area Above 6000 Ft [%]	55.3
	Percentage of Area Covered By Forest [%]	21
	Percentage of Lakes And Ponds [%]	0
	Percentage of Developed (Urban) Land (NLCD 2011 Classes 21-24) [%]	0.4
	Percentage of Imperviousness (NLCD 2001 Impervious Dataset) [%]	0.146
	Percentage of Imperviousness (NLCD 2011 Impervious Dataset) [%]	0.147
	Percentage of Imperviousness (NLCD 2019 Impervious Dataset) [%]	0.147
Stream Management Controls	Developed or Natural	Natural
	Regulation	Unregulated*
	Geological or Hydrological Control	None
	Dam Outlet	No
	Agricultural Control	None
	(Waste)water Inputs	None
	Water Withdrawals	Yes**
	Other Factors Affecting Runoff	Steep Watershed***

*Mostly undeveloped. No regulation upstream from station.
**Diversion (station 10256550) 10 ft upstream, generally taking most of the base flow. Published record prior to 1989 represents entire flow from basin (combined creek plus diversion prior to March 1927 and October 1978 to September 1988; creek only, upstream from diversion, December 1927 to September 1931, and October 1959 to September 1978). Both creek only and combined flow published beginning October 1989. Statistics for station 10256501 (combined flow) reflect equivalent total flow from basin.
***Relatively Small Steep Watershed off San Jacinto Peak.
Ref. waterdata.usgs.gov

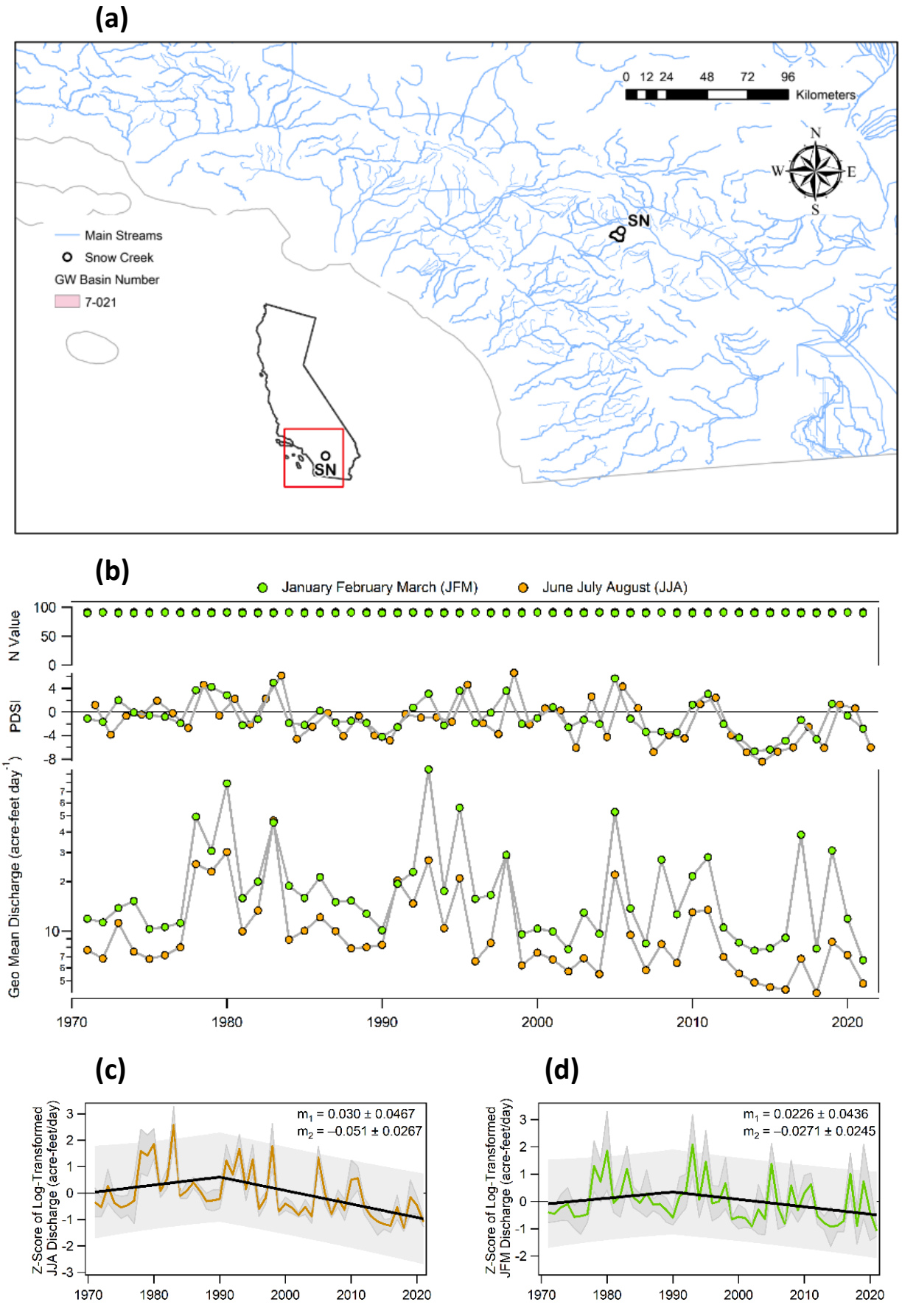
(a)
0 12 24 48 72 96
Kilometers
N
W
E
S
SN
Main Streams
Snow Creek
GW Basin Number
7-021
SN
(b)
January February March (JFM)
June July August (JJA)
N Value
PDSI
Geo Mean Discharge (acre-feet day-1)
1970
1980
1990
2000
2010
2020
(c)
m1 = 0.030 ± 0.0467
m2 = –0.051 ± 0.0267
Z-Score of Log-Transformed JJA Discharge (acre-feet/day)
(d)
m1 = 0.0226 ± 0.0436
m2 = –0.0271 ± 0.0245
Z-Score of Log-Transformed JFM Discharge (acre-feet/day)

SANTA YSABEL C NR RAMONA CA

Gauge Information	USGS Station ID	11025500
	Hydrologic Unit Code	18070304
	Latitude (NAD27)	33°06'25"
	Longitude (NAD27)	116°51'55"
	Drainage Area [Mi^2]	112
	Elevation of The Stream Outlet Above NAVD88 [Ft]	873
	County	San Diego
Watershed Characteristics	Mean Maximum January Temperature [°F]	59.11
	Mean Minimum January Temperature [°F]	36.31
	Mean Annual Precipitation [In]	24.4
	Hydrological Soil Group (HSG) [% of Covered Area]	D(100%)
	Length of Longest Flow Path [Mi]	25
	Mean Basin Elevation [Ft]	2926
	Maximum Basin Elevation [Ft]	5655
	Minimum Basin Elevation [Ft]	863
	Percentage of Area Above 6000 Ft [%]	0
	Percentage of Area Covered By Forest [%]	17.1
	Percentage of Lakes And Ponds [%]	0.24
	Percentage of Developed (Urban) Land (NLCD 2011 Classes 21-24) [%]	3.4
	Percentage of Imperviousness (NLCD 2001 Impervious Dataset) [%]	0.114
	Percentage of Imperviousness (NLCD 2011 Impervious Dataset) [%]	0.118
	Percentage of Imperviousness (NLCD 2019 Impervious Dataset) [%]	0.121
Stream Management Controls	Developed or Natural	Natural*
	Regulation	Regulated**
	Geological or Hydrological Control	None
	Dam Outlet	No
	Agricultural Control	None
	(Waste)water Inputs	None
	Water Withdrawals	Yes***
	Other Factors Affecting Runoff	-

*Mostly natural undeveloped watershed
**Flow regulated by Sutherland Reservoir, capacity, 29,680 acre-ft, since July 1954.
***Some small diversions upstream from station.
Ref. waterdata.usgs.gov

(a)

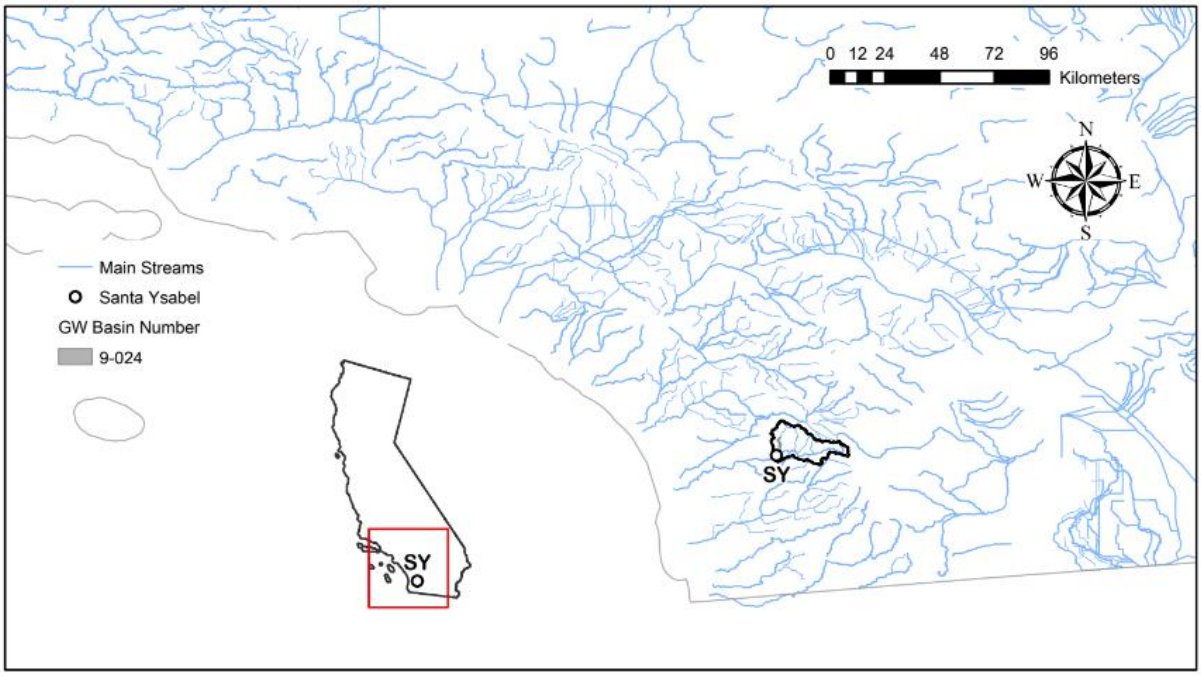
0 12 24 48 72 96
Kilometers
N
W
E
S
Main Streams
Santa Ysabel
GW Basin Number
9-024
SY
SY

(b)

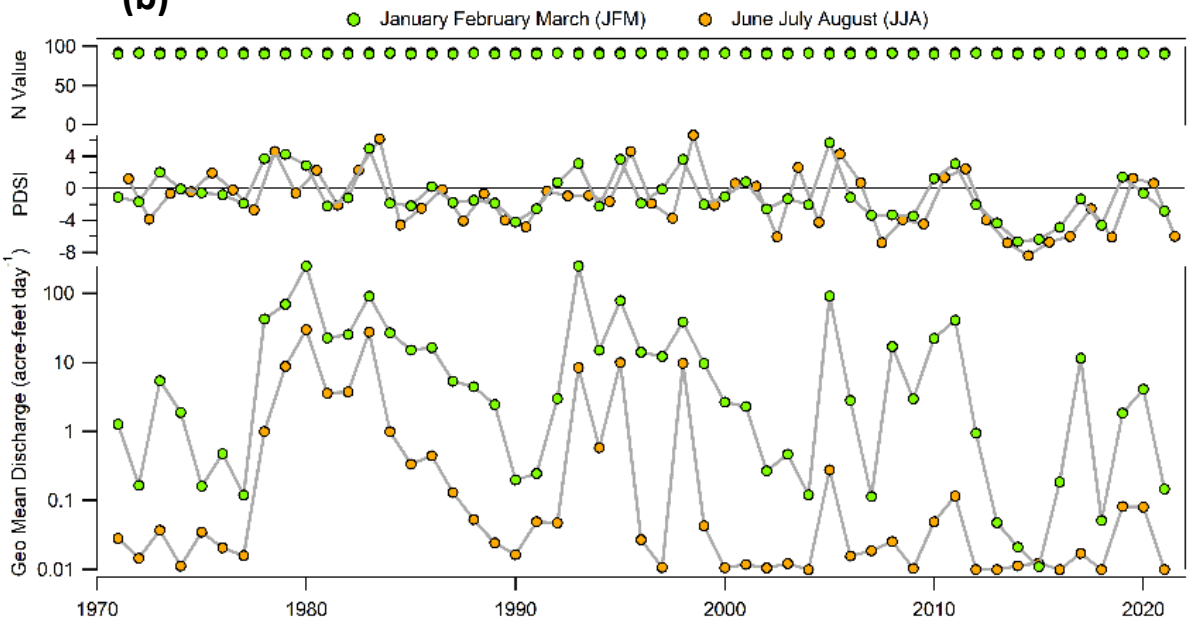
January February March (JFM)
June July August (JJA)
N Value
PDSI
Geo Mean Discharge (acre-feet day-1)
1970
1980
1990
2000
2010
2020

(c)

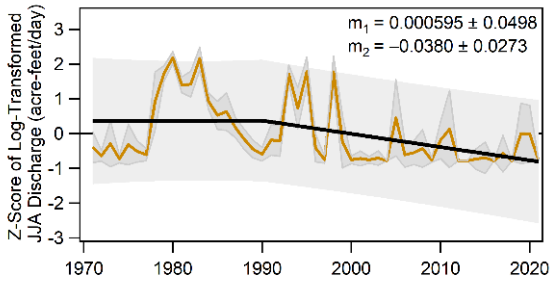
m1 = 0.000595 ± 0.0498
m2 = −0.0380 ± 0.0273
Z-Score of Log-Transformed JJA Discharge (acre-feet/day)
1970
1980
1990
2000
2010
2020

(d)

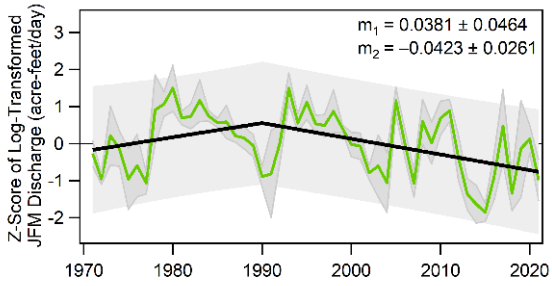
m1 = 0.0381 ± 0.0464
m2 = −0.0423 ± 0.0261
Z-Score of Log-Transformed JFM Discharge (acre-feet/day)
1970
1980
1990
2000
2010
2020

SESPE C NR FILLMORE

Gauge Information	USGS Station ID	11113000
	Hydrologic Unit Code	18070102
	Latitude (NAD27)	34°26'30"
	Longitude (NAD27)	118°55'35"
	Drainage Area [Mi^2]	252
	Elevation of The Stream Outlet Above NAVD88 [Ft]	552
	County	Ventura
Watershed Characteristics	Mean Maximum January Temperature [°F]	53.92
	Mean Minimum January Temperature [°F]	33.06
	Mean Annual Precipitation [In]	26.7
	Hydrological Soil Group (HSG) [% of Covered Area]	D(100%)
	Length of Longest Flow Path [Mi]	57
	Mean Basin Elevation [Ft]	4091
	Maximum Basin Elevation [Ft]	7467
	Minimum Basin Elevation [Ft]	552
	Percentage of Area Above 6000 Ft [%]	4.98
	Percentage of Area Covered By Forest [%]	30.9
	Percentage of Lakes And Ponds [%]	0.009
	Percentage of Developed (Urban) Land (NLCD 2011 Classes 21-24) [%]	1.1
	Percentage of Imperviousness (NLCD 2001 Impervious Dataset) [%]	0.074
	Percentage of Imperviousness (NLCD 2011 Impervious Dataset) [%]	0.077
	Percentage of Imperviousness (NLCD 2019 Impervious Dataset) [%]	0.079
Stream Management Controls	Developed or Natural	Natural
	Regulation	Unregulated*
	Geological or Hydrological Control	None
	Dam Outlet	No
	Agricultural Control	None
	(Waste)water Inputs	None
	Water Withdrawals	Yes*
	Other Factors Affecting Runoff	No Apparent Anthropogenic Sources

*No regulation upstream from station. Fillmore Irrigation Co. has diverted water 1 mi upstream since September 1911. Ref. waterdata.usgs.gov

(a)

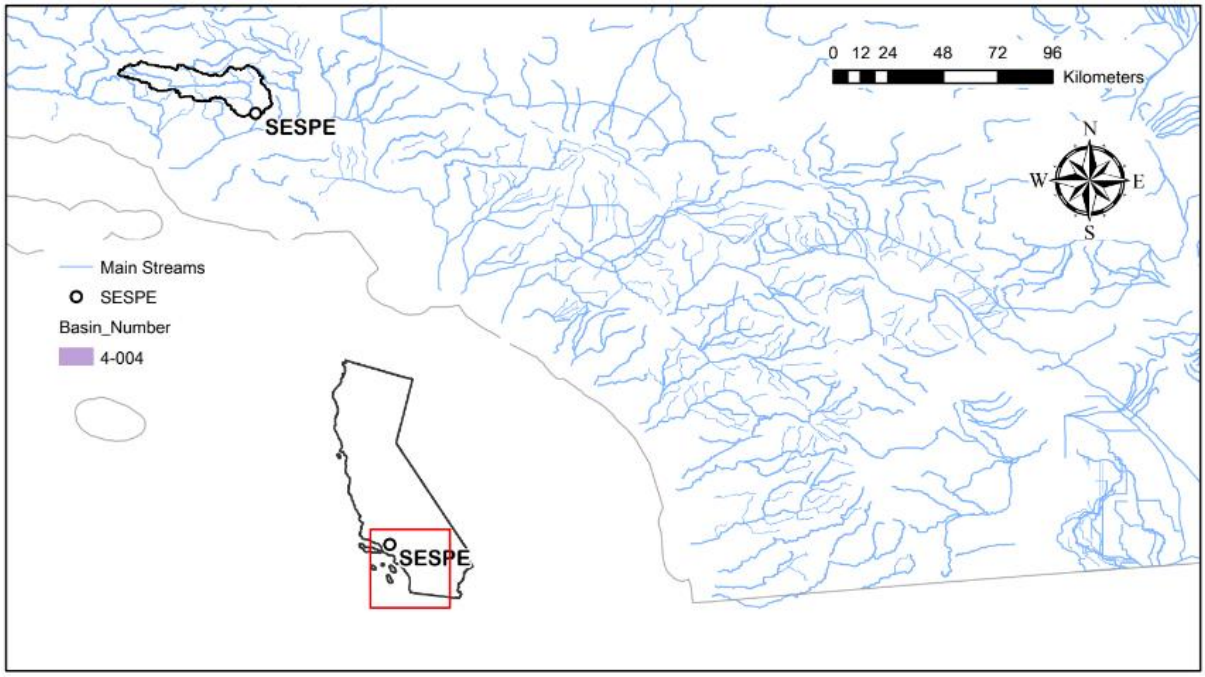
SESPE
0 12 24 48 72 96
Kilometers
N
W
E
S
Main Streams
SESPE
Basin_Number
4-004
SESPE

(b)

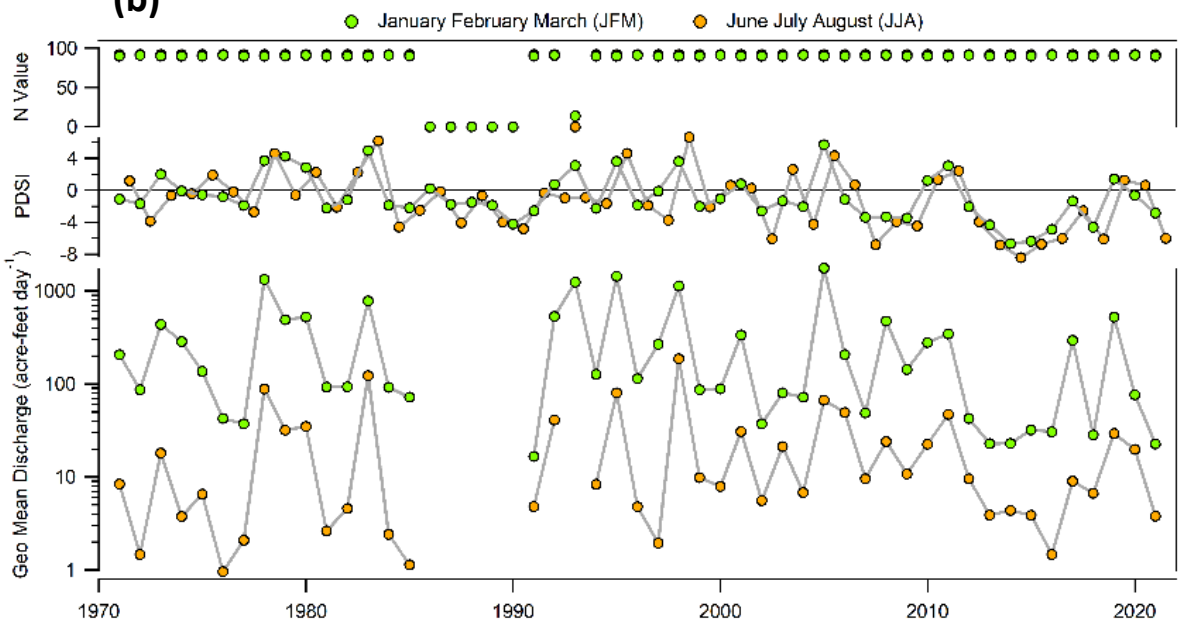
January February March (JFM)
June July August (JJA)
N Value
PDSI
Geo Mean Discharge (acre-feet day-1)
1970
1980
1990
2000
2010
2020

(c)

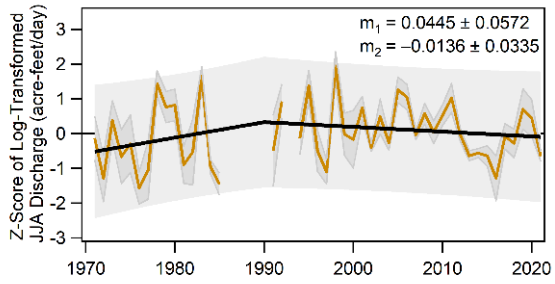
m1 = 0.0445 ± 0.0572
m2 = −0.0136 ± 0.0335
Z-Score of Log-Transformed JJA Discharge (acre-feet/day)
1970
1980
1990
2000
2010
2020

(d)

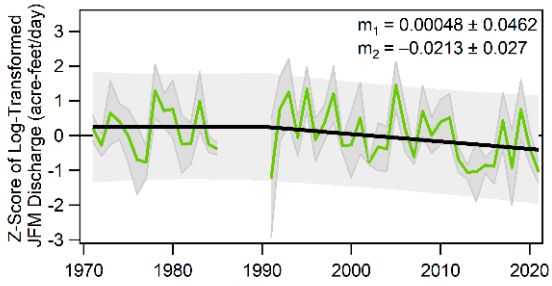
m1 = 0.00048 ± 0.0462
m2 = −0.0213 ± 0.027
Z-Score of Log-Transformed JFM Discharge (acre-feet/day)
1970
1980
1990
2000
2010
2020

Appendix B

Suplemental Information for Chapter 3

B.1 Derivation of Solution I

In this section we derive a formula for the concentration of free microorganisms at any depth z and time t in the interstitial pore fluids of the soil media, $C(z,t)$, under the assumption that all microorganisms originated from a single microbial population initially attached to the soil media at depth $z = z_0$ and time $t = 0$. We begin with the original form of the governing conservation equation for free microorganisms (equation (1a)) in the main text:

$$\frac{\partial C^{\mathrm{I}}}{\partial t} = -v_z(t)\frac{\partial C^{\mathrm{I}}}{\partial z} + v_z(t)\alpha_D\frac{\partial^2 C^{\mathrm{I}}}{\partial z^2} - \lambda_f v_z(t)C^{\mathrm{I}}(z,t) + \frac{\rho_b\lambda_s}{\theta}v_z(t)C_s^{\mathrm{I}}(z,t) + (\mu - k)C^{\mathrm{I}}(z,t) \quad \text{(B.1)}$$

We begin by applying the integrating factors, $\bar{C}^{\mathrm{I}}(z,t) = C^{\mathrm{I}}(z,t)e^{-(\mu-k)(t-t_0)}u(t-t_0)$ and $\bar{C_s}^{\mathrm{I}}(z,t) = C_s^{\mathrm{I}}(z,t)e^{-(\mu-k)(t-t_0)}u(t-t_0)$, where t_0 is an initial condition-dependent time delay

(see below) and $u(t)$ is the unit step function (equal to zero for $t < 0$ and unity for $t \geq 0$):

$$\frac{\partial \bar{C}^{\mathrm{I}}}{\partial t} = -v_z(t)\frac{\partial \bar{C}^{\mathrm{I}}}{\partial z} + v_z(t)\alpha_D \frac{\partial^2 \bar{C}^{\mathrm{I}}}{\partial z^2} - \lambda_f v_z(t)\bar{C}^{\mathrm{I}}(z,t) + \frac{\rho_b \lambda_s}{\theta} v_z(t)\bar{C}_s^{\mathrm{I}}(z,t) \tag{B.2}$$

Next we introduce flow-weighted time $\tau(t)$ (units of hours) where K_s (units meters per second) is the saturated hydraulic conductivity of the soil media, $q(t)$ (units of meters per second) is the Darcy flux of water infiltrating through the soil media with time, and x is a dummy integration variable:

$$\tau(t) = \frac{1}{K_s}\int_0^t q(x)\,dx \tag{B.3}$$

Taking the derivative of equation (B.3) with respect to time, we obtain the following relationship between a differential increase in flow-weighted time and a differential increase in calendar time: $d\tau = \frac{q(t)dt}{K_s}$. Substituting this last result into equations (B.2), along with the relationship between interstitial velocity and Darcy flux described in the main text, $v_z(t) = \alpha_V q(t)$, we obtain a simplified form of the equation in which the unsteady vertical velocity function, $v_z(t)$, has been replaced with the constant velocity, $u = \alpha_V K_s$:

$$\frac{\partial \bar{C}^{\mathrm{I}}}{\partial \tau} = -u\frac{\partial \bar{C}^{\mathrm{I}}}{\partial z} + u\alpha_D \frac{\partial^2 \bar{C}^{\mathrm{I}}}{\partial z^2} - k_f \bar{C}^{\mathrm{I}}(z,t) + \frac{\rho_b k_s}{\theta}\bar{C}_s^{\mathrm{I}}(z,t) \tag{B.4}$$

The filtration and re-entrainment rate constants are $k_f = u\lambda_f$ and $k_s = u\lambda_s$, respectively (both units of inverse time). For Solution I, all microorganisms are from a single population initially attached to the soil media at depth $z = z_0$ at time $\tau = t = 0$. Thus, the initial and boundary conditions for the governing equation of free microorganisms (equation (B.4)) are:

$$\bar{C}^{\mathrm{I}}(z, \tau = 0) = 0 \tag{B.5a}$$

$$\bar{C}^{\mathrm{I}}(z \to \pm\infty, \tau) = 0 \tag{B.5b}$$

Performing the same set of transformations (i.e., applying an integrating factor and flow-weighting time) to the governing equation for attached microorganisms (equation (1b) in the main text) we arrive at the following equation for $\bar{C}_s^{\mathrm{I}}(z,\tau)$:

$$\frac{\partial \bar{C}_s^{\mathrm{I}}}{\partial \tau} = \frac{\theta k_f}{\rho_b}\bar{C}^{\mathrm{I}}(z,\tau) - k_s \bar{C}_s^{\mathrm{I}}(z,\tau) \tag{B.6}$$

The initial condition for surface-attached microorganisms is as follows:

$$\bar{C}_s^{\mathrm{I}}(z,0) = M_s''\delta(z-z_0)/\rho_b \tag{B.7}$$

where M_s'' is the source strength of soil attached microorganisms (in units of soil-attached microorganism count per unit cross-sectional area) at flow-weighted time $\tau = 0$ and depth $z = z_0$, and $\delta(z)$ is the Dirac Delta function (units of inverse meters).

To solve equations (B.4) through (B.7) we proceed step-wise as follows. First, we remove the advective term from equation (B.4) by performing the following substitution for the dependent variable: $\bar{C}^{\mathrm{I}}(z,\tau) = \Gamma(z,\tau)\exp\left(\frac{z}{2\alpha_D} - \frac{u\tau}{4\alpha_D}\right)$ and $\bar{C}_s^{\mathrm{I}}(z,\tau) = \Gamma_s(z,\tau)\exp\left(\frac{z}{2\alpha_D} - \frac{u\tau}{4\alpha_D}\right)$. After substituting these expressions into equation (B.4) and simplifying, the governing equation, initial condition and boundary conditions for free microorganisms becomes:

$$\frac{\partial \Gamma}{\partial \tau} = \alpha_D u \frac{\partial^2 \Gamma}{\partial z^2} - k_f \Gamma(z,\tau) + \frac{k_s \rho_b}{\theta}\Gamma_s(z,\tau) \tag{B.8a}$$

$$\Gamma(z,\tau=0) = 0 \tag{B.8b}$$

$$\Gamma(z\to\pm\infty,\tau) = 0 \tag{B.8c}$$

The same transformation applied to equations (B.6) and (B.7) yields:

$$\frac{\partial \Gamma_s}{\partial \tau} = \frac{k_f\theta}{\rho_b}\Gamma(z,\tau) - \left(k_s - \frac{u}{4\alpha_D}\right)\Gamma_s(z,\tau) \tag{B.9a}$$

$$\Gamma_s(z,\tau=0) = \frac{M_s''}{\rho_b}e^{-\frac{z}{2\alpha_D}}\delta(z-z_0) \tag{B.9b}$$

Equations (B.9a) and (B.9b) can be solved directly, yielding the following formula for soil-attached microorganisms where the symbol $*$ denotes a convolution integral:

$$\Gamma_s(z,\tau) = \frac{k_f\theta}{\rho_b}\Gamma(z,\tau) * e^{-\beta\tau} + \Gamma_s(z,\tau=0)e^{-\beta\tau} \tag{B.10a}$$

$$\beta = k_s - \frac{u}{4\alpha_D} \tag{B.10b}$$

Combining equations (B.8a) and (B.10a) , we obtain an equation for $\Gamma(z,\tau)$:

$$\frac{\partial\Gamma}{\partial\tau} = \alpha_D u\frac{\partial^2\Gamma}{\partial z^2} - k_f\Gamma(z,\tau) + k_f k_s\Gamma(z,\tau) * e^{-\beta\tau} + \phi e^{-\frac{z}{2\alpha_D}}\delta(z-z_0)e^{-\beta\tau} \tag{B.11a}$$

$$\phi = \frac{k_s M_s''}{\theta} \tag{B.11b}$$

Here, the variable ϕ has units of microbial flux (microorganism count per area per time), while the source strength variable M_s'' has units of attached microorganism count per unit cross-sectional area. To solve this last equation we begin by taking its Laplace Transform with respect to flow-weighted time, utilizing the initial condition (equation (B.8b)):

$$s\tilde{\Gamma}(z,s) = \alpha_D u\frac{d^2\tilde{\Gamma}}{dz^2} - k_f\tilde{\Gamma}(z,s) + k_f k_s\frac{\tilde{\Gamma}(z,s)}{s+\beta} + \frac{\phi e^{-\frac{z}{2\alpha_D}}\delta(z-z_0)}{s+\beta} \tag{B.12}$$

Here, $\tilde{\Gamma}(z,s)$ denotes the Laplace Transform of $\Gamma(z,\tau)$: $\tilde{\Gamma}(z,s) = \int_0^\infty e^{-s\tau}\Gamma(z,\tau)d\tau$. We next take the Fourier Transform of equation (B.12), $\widehat{\tilde{\Gamma}}(k,s) = \int_{-\infty}^{\infty}\tilde{\Gamma}(z,s)e^{ikz}dz$, and solve for $\widehat{\tilde{\Gamma}}(k,s)$:

$$\widehat{\tilde{\Gamma}}(k,s) = \phi e^{-\frac{z_0}{2\alpha_D}(1+2\alpha_D ik)}F(s) \tag{B.13a}$$

$$F(s) = \frac{1}{(s+\beta)\left(s + k_f - \frac{k_f k_s}{s+\beta} + \alpha_D u k^2\right)} \tag{B.13b}$$

To invert this Laplace-Fourier solution, we must first perform a few manipulations on the image function, $F(s)$. First we define a new image function, $F_1(s)$, such that $F_1(s+\beta) =$

$F(s)$:

$$F_1(s) = \left(\frac{1}{s}\right)\left(\frac{1}{s - \frac{k_f k_s}{s} + \gamma}\right) \tag{B.14a}$$

$$\gamma = k_f - \beta + \alpha_D u k^2 \tag{B.14b}$$

Using the identity, $\frac{1}{b} = \int_0^\infty e^{-bx}dx$, the new image function can also be expressed in the following form:

$$F_1(s) = \frac{1}{s}\int_0^\infty e^{-(s - \frac{k_f k_s}{s} + \gamma)x}dx = \frac{1}{s}F_2(s - \frac{k_f k_s}{s}) \tag{B.15a}$$

$$F_2(s) = \int_0^\infty e^{-(s+\gamma)x}dx \tag{B.15b}$$

Note that the inverse Laplace Transform of $F_2(s)$ is $f_2(\tau) = \int_0^\infty \delta(\tau - x)e^{-\gamma x}dx = e^{-\gamma\tau}$. Next we utilize Efros' Theorem (Graf, 2015). Suppose that the inverse Laplace Transform of the image function $F_2(s)$ is the function $f_2(\tau)$ *and* the inverse Laplace Transform of $G(s)e^{-q(s)\xi}$ is the function $g(\tau, \xi)$. Then the theorem states that the inverse Laplace Transform of $G(s)F_2[q(s)]$ is equal to $\int_0^\infty g(\tau, \xi)f_2(\xi)d\xi$.

Applying Efros' Theorem to our present problem, we have: (1) the inverse Laplace Transform of $F_2(s)$ is the function $f_2(\tau) = e^{-\gamma\tau}$; (2) $q(s) = s - \frac{k_f k_s}{s}$; (3) $G(s) = 1/s$; and (4) $G(s)e^{-q(s)\xi} = e^{-\xi s} \times (\frac{1}{s}e^{k_f k_s \xi/s})$. In this case, the inverse Laplace Transform of $G(s)e^{-q(s)\xi}$ is $g(\tau, \xi) = I_0[2\sqrt{k_f k_s \xi(\tau - \xi)}]u(\tau - \xi)$, where $I_0[\cdot]$ is the Bessel Function of the first kind and $u(\tau)$ is the unit step function. Thus, from Efros' Theorem we have that the inverse Laplace Transform of $F_1(s) = \frac{F_2(s - \frac{k_f k_s}{s})}{s}$ is $f_1(\tau) = \int_0^\tau I_0[2\sqrt{k_f k_s \xi(\tau - \xi)}]e^{-\gamma\xi}d\xi$. Further, from the similarity rule (Graf, 2015), the relationship $F_1(s+\beta) = F(s)$ implies that the inverse Laplace Transform of $F(s)$ is $e^{-\beta\tau}f_1(\tau)$. Thus, the inverse Laplace Transform of equation (B.13a) is

as follows:

$$\widehat{\Gamma}(k,\tau) = \phi e^{-\frac{z_0}{2\alpha_D}-\beta\tau}\int_0^\tau I_0\Big[2\sqrt{k_f k_s \xi(\tau-\xi)}\Big]e^{-(k_f-\beta)\xi}\Big(e^{-z_0 ik-\alpha_D u k^2\xi}\Big)d\xi \tag{B.16}$$

Taking the Inverse Fourier Transform of this last result we obtain:

$$\Gamma(z,\tau) = \frac{\phi e^{-\frac{z_0}{2\alpha_D}-\beta\tau}}{2\sqrt{\pi}}\int_0^\tau I_0\Big[2\sqrt{k_f k_s \xi(\tau-\xi)}\Big]e^{-(k_f-\beta)\xi}\Big(\frac{e^{-\frac{(z-z0)^2}{4\alpha_D u\xi}}}{\sqrt{\alpha_D u\xi}}\Big)d\xi \tag{B.17}$$

The corresponding expression for $\bar{C}(z,\tau)$ is:

$$\bar{C}^{\mathrm{I}}(z,\tau) = \frac{\phi e^{\frac{z-z_0}{2\alpha_D}-k_s\tau}}{2\sqrt{\pi}}\int_0^\tau I_0\Big[2\sqrt{k_f k_s \xi(\tau-\xi)}\Big]e^{-(k_f-k_s+\frac{u}{4\alpha_D})\xi}\Big(\frac{e^{-\frac{(z-z0)^2}{4\alpha_D u\xi}}}{\sqrt{\alpha_D u\xi}}\Big)d\xi \tag{B.18}$$

Because the attached microbial population was present in the soil media at time $\tau = t = 0$, growth or decay processes would begin immediately. Thus, the time delay appearing in the integrating factor is zero in this case: $t_0 = 0$. Accounting for growth or decay processes and substituting the mass source term, $\phi = \frac{k_s M_s''}{\theta}$, we arrive at the final solution:

$$C^{\mathrm{I}}(z,\tau) = \frac{k_s M_s'' e^{\frac{z-z_0}{2\alpha_D}-k_s\tau-(k-\mu)t(\tau)}}{2\theta\sqrt{\pi}}\int_0^\tau I_0\Big[2\sqrt{k_f k_s \xi(\tau-\xi)}\Big]e^{-(k_f-k_s+\frac{u}{4\alpha_D})\xi}\Big(\frac{e^{-\frac{(z-z0)^2}{4\alpha_D u\xi}}}{\sqrt{\alpha_D u\xi}}\Big)d\xi \tag{B.19}$$

B.2 Derivation of Solution II

In this section we derive a formula for the concentration of free microorganisms at any depth z and time t in the interstitial pore fluids of the soil media, $C(z,t)$, under the assumption that all microorganisms originated from a pulse of stormwater entering the soil media at $z = 0$ and time $t = t_i$. We begin with the simplified form of the governing equation for free microorganisms, after applying the integrating factor and moving the equation to flow-

weighted time (see derivation of equation B.4):

$$\frac{\partial \bar{C}^{\mathrm{II}}}{\partial \tau} = -u\frac{\partial \bar{C}^{\mathrm{II}}}{\partial z} + u\alpha_D \frac{\partial^2 \bar{C}^{\mathrm{II}}}{\partial z^2} - k_f \bar{C}^{\mathrm{II}}(z,t) + \frac{\rho_b k_s}{\theta}\bar{C}_s^{\mathrm{II}}(z,t) \tag{B.20}$$

The corresponding set of initial and boundary conditions are as follows, where for the moment we assume that the stormwater pulse enters the soil media at $t_i = 0$ (the time shift for the stormwater pulse will be introduced later):

$$\bar{C}^{\mathrm{II}}(z, \tau = 0) = \frac{M_R'' \delta(z)}{\theta} \tag{B.21a}$$

$$\bar{C}^{\mathrm{II}}(z \to \pm\infty, \tau) = 0 \tag{B.21b}$$

Here, the variable M_R'' is the source strength of the stormwater pulse in units of microorganism count per unit cross-sectional area. Performing the same set of transformations (i.e., applying an integrating factor and flow-weighting time) on the governing equation for attached microorganisms (equation (1b) in the main text) we arrive at the following equation for $\bar{C}_s^{\mathrm{II}}(z,\tau)$:

$$\frac{\partial \bar{C}_s^{\mathrm{II}}}{\partial \tau} = \frac{\theta k_f}{\rho_b}\bar{C}^{\mathrm{II}}(z,\tau) - k_s \bar{C}_s^{\mathrm{II}}(z,\tau) \tag{B.22}$$

In Solution II, all microorganisms originate in a stormwater pulse, and therefore the initial condition for the attached-microorganism concentration is zero (i.e., the initial source strength of soil-attached microorganisms is, $M_s'' = 0$:

$$\bar{C}_s^{\mathrm{II}}(z, 0) = 0 \tag{B.23}$$

Solving equations (B.22) and (B.23) in the Laplace domain, we obtain:

$$\bar{C}_s^{\mathrm{II}}(z,\tau) = \frac{\theta k_f}{\rho_b}\bar{C}^{\mathrm{II}}(z,\tau) * e^{-k_s \tau} \tag{B.24}$$

Substituting this result back into equation (B.20), we arrive at a final version of the governing equation for free microorganisms:

$$\frac{\partial \bar{C}^{\mathrm{II}}}{\partial \tau} = -u\frac{\partial \bar{C}^{\mathrm{II}}}{\partial z} + u\alpha_D \frac{\partial^2 \bar{C}^{\mathrm{II}}}{\partial z^2} - k_f \bar{C}^{\mathrm{II}}(z,t) + k_s k_f \bar{C}^{\mathrm{II}}(z,\tau) * e^{-k_s \tau} \tag{B.25a}$$

$$\bar{C}^{\mathrm{II}}(z,\tau=0) = \frac{M_R'' \delta(z)}{\theta} \tag{B.25b}$$

$$\bar{C}^{\mathrm{II}}(z \to \pm\infty, \tau) = 0 \tag{B.25c}$$

Taking the double Laplace and Fourier Transform of these equations, and solving for the transformed dependent variable and utilizing the identity, $\frac{1}{b} = \int_0^\infty e^{-bx} dx$, we obtain the following solution for $\widehat{\bar{C}}^{\mathrm{II}}(k,s)$:

$$\widehat{\bar{C}}^{\mathrm{II}}(k,s) = \frac{M_R''}{\theta} \int_0^\infty e^{-\left(s + k_f - \frac{k_f k_s}{k_s + s}\right)\xi} e^{-u(ik + \alpha_D k^2)\xi} d\xi \tag{B.26}$$

We note that the inverse Laplace Transform of the image function $F_1(s) = e^{\frac{k_f k_s \xi}{k_s + s}}$ is the time-domain function: $f_1(t) = e^{-k_s \tau}\left(\sqrt{\frac{k_f k_s \xi}{\tau}} I_1\left[2\sqrt{k_f k_s \xi \tau}\right] + \delta(\tau)\right)$, where $\delta(\cdot)$ is the Dirac Delta function and $I_1[\cdot]$ is the Bessel Function of the First Kind. Therefore, the inverse Laplace Transform of $e^{-s\xi} F_1(s)$ is, by the Original Shift Rule (Graf, 2015): $e^{-k_s(\tau-\xi)}\sqrt{\frac{k_f k_s \xi}{\tau - \xi}} I_1\left[2\sqrt{k_f k_s \xi(\tau - \xi)}\right] u(\tau - \xi) + e^{-k_s(\tau-\xi)} u(\tau - \xi)\delta(\tau - \xi)$, where $u(\cdot)$ is the unit step function defined above. The inverse Fourier Transform of $e^{-u(ik + \alpha_D k^2)\xi}$ is $\frac{1}{2\sqrt{\pi \alpha_D u \xi}} e^{-\frac{(z-u\xi)^2}{4\alpha_D u \xi}}$. Therefore, Solution II takes the following form when microorganisms enter the soil media with a stormwater pulse at time $t = \tau = 0$:

$$\bar{C}^{\mathrm{II}}(z,\tau) = \frac{M_R'' e^{-k_s \tau}}{2\theta\sqrt{\pi}} \int_0^\tau e^{(k_s - k_f)\xi} \sqrt{\frac{k_f k_s \xi}{\tau - \xi}} I_1\left[2\sqrt{k_f k_s \xi(\tau - \xi)}\right] \frac{e^{-\frac{(z-u\xi)^2}{4\alpha_D u \xi}}}{\sqrt{\alpha_D u \xi}} d\xi + \frac{M_R'' e^{-k_f \tau}}{2\theta\sqrt{\pi}} \frac{e^{-\frac{(z-u\tau)^2}{4\alpha_D u \tau}}}{\sqrt{\alpha_D u \tau}} \tag{B.27}$$

When the microorganisms enter the soil media with a stormwater pulse at time t_i, then solution is modified as follows, where $\tau_i = \tau(t_i)$ and $\tau = \tau(t) > \tau_i$:

$$\bar{C}^{\mathrm{II}}(z,\tau,\tau_i) = \frac{M_R'' e^{-k_s(\tau-\tau_i)}}{2\theta\sqrt{\pi}} \int_0^{\tau-\tau_i} e^{(k_s-k_f)\xi} \sqrt{\frac{k_f k_s \xi}{\tau-\tau_i-\xi}}$$
$$\times I_1\left[2\sqrt{k_f k_s \xi(\tau-\tau_i-\xi)}\right] \frac{e^{-\frac{(z-u\xi)^2}{4\alpha_D u\xi}}}{\sqrt{\alpha_D u\xi}} d\xi + \frac{M_R'' e^{-k_f(\tau-\tau_i)}}{2\theta\sqrt{\pi}} \frac{e^{-\frac{(z-u(\tau-\tau_i))^2}{4\alpha_D u(\tau-\tau_i)}}}{\sqrt{\alpha_D u(\tau-\tau_i)}}, \quad \tau > \tau_i \quad \text{(B.28)}$$

Using the same general procedure, it is easy to derive a solution for the case where microorganisms entering the soil media with stormwater at time $t = \tau = 0$ but do not attach to the soil media or undergo first-order decay or growth:

$$C^{\mathrm{II}}_{\mathrm{cons}}(z,\tau) = \frac{M_R'' e^{-\frac{(z-u\tau)^2}{4\alpha_D u\tau}}}{2\theta\sqrt{\pi\alpha_D u\tau}} \quad \text{(B.29)}$$

Therefore, equation (B.30) can be written in the following more compact form, where the function $\bar{C}^{\mathrm{II}}_{\mathrm{cons}}(z,\tau)$ serves as the Green's function for the more general solution:

$$\bar{C}^{\mathrm{II}}(z,\tau,\tau_i) = e^{-k_s(\tau-\tau_i)} \int_0^{\tau-\tau_i} e^{-(k_f-k_s)\xi} \sqrt{\frac{k_f k_s \xi}{\tau-\tau_i-\xi}} I_1$$
$$\left[2\sqrt{k_f k_s \xi(\tau-\tau_i-\xi)}\right] C^{\mathrm{II}}_{\mathrm{cons}}(z,\xi) d\xi + e^{-k_f(\tau-\tau_i)} C^{\mathrm{II}}_{\mathrm{cons}}(z,\tau-\tau_i), \quad \tau > \tau_i \quad \text{(B.30)}$$

This is the general expression for the pulsatile version of Solution II that appears in the main text (equations (7) and (8)).

B.3 Limiting Expressions

B.3.1 Limiting expressions for Solution I

B.3.2 Re-entrainment Alone: $\mathbf{R^I}$

The solution for this limiting case follows from equation (6) in the main text, by setting $k = \mu = k_f = 0$:

$$C_{\mathrm{R}}^{\mathrm{I}}(z,\tau) = \frac{k_s \rho_b C_{si}}{2\theta} \int_0^\tau e^{-k_s(\tau-\xi)} \Big(\mathrm{erf}\Big[\frac{d-z+u\xi}{2\sqrt{\alpha_D u\xi}}\Big] + \mathrm{erf}\Big[\frac{z-u\xi}{2\sqrt{\alpha_D u\xi}}\Big] \Big) d\xi \tag{B.31}$$

B.3.3 Re-entrainment and Filtration: $\mathbf{(R+F)^I}$

The solution for this limiting case follows from equation (6) in the main text, by setting $k = \mu = 0$:

$$\begin{aligned} C^{\mathrm{I}}(z,\tau) = {} & \frac{k_s \rho_b C_{si} e^{-k_s \tau}}{2\theta} \\ & \times \int_0^\tau I_0\Big[2\sqrt{k_f k_s \xi(\tau-\xi)}\Big] e^{-(k_f-k_s)\xi} \Big(\mathrm{erf}\Big[\frac{d-z+u\xi}{2\sqrt{\alpha_D u\xi}}\Big] + \mathrm{erf}\Big[\frac{z-u\xi}{2\sqrt{\alpha_D u\xi}}\Big] \Big) d\xi \end{aligned} \tag{B.32}$$

B.3.4 Re-entrainment and Growth or Decay: $\mathbf{(R+G/D)^I}$

The solution for this limiting case follows from equation (6) in the main text, by setting $k_f = 0$:

$$C_{\mathrm{R}}^{\mathrm{I}}(z,\tau) = \frac{k_s \rho_b C_{si}}{2\theta} e^{-(k-\mu)t(\tau)} \int_0^\tau e^{-k_s(\tau-\xi)} \Big(\mathrm{erf}\Big[\frac{d-z+u\xi}{2\sqrt{\alpha_D u\xi}}\Big] + \mathrm{erf}\Big[\frac{z-u\xi}{2\sqrt{\alpha_D u\xi}}\Big] \Big) d\xi \tag{B.33}$$

B.4 Limiting expressions for Solution II

B.4.1 Filtration Alone: F^{II}

For this limit, a pulse of stormwater-associated microbial pollution enters the soil media at flow-weighted time $\tau_i = 0$ (a time shift will be introduced later). It then transports through the soil media by advection and dispersion during storm events, and is removed by filtration onto the soil media. In this case, the governing equations for the concentration of free microorganisms are as follows:

$$\frac{\partial C}{\partial \tau} = -u\frac{\partial C}{\partial z} + u\alpha_D\frac{\partial^2 C}{\partial z^2} - k_f C(z,t) \tag{B.34a}$$

$$C(z, \tau = 0) = \frac{M_R''\delta(z)}{\theta} \tag{B.34b}$$

$$C(z \to \pm\infty, \tau) = 0 \tag{B.34c}$$

This set of equations can readily be solved using the same procedure outlined in Section 2. After delaying the entrance time of the pollution pulse by τ_i, the solution takes the following form:

$$C_{\mathrm{F}}^{\mathrm{II}}(z,\tau,\tau_i) = \frac{M_R''}{2\theta\sqrt{\pi}}\frac{e^{-\frac{(z-u(\tau-\tau_i))^2}{4\alpha_D u(\tau-\tau_i)} - k_f(\tau-\tau_i)}}{\sqrt{\alpha_D u(\tau-\tau_i)}} \tag{B.35}$$

Substituting the differential source strength, $dM_R'' = u\theta C_{sw}(\tau_i)d\tau_i$ where $C_{sw}(\tau_i)$ is the microbe inflow concentration (in the stormwater) at time τ_i, and integrating over a step change in the inflow concentration from C_{SO} (during the sewage-contaminated storm, $0 \le \tau \le \tau_{SO}$) to C_f (in subsequent sewage-free storms, $\tau > \tau_{SO}$), we arrive at the following solution for

this limiting case:

$$C_{\mathrm{F}}^{\mathrm{II}}(z,\tau) = \begin{cases} C_{\mathrm{SO}} D(z,\tau), \ 0 < \tau \leq \tau_{\mathrm{SO}} \\ C_{\mathrm{SO}} D(z,\tau) - (C_{\mathrm{SO}} - C_f) D(z, \tau - \tau_{\mathrm{SO}}), \ \tau > \tau_{\mathrm{SO}} \end{cases} \tag{B.36a}$$

$$D(z,\tau) = \frac{e^{\frac{(1-\gamma)z}{2\alpha_D}}}{2\gamma} \left(\operatorname{erfc}\left[\frac{z - \gamma\tau u}{2\sqrt{\alpha_D \tau u}} \right] - e^{\frac{\gamma z}{\alpha_D}} \operatorname{erfc}\left[\frac{z + \gamma\tau u}{2\sqrt{\alpha_D \tau u}} \right] \right) \tag{B.36b}$$

$$\gamma = \sqrt{1 + \frac{4\alpha_D k_f}{u}} \tag{B.36c}$$

Note that this solution collapses to equations (9a) and (9b) in the main text, when the filtration rate constant is set to zero, $k_f = 0$.

B.4.2 Growth or Decay: (G/D)$^{\mathrm{II}}$

For this limit, we amend the conservative version of Solution II (equation (B.29)) to account for first-order growth or decay, accounting specifically for the elapsed time since a pulse of microbial pollution entered the soil media with stormwater at $\tau = \tau_i$. The final expression is represented as a sum over N pollution pulses, each of which has a source strength of $\Delta M''_{R,i} = u\theta C_{sw}(\tau_i)\Delta\tau$ where $C_{sw}(\tau_i)$ is the microbe inflow concentration (in the stormwater) at time τ_i, $\Delta\tau$ is the duration of each pulse in flow-weighted time, and Floor(x) gives the

greatest integer less than or equal to x:

$$C^{\mathrm{II}}_{\mathrm{G/D}}(z,\tau) = \frac{u\Delta\tau}{2\sqrt{\pi}} \times \begin{cases} C_{\mathrm{SO}} \sum_{i=0}^{N} E(z,\tau,\tau_i), \ 0 < \tau \leq \tau_{\mathrm{SO}} \\ C_{\mathrm{SO}} \sum_{i=0}^{N_{\mathrm{SO}}} E(z,\tau,\tau_i) \\ \quad + C_f \sum_{i=N_{\mathrm{SO}}+1}^{N} E(z,\tau,\tau_i), \ \tau > \tau_{\mathrm{SO}} \end{cases} \tag{B.37a}$$

$$E(z,\tau,\tau_i) = e^{-(k-\mu)(t(\tau)-t(\tau_i))} \frac{e^{-\frac{(z-u(\tau-\tau_i))^2}{4\alpha_D u(\tau-\tau_i)}}}{\sqrt{\alpha_D u(\tau-\tau_i)}} \tag{B.37b}$$

$$\tau_i = i\Delta\tau \tag{B.37c}$$

$$N = \mathrm{Floor}(\tau/\Delta\tau) \tag{B.37d}$$

$$N_{\mathrm{SO}} = \mathrm{Floor}(\tau_{\mathrm{SO}}/\Delta\tau) \tag{B.37e}$$

Because first-order growth or decay occurs over time (not flow-weighted time), this solution requires that we invert flow-weighted time to calendar time: $t(\tau) = \tau^{-1}(t)$.

B.4.3 Filtration and Growth or Decay: $(\mathbf{F+G/D})^{\mathbf{II}}$

For this limit, we amend the filtration-only limiting case for Solution II (equation (B.35)) to account for growth or decay, again summing over N pollution pulses:

$$C^{\mathrm{II}}_{\mathrm{F+G/D}}(z,\tau) = \frac{u\Delta\tau}{2\sqrt{\pi}} \times \begin{cases} C_{\mathrm{SO}} \sum_{i=0}^{N} F(z,\tau,\tau_i), \ 0 < \tau \leq \tau_{\mathrm{SO}} \\ C_{\mathrm{SO}} \sum_{i=0}^{N_{\mathrm{SO}}} F(z,\tau,\tau_i) \\ \quad + C_f \sum_{i=N_{\mathrm{SO}}+1}^{N} F(z,\tau,\tau_i), \ \tau > \tau_{\mathrm{SO}} \end{cases} \tag{B.38a}$$

$$F(z,\tau,\tau_i) = e^{-(k-\mu)(t(\tau)-t(\tau_i))} \frac{e^{-\frac{(z-u(\tau-\tau_i))^2}{4\alpha_D u(\tau-\tau_i)} - k_f(\tau-\tau_i)}}{\sqrt{\alpha_D u(\tau-\tau_i)}} \tag{B.38b}$$

$$\tau_i = i\Delta\tau \tag{B.38c}$$

$$N = \mathrm{Floor}(\tau/\Delta\tau) \tag{B.38d}$$

$$N_{\mathrm{SO}} = \mathrm{Floor}(\tau_{\mathrm{SO}}/\Delta\tau) \tag{B.38e}$$

B.4.4 Filtration and Re-Entrainment: $(\mathbf{F+R})^{\mathbf{II}}$

To derive a solution for this limiting case, we simply drop the growth/decay term from Solution II (equation (10), main text), and again sum over the N pulses:

$$C^{\mathrm{II}}_{\mathrm{F+R}}(z,\tau) = \frac{u\Delta\tau}{2\sqrt{\pi}} \times \begin{cases} C_{\mathrm{SO}} \sum_{i=0}^{N} G(z,\tau,\tau_i), \ 0 < \tau \leq \tau_{\mathrm{SO}} \\ C_{\mathrm{SO}} \sum_{i=0}^{N_{\mathrm{SO}}} G(z,\tau,\tau_i) \\ \quad + C_f \sum_{i=N_{\mathrm{SO}}+1}^{N} G(z,\tau,\tau_i), \ \tau > \tau_{\mathrm{SO}} \end{cases} \tag{B.39a}$$

$$\tau_i = i\Delta\tau \tag{B.39b}$$

$$N = \mathrm{Floor}(\tau/\Delta\tau) \tag{B.39c}$$

$$N_{\mathrm{SO}} = \mathrm{Floor}(\tau_{\mathrm{SO}}/\Delta\tau) \tag{B.39d}$$

Here, the function $G(z,\tau,\tau_i)$ takes on the following form:

$$G(z,\tau,\tau_i) = e^{-k_s(\tau-\tau_i)} \int_0^{\tau-\tau_i} e^{-(k_f-k_s)\xi} \sqrt{\frac{k_f k_s \xi}{\tau-\tau_i-\xi}} \times I_1\left[2\sqrt{k_f k_s \xi(\tau-\tau_i-\xi)}\right] C^{\mathrm{II}}_{\mathrm{cons}}(z,\xi)d\xi + e^{-k_f(\tau-\tau_i)} C^{\mathrm{II}}_{\mathrm{cons}}(z,\tau-\tau_i) \quad \text{(B.40)}$$

B.5 Numerical Implementation of Pulsatile Solutions

All of the limiting cases for Solution I are readily represented as explicit formula (e.g., involving complementary error functions, integrals of Bessel functions, and so on), and thus are straightforward to implement numerically. In our case, we simply coded these explicit formula as functions in Wolfram Mathematica (v 13.0) and then utilized the "NonLinearModel" within Mathematica to estimate experimental parameters and associated errors. This was also the case for all limiting cases for Solution II which do not involve summing over pollution pulses. An example of this approach is our implementation of the conservative solution, and its use for estimating the transport parameters, α_V and α_D, and the duration of the (bromide-spiked) sewage pulse τ_{SO}. The Mathematica code is shown in Figure B.1 (compare with equation (B.29)).

A number of the limiting solutions, especially for Solution II, involve a summation over multiple pollution pulses. As an example, consider the limiting case $\mathrm{G/D^{II}}$ (equation (B.37a)). To implement this solution numerically we must make several choices. First, we need to decide the resolution at which we want to resolve the breakthrough curve, which is determined by the duration of each pulse in flow-weighted time, $\Delta\tau$ (smaller values of $\Delta\tau$ will lead to a more refinely resolved breakthrough curve). Second, we need to decide where to place the pulse within each $\Delta\tau$ interval (e.g., at the beginning, middle, or end). In the first instance, we calculated $\Delta\tau$ by including in the function call a fixed integer, N_{SO}, which

```
depth = 0.6; Ksat = .174; initialconc = .124;

a[z_, tau_, ad_, u_] := (1 / 2) Erfc[(z - tau u) / (2 Sqrt[ad tau u])] -
  (1 / 2) Exp[z / ad] Erfc[(z + tau u) / (2 Sqrt[ad tau u])]

cConsII[z_, tau_, ad_, u_, tauSO_, cSO_] :=
 cSO (a[z, tau, ad, u] - a[z, tau - tauSO, ad, u] UnitStep[tau - tauSO])

nlmbro = NonlinearModelFit[bromidedata, cConsII[depth, tau, aD, Ksat aV, tauSO, initialconc],
  {{tauSO, 2.2}, {aV, 2}, {aD, .1}}, tau]
```

FittedModel[0.124 (1/2 Erfc[(≪19≫ (0.6 − ≪1≫))/√tau] − ≪1≫ − (1/2 Erfc[≪1≫/≪1≫] − ≪1≫) ≪1≫)]

```
nlmbro["ParameterTable"]
```

	Estimate	Standard Error	t-Statistic	P-Value
tauSO	1.99655	0.0360181	55.4319	1.47787×10^{-98}
aV	3.54049	0.155083	22.8297	1.54061×10^{-49}
aD	0.535222	0.0501441	10.6737	6.33111×10^{-20}

```
nlmbro[{"AICc", "RSquared"}]
{-1184.53, 0.972815}
```

Figure B.1: Mathematica code for implementing the conservative solution in flow-weighted time, and its application to bromide breakthrough measurements during and following the sewage-contaminated runoff event.

represents the number pulses assigned to the sewage-contaminated storm. Recalling that the flow-weighted duration of the sewage-contaminated storm is, τ_{SO}, the duration of each pulse in flow-weighted time is calculated as follows: $\Delta\tau = \tau_{SO}/N_{SO}$. In the second instance we placed the pulse in the middle of each $\Delta\tau$ interval. Therefore, the jth pulse is release at flow-weighted time, $\tau_i = (j - 1/2)\Delta\tau$, where the integer j ranges between 1 and Floor$(\tau/\Delta\tau)$ if $\tau \leq \tau_{SO}$, or N_{SO} if $\tau > \tau_{SO}$. The Mathematica code for this solution therefore took the form indicated in Figure 2, where the function "e" corresponds to equation (B.40) and "numsum" is N_{SO}. Note that the interpolating function for the inverse function $t(\tau) = \tau^{-1}(t)$ is represented here by the function, "tauInverseFuncInvert". Data used to generate interpolating functions for flow-weighted time, $\tau(t)$, and its inverse function, $t(\tau)$, are both available from the data repository prepared for this manuscript.

To inform our decision about how finely to resolve the breakthrough curve, we compared breakthrough curves predicted by the exact solution and the pulsatile solution illustrated in

```
e[z_, tau_, taui_, u_, ad_, k_, mu_] :=
 UnitStep[tau - taui]
  Exp[-(k - mu) (tauInverseFuncInterp[tau] - tauInverseFuncInterp[taui])]
  Exp[-((z - u (tau - taui))^2) / (4 ad u (tau - taui))] / Sqrt[ad u (tau - taui)]

cGDII[z_, tau_, sumnum_, taus0_, u_, ad_, k_, mu_, cs0_] :=
 cs0 (u (taus0 / sumnum) / (2 Sqrt[Pi]))
  (UnitStep[taus0 - tau]
     Module[{deltau = taus0 / sumnum, maxsum = Floor[tau (sumnum) / taus0]},
      Sum[e[z, tau, deltau (j - 1 / 2), u, ad, k, mu], {j, 1, maxsum}]] +
    UnitStep[tau - taus0] Module[{deltau = taus0 / sumnum},
      Sum[e[z, tau, deltau (j - 1 / 2), u, ad, k, mu], {j, 1, sumnum}]])
```

Figure B.2: Mathematica code for implementing the pulsatile solution for the limiting case, G/D$^{\text{II}}$ (compare with equation (B.37a)).

Figure 2 (for $k = \mu = 0$) for different choices of the number N_{SO}. As indicated in Figure 3, the breakthrough curve (in this case for coliphage) is very well represented for any choice of this integer greater than 20. We therefore set $N_{SO} = 30$ for all of our simulations.

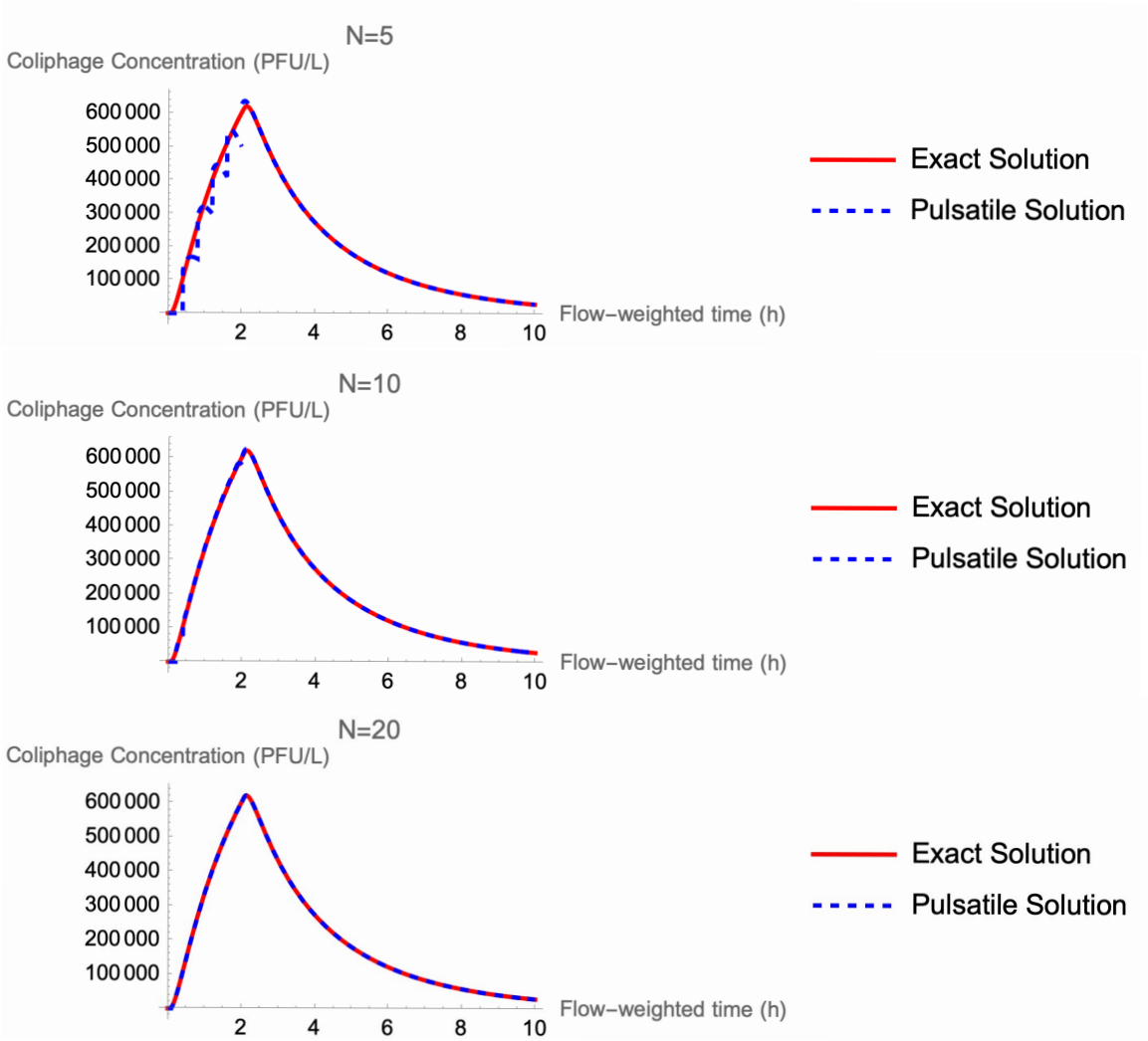

Figure B.3: Breakthrough curves predicted from the exact formula (equations (9a) and (9b) in the main text) and the pulsatile version of G/D^{II} for the choice of $k = \mu = 0$ (equation (B.37a)) and various choices of the parameter N_{SO}. The two breakthrough curves are indistinguishable for $N_{SO} > 20$.

Appendix C

Suplemental Information for Chapter 4

C.1 Bucket Model of Biofilter Hydrology

A bucket model was used to generate high frequency (ca., 1 min.$^{-1}$) estimates for the water stored in the pore spaces of the biofilter media ("storage", $S(t)$ [units of L)]), the transfer of water from the ponding zone into the biofilter across its upper boundary ("infiltration", $J(t)$ [units of L T^{-1})]), the transfer of water out of the biofilter by gravitational drainage across its lower boundary ("outflow", $Q(t)$ [units of L T^{-1})]) and evapotranspiration across its upper boundary (ET(t) [units of L T^{-1})]) (note that all volumes and flow rates have been normalized by the area of the biofilter):

$$\frac{dS}{dt} = J(t) - Q(t) - ET(t) \tag{C.1a}$$

$$S(t = 0) = S_0 \tag{C.1b}$$

The variable S_0 represents the volume of water initially present in the biofilter. The bucket model is forced by measured (or modeled, depending on context) inflow to the ponding zone ("inflow", $I(t)$ [units of L T^{-1})]) and hourly ET, calculated as reference crop potential ET (cPET) using the Penman-Monteith equation following FAO guidelines (Allen et al., 1998) and taking into account local environmental conditions (wind speed, vapor pressure deficit, temperature) and plant-specific characteristics (for details see Supplemental Materials in Parker et al., 2021).

The infiltration term $J(t)$ appearing in equation (C.1a) was estimated from measured or modeled inflow to the ponding zone $I(t)$ as follows, where the variables represent the biofilter media's average saturated hydraulic conductivity (K_{sat} [units of L T^{-1})]) and the biofilter's maximum water storage volume (S_{max} [units L]) equal to the area-normalized void volume of the biofilter's media:

$$J(t) = \begin{cases} I(t), \ 0 < S(t) < S_{max} \\ K_{\text{sat}}, \ S(t) = S_{max} \end{cases} \tag{C.2}$$

As noted in Parker et al. (2021), this simple expression approximates the infiltration process as three distinct phases: (1) infiltration equals inflow during the filling phase, which begins when storm water first enters the ponding zone and infiltration is dominated by capillary forces ($S(t) < S_{max}$, $J(t) = I(t)$); (2) infiltration equals the saturated hydraulic conductivity during the transition phase as the biofilter approaches full saturation ($S(t) = S_{max}$, $J(t) = K_{\text{sat}}$); and (3) infiltration equals zero during the draining phase, which commences once inflow has ceased and the ponding zone has drained ($S(t) < S_{max}, J(t) = I(t) = 0$). While process-based models of infiltration are available (e.g., Green and Ampt, 1911), equation (C.2) is consistent with field observations of infiltration described in Parker et al. (2021), and its sole variables (K_{sat} and S_{max}) are easily measured biofilter design parameters.

The gravitational discharge term $Q(t)$ appearing in equation (C.1a) was modeled as a power-

law function of the water in storage (Kirchner, 2009):

$$Q(t) = K_{\text{sat}} \left(\frac{S(t) - S_{min}}{S_{max} - S_{min}} \right)^{g} \tag{C.3}$$

The new variables S_{min} and g represent the minimum storage below which all gravitational drainage ceases and an empirical power-law exponent, respectively. Based on numerical simulations of the Richards equation for transient flow through the OCPW biofilter, Parker et al. (2021) suggest a power-law exponent of $g = 5$. As noted in the main text, the parameter S_{min} can be equated to the pore volume of the saturation zone, created by elevating the outlet of lined biofilters (the drain was not elevated for the OCPW experiments described in the main text, and thus $S_{min} = 0$ for that system).

After specifying measured or modeled timeseries of inflow $I(t)$ and evapotranspiration $ET(t)$, equation (C.1a) was integrated numerically using the NDSolve command in Mathematica v. 12 (Wolfram Research, Champaign, IL), to yield high frequency (ca., 1 min.$^{-1}$) timeseries of infiltration $J(t)$, storage $S(t)$ and discharge $Q(t)$ for use in the TTD model of solute transport.

C.2 Derivation of TTD Model of Solute Breakthrough

The breakthrough concentration of the m-th solute at any time t can be represented as a convolution of the probability density function (PDF) form of the age distribution of water leaving the biofilter in gravitational outflow, $p_Q(T, t)$ [units of T^{-1}], and the concentration of the solute that was either present in the biofilter at time $t = 0$ (i.e., "original water") or entered the biofilter from the ponding zone at time $t = t_i$ ("new water") where the integration

is taken with respect to water parcel age, T:

$$C_{Q,m}(t) = \int_0^t \Big(C_m^{\text{original}}(t_i = 0, T) + C_{J,m}^{\text{new}}(t_i = t - T, T) \Big) p_Q(T, t) dT \tag{C.4}$$

Physically, the product, $p_Q(T,t)dT$, represents the fraction of gravitational discharge at time t with ages in the range T to $T + dT$. The age distribution $p_Q(T,t)$ is itself a function of time due to the transient nature of the biofilter's water balance (e.g., one might expect that the age distribution will skew older after a long antecedent dry period). The age distribution can be calculated directly from the age-ranked storage function, $S_T(T,t)$, which is tailored to the hydrologic system of interest and takes into account the time history of inflows, outflows and storage. The time evolution of age-ranked storage is governed by the so-called age conservation equation (ACE) (Harman, 2015):

$$\frac{\partial S_T}{\partial t} = J(t) - Q(t) P_Q(T,t) - ET(t) P_{ET}(T,t) - \frac{\partial S_T}{\partial T} \tag{C.5a}$$

$$S_T(T = 0, t) = 0 \tag{C.5b}$$

$$S_T(T, t = 0) = S_0 H(T - T_0) \tag{C.5c}$$

$$H(x) = \begin{cases} 0, x < 0 \\ 1, x \geq 0 \end{cases} \tag{C.5d}$$

The ACE equates the time rate of change of age-ranked storage (left hand side) to the inflow of new water of age $T = 0$ (first term on right hand side); outflow of water by gravitational drainage and evapotranspiration with age distributions of $P_Q(T,t)$ (second term) and $P_{ET}(T,t)$ (third term), respectively; and aging of water in storage (fourth term). The boundary condition ((equation (C.5b)) ensures that no water in storage has an age less than $T = 0$. The initial condition (equation (C.5c)) implies that, at time $t = 0$, all original water in storage, S_0, has a single age, $T = T_0$. The age distributions, $P_Q(T,t)$ and $P_{ET}(T,t)$ are CDFs, and hence represent the fraction of water leaving the control volume as either

gravitational discharge or ET at time, t, with age less than or equal to T. The function $H(\cdot)$ is a unit step or Heaviside function.

Before the ACE can be solved an additional closure relationship, called the StorAgeSelection (SAS) function, is required to relate the age distributions of water in gravitational discharge and ET to the age-distribution of water in storage: $P_Q(T,t) = \Omega_Q(S_T(T,t),t)$ and $P_{ET}(T,t) = \Omega_{ET}(S_T(T,t),t)$. In our previous study (Parker et al., 2021), we found that bromide breakthrough data were well described by a uniform SAS, implying that water in outflow is selected more-or-less randomly from storage by age (colored discharge arrows in Figure (1C)). For the choice of a uniform SAS, equations (C.5a) - (C.5d) yield an exact solution for age-ranked storage in the biofilter's soil media (Parker et al., 2021):

$$S_T(T,t) = S_0 H(T-t-T_0)e^{-\bar{\tau}(t,0)} + \int_w^t e^{-\bar{\tau}(t,\nu)} J(\nu)\, d\nu \tag{C.6a}$$

$$\bar{\tau}(t,\nu) = \int_\nu^t \frac{Q(x)+ET(x)}{S(x)}\, dx \tag{C.6b}$$

$$w = \begin{cases} 0,\, T-t \geq 0 \\ t-T,\, T-t < 0 \end{cases} \tag{C.6c}$$

Under uniform sampling the age distribution of water in outflow is equal to the age-distribution of water in storage (i.e., $P_{RTD}(T,t) = P_Q(T,t) = P_{ET}(T,t)$), and therefore the PDF form of the age distribution of water discharged from the biofilter by gravity can be calculated directly from the definition of age-ranked storage (Parker et al., 2021):

$$p_Q(T,t) = \frac{1}{S(t)}\frac{\partial S_T}{\partial T} = \delta(t+T_0-T)\frac{S_0}{S(t)}e^{-\bar{\tau}(t,0)} + H(t-T)\frac{J(t-T)}{S(t)}e^{-\bar{\tau}(t,t-T)} \tag{C.7}$$

The first and second terms on the right hand side equation (C.7) represent the contributions of original water and new water, respectively, where $\delta(\cdot)$ is the Dirac Delta function. Letting $T_0 = 0$, combining equations (C.4) and (C.7) and utilizing the combing property of the Dirac

delta function, we arrive at the TTD model for solute breakthrough described in the main text (see equation (1a)).

C.3 TTD Theory with Equilibrium Sorption

Here we demonstrate that the breakthrough concentration predicted by TTD theory can be modified to account for equilibrium sorption (e.g., by ion exchange), as represented by a linear isotherm. In every differential volume of the biofilter media, we can express the mass of an adsorbing solute (such as ammonium) as follows

$$m = C\theta dV + C_s \rho_b dV \tag{C.8}$$

Variables appearing here include all solute mass m in the differential volume dV present in either the pore fluids or adsorbed to the solid matrix; the pore fluid concentration of solute C (units of solute mass per pore fluid volume); the adsorbed concentration of the solute C_s (units of solute mass per mass of biofilter matrix); the porosity θ of the biofilter matrix (unitless); and the bulk density of the biofilter matrix ρ_b (units mass of biofilter matrix per unit bulk volume).

Provided that any reactions involving the solute do not depend on whether the solute is in an adsorbed or free state, the corresponding reaction rates can be represented in terms of an effective concentration that includes solute mass in both phases expressed on a per unit pore volume basis: $C_m = m/(\theta dV)$ (units mass of solute per pore fluid volume):

$$C_m = C + \frac{C_s \rho_b}{\theta} \tag{C.9}$$

Next we adopt a linear isotherm to relate the equilibrium partitioning of solute between free and adsorbed states, where the partition coefficient is defined as follows (refs): $K_d =$

$\frac{C_s}{C}$. Substituting the linear isotherm into equation (C.9) and rearranging, we arrive at the following relationship between the model and pore fluid solute concentrations where R (unitless) is the retardation coefficient:

$$C = C_m/R \tag{C.10a}$$

$$R = 1 + \frac{K_d \rho_b}{\theta} \tag{C.10b}$$

In summary, the solute breakthrough concentration, C, in water draining from a biofilter can be computed by dividing the solute concentration predicted by the TTD model, C_m, by the retardation coefficient, R. In the event that the solute in question does not adsorb to the biofilter matrix, then the partition coefficient is, $K_d = 0$, the retardation coefficient is unity, $R = 1$, and the model and pore fluid solute concentrations are equivalent, $C = C_m$. If the solute undergoes adsorption, the partition coefficient is greater than zero, $K_d > 0$, the retardation coefficient is greater than unity, $R > 1$, and the pore fluid solute concentration is proportionally less than the model-predicted solute concentration following equation (C.10a).

C.4 Ammonium Breakthrough: Solution I

The N-cycle model (equations (2) and (3) in the main text) tracks the evolution of dissolved organic carbon (DOC), oxygen, ammonium and nitrate as new and original water age and wash-out of the biofilter. The fully-coupled and non-linear nature of the N-cycle model precludes writing out an exact solution for the concentration of these four solutes; instead, solution of the full N-cycle model must be carried out numerically. However, under certain simplifying assumptions the N-cycle model can be solved analytically to yield, when coupled to TTD theory, explicit formulae for the breakthrough concentrations of ammonium and nitrate.

In this section we derive one such solution for the breakthrough concentration of ammonium ("Solution I" in the main text) given two simplifications of the N-cycle model: (Assumption 1) pore fluids in the biofilter are oxygen saturated; and (Assumption 2) the generation of ammonia by ammonification occurs by the respiration of autochthonous organic material (i.e., organic material mixed into the biofilter media) and not by respiration of allochthonous organic material (i.e., organic material transported into the biofilter with new water during storms). Assumption (1) implies that the rate equation for the evolution of oxygen concentration with age (equation (2b) in the main text) can be dropped because the oxygen concentration is now a fixed constant equal to its saturation value ($C_{O_2}(T) = C_{O_2}^{\text{sat}}$), and the oxygen inhibition term (equation (3g) in the main text) is approximately equal to zero, $\theta_{\text{O}_2}^{\text{inh}}(T) \approx 0$. Assumption (2) implies that the rate equation for the evolution of DOC concentration with age (equation (2a) in the main text) can be dropped, and the allocthonous mineralization rate term can be set to zero, $R_{\text{MIN}}^{\text{alloc}}(T) = 0$. The net result is that the rate equation for the age evolution of ammonium simplifies as follows:

$$\frac{dC_{\text{NH}_4^+}}{dT} = \frac{R_{\text{MIN}}^{\text{auto}}}{\gamma_{CN}} - k'_{\text{NI}} C_{\text{NH}_4^+}(T) \tag{C.11}$$

where $k'_{\text{NI}} = k_{\text{NI}} C_{O_2}^{\text{sat}}$ is a pseudo-first-order nitrification rate constant. Letting the variables C_{0,NH_4^+} and $C_{J,\text{NH}_4^+}(t_i)$ represent the initial concentration of ammonium in, respectively, original water (at time $t = 0$) and new water (as it enters the biofilter at time, t_i), equation (C.11) can be solved to yield the following two equations for the concentration of ammonium in water parcels of original and new water, respectively:

$$C_{\text{NH}_4^+}^{\text{original}}(t) = C_{0,\text{NH}_4^+}^{\text{original}} e^{-k'_{\text{NI}} t} + \frac{R_{\text{MIN}}^{\text{auto}}}{\gamma_{CN} k'_{\text{NI}}} \left(1 - e^{-k'_{\text{NI}} t}\right) \tag{C.12a}$$

$$C_{J,\text{NH}_4^+}^{\text{new}}(t_i, T) = C_{J,\text{NH}_4^+}^{\text{new}}(t_i) e^{-k'_{\text{NI}} T} + \frac{R_{\text{MIN}}^{\text{auto}}}{\gamma_{CN} k'_{\text{NI}}} \left(1 - e^{-k'_{\text{NI}} T}\right) \tag{C.12b}$$

Equation (C.13) is the corresponding TTD prediction for the breakthrough concentration of

ammonium where $R_{\mathrm{NH}_4^+}$ is the retardation coefficient for ammonium in the biofilter (compare with equation (8) in the main text).

$$C_{Q,\mathrm{NH}_4^+}(t) = \frac{S_0 e^{-\bar{\tau}(t,0)}}{R_{\mathrm{NH}_4^+} S(t)} C^{\mathrm{original}}_{\mathrm{NH}_4^+}(t) + \frac{1}{R_{\mathrm{NH}_4^+} S(t)} \int_0^t C^{\mathrm{new}}_{J,\mathrm{NH}_4^+}(t_i, T = t - t_i) J(t_i) e^{-\bar{\tau}(t,t_i)}\, dt_i \quad \text{(C.13)}$$

The first term on the right hand side of equation (C.13), which captures the contribution of old water to the export of ammonium from the biofilter, is straightforward to numerically evaluate. Numerical evaluation of the second term, which captures the contribution of new water to the export of ammonium, requires some care because the integrand is highly oscillatory (due to the highly transient nature of inflow, $J(t)$, to the biofilter during storms). Substituting equation (C.12b), the second term of equation (C.13) can be written as follows where $b = \frac{R^{\mathrm{auto}}_{\mathrm{MIN}}}{\gamma_{CN} k'_{\mathrm{NI}}}$:

$$\begin{aligned} &\frac{1}{R_{\mathrm{NH}_4^+} S(t)} \int_0^t C^{\mathrm{new}}_{J,\mathrm{NH}_4^+}(t_i, t - t_i) J(t_i) e^{-\bar{\tau}(t,t_i)}\, dt_i \\ &= \frac{1}{R_{\mathrm{NH}_4^+} S(t)} \int_0^t C^{\mathrm{new}}_{J,\mathrm{NH}_4^+}(t_i) e^{-k'_{\mathrm{NI}}(t-t_i)} J(t_i) e^{-\bar{\tau}(t,t_i)}\, dt_i + \\ &\qquad \frac{b}{R_{\mathrm{NH}_4^+} S(t)} \int_0^t J(t_i) e^{-\bar{\tau}(t,t_i)}\, dt_i - \frac{b}{R_{\mathrm{NH}_4^+} S(t)} \int_0^t e^{-k'_{\mathrm{NI}}(t-t_i)} J(t_i) e^{-\bar{\tau}(t,t_i)}\, dt_i \end{aligned} \quad \text{(C.14)}$$

Because ammonium flows into the biofilter only during storm events, the concentration of ammonium entering the biofilter with new water, $C^{\mathrm{new}}_{J,\mathrm{NH}_4^+}(t_i)$, can be expressed as the following sum over all N storm events where $C^{\mathrm{NH}_4^+}_{J,k}$, $t_{k,s}$ and $t_{k,e}$ represent, respectively, the ammonium concentration, starting time and ending time of the k-th storm event:

$$C^{\mathrm{new}}_{J,\mathrm{NH}_4^+}(t_i) = \sum_{k=1}^{N} C^{\mathrm{NH}_4^+}_{J,k} H(t_i - t_{k,s}) H(t_{k,e} - t_i) \quad \text{(C.15)}$$

Substituting equation (C.15) into equation (C.14) yields, after some rearrangement, the

following result for the second term of equation (C.13):

$$\frac{1}{R_{\mathrm{NH_4^+}}S(t)}\int_0^t C^{\mathrm{new}}_{J,\mathrm{NH_4^+}}(t_i,t-t_i)J(t_i)e^{-\bar{\tau}(t,t_i)}\,dt_i =$$
$$\frac{1}{R_{\mathrm{NH_4^+}}S(t)}\sum_{k=1}^{N} C^{\mathrm{NH_4^+}}_{J,k}H(t-t_{k,s})\int_{t_{k,s}}^{y} e^{-k'_{\mathrm{NI}}(t-t_i)}J(t_i)e^{-\bar{\tau}(t,t_i)}\,dt_i +$$
$$\frac{b}{R_{\mathrm{NH_4^+}}S(t)}\int_0^t J(t_i)e^{-\bar{\tau}(t,t_i)}\,dt_i - \frac{b}{R_{\mathrm{NH_4^+}}S(t)}\int_0^t e^{-k'_{\mathrm{NI}}(t-t_i)}J(t_i)e^{-\bar{\tau}(t,t_i)}\,dt_i \quad \text{(C.16)}$$

The magnitude of the variable y appearing in the upper limit of the first integral on the right hand side of equation (C.16) depends on time t:

$$y = \begin{cases} t,\ t < t_{k,e} \\ \\ t_{k,e},\ t \geq t_{k,e} \end{cases} \quad \text{(C.17)}$$

To quickly evaluate these integrals, they can be re-expressed in terms of the following function which is evaluated only once (e.g., using the ParametricNDSolve command in Wolfram Mathematica v. 12, see accompanying solution code C1):

$$h(u,k'_{\mathrm{NI}}) = \int_0^u J(t_i)e^{-k'_{\mathrm{NI}}(t_{max}-t_i)-\bar{\tau}(t_{max},t_i)}\,dt_i \quad \text{(C.18)}$$

The variable t_{max} represents the maximum time over which the simulations are to be run (i.e., time is bounded by, $0 \leq t \leq t_{max}$). Given this definition for the function $h(u,k'_{\mathrm{NI}})$, equation (C.16) can be reformulated as a simple algebraic expression:

$$\frac{1}{R_{\mathrm{NH_4^+}}S(t)}\int_0^t C^{\mathrm{new}}_{J,\mathrm{NH_4^+}}(t_i,t-t_i)J(t_i)e^{-\bar{\tau}(t,t_i)}\,dt_i =$$
$$\frac{e^{-\bar{\tau}(t,0)+\bar{\tau}(t_{max},0)}}{R_{\mathrm{NH_4^+}}S(t)}\Bigg(e^{-k'_{\mathrm{NI}}(t-t_{max})}\sum_{k=1}^{N} C^{\mathrm{NH_4^+}}_{J,k}H(t-t_{k,s})\Big(h(y,k'_{\mathrm{NI}})-h(t_{k,s},k'_{\mathrm{NI}})\Big)$$
$$+\,bh(t,0)-be^{-k'_{\mathrm{NI}}(t-t_{max})}h(t,k'_{\mathrm{NI}})\Bigg) \quad \text{(C.19)}$$

Combining equations (C.13) and (C.19) we arrive at the final form of Solution I for the ammonium breakthrough concentration (see Code C1 for our Mathematica implementation of Solution I):

$$C_{Q,\mathrm{NH}_4^+}(t) = \frac{S_0 e^{-\bar{\tau}(t,0)}}{R_{\mathrm{NH}_4^+} S(t)} \left(C_{0,\mathrm{NH}_4^+}^{\mathrm{original}} e^{-k'_{\mathrm{NI}} t} + \frac{R_{\mathrm{MIN}}^{\mathrm{auto}}}{\gamma_{CN} k'_{\mathrm{NI}}} \left(1 - e^{-k'_{\mathrm{NI}} t}\right) \right)$$
$$+ \frac{e^{-\bar{\tau}(t,0)+\bar{\tau}(t_{max},0)}}{R_{\mathrm{NH}_4^+} S(t)} \left(e^{-k'_{\mathrm{NI}}(t-t_{max})} \sum_{k=1}^{N} C_{J,k,\mathrm{NH}_4^+}^{\mathrm{new}} H(t - t_{k,s}) \right.$$
$$\left. \left(h(y, k'_{\mathrm{NI}}) - h(t_{k,s}, k'_{\mathrm{NI}})\right) + \frac{R_{\mathrm{MIN}}^{\mathrm{auto}}}{\gamma_{CN} k'_{\mathrm{NI}}} h(t, 0) - \frac{R_{\mathrm{MIN}}^{\mathrm{auto}}}{\gamma_{CN} k'_{\mathrm{NI}}} e^{-k'_{\mathrm{NI}}(t-t_{max})} h(t, k'_{\mathrm{NI}}) \right) \quad \text{(C.20)}$$

Provided that the concentrations of ammonium in original water ($C_{0,\mathrm{NH}_4^+}^{\mathrm{original}}$) and new water (associated with each storm pulse, $C_{J,k,\mathrm{NH}_4^+}^{\mathrm{new}}$) are known and the carbon-to-nitrogen ratio of organic material is fixed at $\gamma_{CN} = 14$ (see main text), equation (C.20) has three unknowns: the pseudo-first-order nitrification rate constant, k'_{NI}, the fixed (autochthonous organic material) mineralization rate, $R_{\mathrm{MIN}}^{\mathrm{auto}}$, and the retardation coefficient associated with the linear equilibrium adsorption of ammonium to the biofilter media, $R_{\mathrm{NH}_4^+}$.

C.5 Ammonium Breakthrough: Solution II

In this section we amend the above solution for ammonium breakthrough to account for the mineralization of (allochthonous) DOC that is transported into the biofilter with new water during storms. Mathematically this involved making the following adjustments: (1) expressing the mineralization rate as a function of the DOC concentration: $R_{\mathrm{MIN}}^{\mathrm{total}} = k_{\mathrm{MIN}}^{\mathrm{alloc}} C_{\mathrm{DOC}}(T)$ where $k_{\mathrm{MIN}}^{\mathrm{alloc}}$ is a first-order mineralization rate constant for allocthonous DOC; and (2) tracking the inflow of allochthonous DOC into the biofilter with new water during storms. The first adjustment implies that the rate equations for ammonium and allochthonous DOC are

now coupled (compare with equation (C.11) above):

$$\frac{dC_{\mathrm{NH}_4^+}}{dT} = \frac{k_{\mathrm{MIN}}^{\mathrm{alloc}} C_{\mathrm{DOC}}(T)}{\gamma_{CN}} - k'_{\mathrm{NI}} C_{\mathrm{NH}_4^+}(T) \tag{C.21a}$$

$$\frac{dC_{\mathrm{DOC}}}{dT} = -k_{\mathrm{MIN}}^{\mathrm{alloc}} C_{\mathrm{DOC}} \tag{C.21b}$$

The second adjustment requires that we track the concentration of DOC in both original and new water: $C_{0,\mathrm{DOC}}^{\mathrm{original}}$ and $C_{J,\mathrm{DOC}}^{\mathrm{new}}(t_i)$ where, as before, the variable t_i represents the time a new water parcel enteered the biofilter during a storm. With these two adjustments, equations (C.21a) and (C.21b) can be solved to yield the following formula for the age-dependence of the ammonium concentration in original water:

$$C_{\mathrm{NH}_4^+}^{\mathrm{original}}(T=t) = \begin{cases} C_{0,\mathrm{NH}_4^+}^{\mathrm{original}} e^{-k'_{\mathrm{NI}} t} \\ +C_{0,\mathrm{DOC}}^{\mathrm{original}} \frac{k_{\mathrm{MIN}}^{\mathrm{alloc}}/\gamma_{CN}}{(k_{\mathrm{MIN}}^{\mathrm{alloc}} - k'_{\mathrm{NI}})} \left(e^{-k'_{\mathrm{NI}} t} - e^{-k_{\mathrm{MIN}}^{\mathrm{alloc}} t} \right), \ k'_{\mathrm{NI}} \neq k_{\mathrm{MIN}}^{\mathrm{alloc}} \\ e^{-k_{\mathrm{MIN}}^{\mathrm{alloc}} t} \left(C_{0,\mathrm{NH}_4^+}^{\mathrm{original}} + \frac{k_{\mathrm{MIN}}^{\mathrm{alloc}}}{\gamma_{CN}} C_{0,\mathrm{DOC}}^{\mathrm{original}} t \right), \ k'_{\mathrm{NI}} = k_{\mathrm{MIN}}^{\mathrm{alloc}} \end{cases} \tag{C.22}$$

The corresponding solution for the age-evolution of ammonium in new water is as follows:

$$C_{\mathrm{NH}_4^+}^{\mathrm{new}}(t_i, T) = \begin{cases} C_{J,\mathrm{NH}_4^+}^{\mathrm{new}}(t_i) e^{-k'_{\mathrm{NI}} T} \\ +C_{J,\mathrm{DOC}}^{\mathrm{new}}(t_i) \frac{k_{\mathrm{MIN}}^{\mathrm{alloc}}/\gamma_{CN}}{(k_{\mathrm{MIN}}^{\mathrm{alloc}} - k'_{\mathrm{NI}})} \left(e^{-k'_{\mathrm{NI}} T} - e^{-k_{\mathrm{MIN}}^{\mathrm{alloc}} T} \right), \ k'_{\mathrm{NI}} \neq k_{\mathrm{MIN}}^{\mathrm{alloc}} \\ e^{-k_{\mathrm{MIN}}^{\mathrm{alloc}} T} \left(C_{J,\mathrm{NH}_4^+}^{\mathrm{new}}(t_i) + \frac{k_{\mathrm{MIN}}^{\mathrm{alloc}}}{\gamma_{CN}} C_{J,\mathrm{DOC}}^{\mathrm{new}}(t_i) T \right), \ k'_{\mathrm{NI}} = k_{\mathrm{MIN}}^{\mathrm{alloc}} \end{cases} \tag{C.23}$$

The next step involves coupling the above solutions for the age-dependence of ammonium in original and new water with the TTD model for solute breakthrough from the biofilter (equation (C.13) in the last section). As with our discussion of Solution I, the second term requires further manipulation. Substituting equation (C.23) and assuming for the moment that $k'_{\mathrm{NI}} \neq k_{\mathrm{MIN}}^{\mathrm{alloc}}$, the second term of equation (C.13) can be written as follows

where $b = \frac{k_{\mathrm{MIN}}^{\mathrm{alloc}}}{\gamma_{CN}(k_{\mathrm{MIN}}^{\mathrm{alloc}} - k'_{\mathrm{NI}})}$:

$$\frac{1}{R_{\mathrm{NH}_4^+} S(t)} \int_0^t C_{J,\mathrm{NH}_4^+}^{\mathrm{new}}(t_i, t - t_i) J(t_i) e^{-\bar{\tau}(t,t_i)}\, dt_i =$$
$$\frac{1}{R_{\mathrm{NH}_4^+} S(t)} \int_0^t C_{J,\mathrm{NH}_4^+}^{\mathrm{new}}(t_i) e^{-k'_{\mathrm{NI}}(t-t_i)} J(t_i) e^{-\bar{\tau}(t,t_i)}\, dt_i$$
$$+ \frac{b}{R_{\mathrm{NH}_4^+} S(t)} \int_0^t e^{-k'_{\mathrm{NI}}(t-t_i)} C_{J,\mathrm{DOC}}^{\mathrm{new}}(t_i) J(t_i) e^{-\bar{\tau}(t,t_i)}\, dt_i$$
$$- \frac{b}{R_{\mathrm{NH}_4^+} S(t)} \int_0^t e^{-k_{\mathrm{MIN}}^{\mathrm{alloc}}(t-t_i)} C_{J,\mathrm{DOC}}^{\mathrm{new}}(t_i) J(t_i) e^{-\bar{\tau}(t,t_i)}\, dt_i \quad \text{(C.24)}$$

Provided that the inflow concentrations of ammonium and DOC are constant over a given storm (as they were for the storm sequence we simulated in the field), the terms $C_{J,\mathrm{NH}_4^+}^{\mathrm{new}}(t_i)$ and $C_{J,\mathrm{DOC}}^{\mathrm{new}}(t_i)$ can be expressed as sums over all N storm events where $C_{J,k}^{\mathrm{NH}_4^+}$, $C_{J,k}^{\mathrm{DOC}}$, $t_{k,s}$ and $t_{k,e}$ represent, respectively, the k-th storm event's ammonium concentration, DOC concentration, starting time, and ending time:

$$C_{J,\mathrm{NH}_4^+}^{\mathrm{new}}(t_i) = \sum_{k=1}^{N} C_{J,k}^{\mathrm{NH}_4^+} H(t_i - t_{k,s}) H(t_{k,e} - t_i) \quad \text{(C.25a)}$$

$$C_{J,\mathrm{DOC}}^{\mathrm{new}}(t_i) = \sum_{k=1}^{N} C_{J,k}^{\mathrm{DOC}} H(t_i - t_{k,s}) H(t_{k,e} - t_i) \quad \text{(C.25b)}$$

Substituting equations (C.25a) and (C.25b) into equation (C.24) yields, after some rearrange-

ment, the following result for the second term of the right hand side of equation (C.13):

$$\frac{1}{R_{\mathrm{NH}_4^+}S(t)}\int_0^t C^{\mathrm{new}}_{J,\mathrm{NH}_4^+}(t_i,t-t_i)J(t_i)e^{-\bar{\tau}(t,t_i)}\,dt_i =$$
$$\frac{1}{R_{\mathrm{NH}_4^+}S(t)}\sum_{k=1}^{N} C^{\mathrm{NH}_4^+}_{J,k}H(t-t_{k,s})\int_{t_{k,s}}^{y} e^{-k'_{\mathrm{NI}}(t-t_i)}J(t_i)e^{-\bar{\tau}(t,t_i)}\,dt_i$$
$$+\frac{b}{R_{\mathrm{NH}_4^+}S(t)}\sum_{k=1}^{N} C^{\mathrm{DOC}}_{J,k}H(t-t_{k,s})\int_{t_{k,s}}^{y} e^{-k'_{\mathrm{NI}}(t-t_i)}J(t_i)e^{-\bar{\tau}(t,t_i)}\,dt_i$$
$$-\frac{b}{R_{\mathrm{NH}_4^+}S(t)}\sum_{k=1}^{N} C^{\mathrm{DOC}}_{J,k}H(t-t_{k,s})\int_{t_{k,s}}^{y} e^{-k^{\mathrm{alloc}}_{\mathrm{MIN}}(t-t_i)}J(t_i)e^{-\bar{\tau}(t,t_i)}\,dt_i \quad \text{(C.26)}$$

As with Solution I, the value of the variable y appearing in the upper limit depends on time t:

$$y=\begin{cases} t,\ t<t_{k,e} \\ \\ t_{k,e},\ t\geq t_{k,e}\end{cases} \quad \text{(C.27)}$$

Equation (C.26) can be simplified by bringing the first two terms on the right hand side of the equation under the same summation:

$$\frac{1}{R_{\mathrm{NH}_4^+}S(t)}\int_0^t C^{\mathrm{new}}_{J,\mathrm{NH}_4^+}(t_i,t-t_i)J(t_i)e^{-\bar{\tau}(t,t_i)}\,dt_i =$$
$$\frac{1}{R_{\mathrm{NH}_4^+}S(t)}\sum_{k=1}^{N}\left(C^{\mathrm{NH}_4^+}_{J,k}+bC^{\mathrm{DOC}}_{J,k}\right)H(t-t_{k,s})\int_{t_{k,s}}^{y} e^{-k'_{\mathrm{NI}}(t-t_i)}J(t_i)e^{-\bar{\tau}(t,t_i)}\,dt_i$$
$$-\frac{b}{R_{\mathrm{NH}_4^+}S(t)}\sum_{k=1}^{N} C^{\mathrm{DOC}}_{J,k}H(t-t_{k,s})\int_{t_{k,s}}^{y} e^{-k^{\mathrm{alloc}}_{\mathrm{MIN}}(t-t_i)}J(t_i)e^{-\bar{\tau}(t,t_i)}\,dt_i \quad \text{(C.28)}$$

To quickly evaluate these integrals, they can be re-expressed in terms of the function $h(u,k'_{\mathrm{NI}})$

introduced in the last section (see equation (C.18)):

$$\frac{1}{R_{\mathrm{NH}_4^+}S(t)}\int_0^t C^{\mathrm{new}}_{J,\mathrm{NH}_4^+}(t_i,t-t_i)J(t_i)e^{-\bar{\tau}(t,t_i)}\,dt_i =$$
$$\frac{e^{-\bar{\tau}(t,0)+\bar{\tau}(t_{max},0)}}{R_{\mathrm{NH}_4^+}S(t)}\Bigg(e^{-k'_{\mathrm{NI}}(t-t_{max})}\sum_{k=1}^{N}\Big(C^{\mathrm{NH}_4^+}_{J,k}+bC^{\mathrm{DOC}}_{J,k}\Big)H(t-t_{k,s})$$
$$\Big(h(y,k'_{\mathrm{NI}})-h(t_{k,s},k'_{\mathrm{NI}})\Big)-be^{-k^{\mathrm{alloc}}_{\mathrm{MIN}}(t-t_{max})}\sum_{k=1}^{N}C^{\mathrm{DOC}}_{J,k}H(t-t_{k,s})$$
$$\Big(h(y,k^{\mathrm{alloc}}_{\mathrm{MIN}})-h(t_{k,s},k^{\mathrm{alloc}}_{\mathrm{MIN}})\Big)\Bigg) \quad \text{(C.29)}$$

Combining equations (C.13), (C.22), and (C.29) we arrive at the following solution for the ammonium breakthrough concentration:

$$C_{Q,\mathrm{NH}_4^+}(t)=\frac{S_0e^{-\bar{\tau}(t,0)}}{R_{\mathrm{NH}_4^+}S(t)}\Bigg(e^{-k'_{\mathrm{NI}}t}\Big(C^{\mathrm{original}}_{0,\mathrm{NH}_4^+}+bC^{\mathrm{original}}_{0,\mathrm{DOC}}\Big)-be^{-k^{\mathrm{alloc}}_{\mathrm{MIN}}t}C^{\mathrm{original}}_{0,\mathrm{DOC}}\Bigg)$$
$$+\frac{e^{-\bar{\tau}(t,0)+\bar{\tau}(t_{max},0)}}{R_{\mathrm{NH}_4^+}S(t)}\Bigg(e^{-k'_{\mathrm{NI}}(t-t_{max})}\sum_{k=1}^{N}\Big(C^{\mathrm{NH}_4^+}_{J,k}+bC^{\mathrm{DOC}}_{J,k}\Big)H(t-t_{k,s})$$
$$\Big(h(y,k'_{\mathrm{NI}})-h(t_{k,s},k'_{\mathrm{NI}})\Big)-e^{-k^{\mathrm{alloc}}_{\mathrm{MIN}}(t-t_{max})}\sum_{k=1}^{N}bC^{\mathrm{DOC}}_{J,k}H(t-t_{k,s})$$
$$\Big(h(y,k^{\mathrm{alloc}}_{\mathrm{MIN}})-h(t_{k,s},k^{\mathrm{alloc}}_{\mathrm{MIN}})\Big)\Bigg),\ k'_{\mathrm{NI}}\neq k^{\mathrm{alloc}}_{\mathrm{MIN}} \quad \text{(C.30)}$$

Provided that the concentrations of ammonium and DOC in original water ($C^{\mathrm{original}}_{0,\mathrm{NH}_4^+}$ and $C^{\mathrm{original}}_{0,\mathrm{DOC}}$) and new water (associated with each storm pulse, $C^{\mathrm{new}}_{J,k,\mathrm{NH}_4^+}$ and $C^{\mathrm{new}}_{J,k,\mathrm{DOC}}$) are known, equation (C.30) has three unknowns: (1) the retardation coefficient for ammonium, $R_{\mathrm{NH}_4^+}$; (2) the pseudo-first-order rate constant for nitrification, k'_{NI}; and (3) the dissolved organic carbon mineralization rate, $k^{\mathrm{alloc}}_{\mathrm{MIN}}$. The remaining parameter $b=\frac{k^{\mathrm{alloc}}_{\mathrm{MIN}}}{\gamma_{CN}(k^{\mathrm{alloc}}_{\mathrm{MIN}}-k'_{\mathrm{NI}})}$ can be calculated from k'_{NI} and $k^{\mathrm{alloc}}_{\mathrm{MIN}}$ for the choice of $\gamma_{CN}=14$ (see main text). An alternative solution for $C_{Q,\mathrm{NH}_4^+}(t)$ can be derived when $k'_{\mathrm{NI}}=k^{\mathrm{alloc}}_{\mathrm{MIN}}$, although this limiting case was not needed for the optimization studies described in the main text.

C.6 Nitrate Breakthrough: Solution III

In this section we derive a solution for the breakthrough of nitrate, adopting the same set of assumptions used to derive Solution I for the breakthrough of ammonium: (Assumption 1) pore fluids in the biofilter are oxygen saturated; and (Assumption 2) the generation of ammonium by ammonification occurs by the respiration of autochthonous organic material (i.e., organic material mixed into the biofilter media) and not by respiration of allochthonous organic material (i.e., organic material transported into the biofilter with new water during storms). Under these conditions, rate equation governing the change in nitrate concentration with age simplifies as follows:

$$\frac{dC_{\mathrm{NO_3^-}}}{dT} = k_{\mathrm{NI}} C_{O_2}^{\mathrm{sat}} C_{\mathrm{NH_4^+}}(T) = k'_{\mathrm{NI}} C_{\mathrm{NH_4^+}}(T) \tag{C.31}$$

where k'_{NI} is a pseudo-first-order rate constant for nitrification. This rate equation can be integrated to yield the following formula for the age-dependence of nitrate concentration in old and new water, respectively, where we have assumed that the initial age of original water is $T_0 = 0$:

$$C_{\mathrm{NO_3^-}}^{\mathrm{original}}(t) = C_{0,\mathrm{NO_3^-}}^{\mathrm{original}} + k'_{\mathrm{NI}} \int_0^t C_{\mathrm{NH_4^+}}^{\mathrm{original}}(x)dx \tag{C.32a}$$

$$C_{J,\mathrm{NO_3^-}}^{\mathrm{new}}(t_i, T) = C_{J,\mathrm{NO_3^-}}^{\mathrm{new}}(t_i) + k'_{\mathrm{NI}} \int_0^T C_{J,\mathrm{NH_4^+}}^{\mathrm{new}}(t_i, x)dx \tag{C.32b}$$

Substituting the corresponding formulae for the evolution of ammonium with age from Solution I (equations (C.12a) and (C.12b)) we arrive at the following algebraic expression for

the time-evolution of nitrate concentration in original and new water.

$$C^{\text{original}}_{\text{NO}_3^-}(t) = C^{\text{original}}_{0,\text{NO}_3^-} + C^{\text{original}}_{0,\text{NH}_4^+}\Big(1 - e^{-k'_{\text{NI}}t}\Big) + \frac{R^{\text{auto}}_{\text{MIN}}}{\gamma_{CN}k'_{\text{NI}}}\Big(k'_{\text{NI}}t - (1 - e^{-k'_{\text{NI}}t})\Big) \tag{C.33a}$$

$$C^{\text{new}}_{J,\text{NO}_3^-}(t_i, T) = C^{\text{new}}_{J,\text{NO}_3^-}(t_i) + C^{\text{new}}_{J,\text{NH}_4^+}(t_i)\Big(1 - e^{-k'_{\text{NI}}T}\Big) + \frac{R^{\text{auto}}_{\text{MIN}}}{\gamma_{CN}k'_{\text{NI}}} \Big(k'_{\text{NI}}T - (1 - e^{-k'_{\text{NI}}T})\Big) \tag{C.33b}$$

From equation (1a) in the main text, the TTD prediction for nitrate breakthrough can be written as follows where we have assumed that nitrate does not undergo adsorption (i.e., the retardation factor is unity, $R = 1$):

$$C_{Q,\text{NO}_3^-}(t) = \frac{S_0 e^{-\bar{\tau}(t,0)}}{S(t)} C^{\text{original}}_{\text{NO}_3^-}(t) + \frac{1}{S(t)}\int_0^t C^{\text{new}}_{J,\text{NO}_3^-}(t_i, T = t - t_i) J(t_i) e^{-\bar{\tau}(t,t_i)}\, dt_i \tag{C.34}$$

The first term on the right hand side of equation (C.34) is straight forward to evaluate numerically, while the second term requires some consideration. First, we re-express the nitrate and ammonium concentration entering the biofilter with new water as a series of storm events or pulses (where the inflow concentration is constant during each pulse):

$$C^{\text{new}}_{J,\text{NH}_4^+}(t_i) = \sum_{k=1}^{N} C^{\text{NH}_4^+}_{J,k} H(t_i - t_{k,s}) H(t_{k,e} - t_i) \tag{C.35a}$$

$$C^{\text{new}}_{J,\text{NO}_3^-}(t_i) = \sum_{k=1}^{N} C^{\text{NO}_3^-}_{J,k} H(t_i - t_{k,s}) H(t_{k,e} - t_i) \tag{C.35b}$$

Substituting equations (C.33b), (C.35a) and (C.35b) into the second term on the right hand side of equation (C.34) we obtain:

$$\begin{aligned}
&\frac{1}{S(t)}\int_0^t C^{\text{new}}_{J,\text{NO}_3^-}(t_i, T=t-t_i)J(t_i)e^{-\bar{\tau}(t,t_i)}\,dt_i = \\
&\frac{1}{S(t)}\sum_{k=1}^{N}\Big(C^{\text{NO}_3^-}_{J,k}+C^{\text{NH}_4^+}_{J,k}\Big)H(t-t_{k,s})\int_{t_{k,s}}^{y} J(t_i)e^{-\bar{\tau}(t,t_i)}\,dt_i \\
&-\frac{1}{\gamma_{CN}k'_{\text{NI}}S(t)}\sum_{k=1}^{N}C^{\text{NH}_4^+}_{J,k}H(t-t_{k,s})\int_{t_{k,s}}^{y} e^{-k'_{\text{NI}}(t-t_i)}J(t_i)e^{-\bar{\tau}(t,t_i)}\,dt_i \\
&+\frac{R^{\text{auto}}_{\text{MIN}}}{S(t)}\Big(k'_{\text{NI}}t-1\Big)\int_0^t J(t_i)e^{-\bar{\tau}(t,t_i)}\,dt_i \\
&-\frac{R^{\text{auto}}_{\text{MIN}}}{\gamma_{CN}S(t)}\int_0^t t_iJ(t_i)e^{-\bar{\tau}(t,t_i)}\,dt_i \\
&+\frac{R^{\text{auto}}_{\text{MIN}}}{\gamma_{CN}k'_{\text{NI}}S(t)}\int_0^t e^{-k'_{\text{NI}}(t-t_i)}J(t_i)e^{-\bar{\tau}(t,t_i)}\,dt_i
\end{aligned} \tag{C.36}$$

For ease of numerical implementation, we can rewrite the above result in terms of the function $h(u,a)$ (see equation (C.18)):

$$\begin{aligned}
&\frac{1}{S(t)}\int_0^t C^{\text{new}}_{J,\text{NO}_3^-}(t_i, T=t-t_i)J(t_i)e^{-\bar{\tau}(t,t_i)}\,dt_i = \\
&\frac{e^{-\bar{\tau}(t,0)+\bar{\tau}(t_{\max},0)}}{S(t)}\Bigg(\sum_{k=1}^{N}\Big(C^{\text{NO}_3^-}_{J,k}+C^{\text{NH}_4^+}_{J,k}\Big)H(t-t_{k,s})(h(y,0)-h(t_{k,s},0)) \\
&-e^{-k'_{\text{NI}}(t-t_{max})}\sum_{k=1}^{N}C^{\text{NH}_4^+}_{J,k}H(t-t_{k,s})(h(y,k'_{\text{NI}})-h(t_{k,s},k'_{\text{NI}})) \\
&+\frac{R^{\text{auto}}_{\text{MIN}}}{\gamma_{CN}k'_{\text{NI}}}\Big(k'_{\text{NI}}t-1\Big)h(t,0)-\frac{R^{\text{auto}}_{\text{MIN}}}{\gamma_{CN}}h_2(t)+\frac{R^{\text{auto}}_{\text{MIN}}}{\gamma_{CN}k'_{\text{NI}}} \\
&\qquad\qquad e^{-k'_{\text{NI}}(t-t_{\max})}h(t,k'_{\text{NI}})\Bigg)
\end{aligned} \tag{C.37}$$

The new function, $h_2(t)$, is defined as follows:

$$h_2(t) = \int_0^t t_i J(t_i) e^{-\bar{\tau}(t_{\max}, t_i)}\, dt_i \tag{C.38}$$

Combining equations (C.32a), (C.34) and (C.37) we arrive at the following formula for the calculation of nitrate breakthrough under fully oxygen saturated conditions and assuming that ammonification occurs by mineralization of autochthonous organic material:

$$\begin{aligned} C_{Q,\mathrm{NO_3^-}}(t) = \frac{S_0 e^{-\bar{\tau}(t,0)}}{S(t)} \Bigg(& C^{\text{original}}_{0,\mathrm{NO_3^-}} + C^{\text{original}}_{0,\mathrm{NH_4^+}} \Big(1 - e^{-k'_{\mathrm{NI}} t}\Big) + \frac{R^{\text{auto}}_{\mathrm{MIN}}}{\gamma_{CN} k'_{\mathrm{NI}}} \\ & \Big(k'_{\mathrm{NI}} t - (1 - e^{-k'_{\mathrm{NI}} t})\Big)\Bigg) + \frac{e^{-\bar{\tau}(t,0) + \bar{\tau}(t_{\max},0)}}{S(t)} \Bigg(\sum_{k=1}^{N} \Big(C^{\mathrm{NO_3^-}}_{J,k} + C^{\mathrm{NH_4^+}}_{J,k} \Big) \\ & H(t - t_{k,s}) \Big(h(y,0) - h(t_{k,s},0) \Big) - e^{-k'_{\mathrm{NI}}(t - t_{max})} \sum_{k=1}^{N} C^{\mathrm{NH_4^+}}_{J,k} H(t - t_{k,s}) \\ & \Big(h(y, k'_{\mathrm{NI}}) - h(t_{k,s}, k'_{\mathrm{NI}}) \Big) + \frac{R_{\min}}{\gamma_{CN} k'_{\mathrm{NI}}} \Big(k'_{\mathrm{NI}} t - 1 \Big) h(t,0) - \frac{R_{\min}}{\gamma_{CN}} h_2(t) + \\ & \frac{R_{\min}}{\gamma_{CN} k'_{\mathrm{NI}}} e^{-k'_{\mathrm{NI}}(t - t_{\max})} h(t, k'_{\mathrm{NI}}) \Bigg) \end{aligned} \tag{C.39}$$

C.7 Figures

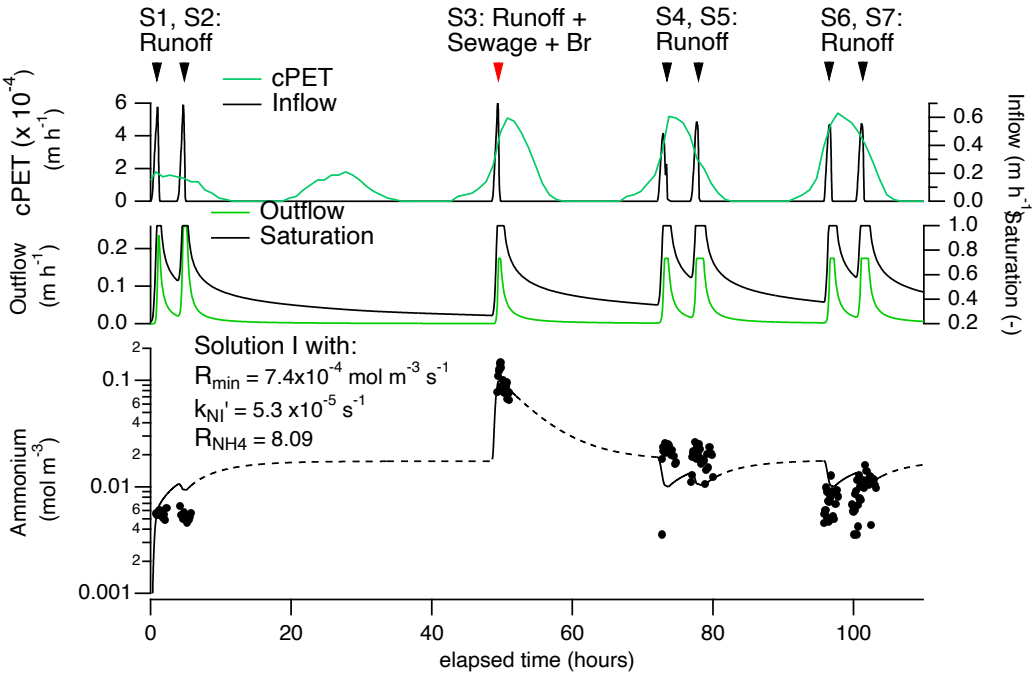

Figure C.1: A model test of hypothesis H1 in the main text (Solution I with the $R_{\min}$, k'_{NI} and $R_{\mathrm{NH}_4^+}$ values shown).

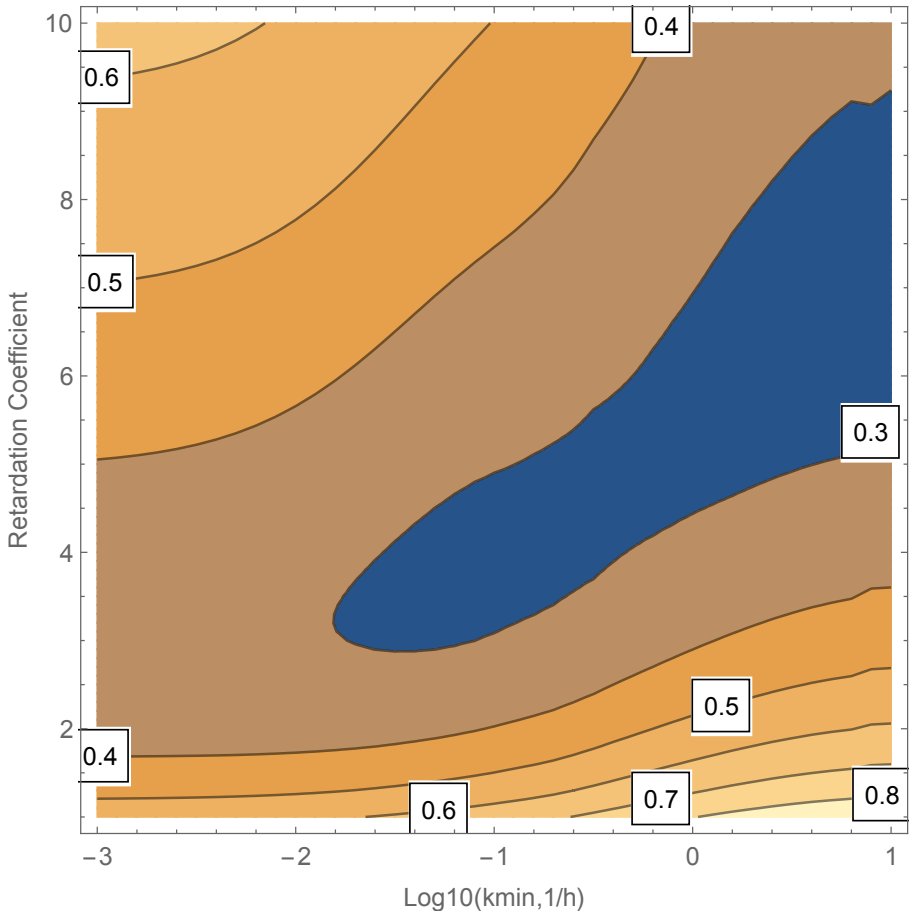

Figure C.2: The Solution II RMSE (contours) as a function of the log-transformed mineralization rate constant (horizontal axis) and the retardation coefficient (vertical axis). Here, the equifinality issue manifests as a diagonal band of low RMSE (see dark blue region) which indicates an infinite set of $k_{\min}^{\text{alloc}}$ and $R_{\text{NH}_4^+}$ values equally well minimize the RMSE, with an increase in one balanced by an increase in the other, see discussion in main text.

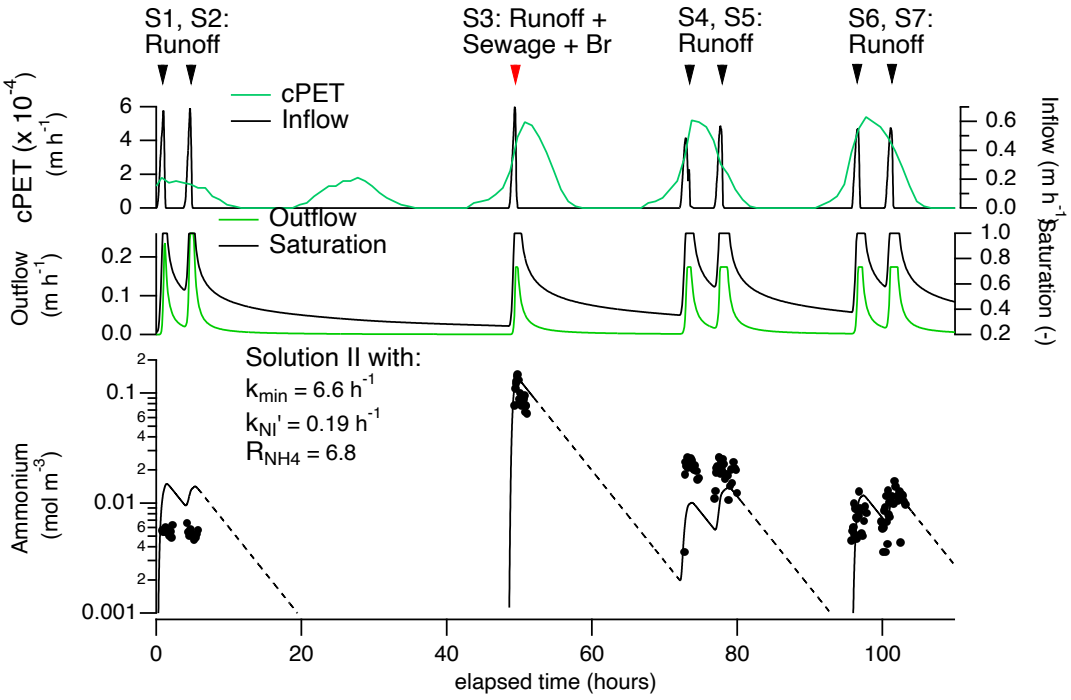

Figure C.3: A model test of hypothesis H2 in the main text (Solution II with the $k_{\min}$, k'_{NI} and $R_{\mathrm{NH}_4^+}$ values shown).